Molecular and Behavioural Analysis of *D. melanogaster* as an alternative model of Alternating Hemiplegia of Childhood

Jennifer Abisola Omoese Ogbeta

Submitted in accordance with the requirements for the degree of Doctor in Philosophy

University of Leeds

School of Biomedical Sciences

October 2024

I confirm that the work submitted is my own, except where work which has formed part of jointly authored publications has been included. My contribution and the other authors to this work has been explicitly indicated below. I confirm that appropriate credit has been given within the thesis where reference has been made to the work of others.

Introduction contains work published in the following review article: **'Genetically altered animal models for ATP1A3-related disorders'**, Ng, H.W., Ogbeta, J.A. and Clapcote, S.J. (2021). *Disease Models & Mechanisms*.

The work within the publication directly attributable to me: Fruit fly (*Drosophila melanogaster*); Zebrafish (*Danio rerio*) and Nematode (*Caenorhabditis elegans*); Hannah Ng: Mouse (*Mus musculus*), Schematic figure; Steve Clapcote: Overall editing of manuscript

Acknowledgements

This research has been carried out by a team which included Dr Steve Clapcote, Prof. Elwyn Isaac and Prof. Amanda Bretman. My own contributions, fully and explicitly indicated in thesis have been: fly genotyping, fly backcrossing, molecular cloning, PCRs, RT-PCR, all behavioural experiments (negative geotaxis assay, cold-shock assay and locomotor activity assay), data processing and analysis done for this thesis. The other members of the group and their contributions have been as follows: the Cambridge Fly Facility and Korea Drosophila Resource Centre (KDRC) for helping to make transgenic flies; Pariya Anaongjanya, Dr Paul Armstrong and Kate Moroney for helping with western blot experiments; Dr Bill Budenberg and Dr Shanelle Kohler for assisting with scripting for Zantiks experiment; Dr Arijit Ghosh for writing an R script for conversion of Zantiks data into a DAM system format.

First and foremost, I would like to thank God for His provision and grace to run with endurance to finish this race titled a PhD.

I would like to extend my gratitude to my PhD supervisors, Dr Steve Clapcote, Prof. Elwyn Isaac and Prof. Amanda Bretman for their continual guidance and valuable feedback throughout this project. A special thanks to Prof. Elwyn Issac whose mentorship from master's to PhD level has been instrumental in my development as a scientist. A huge thanks to all the academics who have helped me reach this stage, particularly Prof. Susan Deuchars for her invaluable counsel.

I would like to acknowledge the University of Leeds for their extensive support in facilitating the completion of project and thesis.

It has been a thrilling experience working in three different labs. Thank you to Claire, Meg, Emily, Steph, Nok and Pariya for your advice and help with my experiments. Thank you to Andreea, Shilpa, Shan, Deborah and Damarie for your friendship and continual emotional support. I would also like to thank the Leeds cohort of women from the WHEN 2023 programme for their shared words of encouragement and wisdom.

A huge thanks to my family for their constant support, especially my mom, who is my biggest cheerleader. Without her words of encouragement, I would not have applied for this PhD. So, I would like to dedicate this thesis to you mom.

Abstract

Alternating Hemiplegia of Childhood (AHC) is a rare and complex neurodevelopmental disorder hallmarked by infantile onset (<18 months) of recurrent temporal paralysis affecting either one (Hemiplegia) or both sides (Quadriplegia) of the body. These episodes are spontaneous but are also triggered by external stressors and are alleviated during sleep. They can present alone or alongside movement, cognitive, and behavioural symptoms that become more apparent with age. The majority of AHC cases are caused by heterozygous de novo mutations in the ATP1A3 gene, encoding the catalytic α3-subunit of the neuronal Na+/K+ ATPase (NKA) pump. The NKA α3 subunit is responsible for the rapid restoration of basal intracellular Na+ in neurons following sustained discharge. A Drosophila melanogaster mutant carrying the fly equivalent (p.Gly744Ser) of the human AHC p.Gly755Ser mutation within its NKA α-subunit (ATPα) showcased mechanical-stress induced paralysis, suggesting conservation of NKA α-subunit function between species thus the potential to be used as an alternative animal model for in vivo studies of AHC. Consistent with this, further characterisation of the heterozygous p.Gly744Ser and null NKA α flies showed AHC-relevant phenotypes including defective walking speed, heightened sensitivity to cold stress and sleep disturbances. Utilization of the Gal4/UAS system to ubiquitously express a copy of the wildtype human ATP1A3, confirmed by qualitative RT-PCR, rescues sensitivity to cold stress in both p.Gly744Ser and null NKA α flies. Hemizygous transgenic flies expressing the p.Asp801Asn ATP1A3 transgene via the Gal4/UAS system did not exhibit AHC-relevant phenotypes, potentially due to the presence of functional endogenous wildtype ATPα alleles. Overall, the capability of NKA α-modified flies to display other AHC-relevant phenotypes and evidence of functional equivalence between species showcases the fly as a suitable in vivo model for AHC research. Thus, a step in the right direction to successfully implement the replacement principle of the 3Rs.

Table of Contents

List of Tables

List of Figures

Abbreviation List

AHC	Alternating Hemiplegia of Childhood
ADHD	Attention deficit hyperactivity disorder
ADP	Adenosine diphosphate
AKT	Protein kinase B
ATP	Adenosine Triphosphatase
ATP1A2	*ATPase Na+/K+ Transporting Subunit Alpha 2*
ATP1A3	*ATPase Na+/K+ Transporting Subunit Alpha 3*
Ca^{2+}	Calcium ions
CACNA1A	Calcium voltage-gated channel subunit alpha1
SLC1A3	Solute carrier family 1 member 3
SLC2A1	Solute carrier family 2 member 1
CLDN5	Claudin 5
ERK	Extracellular signal-regulated kinase
FXYD	Phe-X-Tyr-Asp protein family
GABA	Gamma-aminobutyric acid
H^+	Hydrogen ion
K^+	Potassium ions
KDa	Kilodalton
Na^+	Sodium ions
NKA	Sodium-potassium ATPase
NKA α	Sodium-potassium ATPase alpha subunit

OMIM	*Online Mendelian Inheritance in Man*
p.	Protein
Pi	Inorganic phosphate
α1	Alpha 1
α2	Alpha 2
$\alpha 3$	Alpha 3
β	Beta
WT	Wildtype
SUDEP	Sudden unexpected death in epilepsy
NMDA	N-methyl-D-aspartate
LoF	Loss-of-function
GoF	Gain-of-function
TS	Temperature Sensitive
DTS	Dominant Temperature Sensitive
h-NKA	Human Sodium-potassium ATPase
m-NKA	Mouse Sodium-potassium ATPase
d-NKA	*D. melanogaster* Sodium-potassium ATPase

I. General Introduction

1.1 Alternating Hemiplegia of Childhood (AHC)

1.1.1 Clinical features of classic AHC

Alternating Hemiplegia of Childhood (AHC, OMIM #614820) is a rare neurodevelopmental syndrome that was first described over fifty years ago in six children (Verret and Steele, 1971). The disorder is characterised by episodes of temporal paralysis involving either one (unilateral) or both sides (bilateral) of the body, usually appearing before 18 months of age (Verret and Steele, 1971). The frequency of episodes ranges from a single episode every few months to multiple episodes per day (Verret and Steele, 1971). Recovery following an episode usually occurs within minutes to hours, however episodes can persist for days or weeks (Verret and Steele, 1971). Other neurological abnormalities reported in early childhood (0-8 years) include developmental delays, epilepsy, headaches, involuntary muscle movement causing stiffness (dystonia) or jerky/twisting (choreoathetosis), rapid involuntary eye movement (paroxysmal nystagmus), difficulty speaking (dysarthria) and episodes of autonomic dysfunction (Verret and Steele, 1971; Aicardi, 1987; Bourgeois et al., 1993). Usually beginning abruptly, plegic and dystonic episodes (or attacks) can be triggered or exacerbated by a range of environmental (e.g., extreme heat/cold and lighting changes), physical (e.g., exercise), and emotional (e.g., excitement and frustration) stressors (Mikati et al., 2000; Sweney et al., 2009), which are detailed in Table 1. Moreover, in majority of AHC patients, plegic and dystonic attacks are reported to disappear upon sleep, with frequent reoccurrence shortly (10-20 minutes) after waking (Aicardi, 1987; Bourgeois et al., 1993; Sweney et al., 2009; Panagiotakaki et al., 2010; Panagiotakaki et al., 2015). There have also been reports of AHC patients being underweight and small in stature, which is thought to be due to

difficulties with eating during plegic attacks (Neville and Ninan, 2007; Panagiotakaki et al., 2010).

1.1.2 Clinical features of atypical AHC

In addition to the classic symptoms of AHC described in Table 1, several uncommon features have been reported including onset of plegic attacks presenting later in childhood, as late as 4 years old (Verret and Steele, 1971; Mikati et al., 2000; Roubergue et al., 2013). Other atypical features reported are mild to no sign of cognitive impairment (Mikati et al., 2000), greater occurrence of dystonia attacks than hemiplegic attacks (Mikati et al., 2000), absence of quadriplegic attacks or manifestation of single limb paralysis (Mikati et al., 2000; Delorme et al., 2017). Moreover, children with typical signs of AHC have been reported to exhibit features of early-onset encephalopathy, such as early life drug-resistant seizures and microcephaly (Paciorkowski et al., 2015; Schirinzi et al., 2018; Stagnaro et al., 2018).

1.1.3 Diagnostic criteria of AHC

Since the initial establishment of the diagnostic criteria of AHC (Bourgeois et al., 1993; Aicardi et al., 1995), there have been recent revisions to the criteria with clinical features classed into essential, major, and minor criteria Mikati et al. (2021), as summarised in Table 1. It has been proposed that for AHC diagnosis, patients must have the essential criteria in addition to three of the major criteria or two major and three minor criteria (Mikati et al., 2021).

Table 1. Diagnostic criteria of Alternating Hemiplegia of Childhood*

Essential criteria	1. Sudden episodes of hemiplegia attacks that shift between left or right side of the body and/or episode of quadriplegia

	2. Indication of background of abnormal neurological development - Developmental delay (speech and language delay, behavioural problems) - Cognitive impairment (intellectual disability)
Major criteria	1. Onset between 0-18 months of life (classic). Onset after 18 months (atypical) 2. Dystonic attacks 3. Various types of episode occurring either separately or concurrently, with a progression from one or more symptoms to others within the same episode. 4. Sudden episode of involuntary, rhythmic eye movements of both (nystagmus) or one (monocular nystagmus) eye 5. Identification of an *ATP1A3* nutation 6. Observation of symptom relief upon sleeping
Minor criteria	1. Epileptic seizures (partial, myoclonic, convulsive, tonic seizures or status epilepticus) that are independent or concurrent with other symptoms 2. Occurrences of altered consciousness, not epileptic in nature, that is independent or in conjunction with other symptoms 3. Episodes of autonomic dysfunction (bradycardia, bronchospasm, apnoea, nausea, shortness of breath, hypo- or hyperthermia, sleep disturbance) or dysfunction such as muscle tone abnormalities (specifically hypotonia), ataxia, choreoathetosis and oral motor dysfunction

*Information from Gergont and Kaciński (2014); Rosewich et al. (2017); Mikati et al. (2021)

1.1.4 Epidemiology of AHC

AHC has an estimated prevalence of 1 in a million children worldwide according to a review article (Neville and Ninan, 2007). Some research suggests that prevalence

might be influenced by geographic differences, with estimates reported of 1 in 100,000 children (≤16 years) diagnosed with AHC in Denmark (Hoei-Hansen et al., 2014).

1.1.5 Genetic basis of AHC

In over 75% of AHC patients, the identified cause is a *de novo* heterozygous mutation in the *ATP1A3* gene (chromosome 19q13.2), encoding the human alpha 3 (α3) subunit of the Na^+/K^+ ATPase (h-NKA) pump found predominantly in neurons (Heinzen et al., 2012; Rosewich et al., 2012; Ishii et al., 2013; Hoei-Hansen et al., 2014; Sasaki et al., 2014; Panagiotakaki et al., 2015; Viollet et al., 2015; Cordani et al., 2021). Almost all reported cases of AHC are sporadic in nature. However, the few familial cases show autosomal dominant inheritance of AHC (Mikati et al., 1992; Mikati et al., 1995; Kramer et al., 2000; Kanavakis et al., 2003; Heinzen et al., 2012). There are over sixty distinct *ATP1A3* mutations linked to AHC, with 91% being missense mutations and the remaining 9% being small deletion, small insertional, splicing or complex rearrangement mutations (Viollet et al., 2015; Holm, R. et al., 2016; Li et al., 2022). Of the >60 mutations, there are three leading mutations found among AHC patients. One mutation (p.Asp801Asn) explains 30-43% of AHC cases, the second mutation (p.Glu815Lys) explains 16-35%, and the third mutation (p.Gly947Arg) explains 8-15% of reported cases (Yang et al., 2014; Panagiotakaki et al., 2015; Viollet et al., 2015). Genotype-phenotype correlational studies have found the three mutations to show gradient of symptom severity from left to right: p.Glu815Lys > p.Asp801Asn >p.Gly947Arg (Sasaki et al., 2014; Yang et al., 2014; Panagiotakaki et al., 2015; Viollet et al., 2015). Distinct features of the three mutations are summarised in Table 2. Despite the majority of cases being caused by *ATP1A3* mutations, genetic heterogeneity is recognized in AHC, with classic and atypical features of AHC linked to mutations in other membrane transport proteins. Implicated genes include: *ATP1A2*

(chromosome 1q23.2), encoding the $\alpha 2$ subunit of the h-NKA pump (Bassi et al., 2004; Swoboda et al., 2004; Huang et al., 2021); *SLC2A1* (chromosome 1p34.2), encoding a glucose transporter (Weller et al., 2015); *CACNA1A* (chromosome 19p13.13), encoding the $\alpha 1$A subunit of a voltage-dependent Ca^{2+} channel (De Vries et al., 2008; Gajam et al., 2022); *SLC1A3* (chromosome 5p13.2), encoding excitatory amino acid transporter 1 protein (Jen et al., 2005) and *CLDN5* (chromosome 22p11.21), encoding a tight junction protein at the blood-brain barrier (Hashimoto et al., 2022; Desguerre et al., 2023). However, these genes are responsible for very few cases of AHC.

1.1.6 Physiological basis of AHC

Vascular-related mechanisms have been proposed as a possible explanation for the manifestation of hemiplegia in AHC. This is due to several cases reports of patients with a loss of blood flow to their brain before and during attacks (Holm and Lykke-Hartmann, 2016). In a separate study, AHC patients were found to have small blood vessel abnormalities in the skin and muscles (Auvin et al., 2006). Further support for hemiplegia as a vascular phenotype is the effectiveness of the vasodilator flunarizine, the first-line treatment for hemiplegia in AHC (Holm and Lykke-Hartmann, 2016). However, the absence of vascular phenotypes in all patients studied and the limited efficacy of flunarizine suggest the involvement of other mechanisms in hemiplegia development.

Table 2. Clinical features of three most prevalent AHC-causing mutations*

Mutation	Disease severity	Onset of paroxysmal symptoms	Frequency and duration of plegic attacks	Onset and frequency of epilepsy	Severity of cognitive impairment	Severity of motor deficits	Episodes of autonomic dysfunction
p.Glu815Lys (E815K)	Severe	0-4 months	Frequent but shorter bouts	4-7 months More frequent	Severe	Severe	Frequent
p.Asp801Asn (D801N)	Moderate	0-7 months	Fewer but longer bouts	0-18 months Less frequent	Moderate	Moderate	Infrequent
p.Gly947Arg (G947R)	Mild	1-10 months	Fewer but longer bouts	1-14 months Very infrequent	Mild	Mild	Infrequent

*Data taken from Panagiotakaki et al. (2015)

1.1.7 Molecular and Cellular basis of AHC

1.1.7.1 Mammalian Na^+/K^+ ATPase: Structure, Function and Expression

The Na^+, K^+-ATPase pump, commonly referred to as NKA, is responsible for the generation and preservation of Na^+ and K^+ gradients across the cell membrane in all animal cell types. The h/m-NKA establishes Na^+/K^+ homeostasis by utilising the energy released from the hydrolysis of an ATP molecule to transport three Na^+ ions out of the cell in exchange for two extracellular K^+ ions into the cell. The process by which h/m-NKA uses ATP hydrolysis to transport these cations either in or out of the cell is known as forward cycling (Post et al., 1972). The heterodimeric integral membrane protein is composed of a large alpha (α) subunit and a smaller auxiliary beta (β) subunit associated in a 1:1 αβ complex forming the minimal functional unit in mammals (Morth et al., 2007; Kanai et al., 2013). In addition, h/m-NKA also contains an auxiliary tissue-specific subunit belonging to the Phe-X-Tyr-Asp (FXYD) domain protein family (Morth et al., 2007; Kanai et al., 2013). Cellular functions driven by Na^+/K^+ gradients include regulation of cell volume, pH modulation, generation of action potentials (AP) and Na^+-coupled secondary transport of H^+, Ca^{2+}, glucose and amino acids across the plasma membrane (Clausen et al., 2017).

The α-subunit makes up the catalytic unit of the h/m-NKA pump and has a molecular weight of ~110 kDa (Suhail, 2010; Clausen et al., 2017). The h/m-NKA has four α-subunit isoforms (α1, α2, α3, α4) distinguished by properties such as substrate affinities and expression patterns. The most abundant isoform, h/m-NKA α1, is expressed ubiquitously, while the h/m-NKA α2 isoform is expressed in the muscle (skeletal and heart) and brain (astrocytes and glia cells) (Clausen et al., 2017). The h/m-NKA α3 isoform is primarily expressed in neuronal populations but is also highly

expressed in the heart (Richards et al., 2007; Bøttger et al., 2011; Clausen et al., 2017). Although both h/m-NKA α1 and h/m-NKA α3 are co-expressed in many neurons of the central nervous system (CNS), the h/m-NKA α3-subunit is distinct in that it is highly expressed in inhibitory neurons, particularly fast-spiking interneurons, and has a lower affinity for Na^+ and K^+ ions thought to facilitate the rapid restoration of neuronal resting membrane potential after intense firing (Azarias et al., 2013; Smith et al., 2021). The h/m-NKA α4 isoform is exclusively expressed in testis (Clausen et al., 2017). As highlighted by the expression pattern of h/m-NKA α-subunits, h/m-NKA is expressed abundantly in the brain, consuming 50% of energy in ATP form (Harris et al., 2012). Thus, it is reasonable to associate its dysfunction to a series of cellular complications.

Crystal structures of the pig and shark NKA α1-subunit reported by Morth et al. (2007), Shinoda et al. (2009) and Kanai et al. (2013) revealed that the α-subunit is characterised by ten transmembrane α-helices (TM1-TM10) and three cytoplasmic domains harbouring the phosphorylation (P), nucleotide binding (N) and actuator (A) domains (Figure 1). Recently cryo-electron microscopy (cryo-EM) studies have revealed that the structure of the h-NKA α3-subunit overlaps exactly with that of the pig NKA α1-subunit (Nguyen et al., 2022) suggesting that the TM1-TM10 structure of h-NKA α is conserved across mammalian species. The h/m-NKA α-subunit also contains an inhibitor site located between TM1-TM6 (Kanai et al., 2021) where the molecule ouabain binds. Moreover, all three cation binding sites are located to certain transmembrane α-helices, elucidating α-subunit function in binding and movement of cations (Morth et al., 2007; Kanai et al., 2013). Two of the sites (site I and II), located between TM4, TM5 and TM6, bind either Na^+ or K^+ ions (Kanai et al., 2013).

Meanwhile, the third site (site III), found between TM5, TM6 and TM8 amino-acid side chains, binds Na^+ only (Kanai et al., 2013). However, it has been reported that in the absence of extracellular Na^+ and K^+ and at physiological Na^+ and K^+ concentrations, h/m-NKA permits the inward movement of H^+ through site III, creating intracellular H^+ currents which help to regulate cellular processes in the brain such as ion channel activity and neuronal excitability (Mitchell et al., 2014; Ruffin et al., 2014; Vedovato and Gadsby, 2014).

The β-subunit is the regulatory unit of the h/m-NKA pump and has a molecular weight of 40-60 kDa (Geering, 2008; Clausen et al., 2017; Kryvenko et al., 2021). Three β isoforms (β1, β2, β3) exist in mammals which are differentially expressed. The most abundant isoform, β1, is expressed ubiquitously, while the β2 isoform is expressed in skeletal muscle, heart and brain (astrocytes and glia cells), and the β3 isoform is expressed in the central nervous system (CNS) and testis (Suhail, 2010; Clausen et al., 2017). The β-subunit is characterised by a single transmembrane helix with an amino N-terminus in the cytoplasm and a large C-terminal extracellular domain (Figure 1). The subunit is in direct contact with transmembrane αM7 and αM10 (Morth et al., 2007; Kanai et al., 2013). The β-subunit is responsible for the maturation of h/m-NKA, trafficking of the enzyme to the plasma membrane, and stabilization of the K^+-bound E2 state of h/m-NKA (Geering, 2008; Shinoda et al., 2009; Clausen et al., 2017).

The FXYD protein is an additional regulatory unit of the h/m-NKA pump with a molecular weight of ~8-19 kDa (Geering, 2005; Geering, 2006; Mishra et al., 2011; Yap et al., 2021). Mammals express seven FXYD proteins in a tissue-specific manner (Table 3). Similar to the β-subunit, the FXYD subunit is characterised by a single transmembrane helix, however the amino terminus is located in the extracellular space

(Figure 1). The subunit is found in close proximity to αM9 residues (Morth et al., 2007; Kanai et al., 2013). Unlike the α and β subunits, the FXYD subunit is not essential for h/m-NKA function but is reported to regulate the kinetic properties of the enzyme specifically by changing the rates and cation affinities of active Na^+/ K^+ transport to suit the physiological needs of different cell types (Geering, 2005; Mishra et al., 2011).

Table 3. Summary of mammalian FXYD protein expression*

FXYD protein	Other given names	Expression patterns
FXYD1	Phospholemman	Mainly expressed in skeletal muscle, heart, and liver tissue
FXYD2	Gamma (γ) subunit of NKA	Exclusively expressed in kidney and pancreatic tissue
FXYD3	Mammary tumor (Mat-8)	Mainly expressed in uterus, stomach, colon, skin tissue. Overexpressed in breast tissue
FXYD4	Corticosteroid hormone-induced factor (CHIF)	Exclusive to kidney and colon tissue
FXYD5	Dysadherin	Expressed in multiple tissue types but to a significantly lesser extent in brain tissue. Overexpressed in liver tissue
FXYD6	Phosphohippolin	Expressed in multiple tissues
FXDY7	N/A	Expressed exclusively in brain tissue

*Information from Geering (2006); Clausen et al. (2017); Yap et al. (2021)

1.1.7.2 The catalytic mechanism of Na^+/K^+ ATPase

Ion transport is achieved by the h/m-NKA α-subunit undergoing confirmational changes, illustrated by the Post-Albers model (Post et al., 1972) (Figure 2). The E_1 states are cytoplasmic facing with a high affinity for Na^+ and ATP, while E_2 states are

extracellular facing with high affinity for K^+ (Morth et al., 2007; Kanai et al., 2013). In E_1 state, the pump binds three intracellular Na^+ ions while bound to ATP. Following Na^+ binding, ATP hydrolysis occurs (ADP + Pi), and the pump is phosphorylated at the highly conserved Asp366 residue within the P-domain, leading to E_1P state (Kanai et al., 2013). Conformational change results in release of Na^+ ions into the extracellular space, leading to the E_2P (a low affinity for Na^+ and ATP, extracellular facing). The pump can now bind two K^+ ions on the extracellular side. Binding of K^+ ions causes the pump to dephosphorylate by hydrolysis of the Asp366 residue and transition to the E_2 state. The state having a low affinity for ATP results in transition to E_1 state, which is characterised by low K^+ affinity, thus the release of the cation into the cytoplasm (Kanai et al., 2013).

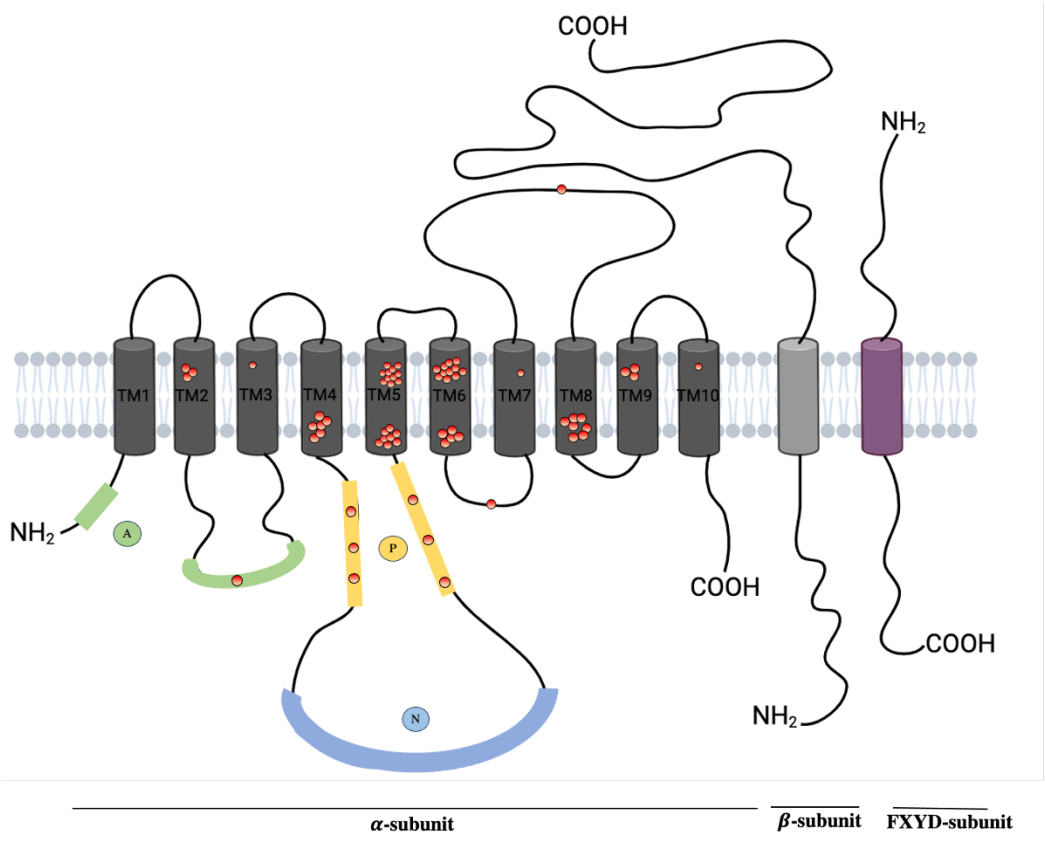

Figure 1. Schematic illustration of the mammalian NKA ion pump structure. The heterodimeric integral membrane-spanning protein consist of a single α-subunit (dark grey), β-subunit (light grey) and the auxiliary FXDY-subunit (purple). Ten

transmembrane segments (TM1-TM10) and three cytoplasmic domains (A, P and N) make up the α-subunit. The Actuator (A) domain; shown in green, Phosphorylation (P) domain; shown in yellow and Nucleotide (N) domain; shown in blue reside within the intracellular loops. Both the glycosylated β-subunit and FXDY-subunit contain a single transmembrane region. From the extracellular space, 2K+ ions are exchanged for 3 intracellular Na+ ions. The red circle (n = 67) are indicative of the location of AHC-related mutations which show majority of ATP1A3 variants reside in TM5 and TM6. Figure was adapted from Ng et al. (2021) and partially created in BioRender.com.

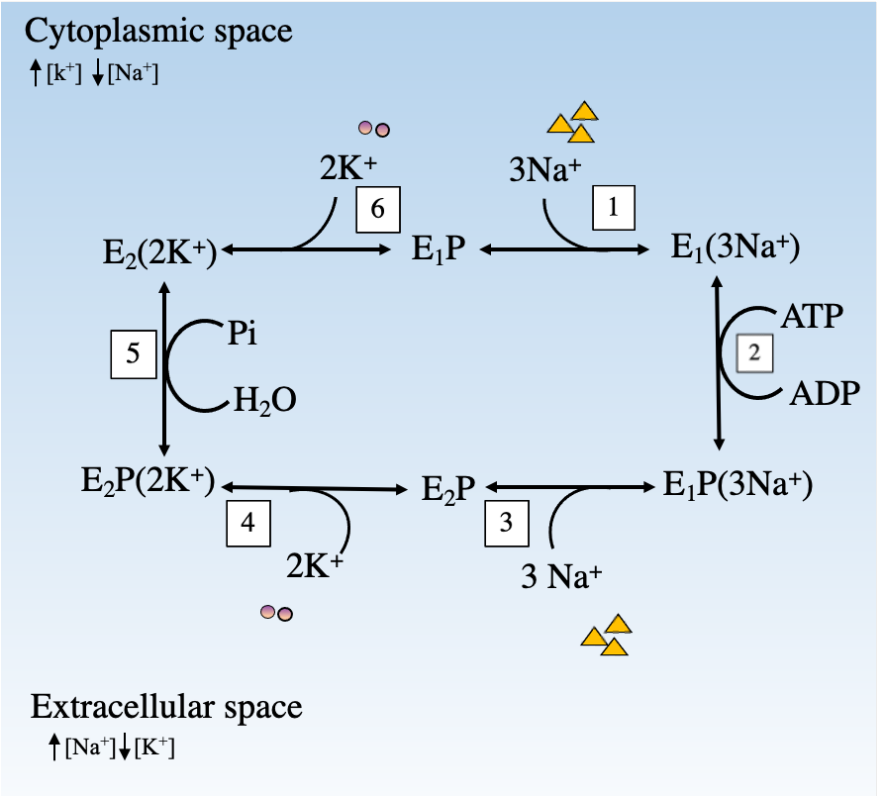

Figure 2. Schematic illustration of Post-Albers model for NKA reaction cycle. Active transport of cations across the cell membrane facilitated by conformation changes (The E1 and E2 states) of the catalytic component of the NKA pump, the α-subunit, occurs in sequential manner both the forward and reverse direction. The binding of the cations in the protein cavity are indicated by brackets. The movement of 3 Na+ ion out of cell (Step 3) and 2 K+ ions into the cell (Step 6) shown in the forward direction generates ionic balance across cell membranes. Figure was adapted from Heinzen et al. (2014).

1.1.8 Molecular pathology of AHC mutations

1.1.8.1 Cell culture studies

Approximately 70% of AHC mutations reside within TM domains, specifically TM4-TM6 helices, where Na^+/ K^+ binding occurs (Heinzen et al., 2012; Sweadner et al., 2019). Thus, *in vitro* studies have been carried out to understand the mechanistic actions of AHC mutations on h-NKA protein function. Co-injection of h-NKA α_3 wildtype (WT) and mutant (p.Asp801Asn, p.Glu815Lys and p.Gly947Arg) complementary RNA (cRNA) into oocytes resulted in a marked decline in WT h-NKA α_3 function, indicating competition between disease and WT α_3-subunit for use within the h-NKA pump (Li et al., 2015). The proposed dominant negative effect of AHC mutations was considered unlikely to explain differences in AHC severity since the extent of inhibition by all mutations was similar (Li et al., 2015). ATPase activity and phosphorylation assays revealed that several mutated protein including the three most common (p.Gly947Arg, p.Asp801Asn and p.Glu815Lys), could not breakdown ATP or add a phosphate group to themselves, indicated by ATPase activity and phosphorylation levels being similar to that of the mock control (Weigand et al., 2014; Holm, R. et al., 2016). Ouabain binding studies also facilitated the evaluation of K^+ binding of h-NKA α_3 mutants, as the cation is a ouabain antagonist (Weigand et al., 2014). Three mutants (p.Ile274Asn, p.Gly947Arg and p.Glu815Lys) showed no ouabain-binding capacity at varying concentrations (5-40 nM). Meanwhile, two mutants (p.Asp801Asn and p.Ser137Tyr) showed similar binding to WT h-NKA, which allowed for K^+ binding analysis (Weigand et al., 2014). Increased ouabain binding at increasing concentrations of potassium chloride (KCl) was observed in p.Asp801Asn and p.Ser137Tyr mutants, indicating impairment of K^+ binding in these mutants (Weigand et al., 2014). K^+/ouabain results indicate that AHC mutations lead

to alterations in the cation binding site, impairing h-NKA function (Weigand et al., 2014). Protein expression studies revealed ATP1A3 expression was unaffected in AHC mutated protein via western blot analysis (Heinzen et al., 2014; Lazarov et al., 2020). However, the Glu277Lys mutation expressed in COS-7 cells were found to significantly reduce protein expression to an undetectable level (Heinzen et al., 2012; Boelman et al., 2014). Neuron-differentiated induced pluripotent stem cells (iPSCs) from AHC patients with p.Gly947Arg exhibited diminished pump current, a depolarized K^+ equilibrium and altered resting potential (Simmons et al., 2018). This provides direct evidence of the functional impact of AHC mutations on the h-NKA α_3 pump (Simmons et al., 2018). As the severity of AHC phenotypes could not be solely attributed to loss of h-NKA activity, the effects of the p.Glu815Lys mutation on aspects of h-NKA biosynthesis, including protein folding, α_1/α_3 competition for β-subunit and post-translational processing of the β-subunit, was explored (Arystarkhova et al., 2019). However, cells expressing this mutation showed no evidence of h-NKA α_3 misfolding, retention of the β-subunit in endoplasmic reticulum or competition between α-subunits (Arystarkhova et al., 2019).

Furthermore, in addition to a dominant negative effect, haploinsufficiency has also been suggested as a possible pathophysiological mechanism of AHC, as functional studies indicate missense mutations are independently able to impair h-NKA pump activity. But, to date, it is not clear which mechanism fundamentally underpins AHC.

1.1.8.2 Structural modelling studies of common AHC mutations

Results from homology modelling can provide possible reasons for impaired ATPase activity in mutated h-NKA α3 pumps. Modelling the p.Asp801Asn mutant revealed that the Asp801 residue lies within Na^+/K^+ binding sites and substitution of the

terminal oxygen with nitrogen leads to a loss of the electrostatic interaction between Asp801 and two K^+ ions (Kirshenbaum et al., 2013; Li et al., 2015). This is predicted to directly affect the movement of K^+ along the narrow corridor of the K^+ pore and may influence Na^+/K^+ binding affinity. These findings shed light on the previously reported lack of ATPase activity and diminished K^+ binding in this mutant (Weigand et al., 2014). In the case of the p.Glu815Lys mutant, the absence of ATPase activity may be attributed to the substitution of the negatively charged Glu residue with a positively charged Lys residue. Modelling revealed that p.Glu815 is distant from the cation binding site but accessible from the cytoplasm, potentially creating an unfavourable environment for the movement of H^+, K^+, and Na^+ ions through the h-NKA pump (Li et al., 2015). *In vitro* experiments indicated that the p.Glu815Lys mutation impairs h-NKA proton transport by blocking the passage of intracellular H^+ currents through the h-NKA pump (Li et al., 2015). Studies toward understanding the involvement of h-NKA proton transport in regulating neuronal excitability suggest a role of pH regulation in the pathophysiology of severe AHC phenotypes (Li et al., 2015), although its importance *in vivo* remains to be determined.

The p.Gly947Arg mutation is predicted to directly interfere with normal Na^+/K^+ binding of the h-NKA as modelling of the mutant revealed the Gly947 residue to be situated next to the Glu951 residue implicated in Na^+ binding (Li et al., 2015). Study of the crystal structure of the Na^+-bound state suggested that p.Gly947Arg impacts the third Na^+ binding site of h-NKA, crucial for the release of Na^+ ions after the transition from E_1P-ADP to the E_2P state (Kanai et al., 2013).

1.1.8.3 Structural modelling studies of other AHC mutations

The modelled structure of p.Ile274Asn m-NKA α3 revealed a loss of interaction between the Glu776 residue and its K^+ ion, the introduction of a polar side chain into the K^+ pore at position 274, and the absence of side chain contact between p.Thr272 and p.Ile274 (Kirshenbaum et al., 2013). These alterations were predicted to significantly impact protein functionality, providing a plausible explanation for the observed lack of ATPase activity in the p.Ile274Asn mutant (Weigand et al., 2014). Both p.Ile810Asn and p.Ile810Ser mutations were predicted to affect the M6 helix bordering the cytoplasmic end of the K^+ pore by substituting the hydrophobic residue (Ile) with polar residues (Asn and Ser) (Kirshenbaum et al., 2013). This is expected to impair the interaction of a neighbouring residue (Glu776) with its K^+ ion and change the protein's pore structure, thereby affecting the routing of K^+ ions (Kirshenbaum et al., 2013).

The Glu815 residue makes up part of the h-NKA opening at the cytoplasmic end for passage of cations, thus the prediction that substitution of Ser137 residue with a bulky Tyr residue could severely affect the H-bond interaction between Ser137 and Glu85 residue may explain observations of impaired K^+ binding in the p.Ser137Tyr mutant following K^+/ouabain binding studies (Weigand et al., 2014).

1.1.9 Treatment of AHC

Currently, there is no cure for AHC, available treatment focuses on symptom management. The first choice of treatment is the non-selective calcium channel blocker, flunarizine, recognized for over 35 years for its efficacy in alleviating hemiplegic episodes (Casaer et al., 1987). While flunarizine rarely prevents the onset of hemiplegic attacks, studies indicate a reduction in severity, duration, or frequency

in 30-78% of AHC patients (Samanta, 2020; Pavone et al., 2022). The proposed mechanism involves inhibiting intracellular Ca^{2+} build-up by blocking inactivated Na^{+}/Ca^{2+} exchanger or N-type voltage-gated calcium channels resulting from intracellular Na^{+} accumulation (Samanta, 2020; Kusunoki et al., 2021). This mitigates cell death and neuronal hyperexcitability linked to intracellular Ca^{2+} build-up (Samanta, 2020; Kusunoki et al., 2021). The reasons for the effectiveness of flunarizine over other Ca^{2+} channel inhibitors remains unclear. In addition to flunarizine, the ketogenic diet/modified Atkins diet (KD/MAD) shows promise for managing acute dystonic and plegic attacks. It has led to complete relief in some cases during follow-up periods (Ulate-Campos et al., 2014; Roubergue et al., 2015). The therapeutic mechanism is not fully understood, but it is suggested that ketones serve as an alternative energy source, countering abnormal cerebral glucose metabolism observed in AHC patients (Ulate-Campos et al., 2014; Roubergue et al., 2015).Various drug treatments, such as beta blockers, anticonvulsants, and glutamate receptor antagonists, are available following failure of flunarizine, but their efficacy remains inconsistent (Samanta, 2020). Verapamil, a Ca^{2+} channel blocker, has shown potential in reducing the severity and frequency of attacks in one individual (Van Hillegondsberg and Michaelis, 2019). Supportive measures include sedatives like buccal midazolam and diazepam rectal for symptom relief during AHC episodes (Bourgeois et al., 1993). Epilepsy management in AHC is challenging due to frequent resistance to anti-epilepsy drugs (AEDs). AEDs are commonly given but may be stopped if adverse effects or poor efficacy occurred (Neville and Ninan, 2007; Alyoubi et al., 2016; Samanta, 2020).

1.1.10 Prognosis of AHC

While AHC is a lifelong condition, research indicates that the frequency and duration of paroxysmal episodes, including hemiplegic attacks, abnormal eye movements, and hypotonia, tend to decrease with age (Mikati et al., 2000; Panagiotakaki et al., 2010; Incorpora et al., 2012). Flunarizine treatment has shown promise in reducing the frequency and severity of attacks, potentially enhancing individuals' quality of life. Notably, patients with p.Asp801Asn or p.Gly947Arg mutations generally exhibit better clinical outcomes than those with the p.Glu815Lys mutation (Sasaki et al., 2014; Yang et al., 2014). Despite this, the long-term prognosis for AHC patients is often poor due to the risk of cognitive decline and a gradual or abrupt decline in motor function (Neville and Ninan, 2007; Sasaki et al., 2017). Furthermore, there is a substantial likelihood of developing epilepsy, with 53% (83/137) to 62% (24/39) of AHC patients experiencing at least one epileptic seizure in their lifetime (Panagiotakaki et al., 2010; Uchitel et al., 2019). Patients suffering frequent convulsive status epilepticus may experience a deterioration in psychomotor skills, potentially leading to wheelchair dependence (Algahtani et al., 2017). While there is no evidence that AHC shortens life expectancy, there is a risk of sudden death following or during severe epileptic seizures or prolonged states of quadriplegia (Panagiotakaki et al., 2010)

1.2 *In vivo* studies of AHC

1.2.1 Mouse models of AHC

Researchers are heavily reliant on the use of genetically-altered *Atp1a3* mouse models to explore the functional and phenotypic consequences of h-NKA α3 dysfunction (summarised in Table 4), given their high genomic similarity to humans. The mouse orthologue, *Atp1a3,* is composed of 23 exons positioned on chromosome 7, sharing

90.8% DNA and 99.6% protein sequence homology with the human *ATP1A3* gene (Ng et al., 2021). In contrast to humans with three, mice have two *Atp1a3* transcript variants arising from alternative splicing, which produces two isoforms: variant 1/ isoform 1 (3615 bp/ 1026 aa; NM_001374627.1) and variant 2/ isoform 2 (3609 bp/ 1013 aa; NM_001290469.2) (Brown et al., 2015). The use of heterozygous knock-out and knock-in mouse models have also offered insight into AHC pathophysiology. The cerebellar inhibitory network is implicated in dystonia pathogenesis following the sudden disruption of the network in *Atp1a3*$^{tm2Kwk/+}$ mice by administration of the neuroexcitatory toxin kainate into their cerebellum vermis, leading to a prolonged dystonic response and recovery period (i.e. disappearance of dystonia) relative to WT littermates (Ikeda et al., 2013). Observations of the enhancement of GABAergic transmission at the synapse between molecular-layer interneurons and Purkinje cells in the cerebellar cortex of *Atp1a3*$^{tm2Kwk/+}$ mice, due to intracellular Na^+ and Ca^{2+} accumulation, may offer insight into how h-NKA dysfunction may affect synaptic plasticity and motor learning (Ikeda et al., 2013). *In vitro* electrophysiology of hippocampal slices from a genetically-altered mouse model carrying the heterozygous AHC Ile810Asn mutation in its *Atp1a3* gene (*Myshkin* mice, Table 4) revealed neuronal hyperexcitability, a phenomenon associated with triggering recurrent seizures (Clapcote et al., 2009). This discovery has been suggested to provide a possible pathophysiological mechanism in understanding the link to h-NKA α3 dysfunction in epilepsy (Clapcote et al., 2009). It is hypothesised that the diminished activity of the m-NKA pump in *Myshkin* mice (Table 4) may cause hyperexcitability due to the pump's failure to effectively clear K^+ ions from the extracellular space, leading to neuronal depolarization. Subsequent effects are post-tetanic accumulation of Na^+ ions, causing increased intracellular Ca^{2+} levels (due inhibition of the Na^+/Ca^{2+}

exchanger) and accumulation of the excitatory neurotransmitter glutamate in the synaptic cleft, rendering the CNS more susceptible to seizures (Clapcote et al., 2009; Kinoshita et al., 2016). Moreover, cerebral glucose hypometabolism in *Myshkin* mice, a phenotype also reported in asymptomatic AHC patients, could be linked casually to seizure generation (Sasaki et al., 2009; Tenney and Schapiro, 2010; Kirshenbaum et al., 2013). Although *Atp1a3*$^{D801Y/+}$ mice did not exhibit spontaneous seizures, they were reported, along with *Myshkin* mice, to have a reduced threshold for flurothyl-induced seizures, indicating higher seizure susceptibility (Hunanyan et al., 2015; Holm, T.H. et al., 2016). This provides evidence that loss-of-function of the neuronal m-NKA pump increases seizure susceptibility in young adult mice (Hunanyan et al., 2015; Holm, T.H. et al., 2016). To explore how m-NKA α3 dysfunction may impact learning and memory in *Atp1a3*$^{tm1Ling/+}$ mice, expression of the hippocampal NMDA receptor (NMDAR), a glutamate-activated Ca^{2+} channel, was studied via western blot analysis (Moseley et al., 2007). The *Atp1a3*$^{tm1Ling/+}$ mice showed significant downregulation of the NR1 isoform of the NMDAR, suggesting a link between h/m-NKA α3 and the NMDAR (Moseley et al., 2007). The observed decline in m-NKA α3 expression in *Atp1a3*$^{tm1Ling/+}$ adult mice is suggested to induce chronic neuronal depolarization, lowering overall neuronal activity and leading to NMDAR downregulation (Moseley et al., 2007). However, when investigated in *Myshkin* adults, expression levels of NR1 protein did not differ from WT littermates (Clapcote et al., 2009). It is recognised that various brain regions other than the hippocampus could be implicated in governing spatial memory (Moseley et al., 2007). Analysis of energy metabolism in *Myshkin* mice indicated elevated basal metabolic rates and decreased visits to food hopper, suggesting both feeding deficits and high metabolic rate contribute to their lower weight (Timothy et al., 2018). Moreover, WT *Atp1a3*

transgenic rescue of *Myshkin* mouse body weight provides supporting evidence of a correlation between h-NKA α3 activity and manifestation of AHC features (Kirshenbaum et al., 2016a). The hippocampus plays a role in regulating emotional and motivated behaviours. Up-regulation of signalling pathways downstream of m-NKA α3, specifically the phosphorylation of ERK and AKT, known to regulate excitatory behaviour in rodents, has been observed in *Myshkin* mice. This suggests the probable involvement of h/m-NKA α3 in the regulation of behaviour (Kirshenbaum et al., 2011; Holm and Lykke-Hartmann, 2016).

Table 4. Summary of genetically-modified mouse models of AHC

Mouse Models	Other Given Names	Genetic Background	Genetic Modifications of *Atp1a3*	Observed Phenotypes	References
Atp1a3$^{tm1Ling/+}$ (Knock-out)	*Atp1a3*$^{-/+}$ *α3*$^{-/+}$	129/Black Swiss (MGI: 3696954)	Heterozygous knockout of *Atp1a3* by an introduction of a single base pair in intron 4, neighbouring the exon-intron splice site leading to abnormal splicing of the gene. Splicing resulted in the addition of 126 bp to the mRNA transcript causing the loss of *Atp1a3* expression	1. Homozygous lethality 2. ~33% reduction in hippocampal m-NKA α3 expression 3. ~16% reduction in total brain m-NKA activity (a1, a2, a3) 4. Locomotor hyperactivity 5. Increased sensitivity to amphetamine 6. Impaired spatial learning and memory 7. Stress-induced dystonic movements	(Moseley et al., 2007) (DeAndrade et al., 2011)
Myshkin (Knock-in)	*Myk*/+ *Atp1a3*$^{Myk/+}$, *Atp1a3*$^{I810N/+}$	C57BL/6NCr (MGI: 4356167)	Chemical (N-ethyl-N-nitrosourea, ENU) mutagenesis induced T to A transversion at	1. Homozygous lethality 2. 36-42% reduction in total brain m-NKA enzymatic activity (α1, α2, α3)	(Clapcote et al., 2009)

$\alpha 3^{I810N/+}$	nucleotide 2562 resulting in amino acid substitution of an Ile (I) for an Asn (N) at position 810 (I810N)	3. Stress-induced hemiplegia attacks 4. Locomotor hyperactivity 5. Increased sensitivity to amphetamine 6. Reduction in body mass 7. Motor deficits 8. Higher susceptibility to epileptic seizures 9. Neuronal hyperexcitability 10. Learning and memory deficits 11. Signs of mania-like behaviour 12. Aberrant circadian rhythms and sleep 13. Social deficits 14. Spontaneous seizures 15. SUDEP 16. Glucose hypometabolism 17. Low body weight	(Kirshenbaum et al., 2011) (Kirshenbaum et al., 2013) (Kirshenbaum et al., 2015) (Kirshenbaum et al., 2016a) (Kirshenbaum et al., 2016b) (Isaksen et al., 2017) (Timothy et al., 2018)

Atp1a3$^{tm1.1Kwk/+}$ (Knock-out)	*Atp1a3*$^{\Delta 2\text{-}6/+}$	C57BL/6J (MGI: 5572809)	Target deletion of exons 2-6 by replacement with an eGFP-*Atp1a3* gene	1. Homozygous lethality 2. Low levels of *Atp1a3* mRNA expression 3. Locomotor hyperactivity 4. Increased motor abilities 5. Increased sensitivity to chemical-inducing dystonia 6. Enhanced inhibitory neurotransmission	(Ikeda et al., 2013) (Sugimoto et al., 2014)
Atp1a3$^{D801Y/+}$ (Knock-in)	*Atp1a3*$^{D801Y/+}$ *α3* $^{D801Y/+}$	C57BL/6JRj (MGI: 6163502)	*Atp1a3* exon 17 replaced with a floxed neomycin resistance cassette and an altered exon 17 containing a single bp change (G>T) resulting in an amino acid change from an aspartic acid (D) to tyrosine (Y) at position 801	1. Homozygous lethality 2. Increased sensitivity to chemically induced epileptic seizures 3. Hypothermia induced dystonia 4. Increased locomotor activity 5. Learning and memory deficits 6. No spontaneous seizures but reduced seizure threshold	(Holm, T.H. et al., 2016) (Isaksen et al., 2017)

Mashlool, (Knock-in)	Mashl Mashl/+ *Atp1a3*$^{D801N/+}$ *α3* $^{D801N/+}$	C57BL/6 (MGI: 6162645)	*Atp1a3* exon 17 replaced with an altered exon 17 containing a single bp change (G>A) resulting in single amino acid change from aspartic acid (D) for asparagine (N) at position 801 (D810N)	1. Homozygous lethality 2. Stress-induced hemiplegic and quadriplegic episodes 3. Locomotor hyperactivity 4. Higher susceptibility to epileptic seizures 5. Learning and memory deficits 6. Motor deficits 7. Low body weight 8. Spontaneous seizures 9. SUDEP	(Hunanyan et al., 2015)
Matoub, (Knock-in)	Matb *Atp1a3*$^{E815K/+}$ *α3* $^{E815K/+}$	C57BL/6J (MGI: 6197036)	A glutamate to lysine missense mutation at amino acid 815 (E815K) was introduced with a neomycin selection cassette flanked by FRT sites.	1. Homozygous lethality 2. Stress-induced hemiplegic episodes 3. Hypo-locomotive activity 4. Low body weight 5. Motor deficits 6. Learning and memory deficits 7. Spontaneous seizures 8. SUDEP 9. Low body weight	(Helseth et al., 2018)

II. Scope of Research

2.1 The Fruit fly: A Potential Replacement Model

Drosophila melanogaster (D. melanogaster) commonly known as the fruit fly has been used as a model system in biomedical research for over a century, contributing to groundbreaking discoveries of which six were awarded the Noble Prize in Physiology or Medicine. The awards acknowledging the fly's role in understanding chromosomal function in heredity, genetic control of early embryonic development and the circadian clock mechanism have particular relevance to human biology (reviewed in (Prokop, 2016). An attractive feature of the fly includes its sequenced genome, containing ~14,000 conserved genes situated on four chromosomes, facilitating easier manipulation of genes for study of animal behaviour, development and disease (Adams et al., 2000). Additionally, over 75% of human disease-associated genes have functional *Drosophila* orthologues, highlighting the usefulness of the invertebrate system in investigating the cellular and molecular processes underpinning human diseases (Reiter et al., 2001). Practical features that make the fly a favourable selection includes low-cost of breeding, housekeeping and genetic screening. The fly's rapid four-stage life cycle (egg/embryo> instar larva> pupa> adult) also enables fast data generation (Prokop, 2016). Despite, anatomical differences between the human and fly brain, advanced genetic tools, conservation of biological properties shared by both organ systems and ability to model complex behaviours, makes it feasible to study human neurological disorders in the fly (Gargano et al., 2005; Mundiyanapurath et al., 2007; Pfeiffer et al., 2008; Ejima and Griffith, 2011; Malik and Hodge, 2014; Ugur et al., 2016; Qiao et al., 2018; Contreras and Klämbt, 2023). Specifically, the GAL4-upstream activator sequence (UAS) binary expression system derived from yeast allows for the targeted expression of human genes for disease modelling in the fly (Pfeiffer et al., 2008; Pfeiffer et al., 2010). Targeted

transgene expression is established by crossing genetically engineered flies expressing the transcriptional activator GAL4 protein under an endogenous promoter with transgenic flies carrying the gene of interest (GOI) downstream of activator sequence (Figure 3). The resulting progeny from this cross expresses the GOI in regions of GAL4 expression due to the GAL4 protein binding and activating the UAS (Pfeiffer et al., 2008; Pfeiffer et al., 2010; Jenett et al., 2012). The fruit fly has also proven valuable in drug discovery processes for neurodevelopmental disorder like Fragile X syndrome (McBride et al., 2013). The ability to screen for new therapeutic drugs in the fly helps to identify high-quality candidates with desirable traits like oral or transdermal delivery, metabolic stability and low toxicity (Pandey and Nichols, 2011). However, a caveat that has to be considered is the potential difference in pharmacological effects between species, which can impact the translatability of findings to human application (Pandey and Nichols, 2011).

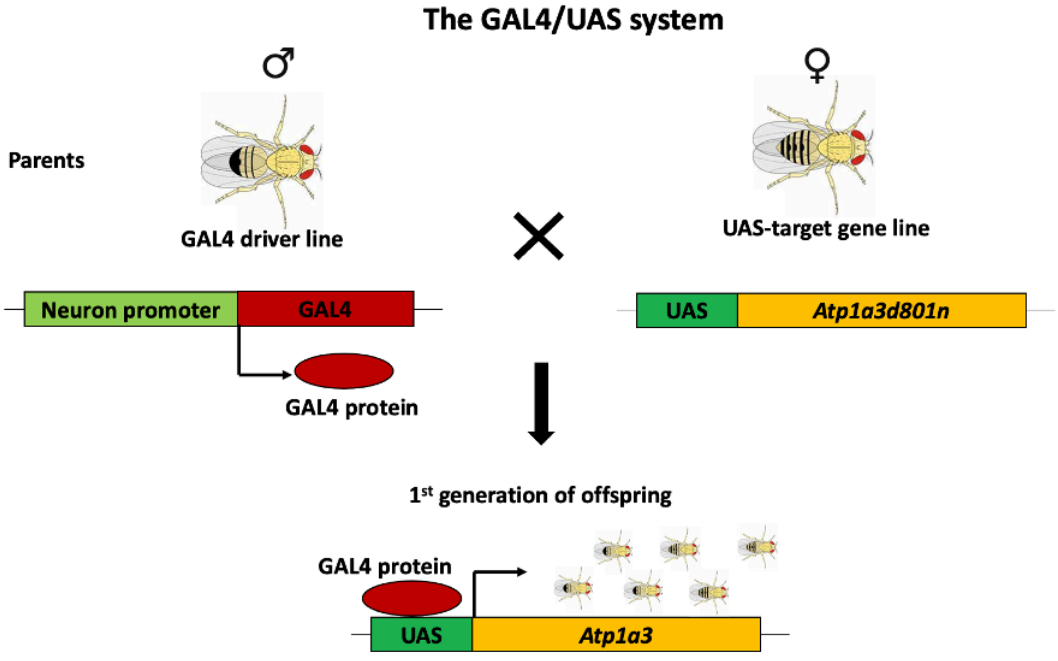

Figure 3. Schematic diagram of the Gal4/UAS system in *Drosophila*. The Gal4 system relies on two components: (1) the driver line, contains the Gal4 coding sequence- a transcriptional activator from yeast, which is inserted into the fly genome under the control of an endogenous promoter to facilitates Gal4 expression in a tissue- or cellular-

specific manner (2) the reporter line, contains a transgene under the control of the upstream activation sequence (UAS) which controls transcription of the gene. The two components are brought together in a simple genetic cross. The resulting progeny of the cross, carry both the Gal4 driver and reporter line thus the transgene is only transcribed in those cells or tissues expressing the Gal4 protein in F1 flies.

The characterization of genetically-altered *Atp1a3* mice models (Table 4) has significantly advanced the understanding of AHC, shedding light on potential pathophysiological mechanisms and establishing itself as a valuable tool for assessing future therapeutic options. However, the use of mice in research poses ethical and financial challenges for researchers. Ethical concerns include the potential pain, suffering, and distress experienced by mice during specific experimental procedures (i.e., forced swim test), given their protection under the Animals (Scientific Procedures) Act 1986. Budgetary constraints arise from the high costs associated with mouse housing (Doke and Dhawale, 2015). As a potential alternative, the phenotypic characterisation of novel mutations within the fruit fly (*Drosophila melanogaster*) NKA (d-NKA) α gene has revealed AHC-relevant phenotypes in adult flies (Palladino et al., 2003; Ashmore et al., 2009). This presents an opportunity to adhere to the replacement principle of the three Rs (replacement, refinement, and reduction) first described by the Universities Federation for Animal Welfare 65 years ago (Russell and Burch, 1959).

2.1.1 Na^+ /K^+ ATPase in *D. melanogaster*

Both structurally and functionally, the d-NKA closely resembles that of the h/m-NKA pump comprising of an α/β-subunit made up of ten TM helices and a single glycosylated TM helix respectively (Lingrel and Kuntzweiler, 1994; Okamura et al., 2003). In addition to previously discussed cellular processes of h/m-NKA (see Section 1.1.7.1), the d-NKA has a structural or scaffolding role in the formation of epithelial barrier junctions and tube-like structures in invertebrates (Krupinski and Beitel, 2009).

The d-NKA α-subunit is encoded by the *ATPalpha* (*ATPα*) gene composed of sixteen exons located on the right arm of chromosome 3 at position 93B (Lebovitz et al., 1989; Brown et al., 2015). This gene, orthologous to all four h/m-NKA α-isoforms (α1, α2, α3 and α4), shares 71.1% DNA and 76.3% protein identity with the human *ATP1A3* gene (Ng et al., 2021). Conserved regions in protein sequences includes the amino acid motifs for phosphorylation of an Asp366 residue, ATP-binding, and ion selectivity (Figure 3). The lack of one-to-one orthology between *ATPα* and human *ATP1A3* is suggested to result from divergence of h-NKA α-isoforms after the split between vertebrates and invertebrates (Okamura et al., 2003). In contrast to humans and mice, flies have eleven *ATPα* transcript variants resulting from alternative splicing, generating eleven protein isoforms: variant A/ isoform A (3558 bp/ 1041 aa; NM_169936.3), variant B/ isoform B (3861 bp/ 1002 aa; NP_732573.1), variant C/ isoform C (4524 bp/ 1002 aa; NP_732574.1), variant D/ isoform D (5099 bp/ 839 aa; NM_169939.2), variant E/ isoform E (5033 bp/ 1002 aa; NM_206528.3), variant F/ isoform F (4524 bp/ 1002 aa; NM_206527.3), variant G/ isoform G (4524 bp/ 1002 aa; NM_206526.3), variant H/ isoform H (4808 bp/ 1002 aa; NM_206525.3), variant J/ isoform J (5545 bp/ 1002 aa; NM_001275861.1), variant K/ isoform K (3721 bp/ 1002 aa; NM_001275862.2). *ATPα* transcripts exhibit widespread expression throughout all developmental stages, with high expression reported in the malpighian tubules, nervous system, flight muscle and tubular muscles (Lebovitz et al., 1989). *ATPα* produces six structurally distinct polypeptides by alternatively splicing four unique exons (6a, 6b, 6c and 6d) in a mutually exclusive manner (Palladino et al., 2003; Gramates et al., 2016). These exons are predicted to encode a partial segment of the TM6 helix and the entire cytosolic loop between the TM6-TM7 helices of the ATPα protein (Palladino et al., 2003). Given the crucial role of the TM6 helix in d-NKA function and differences from the vertebrate

consensus at both conserved and non-conserved residue sites (Figure 3), it is suggested that exon 6a, 6b, 6c and 6d could introduce both structural and functional changes to ATPα protein isoforms (Palladino et al., 2003). Akin to humans, flies also have short and long protein isoforms resulting from alternative splicing at the 5' end of the *ATPα* gene (Palladino et al., 2003).

Similar to mammals, fruit flies express three tissue-specific β-subunits, encoded by *nervana* genes (*nrv1, nrv2 and nrv3*). The *nrv1* gene is expressed in muscle, head, thorax and abdomen of adult flies (Sun et al., 1998; Baumann et al., 2010). The *nrv2* gene is expressed in sensory cells, epidermis and trachea (Paul et al., 2003; Paul et al., 2007; Roy et al., 2013). The *nrv3* gene is neurone-specific with expression in the adult brain and retina (Baumann et al., 2010).

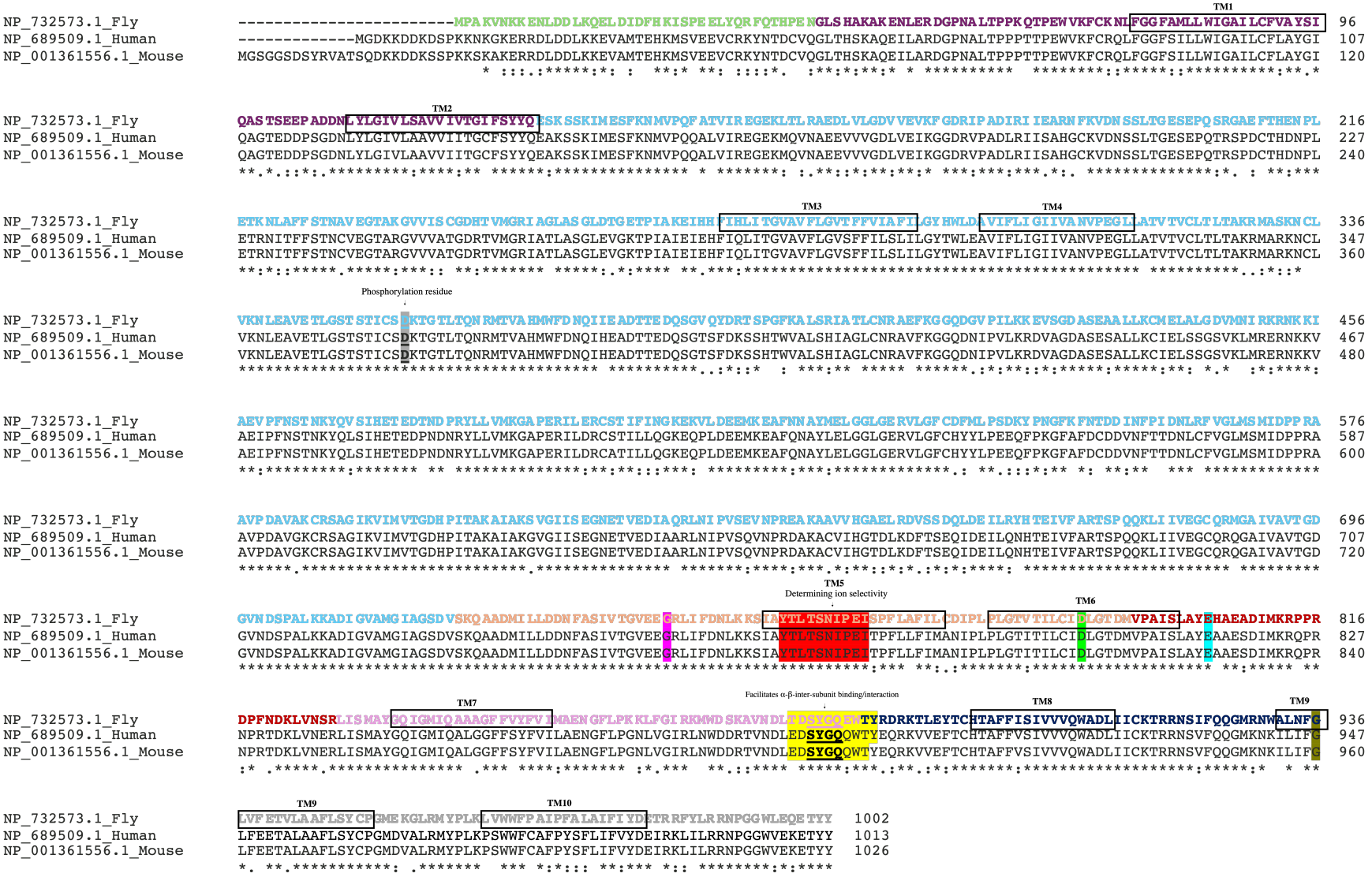

Figure 4. Annotated alignment of the fly NKA α-subunit against the human and mouse NKA α_3-subunit protein sequence. Bold coloured residues indicate the exon sequences of the fly protein (exon 2; shown in green, exon 3; shown in purple, exon 4; shown in light

blue, exon 5; shown in orange, exon 6B; shown in red, exon 7; shown in pink, exon 8; shown in navy blue, exon 9; shown in grey. Residues boxed in black outline indicates the predicted TM1-TM10 segments (Blanco and Mercer, 1998). Highlighted in grey is the evolutionary conserved Asp residue in fly (Asp394) and mouse (Asp379) that corresponds to the human Asp366 residue that is the site for phosphorylation during NKA reaction cycle (Kanai et al., 2013). Highlighted in yellow is the α-β binding site located in the extracellular H7/H8 loop of the alpha subunit. The evolutionarily conserved four residue sequence underlined in bold are important for the facilitation of the α-β complex (Colonna et al., 1997). Highlighted in bright green, bright blue and dark green are the most common AHC-causing mutation p.D801N, p.E818K and p.G479R respectively. In the fly these mutations correspond to D790N, E805K and G936R respectively. Highlighted in pink is AtpalphaCJ10 mutation (p.G744S) which is equivalent to the human NKA α3 mutation, p.G755S. Highlighted in red is the sequence that is reported to be especially important in ion selectivity (Palladino et al., 2003). Multiple protein alignment was created using Clustal Omega (Sievers and Higgins, 2018)

2.1.2 *D. melanogaster* models of NKA α dysfunction

Flies carrying mutations in *Atpα* (transcript b), affecting highly conserved residues, were generated through chemical mutagenesis and selected upon the presence of dominant temperature-sensitive (DTS) or failure to complement *Atpα* null alleles leading to homozygous lethality at embryonic or early larval stage (Palladino et al., 2003; Ashmore et al., 2009). Heterozygous missense *Atpα* mutants detailed in Table 5 used to model *in vivo* consequences of impaired d-NKA α pump activity have been reported to display AHC-relevant phenotypes (Palladino et al., 2003; Ashmore et al., 2009). Importantly, in later years it was revealed that the human AHC Gly755Ser mutation is the equivalent of the fly CJ10 (Gly744Ser) mutation (Heinzen et al., 2014) (Table 5). The Gly755Ser mutation is considered low-frequency as only seven patients have been reported with genotype (Rosewich et al., 2014; Sasaki et al., 2014; Yang et al., 2014; Panagiotakaki et al., 2015; Ito et al., 2018).

Table 5. Chemical mutagenesis generated *D. melanogaster ATPα* mutant alleles

ATPα allele	FlyBase ID number	Change at cDNA level	Change at Protein level	Human ATP1A3 equivalent
$Atp\alpha^{DTS1}$	FBaI0188150	c.2944G>A	Glu982Lys	Asp993Lys
$Atp\alpha^{DTS2}$	FBaI0188149	c.2941G>A	Asp981Asn	Asp992Asn
$Atp\alpha^{DTS1R1}$	FBaI015277	c.2713_2716del	Ile905Trpfs*8	N/A
$Atp\alpha^{CJ4}$	FBaI0282769	c.786C>T	Pro262Leu	Pro273Leu
$Atp\alpha^{CJ5}$	BaI0282770	c.720C>T	Ser201Leu	Ser212Leu
$Atp\alpha^{CJ6}$	BaI0282771	c.1044T>A	Ser348Thr	Ser359Thr
$Atp\alpha^{CJ10}$	FBaI0282773	c.2230G>A	Gly744Ser	$Gly755Ser^{AHC}$
$Atp\alpha^{CJ12}$	BaI0282774	c.1584G>A	Gly528Ser	Gly539Ser
$Atp\alpha^{CJ13}$	BaI0282775	c.1881G>A	Ala588Thr	Ala599Thr

*Information obtained from Öztürk-Çolak et al. (2024); Heinzen et al. (2014)

*Human equivalent mutation causing disease is denoted with AHC.

2.1.3 Phenotypic profile of *ATPα* mutants

2.1.3.1 NKA activity

Western blot analysis revealed the AHC-causing p.Glu277Lys mutation significantly reduced ATP1A3 protein expression (Heinzen et al., 2012; Boelman et al., 2014). In adult heads of *CJ6*/+ (p.Ser348Thr), *CJ13*/+ (p.Ala588Thr) and *DTS1R1*/+ (p. Ile905Trpfs*8) mutants, levels of the Atpα protein were reduced by 30-50% (Ashmore et al., 2009). Additionally, the *DTS1R1*/+ (p. Ile905Trpfs*8) mutant, considered a heterozygous null, displayed lower levels of detectable *ATPα* mRNA transcripts (Palladino et al., 2003). Defect in respiration rates indicated by a 16-27% decrease in carbon dioxide production was observed in heterozygous *DTS1* (p.Glu982Ly), *DTS1R1 (*p.Ile905Trpfs*8*)* and all *CJ* (p.Pro262Leu, p.Ser201Leu, p.Ser348Thr, p. Gly744Ser, p.Gly528Ser and p.Ala588Thr) mutants suggesting impairment of ATPase activity, the main enzyme responsible for energy production (Ashmore et al., 2009). Issues with respiration resulting from respiratory muscle weakness have been report in a patient with Gly755Ser mutation, necessitating mechanical respiratory care and tracheostomy (Rosewich et al., 2014). Further investigation into the *in vivo* consequences of embryos homozygous for *ATPα* mutations revealed that *DTS1R1*/+ (p. Ile905Trpfs*8) and all *CJ*/+ mutants had normal septate junction function and tracheal size, suggesting mutations specifically affect ion-transport rather than structural functions of d-NKA (Ashmore et al., 2009). The C-terminus of the ATPα protein (TM8-10) is understood to interact with the TM1-TM2 region of the protein and the β-subunit (reviewed in Palladino et al., 2003). With knowledge of the *DTS*/+ (p.Glu982Lys and p.Asp981Asn) mutations affecting highly conserved residues located in the C-terminus, it was suggested that mutations may interfere with one or both interactions leading to protein dysregulation and TS paralysis as a phenotypic consequence (Palladino et al., 2003).

Mutagenesis study of Asp995Ala change in sheep NKA α1 revealing the mutation impaired protein maturation rather than cation-enzyme interaction provides valuable insight into the potential molecular consequences of the *DTS2*/+(p.Asp981Asn) mutation as sheep Asp995 is equivalent to fly Asp981 (Palladino et al., 2003). Comparing these mutations across species is useful for determining whether changes at this conserved site disrupts ATPα function through a shared mechanism, which could provide key insights into h-NKA α dysfunction in AHC. Notably, mutations at human p.Asp992 (p.Asp992del, p.Asp992dup and p.Asp992Tyr), a residue equivalent to the fly Asp981 has been implicated in AHC pathogenesis (Heinzen et al., 2014; Ng et al., 2021). Additionally, since *DTS2*/+(p.Asp981Asn) flies exhibit dominant phenotypes that are more severe than ATPα null mutations (Table 6), this could result from the mutation interfering with protein folding, trafficking or the assembly of the d-NKA α/*β*complex.

2.1.3.2 Stress-induced paralysis

Hemiplegia and quadriplegia, distinct symptoms of AHC, were mimicked in mouse models under stressful conditions (Table 4). Similarly, fly models described in Table 6 exhibit stress-induced paralysis characterised by time taken to regain mobility following 15 seconds (s) of vortexing (Palladino et al., 2003; Ashmore et al., 2009). *DTS1*/+ (p.Glu982Lys) and *DTS2*/+ (p.Asp981Asn) adults housed at 28°C rather than ambient temperature (20-22°C) displayed complete paralysis lasting 5-30 s (Palladino et al., 2003). Similarly, *DTS1R1*/+ (p.Ile905Trpfs*8) and all *CJ*/+ (p.Pro262Leu, p.Ser201Leu, p.Ser348Thr, p.Gly744Ser, p.Gly528Ser and p.Ala588Thr) adults displayed paralysis lasting 2-24 s at 25°C, with 100% penetrance seen in older adults aged 15-30 days old (Ashmore et al., 2009). Heat-stress paralysis was also reported in *DTS1*/+ (p.Glu982Lys), *DTS2*/+ (p.Asp981Asn) and *CJ10*/+ (p.Gly744Ser) mutants characterised by time taken to regain mobility following exposure to 37-38°C (Palladino

et al., 2003; Ashmore et al., 2009). All *DTS1*/+ (p.Glu982Lys) and *DTS2*/+ (p.Asp981Asn) adults tested showed paralysis within 10-30 s of exposure and recovered in 1-2 minutes at 30°C (Palladino et al., 2003). Heat-induced paralysis manifested in a progressive manner in *CJ10*/+ (p.Gly744Ser) mutants, as the phenotype was only observed in adults aged over 20 days (Ashmore et al., 2009). Paralysis was observed within 334 ± 17.3 s and recovery took an average of 209 ± 35 s at ~22°C (Ashmore et al., 2009). Notably, both studies reported absence of stress-induced paralysis in age-matched WT flies (Palladino et al., 2003; Ashmore et al., 2009). Akin to *CJ10*/+ (p.Gly744Ser) flies, paralysis manifesting as hemiplegia in a Gly755Ser patient, was present at young (3 months) with consistent occurrence in older age (> 4 years) (Ito et al., 2018).

2.1.3.3 Motor dysfunction

General and startle-induced locomotor activity in aged *CJ*/+ female adults (i.e., 10-12 days old) were assessed using the *Drosophila* Activity Monitoring (DAM) system at 25°C (Ashmore et al., 2009). Hyperactivity, a phenotype observed in all mouse models of AHC except Matoub mice (p.Gly815Lys), was reported in *CJ12*/+ (p.Gly528Ser) mutants (p.Gly528Ser), characterised by significant increase in activity (i.e., the total number of beam breaks) per waking minute compared to WT controls (Ashmore et al., 2009). Conversely, increased locomotor activity exhibited by *DTS1R1*/+ (p. Ile905Trpfs*8) and all *CJ*/+ (p.Pro262Leu, p.Ser201Leu, p.Ser348Thr, p.Gly744Ser, p.Gly528Ser and p.Ala588Thr) mutants in response to startle (i.e., jarring the monitors every three minutes) was significantly less than WT controls (Ashmore et al., 2009). Moreover, total daily activity levels and total time active in *DTS1R1*/+ (p. Ile905Trpfs*8) and all *CJ*/+ (p.Pro262Leu, p.Ser201Leu, p.Ser348Thr, p. Gly744Ser, p.Gly528Ser and p.Ala588Thr) mutants were significantly reduced relative to WT

controls, indicating that *Atpα* mutations compromise peak locomotor performance (Ashmore et al., 2009).

2.1.3 4 Seizure behaviour

Akin to *Myshkin* (Ile810Asn) mice, *DTS1*/+ (p.Glu982Lys), *DTS2*/+ (p.Asp981Asn) mutants display neuronal hyperexcitability at the electrophysiological level (Palladino et al., 2003). The constant bursting activity in the dorsal flight muscles of these *Atpα* mutants at a higher temperature (37°C) phenocopied s*eizure*^{ts2} mutant (Palladino et al., 2003). The seizure fly model (FlyBase ID: FBal0015410), carries a Glu490Lys mutation within the *eag* family of K^+ channels known to cause neuronal hyperexcitability associated with seizure-like activity (Titus et al., 1997). Therefore, provides supporting evidence of the notion that *DTS1*/+ (p.Glu982Lys), and *DTS2*/+ (p.Asp981Asn) mutations cause neuronal hyperexcitability and seizure-like activity (Palladino et al., 2003).

2.1.3.5 Neurodegeneration

Magnetic Resonance Imaging (MRI) and Computed Tomography (CT) scans have revealed progressive brain atrophy in adults with AHC (Sasaki et al., 2017). Similarly, histological analysis revealed progressive loss of neural tissues marked by accumulation of vacuoles in the central brains and optic lobes of middle-aged *DTS*/+ (p.Glu982Lys and p.Asp981Asn) and all *CJ*/+ (p.Pro262Leu, p.Ser201Leu, p.Ser348Thr, p.Gly744Ser, p.Gly528Ser and p.Ala588Thr) mutants (Palladino et al., 2003; Ashmore et al., 2009). Neurodegeneration varied across *Atpα* mutants with *DTS*/+ (p.Glu982Lys and p.Asp981Asn) mutations showing a high prevalence of brain lesions, which were rarely observed in *CJ4*/+ (p.Pro262Leu) and *CJ12*/+ (p.Gly528Ser) mutants (Palladino et al., 2003; Ashmore et al., 2009). The loss of neuronal populations in aged *DTS*/+ (p.Glu982Lys and p.Asp981Asn) mutant brains was thought to be a consequence of

chronic neuronal hyperexcitability (Palladino et al., 2003). However, the extensive vacuolar pathology seen in these *Atpα* mutants was absent in aged-matched s*eizure*^{ts2} mutants, suggesting that hyperexcitability alone is insufficient to cause neurodegeneration in *D. melanogaster* (Palladino et al., 2003). Moreover, histology analysis on the dorsal flight muscles of *CJ* mutants revealed progressive degeneration of myofibrils in aged *CJ12*/+ (p.Gly528Ser) mutants, indicated by vacuolar pathology (Ashmore et al., 2009). Myopathology was observed in *CJ12*/+ (p.Gly528Ser) mutants only suggesting that defective locomotor behaviour exhibited by the other five *CJ*/+ (p.Pro262Leu, p.Ser201Leu, p.Ser348Thr, p.Gly744Ser and p.Ala588Thr) mutants is unlikely to result from muscle-related abnormalities.

2.1.3 6 Longevity

The *DTS1*/+ (p.Glu982Lys), *DTS2*/+ (p.Asp981Asn) and *CJ10*/+ (p.Gly744Ser) mutant lines were reported to live significantly shorter than WT controls by a percentage decrease of ~59%, ~37% and ~13% respectively (Ashmore et al., 2009), a phenotype also reported in *Myshkin* (Ile810Asn) and Matoub (Glu815Lys) mice (Kirshenbaum et al., 2013; Helseth et al., 2018). Reduced longevity in fly models of d-NKA dysfunction could be explained by the severity of the stress-sensitive paralysis and the evident neurodegenerative pathology observed (Ashmore et al., 2009). Moreover, the significantly increased longevity of *CJ6*/+ (p.Ser348Thr), *CJ12*/+ (p.Gly528Ser) and *DTS1R1*/+ (p. Ile905Trpfs*8) mutant lines relative to the WT controls indicated by a percentage increase of ~22%, ~14% and ~9% respectively, suggests that a certain level of ATPα non-functionality could favour animal longevity (Ashmore et al., 2009). This hypothesis was validated by recapitulation of this phenotype (i.e., increase of lifespan by ~20-25%) in a WT strain given low concentrations of ouabain (0.005mM and 0.5mM), a h/m/d-NKA inhibitor (Ashmore et al., 2009). Ashmore et al. (2009) proposed caloric restriction as a possible explanation for the *CJ6*/+ (p.Ser348Thr), *CJ12*/+

(p.Gly528Ser) and *DTS1R1*/+. (p. Ile905Trpfs*8) increased longevity phenotype, citing decreased feeding as an explanatory variable for the increased longevity of *Caenorhabditis elegans* (*C. elegans*) carrying mutations in the *eat-6* gene, orthologous to *ATP1A3* (Ashmore et al., 2009). However, reduced body mass and feeding reported in *eat-6* mutants and *Myshkin* mice (Ile810Asn) was not phenocopied in *CJ*/+ mutant adults (Ashmore et al., 2009). The lack of a correlation between feeding or mass and longevity in *CJ*/+ mutants undermines caloric restriction as a mechanism for longevity in *D. melanogaster ATP*α mutants (Ashmore et al., 2009).

Table 6. Summary of the phenotypes observed in alleles of *ATPα*

Genotype	TS paralysis	BS paralysis	Respiration	Protein level	Neurodegeneration	Myodegeneration	Longevity
Wild type	No	No	→	→	Mild	No	→
DTS1/+ (Glu982Lys)	Yes	Yes	↓↓	→	Severe	N/A	↓↓
DTS2/+ (Asp981Asn)	Yes	Yes	N/A	→	Severe	N/A	↓
DTS1R1/+ (Ile905Trpfs*8)	No	Yes	↓	↓↓↓	Mild	No	↑
CJ4/+ (Pro262Leu)	No	Yes	↓↓↓	→	Mild	No	→
CJ5/+ (Ser201Leu)	No	Yes	↓↓↓	→	Mild	No	→
CJ6/+ (Ser348Thr)	No	Yes	↓↓	↓	Mild	No	↑↑↑
CJ10/+ (Gly744Ser)	Yes	Yes	↓↓↓	→	Moderate	No	↓↓
CJ12/+ (Gly528Ser)	No	Yes	↓	→	Mild	Yes	↑↑
CJ13/+ (Ala588Thr)	No	Yes	↓↓	↓	Moderate	No	→

Table adapted from Ashmore et al., 2009

→ symbol is indication of no change

One arrows in either direction means $p < 0.05$; two arrows mean $p < 0.01$; three arrows means $p < 0.001$

2.2 Project Aims and Objective

The manifestation of AHC-relevant phenotypes such as stress-induced paralysis and reduced lifespan in the *D. melanogaster ATPα CJ10* line, carrying the heterozygous Gly744Ser mutation in its NKA α-subunit (equivalent to the human Gly755Ser mutation in NKA α3-subunit), forms the rationale for the use of *D. melanogaster* as an alternative *in vivo* system to study AHC. Given the evolutionary conservation of NKA function, characterising the *ATPα CJ10* fly line alongside novel *ATP1A3* transgenic fly models could establish *D. melanogaster* as viable animal system for studying NKA α3 dysfunction in AHC. The primary aim of this project is to determine whether NKA α-modified and humanised flies can recapitulate key phenotypes reported in NKA α3 mutant mice and AHC patients, thus providing a high-throughput, cost-effective and genetically tractable *in vivo* system to study AHC disease mechanisms and therapeutic strategies. The objectives of this project were:

1. Quantify the extent that heterozygous *ATPα CJ10* (p. Gly744Ser*)* and *null R1* (p. Ile905Trpfs*8) mutant flies phenocopy essential, major and minor AHC phenotypes. This will help determine whether the p.Gly477Ser mutation specifically drives these phenotypes or whether they result from broader *ATPα* dysfunction.
2. Generate novel AHC fly models expressing the human *ATP1A3* mutation (*ATP1A3*^{D801N}) or wildtype ATP1A3 (*ATP1A3*^{WT}) in a hemizygous manner via Gal4/UAS approach. The introduction of the *ATP1A3*^{D801N} (the most common AHC-causing mutation) into *D. melanogaster* will allow us to directly model AHC-related NKA α3 dysfunction. Moreover, the *ATP1A3*^{WT} fly model will act as a control line to help distinguish between mutation-specific effects verses general *ATP1A3* expression effects in flies.

3. Quantify the extent that hemizygous *ATP1A3*$^{D801N/+}$ transgenic flies are able to phenocopy heterozygous *ATPα CJ10* flies, NKA α3 mutant mice and AHC patients. If *ATP1A3*$^{D801N/+}$ flies exhibit AHC-relevant phenotypes this will further support *D. melanogaster* as a valid model for studying AHC disease mechanisms and therapeutic strategies. Moreover, this experiment will also help to identify conserved verses species-specific phenotypes of NKA α3 dysfunction.
4. Determine whether hemizygous *ATP1A3*$^{WT/+}$ transgenic flies are able to rescue AHC-relevant behaviour exhibited by heterozygous *ATPα CJ10 (p. Gly444Ser)* and *null R1 (*p. Ile905Trpfs*8*) mutant flies. If human *ATP1A3*^{WT} expression rescues behavioural deficits in *ATPα* mutants flies, it would confirm that the AHC-relevant behaviour is a direct consequence of d-NKA *α* dysfunction rather than secondary effects. If complete rescue is observed, it would showcase that the core NKA *α* functions are highly conserved across species reinforcing the use of *D. melanogaster* as model organism for AHC. Additionally, comparing the ability of human *ATP1A3*^{WT} to restore NKA *α* function in *ATPα CJ10 (p. Gly444Ser)* and *null R1 (*p. Ile905Trpfs*8)* mutant flies can help to determine whether AHC-relevant behaviours arose from dominant-negative effect or haploinsufficiency.

III. Materials and Methods

3.1 Molecular Cloning Methods

Molecular cloning refers to the creation of recombinant DNA through the joining of an isolated DNA sequence from any species to a vector and subsequently inserting the recombinant DNA into a host cell for replication and protein expression purposes. Since the introduction of molecular cloning over 50 years ago (Jackson and Symons, 1972), different approaches have been established to achieve recombinant DNA. However, the basic workflow for approaches remain the same: (1) isolation of target DNA sequence, (2) joining of DNA sequence to a suitable cloning vector, (3) transformation of recombinant DNA into a suitable host for replication and (4) screening/selection of host containing desired recombinant DNA.

3.1.1 Cloning Materials

Drosophila SST13-UAS (*SST13*) and *pUAST* vector containing the bacterial attachment site *attB* was kindly provided by Professor Young-Joon Kim Kim (Korea Drosophila Resource Centre, ADDR 61005, 123 Cheomdangwagi-ro, Buk-gu, Gwangju, Republic of Korea) and Dr Simon Collier (Cambridge Fly Facility, University of Cambridge, UK) respectively. The key difference between these two UAS vectors is that the SST13 vector contains a partial non-functional white gene whereas the pUAST vector carries a fully functional white gene. The SST13 vector uses the split white-system which requires a complementary partial white gene at the attP site to restore full white gene function. This system helps to minimise off-target insertions and reduce screening time, thereby improving efficiency and precision of transgene integration (Bischof et al., 2007). The human *ATP1A3* variant 1 ORF sequence (NM_152296.5) modified with the *Drosophila* Kozak consensus sequence (CAAA) (Cavener, 1987) flanking the 5' end of the ORF was synthesised and cloned into the pcDNA3.1(+) mammalian expression vector via HindIII/BamHI by GenScript (Europe, Netherlands). The Drosophila Kozak sequence

was added to optimize expression of the *ATP1A3* transgene in *Drosophila* (Cavener, 1987)

3.1.2 NEBuilder® HiFi DNA Assembly Cloning Method

The one step overlap-based cloning method known as HiFi DNA Assembly was selected to avoid the use of restriction enzymes and for time efficiency purposes. The approach exploits the properties of three common biological enzymes: Taq polymerase, ligase and 5'-3' exonuclease to facilitate the seamless assembly of numerous single or double-stranded DNA fragments in spite of their length or end compatibility by designing PCR-amplified DNA inserts with 15-30-bp overlapping ends (Hochrein et al., 2017; Chart, 2019).

3.1.2.1 Primer Design

For assembly of the *ATP1A3* cDNA full-length fragment and *UAS* vectors, primers were designed in Benchling. Inc to include 18-bp from the 5' (forward) and 3' (reverse) end of the target cDNA (Table 7, highlighted in pink), flanked with a 20-to-26-bp long 5' and 3' regions homologous to the vectors (Table 7, highlighted in red) which included BgIII and XhoI restriction sites (Table 7, highlighted in yellow) to allow for colony screening by REs digest (Table 10). Primer parameter included melting Tm of 55-60°C with a maximum difference of 5°C, and GC content of 35-65%. Annealing Tm of the primer sequence which is expected to bind to *ATP1A3* target sequence (Table 7, highlighted in purple) was calculated using NEB Tm calculator.

Table 7. Oligonucleotides primers for NEBuilder HiFi DNA Assembly

Forward primer	gaattgggaattcgttaa ca^ gatct caaaatgggggacaagaa
Reverse primer	cgtgcagcggtacc c^tcgag tcagtagtaggtttccttc

3.1.2.2 Insert Preparation

The full-length *ATP1A3* cDNA fragment was amplified in duplicates or triplets using primer set above (Table 7) and ThermoFisher high fidelity Taq polymerase (Cat no: F3OS) (Table 8) to minimize mutations. The PCR products generated from PCR programme (Table 9) were run on 1.2% agarose gel at 120 V for ~ 2.5 h before fragments were excised and purified by QIAquick Gel Extraction Kit (Cat no: 28706) following manufacturing instructions and recommendations. The concentration of DNA samples eluted in 30 µL of RNAse/DNase water was determined using Thermo Scientific NanoDrop™ spectrophotometer (Serial no. ND-2000). The samples were pulled together to concentrate DNA using the NEB Monarch® PCR & DNA Cleanup Kit (Cat no: T1130) so desired volume (5 µL) for assembly reaction could be met.

Table 8. Master Mix for PCR reaction following ThermoFisher protocol

Reagents	1X
5 x Phusion buffer	4 µL
10 mM dNTPs	0.4 µL
F+R primers (0.5 µM)	2 µL
DMSO	0.6 µL
Phusion High Fidelity Taq DNA polymerase	0.2 µL
RNAse/DNase free water	Make up to 20 µL
ATP1A3 insert (22ng)	1 µL

Table 9. PCR cycle ThermoFisher 3-step protocol

Cycle Steps	Temp	Duration	Cycles
1 (Initial denaturation)	98°C	30 s	1
Denaturation	98°C	10 s	30
Annealing	56°C	30 s	
Extension	72°C	90 s	
Final Extension	72°C	10 min	1
Hold	10°C	∝	

3.1.2.3 Vector Preparation

The *pUAST* and *SST13_UAS* vector backbones were linearised for the assembly reaction by digestion with BgIII and XhoI enzymes overnight (~18 h) at 37 ℃ (Table 10). Following this, the vectors were quickly purified using the NEB Monarch® PCR & DNA Cleanup Kit (Cat no: T1130). The digested samples were not run on gel to confirm linearization as it was unlikely to see the 16-bp product. Moreover, if the 16-bp product was present, in principle the NEBuilder® HiFi should be able to remove bases due to its ability to remove 3' end mismatches as 5'-3' exonuclease is present in HiFi Assembly Master Mix (Chart, 2019).

Table 10. Master Mix for *BgIII*/*XhoI* double digest of *pUAST* and *SST13_UAS* vector.

Reagents	1X
UAS vector	1µg
10 x NEBuffer (NEBuffer 3.1)	5 µL
R0144S BgIII (10,000 units/mL)	1 µL (10 units)
R0146S XhoI (20,000 units/mL)	0.5 µL (10 units)
RNAse/DNase free water	Make up to 50µL
Total Volume	50µL

3.1.2.4 HiFi DNA Assembly Reaction

The NEBuilder® HiFi DNA Assembly Kit (Cat no: E2621S) and online protocol was used to assembly the *ATP1A3* cDNA full-length fragment and *UAS* vectors (Table 11). Adaption to protocol included using an insert: vector ratio of 10:1 calculated with the NEB ligation calculator, making total volume smaller and extending incubation to 25 minutes (i.e., an extra 10 minutes) to help improve success of assembly. A ligation control sample (backbone + no insert) was also assembled.

Table 11. NEBuilder® HiFi DNA Assembly reaction setup

Reagents	*SST13*	*pUAST*
UAS vector	1 µg (50 ng)	1 µg (50 ng)
ATP1A3 Insert (PCR amplified with overhang)	5 µL (330 ng)	4.04 µL (286.8 ng)
NEBuilder Hifi DNA Assembly Master Mix	6 µL	7 µL
Total Volume	12µL	12µL

3.1.2.5 Bacterial Transformation, Culturing and Plasmid Isolation

The recombinant DNA was transformed into NEB® 5-alpha Competent *E. coli* cells (Cat no: C2998J) following protocol provided online. Alterations to protocol included: (1) pre-chilling tubes for transformation; (2) use of pUC18 plasmid DNA as transformation control due to pUC19 was not provided with kit; (3) added 5 μL of recombinant plasmid to cells; (4) skipped addition of SOC media due to use of Ampicillin (100 mg/mL) and (5) ~55μL of transformed cells were spread on LB/ Ampicillin (Amp) plate. Several colonies were picked (n = 2-5) that were not surrounded by satellite colonies. For bacterial culturing and plasmid purification, the QIAprep Spin Miniprep Kit (Cat no: 27104) and handbook was used. Bacterial colonies were cultured in 50 mL with a higher volume of LB/Amp media (10 mL) because of the assumption that the vectors had a low copy number. Tubes were incubated at 37 ℃ with 225 rpm shaking for 14 h before plasmid extraction and purification.

3.1.2.6 Positive Screening/Selection

The recombinant DNA extracted from selected clones were digested with BgIII and XhoI (Table 12) at 37 ℃ for 1 h before products were ran on a 0.8% agarose gel stained with EtBr for analysis.

Table 12. Master Mix for BgIII/XhoI double digest of *UAS-ATP1A3* plasmids isolated from bacterial colonies.

Reagents	Volume

Plasmid DNA	1 µL (0.5µg)
10 x NEBuffer (NEBuffer 3.1)	2.5µL
R0144S BgIII (10,000 units/mL)	0.5µL (5 units)
R0146S XhoI (20,000 units/mL)	0.5µL (10 units)
RNAse/DNase free water	Make volume up to 15µL
Total Volume	15µL

3.1.2.7 Site-directed mutagenesis

The Quick-Change II Site-directed Mutagenesis Kit (Cat no: 200523) and protocol was used to modify the ATP1A3 protein at a single amino acid by point mutation (D801N; c.2401G>A) within the double-stranded *ATP1A3_UAS* vector plasmids. Mutagenic primers were designed in the online QuickChange Primer Design Tool. According to the kit's handbook, primer pairs were designed to contain the single nucleotide change near the center (Table 13, highlighted in yellow) and anneal to the *ATP1A3* sequence on opposite strands of plasmid. Other set parameters for design included a primer size of 25-45 bases, melting Tm of ≥78 ℃, GC content of >40% and self-dimer ΔG value of >-9 kcal/mole. Modification to cycling parameters for site-directed mutagenesis included adjusting cycle times for a single amino acid change and extension time (Table 14). Following temperature cycling, *Dpn* I digestion and transformation of plasmid into Agilent XL1-Blue Supercompetent cells (Cat no: 200236) was carried out following manufactures instructions. Alterations to transformation protocol included: (1) added 50ng of the modified plasmid DNA, (2) added 0.45 mL of preheated SOC and incubated transformed cells at 37℃ with 225 rpm shaking for 30 minutes and (3) ~250 μL of transformed cells were spread on LB/ Ampicillin (Amp) plate. Several colonies were picked (n = 2-5) that were not surrounded by satellite colonies. Bacterial colonies were cultured in 50 mL with a higher volume of LB/Amp media (10 mL) because of the assumption that the plasmid had a low copy number. Tubes were incubated at 37℃ with

210 rpm shaking for 17 h before plasmid extraction and purification. Bacterial culturing and plasmid purification were achieved using the QIAprep Spin Miniprep Kit (Cat no: 27104) and handbook. The purified plasmid samples (n = 3) were sent off for sequencing to confirm D801N mutation using primers in Table 15. Following this, wildtype and mutant plasmids (~500 ng/ μL) were sent off to microinjection services to generate transgenic flies by phiC31 integrase-mediated transgenesis.

Table 13. Mutagenic primers for Quick-Change II Site-directed Mutagenesis

Forward primer	complement	5'-caccatcctctgcatcaatctgggcactgacat-3'	G>A change
Reverse primer	complement	5'-atgtcagtgcccagattgatgcagaggatggtg-3'	C>T change

Table 14. Cycling Parameters for the Quick-change Site-Directed Mutagenesis Method

Segment	Cycle	Temp	Time
1	1	95°C	30 s
2	15	95°C	30 s
		55°C	60 s
		68°C	7 m 42 s (60 s/kb of plasmid length)
		12°C	Cooling

Table 15. Primers for amplification of region containing D801N point mutation

Forward primer	5'- acctaaagaagtccattgcct-3'
Reverse primer	5'- cgtaaggaaggttatttacaagg -3'

3.2 Fly Materials

3.2.1 Standard Sugar/Yeast agar media

Rearing, maintenance and/or experimentation of fly stocks were achieved using standard sugar/yeast agar (SYA) food (Bass et al., 2007). Trays of 7mL SYA food contained in

75mm x 23.5mm, 23mL polystyrene flat based tubes (Sarstedt Ltd.) were made by the Faculty of Biological Sciences (FBS) technical staff, University of Leeds. Batch recipe for production of SYA food is described in Table 16.

Table 16. Batch recipe for production of a tray of 7 mL standard SYA food.

Material	Volume	Source
Distilled H_2O (dH_2O)	970 mL	Avidity Science
Pure Agar	15 g	Acros Organics, Thermo Scientific
Granulated sugar	50 g	Store bought
Brewer's Yeast	100 g	Buy Wholefoods Online
Nipagin solution (10% w/v)	30 mL per L	VWR Chemicals
Propionic acid, 99% pure	3 mL per L	Acros Organics, Thermo Scientific

Table 17. Batch recipe for production of fly food preservative

Material	Volume	Source
100% Ethanol	950 mL	Fisher Scientific
dH_2O	50 mL	Avidity Science
Nipagin (Methyl 4-hydroxybenzoate)	50 g	VWR Chemicals

3.2.2 Sugar/Agar media

For specified behavioural experiments, flies were kept and fed a 1% or 2% agar-based diet that contained 5% sucrose. This diet was selected to avoid the use of dietary yeast, reported to affect *Drosophila* behaviour such as sleep-wake (Catterson et al., 2010). Moreover, diet was selected for better visualization of video-recorded flies as the transcendent media provided a great contrast. The ingredients in order listed in Table 18 were added to a clean 1 L glass bottle before mixture was shaken and microwaved on

medium heat till bubbling. Any unused media was stored in cold room (4℃) up to a week before discarded.

Table 18. Batch recipe for 1% or 2% agar-based diet containing 5% sucrose

Material	Volume	Source
Pure Agar	1% 2%	
	2.5 g 5 g	Acros Organics, Thermo Scientific
Granulated sugar	12.5 g	Store bought
dH_2O	250 mL	Avidity Science
*Nipagin solution (10% w/v solution)	15 mL per 0.5 L	VWR Chemicals

* The addition of anti-fungal reagent was dependent on the length of the experiment.

3.2.3 Fly stocks

D. melanogaster wild-type Canton Special (CS) strain supplied by Dr Tom Price at the University of Liverpool served as the control for many experiments. *D. melanogaster ATPα* strains (*CJ10/TM6* and *DTS1R1/TM3*) were provided by Prof. M. Palladino at the University of Pittsburgh. Standardized *CJ10* (CS-*CJ10*) and *DTS1R1* (CS-*R1*) fly lines (Section 3.3.2) were established in the Bretman Lab. In addition, a standardized third chromosome balancer, *TM3* carrying the dominant *Stubble* (*Sb*) bristle marker (Section 3.3.2) was established in the Bretman Lab. Transgenic fly lines generated by the Cambridge Fly Facility microinjection services: *pUAST-ATP1A3*^{WT}*/Sm6a,CyO* and *pUAST-ATP1A3*^{D801N}*/Sm6a,CyO* possesses the transgene on the 2L:5,108,448 known as the attP40 landing site (van der Graaf et al., 2022), The Cambridge service also generated transgenic lines for phenotypic rescue of *CJ10*/+ mutants (*pUAST-ATP1A3*^{WT}*/CyO;CJ10/TM6B*) and *R1*/+ mutants (*pUAST-ATP1A3*^{WT}*/CyO;R1/TM6B*). Transgenic fly lines generated by the Korea Drosophila Resource Centre's (KDRC) microinjection services: *SST13-UAS-ATP1A3*^{WT}*/TM3*,Sb$^{[1]}$ and *SST13-UAS-*

ATP1A3^{D801N}/*TM3*,Sb$^{[1]}$ carry the transgene on the 3R:19,074,732 known as theVIE-49 landing site (Zhang et al., 2022). Both facilities used phiC31 integrase-mediated method to integrate the UAS-*ATP1A3* transgene into the fly genome (Bischof et al., 2007). The pan-neuronal *Gal4* driver *elav-Gal4/CyO* (Cat no: 8765) and ubiquitous *Gal4* driver *Actin5C-Gal4/CyO* (Cat no: 4414) were purchased from Bloomington *Drosophila* Stock Centre (BDSC).

3.3 Fly Pushing Methods

3.3.1 Fly husbandry and breeding

Fly stocks have since been maintained in Dr Amanda Bretman's Lab in 7mL SYA food vials (Section 3.2.1). All stocks were maintained with overlapping generations in a controlled temperature (CT) room at 25℃, 45-50% relative humidity (RH) on a 12:12 h light: dark (LD) cycle (lights turn on at 9:18 am). For experiments, newly emerged adults were cultivated by crossing virgin male and female adults (n = 5) on SYA food for three days before removal of parents to allow time for female egg-laying and avoid larvae overcrowding. After 10-13 days, virgin adults were collected under ice or brief CO_2 anaesthesia. Virgin collection involved sorting flies by sex (sexing) every 4-6 h during the day, selecting for adults with a visible dark spot (meconium) in abdomen as this signified the remnants of their final meal before pupation (Prokop, 2015). Flies were then transferred to vials of SYA food with a maximum of fifteen flies per vial. All flies for experimentation were culture and housed in the CT room until day of testing.

3.3.2 Standardization of *ATPα* strains

Parental lines for controlling genetic background effects in *ATPα* strains were not available. This was of particular concern for *ATPα CJ10* experiments as *ebony* expression in flies is known to influence behaviours such as rhythmic locomotion (Newby and Jackson, 1991; Suh and Jackson, 2007), vision (Borycz et al., 2002) and

courtship (Kyriacou et al.,1987; Kyriacou et al., 1987) which were under investigation. To standardise the genetic background and establish a suitable control for future experiments, a backcrossing (BC) scheme was performed (Figure 5). The laboratory CS was the chosen wild-type strain for the procedure as it is commonly used in genetic studies and has a low mutation rate (Colomb and Brembs et al., 2015). To backcross the *CJ10* and *R1* mutation into the CS genetic background, a female from each original *ATPα* mutant stock was mated with a CS male (outcrossing). Mutant females from the outcross scheme were then individually crossed back to its parent, a CS male, for six generation (Evangelou et al., 2019; Toivonen et al., 2007; Toma et al., 2002). Identification of *CJ10* and *R1* females following each backcross was achieved by screening for bang-sensitive paralysis (Ashmore et al., 2009) and/or non-lethal genotyping using PCR and restriction digest analysis (Section 3.6.3). To ensure *ATPα* mutant females were obtained during each stage of backcrossing, crosses were setup in duplicates or triplicates. Flies used in breeding scheme were 3-to-7-day old virgin adults which were reared and collected by CO_2 anaesthesia as described in Section 3.3.1. To prevent losing the homozygous lethal mutation overtime, the new stocks (BC6 flies) were maintained balanced with a TM3,$Sb^{[1]}$ balancer (Figure 5). The balancer, TM3 was chosen as it carries an inversion breakpoint that is very close to the location of the *ATPα* gene, 93A4 (Gramates et al., 2016; Miller et al., 2016). Balancer from the original *ATPα* R1 stock was used following outcross and backcross to the laboratory CS strain (Figure 5). Upon completion of balancing the cantonised *CJ10*/+ and *R1*/+ strains, Sanger sequencing was done to confirm lines possessed correct mutation. Before use in studies, the balancer was removed by crossing the balanced stocks back to CS and selecting for offspring without the $Sb^{[1]}$ phenotype. In future these flies will be referred to as CS-*CJ10* and CS-*R1* flies.

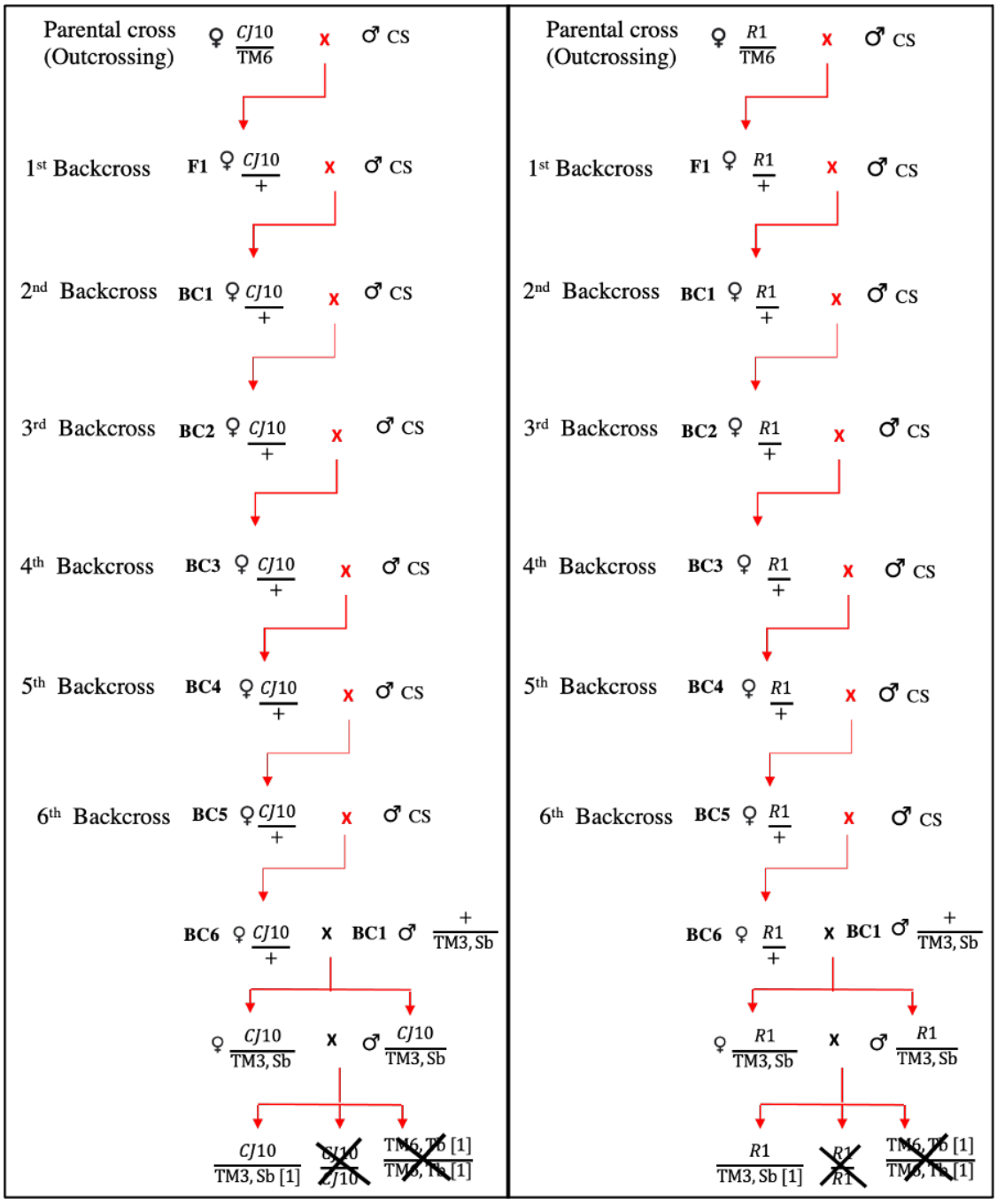

Figure 5. Backcrossing and balancing scheme of the *ATPα CJ10* and *R1* mutant fly lines. The ATPα CJ10 (p.Gly744Ser) and R1 (p. Ile905Trpfs*8) mutation found on the third chromosome were backcrossed six times (BC1-6) into the WT CS strain to standardise the genetic background of mutant fly lines for experimentation. Identification of CJ10 and R1 females following each backcross was achieved by screening for bang-sensitive paralysis and/or non-lethal genotyping using PCR and restriction digest analysis. Following backcrossing, the TM3 balancer line that had been outcrossed and backcrossed once (BC1) to the WT CS strain was crossed to the BC6 mutant flies to balance over mutations.

3.3.3 Generation of *Gal4/UAS-ATP1A3* transgenic fly lines

For phenocopy experiments, female *pUAST-ATP1A3*^{D801N}/*Sm6a,CyO* (*pUAST_α3*$^{D801N/+}$) and *SST13-UAS-ATP1A3*^{D801N}/*TM3* (*SST13_α3*$^{D801N/+}$) were crossed to male *Actin5C-Gal4/CyO* flies for generation of offspring expected to ubiquitously express the human *ATP1A3* transgene under the *Actin5C* (*Act5C*) promoter (*Act5c-Gal4/pUAST_α3*$^{D801N/+}$ *or Act5C-Gal4/SST13_α3*$^{D801N/+}$). Offspring used in experiments were selected against the *CyO* marker. Flies were cultivated, collected by ice anesthesia, and maintained as virgin adults for testing (Section 3.3.1)

3.3.4 Generation of *Gal4/UAS-ATP1A3; ATPα* mutant flies

For rescue experiments, female *pUAST-ATP1A3*^{WT}/*CyO; ATPα*^{CJ10}/*TM6B* (*pUAST_α3; CJ10*) and *pUAST-ATP1A3*^{WT}/*CyO;R1/TM6B* (*pUAST_α3;R1*) flies were crossed to male *Actin5C-Gal4/CyO* flies for generation of offspring expected to ubiquitously express the human *ATP1A3* transgene under the *Actin5C* promoter (*Act5c-Gal4/ pUAST_α3; CJ10* or *Act5C-Gal4/pUAST_α3; R1*). Offspring without *CyO* phenotype were selected for experimentation. Flies were cultivated , collected by ice anesthesia and maintained as virgin adults for testing.

3.4 Behavioural Work

3.4.1. Negative geotaxis assay

Negative geotaxis is a measure of how quickly a fly can climb vertically after the fly has been tapped to the bottom of a vessel to elicit this innate escape response in flies (Gargano et al., 2005). To examine this behaviour, methodology adapted from Gargano et al. (2005) and Nichols et al. (2012) was followed.

3.4.1.1 Construction of Negative Geotaxis apparatus

To facilitate the assaying of multiple individual flies at a time, a similar apparatus described in Gargano et al., 2005 was designed and made with materials that were

readily available in the Bratman's lab. To create negative geotaxis apparatus dimensions of 36.0 x 4.0 cm and 4.0 x 10.0 cm were drawn out on foam board, cut out with a scalpel blade, and assembled with a glue gun. The open-faced rectangular box was made to size to securely fit 10 plastic vials (2.3 x 9.5 cm) which acted as the negative geotaxis tubes. Small holes were cut out of the top of the box to create openings for easy transfer of flies into the negative geotaxis tubes. The openings were closed with a foam stopper to prevent flies from escaping once transferred. Moreover, for analysis purposes, the left outermost tube was marked with lines indicative of 2 cm, 4 cm, 6 cm, and 8 cm which will be referred to in future as the "reference tube".

3.4.1.2 Experimental design

A total of fifty to sixty virgin flies per genotype aged 2-3 days were assayed individually over a span of 2-3 morning blocks (9.30-11.50am). The rearing, collection and maintenance of flies assayed followed description in Section 3.3.1. Experiments involved randomly assigning each experimental group with an ID number and a negative geotaxis tube for each trial using an online random number generator (https://g.co/kgs/W3UwXj). This allowed for blind scoring of behaviour thus preventing potential experimenter bias. On the days of testing, flies from each experimental group were placed in their assigned tubes using a manual pouter. Tubes were then bunged with a foam stopper and flies were given one minute to acclimatize to tube. A standard trial consisted of a firm tap down of the apparatus on a heavy-duty table followed by a single opportunity for flies to perform negative geotaxis under conditions in CT room (24-25°C, 45-50% RH on a 12:12 h LD cycle). Fly behaviour was recorded using either a Handycam Camcorder (Sony HDR-CX405) or an iPhone camera that had been positioned ~30 cm in front of the apparatus (Gargano et al., 2005). Recordings were

started prior to the beginning of each trial and was stopped 30 seconds after eliciting behaviour.

3.4.1.3 Data collection

The distance climbed at 3 seconds (s) was collected for all assayed flies and recorded in an Excel spreadsheet. Data collection occurred by capturing still images at the specified time either using Sony's PlayMemories Home software suite (Version.3.6.01) or the built-in Mac Snipping Tool to save as a jpg file. The images were opened in ImageJ (Version 1.53t) and the brightness/contrast was adjusted and applied across all frames to allow for the clear observation of flies as a black dot. The images were then spatially calibrated by drawing a line with a known distance of 8 cm on each image to set the scale. Following this, the straight-line tool was selected to draw a line from the base of negative geotaxis tubes to the mid-section of each fly to get distance climbed in cm.

The time taken in seconds by all assayed flies at 2-3-day to climb above the 4 cm marking after eliciting negative geotaxis was recorded in an Excel spreadsheet. Data collection occurred by watching climbing assay videos in QuickTime Player (Version 10.5) to determine time taken in centi-seconds for the rear end of flies to pass the 3.0 ± 0.2 cm mark on a standard 15 cm ruler (Tiger Stationary Ltd, England) placed on screen. The measurement equated to the distance from the base of the reference tube to 4 cm marking on the computer screen for each video.

Latency to climb by CS-*ATPα* mutant flies at 2-3-days was recorded in Excel spreadsheet as an additional measure of locomotive behaviour. Data collection occurred by watching climbing assay videos in QuickTime Player (Version 10.5) to determine time taken in centi-seconds for flies to initiate vertical movement after commencement of negative geotaxis.

For all datasets, the genotype and sex of the flies were revealed after scoring had been completed.

3.4.2 Zantiks system setup

Locomotive behaviour of flies was also examined using an automated video tracking unit called the Zantiks Multi Well Plate (MWP) unit (Cambridge, UK). The activity monitor is designed to measure locomotion, activity levels and response to stimuli in small organisms such as *Drosophila*, zebrafish and rodents. The compact unit (190mm width x 230mm length x 480mm height) enables high throughput experiments of *Drosophila* using a standard multi-well plate. Following manufacturer's instructions (https://youtu.be/413nz3j7dKQ), the Zantiks activity monitor was setup on a benchtop in a well-ventilated area of Prof. Isaac's Lab. The Zantiks MWP unit is integrated with a computer that controls its operation, a temperature control system to maintain a set temperature, an experimental chamber that houses the multi-well plate and a camera to track animal movement within each well. Before use, the MWP unit was calibrated with a black 96-well calibration plate supplied with the unit following manufacturer's instructions (https://youtu.be/jJGEo8zC4n4). For experiments, a standard clear flat-bottom 96-well microplate (Greiner Bio-One, UK) was used. To detect the wells defined as "arenas" for accurate fly tracking, the unit required a bitmap file (.bmp) of the 96-well plate to be built and exported to the "Asset directory" on the Zantiks Control Console page. To achieve this, the g96.zs file, was downloaded from the Zantiks website (https://zantiks.com/manuals/asset-building-in-the-mwp) and uploaded into the "Zancript directory" on the Control Console page. The script was then run to generate the 96 arenas, checked for alignment with the well plate and exported as ".a96.bmp" to the "Asset directory" following the manufacturer's instructions (https://youtu.be/jJGEo8zC4n4). To run experiments in Zantiks units, protocols needed

to be written in Zantiks' proprietary software language called Zanscritpt. The demo Zanscript for circadian rhythm, available on the Zantiks website (https://zantiks.com/protocols/circadian-rhythm-monitoring), was downloaded and uploaded to the "Zanscript directory". Necessary modifications were made to the script before added to "Service directory" on the Control Console page to enable running of the experiment in the MWP unit. This included changing command to measure locomotor activity in 5 min bins (DEFINE TIME_BIN: 300); changing the number of samples of movement to 12 (DEFINE NUM_SAMPLES 12) to produce 60 minutes of activity; changing hours of light and dark to 12 h (DEFINE NUM_LIGHT:12; DEFINE NUM_DARK:12); changing the number of L:D cycle to 5 days (DEFINE NUM_DAY_LD: 5); changing arena size to a 96 well plate (DEFINE NUM_WELLS 96); setting temperature to 25℃ (SET THERMOSTAT: 25) and changing auto-reference to 10 seconds (DEFINE AUTOT: 10) to provide a brief period to allow movement of flies before tracking. As an additional measure to distinguish sleeping flies from moving flies, a threshold for pixel changes within each arena was set to the highest recommended value of 6 (MSD_THRESHOLD, 6) (*Measuring pixel difference*, n.d.). In the context of this experiment, the Mean Square Difference (MSD) valued at 6 means that there are pixel changes of 6 units between consecutive frames in a 5 minute window. Thus, a MSD readout of 6 or greater indicated that movement was occurring in the arena, signalling that the fly was awake.

3.4.2.1 Preparation of a 96-well plate and loading of flies

The well microplate (Greiner Bio-One, UK) was aliquoted with 250 μL of fresh 1% agar media containing 5% sucrose and a fungicide agent (Table 18) in each well. The food was allowed to cool to room temperature before immobilization of flies by ice anesthesia for placement in the well plate. The plate was kept on ice to maintain fly immobilization

until all flies were transferred. Each fly genotype received a unique ID number, which was used to assign flies to a well using online random number generator (https://g.co/kgs/W3UwXj). Once all flies were transferred, an air permeable lid (Zantiks, Cambridge, UK) was secured to the top of the plate with Blu Tack creating a humid environment. The well plate, housing the recovered males or females, was placed onto the light stand and inserted into the chamber of the Zantiks MWP instrument. The flies were given a day to acclimatize to new environmental conditions.

3.4.2.2 Experimental design

Flies were cultivated, collected by ice anesthesia, and maintained as virgin adults for testing (Section 3.3.1). Thirty-two virgin CS and CS-*ATPα* mutant males and females aged 2-3 days, were separately entrained at 25±0.5℃ to a 12.03:12.03 h L:D cycle (lights on at 10:10 am) for four full days. The addition of the 0.03 h (2 minutes) was a result of the 10 second delay of tracking every hour to allow for recalibration of tracking to ensure accurate tracking. From this point on, L:D cycle will be referred to as 12h:12h as lights changed within the 12 h period. Fly activity was measured as distance travelled (mm) above the recommended threshold of 1.9 mm (Dr Bill Budenberg, *pers comm*) threshold every 5 minutes.

3.4.2.3 Data Acquisition

Following completion of experiments, the locomotor and sleep activity data saved as a csv file was downloaded from Zantiks system to be reviewed in Excel. Flies that died at any point during the experiment, the data from that fly was omitted. The Zantiks data was converted into a *Drosophila* Activity Monitoring (DAM) system format using a custom R code kindly created by Dr Arijit Ghosh (Ghosh and Sheeba, 2022) to allow for automated data analysis using online-platform tools such as the VANESSA-DAM and Rtivity software (Ghosh and Sheeba, 2022; Silva et al., 2022). However, due to the

25 h usage limit of the VANESSA-DAM app per month and available analysis software unable to account for light changes at 12.03 h, the data was processed in Excel (Table 19) (Isaac et al., 2010; Pfeiffenberger et al., 2010; Miyazaki et al., 2022).

Table 19. Description of the calculation of locomotor and sleep activity in Excel

Behavioural Parameter	Description
Total Locomotor Activity	For each fly, sum of the distance travelled in mm per day (24 h), per light and dark phase (12 h), which was average across the four days.
Profile of Average Locomotor Activity in 5 minute bins in a 24 h cycle	For each fly, each 5 minute bin from each day was average to calculate the average distance travelled in a 24 h cycle every 5 minutes.
Total Sleep Time	For each fly, sum of inactivity (zero distance travelled for at least 5 minutes) per day, per light and dark phase was average across four days.
Sleep Episode Duration	For each fly, sum of minutes of uninterrupted sleep per day, per light and dark phase was average across four days
Number of Sleep Episodes	For each fly, frequency of episodes of uninterrupted sleep per day, per light and dark phase was average across four days
Sleep Latency	For each fly, sum of minutes taken for the start of a sleep episode following the onset of dark phases, average across four days
Wake After Sleep Onset (WASO)	For each fly, the sum of minutes awake during dark phases, average across four days.

3.4.3 Cold-shock assay

To examine cold sensitive-paralysis in young adult flies, a modified version of the cold shock assay described in Ashmore et al. (2009) and Dean et al. (2018) paper was performed. The protocol was adapted to enable the testing of multiple fly strains concurrently. This was achieved by utilizing Bel-Art™ floating racks which allowed for twenty-four individual flies to be assayed at a time in 1.5mL clear plastic tubes (Figure 6). To allow for better visualisation and continual focus of multiple flies during video recording, the tubes were filled with 750μL 2% SA food (Section 3.2.2). Medium sized polystyrene box were used to create cold-shock and recovery water baths (Figure 6).

3.4.3.1 Experimental design

Cold sensitivity testing was examined in virgin adults aged 2-8-day olds. Flies were cultivated, collected by CO2 anaesthesia to avoid pre-exposure to cold and maintained as described in Section 3.3.1. The day before assaying, flies were transferred to cold shock tube via a manual pouter to save time on experimental days and allow acclimatisation period to new conditions. Flies were prevented from escaping by covering tubes with clear plastic film. The plastic films were also pierced with a small hole to allow flies to breathe. Flies contained in tubes were kept in CT room (24-25℃, 45-50% RH on a 12:12 h LD cycle). Experiments involved randomly assigning each genotype and sex with an ID number and a rack place holder for each trial using an online random number generator (https://g.co/kgs/W3UwXj). This allowed for blind scoring of behaviour thus preventing potential experimenter bias. On days of testing, tubes containing flies were firmly placed in their assigned place holders. The tubes were then submerged for six minutes in a thermometer controlled ice water bath that had been chilled to 4℃. In addition to 4℃, the A*ct5C-Gal4/UAS-a3*$^{D80N/+}$ flies were examined at 2℃ to assess behaviour at a colder temperature. Following cold exposure, tubes were then placed in a 24-25℃ (room temp) thermometer controlled water bath until flies were

standing on all four limbs. Fly behaviour was recorded using an iPhone XR camera or Handycam Camcorder (Sony HDR-CX405) which was mounted above cold-shock apparatus. During cold-shock, behaviour of flies was also recorded at times by eye as iPhone camera was unable to keep tube in frame. Testing was done in CT room (24-25°C, 45-50% RH on a 12:12 h LD cycle) which occurred over several afternoon blocks (2-5pm) to assay around fifty flies per genotype.

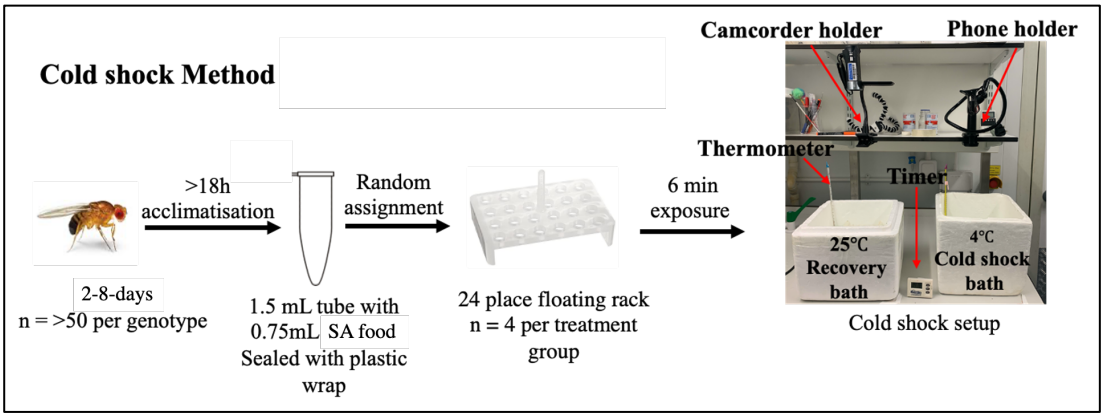

Figure 6. Visual summary of cold-shock experimental setup for assaying of cold sensitive-paralysis in young adult flies.

3.4.3.2 Data collection

Data collection occurred by watching cold-shock assay videos in QuickTime Player (Version 10.5) to determine: (1) number of paralysed and non-paralysed flies (Paralysis Outcome), (2) time taken in seconds for flies to become paralysed (Paralysis Onset Time) and (3) time taken in seconds for paralysed flies to recover (Paralysis Recovery Time). Time to paralysis data revealed that a proportion of flies across all genotypes tested did not experience paralysis within the 360s limit. Thus, to minimise the introduction of bias, all non-paralysed flies were scored the maximum time limit (Time to paralysis of all tested flies). These datasets were recorded in Excel spreadsheets before the genotype and sex of the flies were revealed.

3.5 Statistical Analysis

All datasets were analysed using R (Version 4.2.2) and/or GraphPad Prism (Version 8.02.6). The R package lme4 was used which provides functions to fit and analyse GLM (Bates et al., 2015). Graphical visualisation of data was completed in GraphPad Prism. All datasets were tested for normality using Shapiro-Wilk and extreme outliers were removed using the Iterative Grubbs test (P <0.05) in GraphPad Prism prior to fitting a Generalised Linear Model (GLM) to datasets in R to test the influence of fixed factors such as genotype, sex and their interaction on behavioural responses. The general approach when using GLMs was to fit the most complex model (i.e., interaction between genotype and sex) with the most appropriate distribution (Gamma, Gaussian, Inverse-Gaussian or Poisson) to datasets (Tables 20-23) based on Akaike's Information Criteria (AIC) values (model with lowest AIC value chosen) using the AICcmodavg package, QQ plots and histograms using the fitdistrplus package. This was then followed by testing the significance of interaction by comparing models fitting the data with and without the interaction using F-statistics to compare the fit of models. Models were simplified when interactions were not significant. When genotype and sex were indicated as predictors, sex was removed from model by re-analysis of data grouped into males and females. The simplest statistical model fitted to data was the null model which is a constant of 1. Multiple comparisons of the estimated marginal means (EMMs) of groups were analysed using *emmeans* package (Lenth et al., 2024). As multiple testing was performed, *P*-values were adjusted using Holm-Bonferroni (HB) method to reduce risk of type I error rates. For the height climbed datasets, Gamma error distribution was considered the best fit, however the error distribution cannot handle non-positive values such as zero thus to overcome this, a small noise of 0.01 cm was added to every value to get rid of zero values in data. For categoric datasets, Fisher's Exact test was used and post-hoc analysis were carried using Pairwise Fisher's Exact test from R stats package,

P-values were adjustment by HB method. Moreover, when common GLM error distributions were unable to appropriately fit to datasets, Man-Whitney U (MWU) and Kruskal Wallis (KW) non-parametric testing were used (Table 21 and Table 23). Post-hoc analysis for KW was the Dunn's test.

Table 20. Selected method for statistical analysis of negative geotaxis datasets

Fly Datasets	CS-*ATP*$\boldsymbol{\alpha}$ mutants	*CJ10* rescue transgenics	*R1* rescue transgenics	D801N transgenics
Distance climbed in 3s	GLM Gamma	GLM Gamma	GLM Gamma	GLM Gaussian
Time taken to climb above 4 cm mark	GLM Gamma	GLM Inverse-Gaussian	GLM Gamma	GLM Gamma
Time taken to initiate vertical movement	GLM Gamma	GLM Gamma	GLM Gamma	GLM Gamma

Table 21. Selected method for statistical analysis of locomotor activity datasets

Datasets	CS-*ATP*$\boldsymbol{\alpha}$ mutant females	CS-*ATP*$\boldsymbol{\alpha}$ mutant males
Total distance travelled in 24 h	GLM Gamma	GLM Gamma
Total distance travelled in light phrase	GLM Gamma	GLM Gamma
Total distance travelled in dark phrase	GLM Gamma	GLM Gamma
Locomotor response to lighting	MWU, KW	MWU, KW

Table 22. Selected method for statistical analysis of sleep datasets

Fly Datasets	CS-*ATP*$\boldsymbol{\alpha}$ mutant females	CS-*ATP*$\boldsymbol{\alpha}$ mutant males
Total Sleep per day	GLM Gamma	GLM Gamma

Total Sleep per light phase	GLM Gamma	GLM Gamma
Total Sleep per dark phase	GLM Gamma	GLM Gamma
Number of Sleep episodes per day	GLM Gaussian	GLM Gaussian
Number of Sleep episodes per light phase	GLM Gaussian	GLM Gaussian
Number of Sleep episodes per dark phase	GLM Gaussian	GLM Gaussian
Mean length of Sleep episodes per day	GLM Gamma	GLM Inverse-Gaussian
Mean length of Sleep episodes per light phase	GLM Gamma	GLM Inverse-Gaussian
Mean length of Sleep episodes per dark phase	GLM Gamma	GLM Gamma
Sleep Latency	GLM Gamma	GLM Inverse-Gaussian
Time Awake After Sleep Onset	GLM Gaussian	GLM Gaussian

Table 23. Selected method for statistical analysis of cold-shock paralysis datasets

Fly Datasets	CS-*ATP*$\boldsymbol{\alpha}$ mutants	*CJ10* rescue transgenics	*R1* rescue transgenics	D801N transgenics
Paralysis Outcome	Fisher's Exact	Fisher's Exact	Fisher's Exact	Fisher's Exact
Paralysis Onset Time	GLM Gamma	GLM Gamma	GLM Gamma	GLM Gamma
Paralysis Recovery Time	GLM Gaussian	GLM Gamma	GLM Gamma	GLM Gamma
Paralysis Onset Time for all tested flies	MWU, KW	MWU, KW	MWU, KW	MWU, KW

3.6 Molecular Analysis Methods

3.6.1 Qualitative Reverse Transcriptase-PCR

The molecular technique introduced over thirty years ago (Foley et al., 1993) is commonly used method for detection of many types of ribonucleic acid (RNA) transcripts including ones involved in protein synthesis such as messenger RNA (mRNA), transfer RNA (tRNA) and ribosomal RNA(rRNA). Analysis of RNA is facilitated by the conversion of extracted RNA to complementary DNA (cDNA) using reverse transcriptase enzyme (RT) and amplification of cDNA targets by PCR.

3.6.1.1 RNA extraction and purification

Total RNA was extracted from frozen whole adult flies (n= 8) aged 3-10 days using the ZYMO RESEARCH^{Ò} Direct-zol^{TM} RNA Miniprep Kit protocol (Serial no. R2051). Modifications to protocol included adding 600 μL of RNA lysis buffer (TRI reagent) to tissue samples as weight was less than 50 mg. Following the homogenization of tissues using a sterilised micro-pestle (Melford Biolaboratories Ltd), the mixture was centrifuged for 3 minutes to ensure all debris was pelleted. To avoid disturbing the pellet, only 450 μL of the supernatant was transferred to RNase-free tubes. Total volume in tube was brought to 900 μL by the addition of equal volume of 100% ethanol to promote RNA binding. The contents were thoroughly mixed by gently inverting tubes 10 times. Due to the spin column's maximum capacity of 700 μL, the lysate was loaded and centrifuged in two batches. To ensure RNA samples were free of gDNA contamination, samples were treated with DNase I following kit instructions. Further purification steps included washing bound RNA with Direct-zol RNA prewash and RNA wash buffer. After discarding flow-through of the RNA wash buffer, the column was centrifuged for an extra 2 minutes to remove traces of ethanol following the final wash. Concentrated RNA was eluted by applying 50 µl of DNase/RNase-Free water provided by the kit

directly to the column matrix and centrifuged for 1 minute. The concentration and quality of RNA was determined by loading 2 μL onto the Thermo Scientific NanoDrop^{TM} spectrophotometer (Cat no. ND-2000). Following use, RNA samples were stored at -70°C.

3.6.1.2 cDNA synthesis

Single strand cDNA was generated from RNA using the Thermo Scientific First Strand Synthesis cDNA kit protocol (Serial no. K1612). For a 20 μL reaction, the RNA quantity (~200 ng) was standardised across all samples and random hexamer primer mix provided by kit was used. Negative-RT control reactions were performed to verify the absence of gDNA contamination. If contamination was detected, the reaction was repeated. Following use, cDNA samples were stored at -70°C.

3.6.1.3 Primer design

Primers for *D. melanogaster ATPα* and human *ATP1A3* were designed using the NCBI Primer-BLAST tool. Reference sequence for *ATPα* (NM_169936.3) and human *ATP1A3* (NM_152296.5) gene were obtained from the NCBI Gene database (Brown et al., 2015). Amendments to default parameters included product size (350-600 bp), GC content (40-60%), selecting option for primers to span an exon-exon junction and exhibit specificity for either humans or flies. Selection of a *ATP1A3* primer pair was based on sequence having the fewest identical bp to the *ATPα* sequence as well as showing no hits when searched against the fly genome using the UCSC In-Silico PCR web tool (https://genome.ucsc.edu/cgi-bin/hgPcr). Primers listed in Table 24 were ordered from IDT and reconstituted to 100 μM following manufacturer's instructions before further use or storage at -20°C.

Table 24. Primers used for RT-PCR amplification for *D. melanogaster ATPα* and human *ATP1A3*

Target	Forward Sequence (5'-3')	Reverse Sequence (5'-3')
ATPα	gttaaggtcggattacgagcatgg	cacgatgacgacagcggaaa
ATP1A3	acagactgtgtgcagggttt	tcagcgttcacctgcatctt

3.6.1.4 PCR and Gel electrophoresis protocol

The cDNA quantity was standardised to ~22 ng across all samples to ensure consistency with the cDNA control template. Synthesised cDNA and PCR reagents listed in Table 25 were added to fresh 0.2 mL PCR tubes placed on ice. The contents were mixed by gentle flicking and centrifuged for 5 seconds in a microcentrifuge. PCR reactions were conducted in a thermal cycler (GS4822, G-Storm, Somerton, UK) under conditions described in Table 26. The Total volume of RT-PCR products and 5 μL of 100 bp DNA ladder (Promega) mixed with 6x Blue/Orange Loading Dye (Promega) were loaded onto a 1.2% agarose gel stained with EtBr. Gels were run in 1 x TAE buffer (National Diagnostics) for 1 h at 130 V before imaging bands using the Gel Doc™ EQ imaging system (Bio-Rad).

Table 25. PCR Master Mix for amplification of ATP1A3 cDNA

PCR reagents	Volume (µL)	Source	Cat no.
cDNA template	22ng		
Nuclease free water	Make up to 20.0	Severn Biotech LtD	20-9000-01
5X Fusion HF Buffer	4	APExBIO	K1039
10mM dNTPs Mix (10mM each)	0.4	Appleton Woods Ltd	VC018
Forward Primer (10µM)	0.8	IDT	Custom
Reverse Primer (10µM)	0.8	IDT	Custom
Fusion DNA polymerase	0.4	APExBIO	K1039
TOTAL	20.0		

Table 26. PCR cycle for amplification of ATP1A3 cDNA.

PCR step	Temperature	Duration
1 (Initial denature)	98°C	3 min
2 (Denature)	98°C	30 s
3 (Annealing)	58°C	1 min
4 (Extension)	72°C	40 s
5	Go to 2, 34 times	
6 (Final extension)	72°C	10 min
7 (Hold)	10°C	∞

3.6.2 Western Blotting

The multistep molecular technique, first described over 44 years ago (Towbin et al., 1979) is a frequently used antibody-based method for detection and quantification of protein expression.

3.6.2.1 Protein Extraction

Total protein was extracted from frozen heads of *Elav-Gal4/UAS_ α3* flies (n = 24) or whole *Act5C-Gal4/UAS_α3* flies in duplicates or triplicates. Extraction of cytoplasmic, membrane and nuclear proteins was achieved by homogenizing tissue samples in ChemCruz® RIPA lysis buffer (Cat no. sc-24948) using a micro-pestle (Melford Biolaboratories Ltd). The lysis buffer was supplemented with Protease Inhibitors and Phosphatase Inhibitors to prevent protein degradation and removal of phosphate groups from proteins respectively. Following homogenization, a centrifugation step (15 minutes, 13.3 rpm, at 4℃) was carried out to ensure all debris were pelleted and allow for transfer of the clear supernatant into new and sterile tubes. Protein lysates were stored at -80℃ until required.

3.6.2.2 Protein Quantification

The Pierce™ Bicinchoninic Acid (BCA) Protein Assay Kit (Cat no. 23227) was used to quantify the total protein concentration extracted from fly samples. A serial dilution of the bovine serum albumin (BSA) standard protein with known concentrations from 0-2 mg/mL were made to a final volume of 30 μL using DNase/RNase-Free water. The BCA working reagent was prepared by mixing 50:1 Reagent A and B. As unknown samples were limited, 10 μL instead of 25 μL of unknown samples and BSA standard were pipetted in duplicates into a clear 96-well microplate before the addition of 200 μL of the BCA working mixture to each well. The plate was covered with parafilm and shaken in the Thermo Varioskan® Flash microplate reader for 30 seconds before incubation at 37℃ 30 minutes to allow for colour change. The absorbance was measured at 550 nm in microplate reader and each BSA standard and unknown sample was recorded. A standard curve was plotted in Excel using values of the BSA standards to generate a line-of-best-fit equation to calculate concentrations of fly samples.

3.6.2.3 Sample preparation

Samples were prepared for western blotting at concentrations ranging from 5-50 μg/ μL with distilled water to make a final volume of 20 μL. Into a fresh tubes, 10 μL of sample was aliquoted. To samples, 10 μL of reducing agents β-mercaptoethanol and 2x Laemmli buffer in 1:20 ratio was added to ensure proteins were fully denatured by breakdown of disulfide bonds and separated based on size by giving proteins a negative charge respectively. Samples were then stored at -80℃ until gel running.

3.6.2.4 Polyacrylamide Gel electrophoresis

Prior to loading on Bio-Rad Mini-PROTEAN® TGX Precast Gels (Cat no. 4561083), samples were thawed on ice and heated at 95℃ for 5 minutes to denature proteins. Protein samples (20 μL) and ladder (5 μL) were loaded onto a 4-15% gel in tank filled

with 1% running buffer. Gels were run between ~2 h at 100 V to ensure good separation of proteins.

3.6.2.5 Protein Transfer

Proteins were transferred onto PVDF membrane using the Bio-Rad Trans-Blot® Semi-Dry transfer cell protocol (Cat no. 1703940). Adaption to protocol included equilibrating gels in 1x transfer buffer for 10-20 minutes and running blot at 10 V for 40 minutes. Prior to sandwiching gel, membrane was activated with 100% methanol for >1 minute before rinsed twice with distilled water.

3.6.2.6 Antibody staining

Following transfer, to prevent non-specific antibody binding, membranes were blocked with 5% milk overnight at 4℃ with shaking. The next day, the milk was poured off and membranes were incubated with 5 mL of primary antibody (Table 27) diluted to 1:250-1:4000 with 5% milk to determine optimal conditions. Incubation period was carried out overnight at 4℃ with shaking. The next day, the membrane was washed three times with PBS-Tween (PBS-T) for 10 minutes before the addition of appropriate horseradish peroxidase (HRP)-conjugated secondary antibody (Table 28) at 1:2000 dilution to visualise protein of interest. Membranes were incubated in secondary antibody for 2 h with shaking before washes with PBS-T in preparation for imaging.

Table 27. Details of primary antibodies used in western blotting analysis

Primary Antibody Name	Source	Cat no.	Detail
Anti-Na+/K+ ATPase α3	Merck Millipore	06-172	A polyclonal antibody, produced in rabbit to detect h/m-NKA.
Na+/K+ ATPase α3 (XVIF9-G10)	Santa Cruz	Sc-58631	A monoclonal antibody, produced in mouse to detect h/m-NKA.

Na+/K+ ATPase α-subunit (A5)	DSHB	a5	A monoclonal antibody, produced in mouse to detect h/m/d-NKA.
Anti- β -Tubulin	Sigma-Aldrich	T2200	A polyclonal antibody, produced in rabbit.
Anti β-Actin	Sigma-Aldrich	A1978	A monoclonal antibody produced in mouse.

Table 28. Details of HRP-conjugated secondary antibody used for protein visualization

Secondary Antibody Name	Source	Serial no.	Primary Antibody compatibility
Goat Anti-Rabbit IgG/HRP	Bio-Rad	1721019	Anti-Na+/K+ ATPase α3; Anti- β -Tubulin
Polyclonal Rabbit Anti-Mouse IgG/HRP	Dako	P0260	Na+/K+ ATPase α3 (XVIF9-G10); Anti β-Actin; Na+/K+ ATPase α-subunit (A5)

3.6.2.7 Imaging

The Pierce™ ECL Western Blotting substrate peroxide and luminol enhancer solution (Cat no: 32106) in a 1:1 ratio was used to visualise protein with the Invitrogen™ iBright imaging system.

3.6.3 Genomic DNA (gDNA) Extraction Methods

3.6.3.1 Single fly gDNA extraction

Isolation of gDNA from a single adult fly provides sufficient quantity and quality for genotyping purposes (Nagarajan and Georgiou, 2022). Extraction of gDNA was achieved following a protocol commonly used in Dr Steve Clapcote lab. Ice anaesthesia was used to transfer a single fly to a 1.5 mL sterile Eppendorf tube that had been kept on ice. To ensure cell lysis, the whole fly was homogenized on ice using a sterile yellow pipette tip for 10 seconds before the addition of 600 μL of cell lysis buffer (10 mM Tris-

HCl, 100 mM NaCl, 10 mM EDTA, 0.5 % SDS, pH 8.0) supplemented with 10 μL proteinase K stock solution (10 mg/mL, Merck Millipore). Samples were then mixed well by vortex for 5 seconds and placed in a heating block for overnight incubation (~18 h) at 55°C. Following incubation period, 166.7 μL of 5M NaCl was added to samples and vortexed for 30 seconds to precipitate the cell debris and proteins out of solution. Transferred to fresh 1.5 mL sterile Eppendorf tubes was 725 μL of supernatant containing DNA. An equal volume of 725 μL ice cold 95% ethanol was added to precipitate DNA. The DNA was then pelleted by centrifugation at 13,500 rpm for 5 minutes at room temperature (RT). The supernatant from samples was decanted and the pelleted DNA washed with 1 mL of 70% (v/v) ethanol to ideally remove all salt from the DNA. For the final time, the samples were vortexed for 30 seconds and centrifuged at 13,500 rpm for 5 minutes at room temperature. The supernatant was discarded, and the DNA pellets were air-dried. Following the evaporation of all moisture, the DNA was resuspended in 50 μL of DNAse/RNAse-free water (QIAGEN) and incubated at 65°C for 10 min to ensure DNA was well dissolved in water. DNA concentrations were quantified by measuring the absorbance at 260 nm using the Thermo Scientific NanoDrop™ spectrophotometer (Serial no. ND-2000). DNA samples were diluted to ~50 μg/mL in DNAse/RNAse-free water for PCR. Following use in PCR reactions, the remaining isolated DNA was stored at -20°C for future use.

3.6.3.2 Single wing gDNA extraction

A non-lethal method for isolating fly gDNA during backcrossing scheme of *ATPα* mutants was supplied by Dr Laurin McDowall at the University of Leeds. Each fly was immobilized on a CO2 pad before using sterilized forceps (Dumont no. 4) to remove and transfer a wing to a 0.2 mL PCR tube that was placed on ice. Following wing removal, flies were placed into individual food vial that had been assigned a reference

number. A sterile yellow pipette tip was used to grind fly wing for 10 seconds to release DNA content before wing was carefully covered with 10 μL squishing buffer (10 mM Tris-HCl; 1 mM EDTA; 25 mM NaCl; pH 8.0) supplemented with 0.2 μL proteinase K (10 mg/mL). Samples were placed in PCR blocks and a protocol called soupmaker was run (Table 29). Following use in PCR reactions, the remaining isolated DNA was stored at -20°C for future use.

Table 29. Protocol for DNA extraction from a single fly wing

Steps	Temperature	Duration
Cell lysis reaction	37°C	30 min
Proteinase K inactivation	95°C	3 min
Hold	10°C	∞

3.6.3.3 PCR/RE-based Genotyping Method

PCR is a widely-used method to detect the presence or absence of gene(s) from gDNA extracted from whole or small body parts of flies (Carvalho et al., 2009). For genotyping of the *ATPα CJ10* and *R1* mutations, PCR-restriction digest analysis was used. This was due to identification of commercially available enzymes featuring recognition sites solely within the targeted exonic region of *CJ10* (MlyI) and *R1* (PvuI) mutant by the NEBcutter V2.0 tool.

3.6.3.4 Primer Design for PCR-based genotyping

Primers used for PCR-based genotyping of *ATPα* mutant flies are presented in Table 30. Primers were designed using the Primer3 software (Untergasser et al., 2012) to amplify exonic regions of target genes directly from extracted gDNA. To ensure amplification of whole exons, primers were designed to anneal to intronic sequences flanking each exon. Genomic reference sequences were obtained from the Ensembl Genome Browser (Cunningham et al., 2019). The set parameters for design included a product size of 250-600 bp, primer size of 19-24 bp, primer melting temperature (Tm) of 55-60°C with a

maximum difference of 5°C, and GC content of 35-65%. Primers listed in Table 30 were ordered from IDT and reconstituted to 100 μM following manufacturer's instructions before further use or storage at -20°C.

Table 30. Primers used for PCR-based genotyping and sequencing of *D. melanogaster*

Target gene	Forward Sequence (5'-3')	Reverse Sequence (5'-3')
ATPα Exon 5	tgcctaccaaaatgcctaaa	ccagtgatatggcaggaatc
ATPα Exon 8	acgataatgtaaacagccaagg	cgtaaggaaggttatttacaagg

3.6.3.5 PCR protocol

PCR reagents listed for gDNA amplification from whole flies (Table 31) and single fly wing (Table 32) were added to a fresh 0.2 mL PCR tube and gently mixed by pipetting before centrifugation for 5 seconds in a microcentrifuge. DNA was amplified in a thermal cycler (GS4822, G-Storm, Somerton, UK) under the conditions described in Table 33 for gDNA whole flies and Table 34 for gDNA single fly wing. Following amplification, samples were stored in 4°C fridge until restriction digest.

Table 31. Standard PCR Master Mix for amplification of gDNA from whole flies

PCR reagents	Volume (μL)
dH_2O	19.55
10X buffer	2.5
$MgCl_2$ (50mM)	0.8
dNTPs (25mM each)	0.2
Primer mix (5μM each)	0.75
Taq polymerase	0.2
DNA from whole fly	1
Total	25.0

Table 32. Phusion High-Fidelity PCR Master Mix for amplification of gDNA from single fly wing

PCR reagents	Volume (μL)
dH_2O	11.85
5X Phusion High Fidelity Buffer	4
dNTPs mix (10 mM each)	0.2
Primer mix (5 μM each)	0.75
Phusion Taq polymerase	0.2
DNA from fly wing	3.0
Total	20.0

Table 33. PCR cycle conditions for amplification of gDNA from whole flies

PCR step	Temperature	Duration
1 (Initial denature)	95°C	3 min
2 (Denature)	94°C	30 s
3 (Annealing)	57°C- *CJ10* mutants 53°C- *R1* mutants	1 min
4 (Extension)	72°C	40 s
5	Go to 2, 34 times	
6 (Final extension)	72°C	10 min
7 (Hold)	10°C	∞

Table 34. PCR cycle conditions for amplification of gDNA from single wings

PCR step	Temperature	Duration
1 (Initial denature)	98°C	3 min
2 (Denature)	98°C	30 s
3 (Annealing)	57°C- *CJ10* mutants 53°C- *R1* mutants	1 min
4 (Extension)	72°C	40 s
5	Go to 2, 34 times	
6 (final extension)	72°C	10 min
7 (Hold)	10°C	∞

3.6.3.6 Restriction Enzyme (RE) Digest Protocol for *ATPα* mutants

Following the manufacturer's guidelines (New England Biolabs), reagents listed in Table 35 were added to 0.2 mL PCR tube , gently mixed by pipetting and centrifuged for 5 seconds in a microcentrifuge. The RE digestions were performed in a thermal cycler (GS4822, G-Storm, Somerton, UK) for a minimum of 45 minutes at 37°C. The digested amplicons were visualised and separated according to their size on a 3% agarose gel stained with ethidium bromide (EtBr). Digested samples and 5 μL of 100 bp DNA ladder (Promega) were mixed with the appropriate volume of 6x Blue/Orange Loading Dye (Promega) before loaded into wells. Gels were run in 1 x TAE buffer (National Diagnostics) for 1 h at 130 V. The size of the digested amplicons were determined under UV light using the Gel Doc™ EQ imaging system (Bio-Rad).

Table 35. *MlyI* and *PvuI* restriction enzyme digest Master Mix

Reagents	Volume (μL)
Nuclease free water	2.05
10X CutSmart Buffer	1.9
NEB restriction enzyme (10U/μL)	1.05
PCR product	14.0
Total	19.0

3.6.4. Sanger Sequencing Method

3.6.4.1 PCR product purification

PCR products amplified from fly gDNA were cleaned up using the QIAquick® Gel Extraction Kit (Cat no. 28704) according to instructions provided. Since the purified DNA fragment were required for direct sequencing, the optional steps were carried out. Other modifications included: (1) centrifugation of column for an additional 3 minutes to ensure removal of residual ethanol from Buffer PE and (2) elution of purified DNA with 30 μL of QIAquick® nuclease-free water (Serial no. 129114) following

centrifugation at low speed (1000 rpm) for 30 seconds and letting column stand for 1 minute for increased DNA concentration.

3.6.4.2 Custom DNA Sequencing

The purified DNA templates were prepared for commercial Sanger sequencing following instructions provided by Eurofins Tubeseq or Genewiz's pre-mixed service. Each premixed sample contained either the forward or reverse primer with the DNA template.

3.6.4.3 Sequence Analysis

The .ab1 files provided by the Sanger sequencing service were analysed using the computer programme Benchling, Inc (https://benchling.com). The sequences were then aligned to a consensus sequence published in NCBI (Brown et al., 2015) which set the base numbering. Following alignment powered by Clustal Omega, the chromatogram datasets were viewed simultaneously in forward and/or reverse orientation in comparison with the reference sequence to check for ambiguities/disagreements and correct for any errors in base calls. The protein translations (of the consensus sequence) were also viewed and proofread for any amino acid changes as a result of real base call changes. Chromatograms and alignments were exported as PDF format.

IV. Results

4.1 Molecular analysis of *D. melanogaster ATPα* mutants and *ATP1A3* transgenics

This chapter aims to confirm the successful presence of *ATPα* mutations (p.Gly477Ser and p.Ile905Trpfs*8) following the backcrossing of *ATPα* mutants into a wildtype CS background and the integration of the human wildtype and mutated *UAS-ATP1A3* constructs into the *D. melanogaster* genome located on chromosome 2 (p*UAST_ATP1A3*^{WT} and p*UAST_ATP1A3*^{D801N}) and 3 (*SST13_ATP1A3*^{WT} and *SST13_ATP1A3*^{D801N}) via phiC31 integrase-mediated transgenesis. To verify the presence of the genetic modifications, PCR with restriction enzyme digest (PCR/RE) and Sanger sequencing was used. Additionally, this chapter aims to assess the successful expression of the human *ATP1A3* transgene in *D. melanogaster* using qualitative RT-PCR and western blot analysis. These molecular techniques will address whether wildtype and transgenes are effectively transcribed and translated in the fly model.

4.1.1 Detection of *CJ10* mutation in CS-*CJ10*/+ flies

Genotype analysis of the heterozygous *CJ10* mutation in flies by PCR and restriction enzyme digest resembled agarose gel results predicted by the NEBcutter tool (Figure 7A). The digested amplicons from CS-*CJ10*/+ flies yielded clear bands around 472-bp and 357-bp but not at 115-bp (Figure 7B). DNA sequence chromatograms of CS-*CJ10*/+ flies revealed a heterozygous G>A nucleotide change corresponding to position c.2230, resulting in a codon for serine (AGT; S) rather than the conserved glycine (GGT; G) at position p.744 in the protein sequence (Figure 7C & 7D).

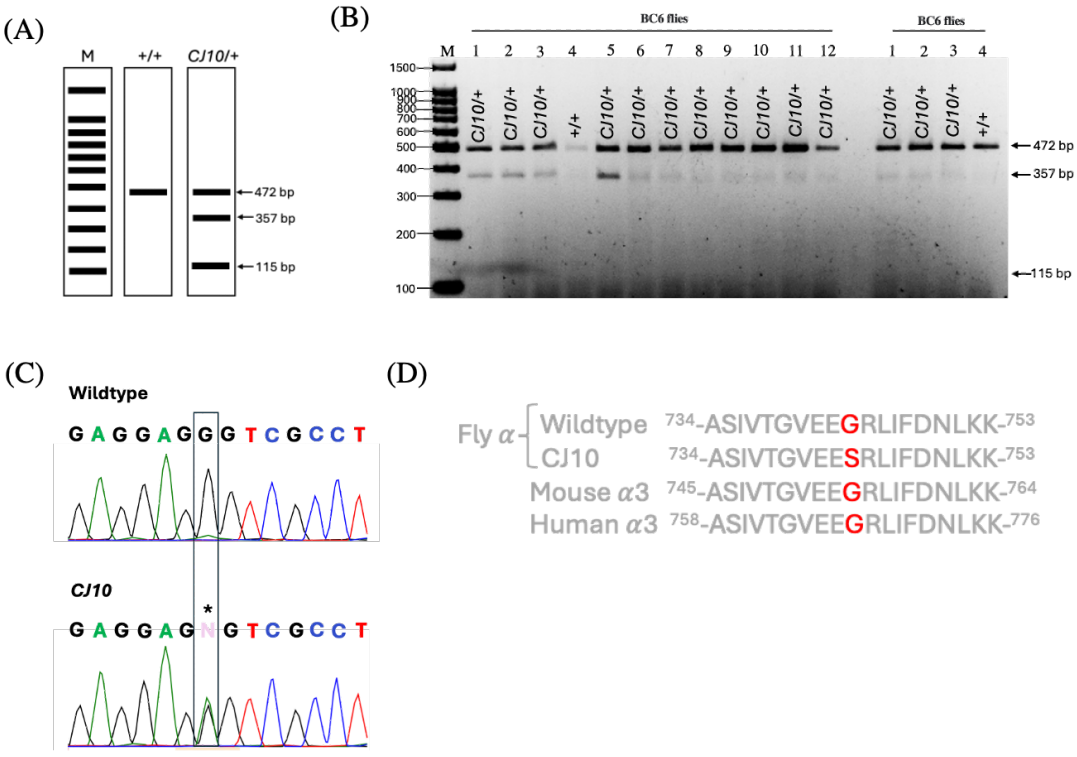

Figure 7. Genotyping of the fly *CJ10* mutation by PCR-restriction enzyme and Sanger sequencing analysis. (A) Schematic diagram of expected gel electrophoresis results following amplification and MlyI digestion of a 472-bp fragment encompassing the heterozygous CJ10 mutation within fly ATP***α*** exon 5 transcript b. **(B)** 3% agarose gel result of digested products of amplified gDNA isolated from flies collected after the sixth generation of Atp***α*** mutant backcrossed into a wildtype CS (+/+) background (BC6). **(C)** DNA sequence traces of Atp***α*** exon 5 confirmed BC6 CJ10 mutants carry a single G>A nucleotide change at position c.2230 in a heterozygous manner. **(D)** Alignment of three partial protein sequences of invertebrate and vertebrate species, showing in red the conserved Glycine(G)744>Serine(S) substitution because of c.2230G>A nucleotide change in flies.

4.1.2 Detection of *R1* mutation in CS-*R*/+ flies

Genotype analysis of the heterozygous *R1* mutation in flies by PCR and restriction enzyme digest resembled agarose gel results predicted by the NEBcutter tool (Figure 8A). The digested amplicons from CS-*R1*/+ flies yielded clear bands at around 615-bp, 374-bp and 241-bp (Figure 8B). DNA sequence chromatograms of CS-*R1*/+ flies revealed an ATCG deletion corresponding to positions c.2713-2716, resulting in the

disruption of the normal reading frame and a premature stop codon being created (Figure 8C & 8D).

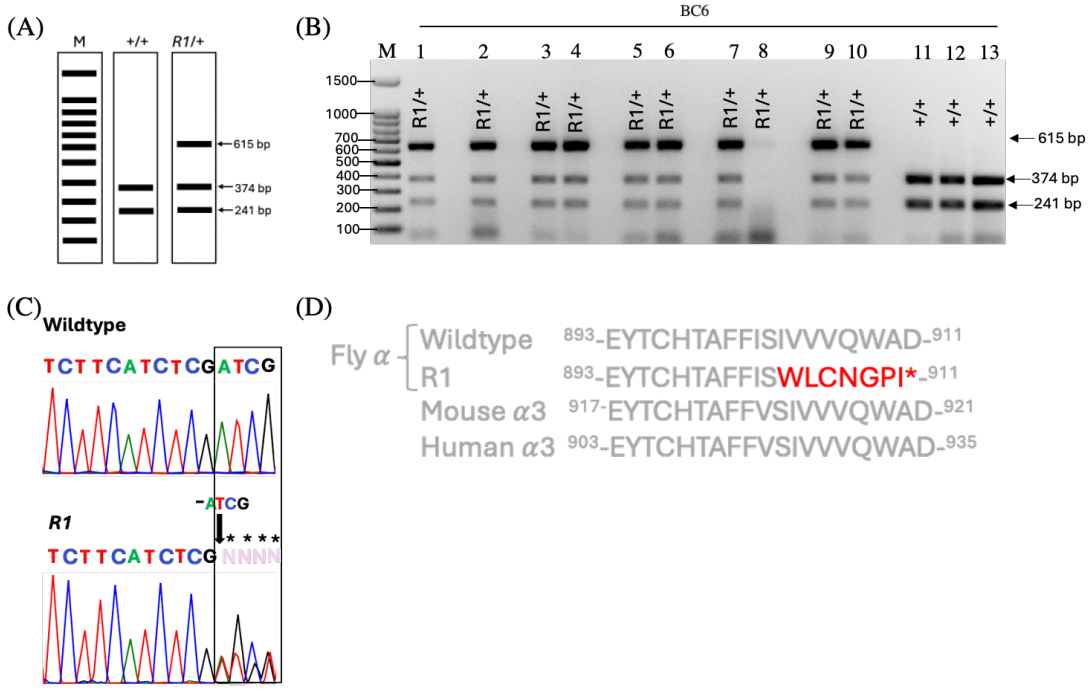

Figure 8. Genotyping of fly *R1* mutation by PCR-restriction enzyme and Sanger sequencing analysis. (A) Schematic diagram of the expected gel electrophoresis results following amplification and PvuI digestion of 615-bp fragment encompassing the heterozygous R1 mutation within fly Atp***α*** exon 8 transcript b. (B) 3% agarose gel result showing digested products of amplified gDNA isolated from flies collected after the sixth generation of Atp***α*** mutant backcrossed into a wildtype CS (+/+) background (BC6). (C) DNA sequence traces of Atp***α*** exon 8 confirmed BC6 R1 mutants carry a c.2713-16delATCG mutation in a heterozygous manner. (D) Alignment of three partial protein sequence of invertebrate and vertebrate species, showing in red the result of the c.2713-16delATCG frameshift mutation leading to a premature stop codon. **4.1.3 Detection of *UAS_ ATP1A3* recombinant clones**

The digested wildtype and mutated p*UAST_ATP1A3* plasmids extracted from bacterial cells yielded two clear bands on agarose gel around 8.5kb and 3.0kb corresponding to the size of the p*UAST* vector and *ATP1A3* insert respectively (Figure 9A). Similarly, digested wildtype and mutated *SST13-UAS_ATP1A3* plasmids yielded two clear bands on agarose gel around 4.7kb and 3.0kb corresponding to the size of the SST13_*UAS*

vector and *ATP1A3* insert respectively (Figure 9B and 9C). This is confirmation of successful ligation.

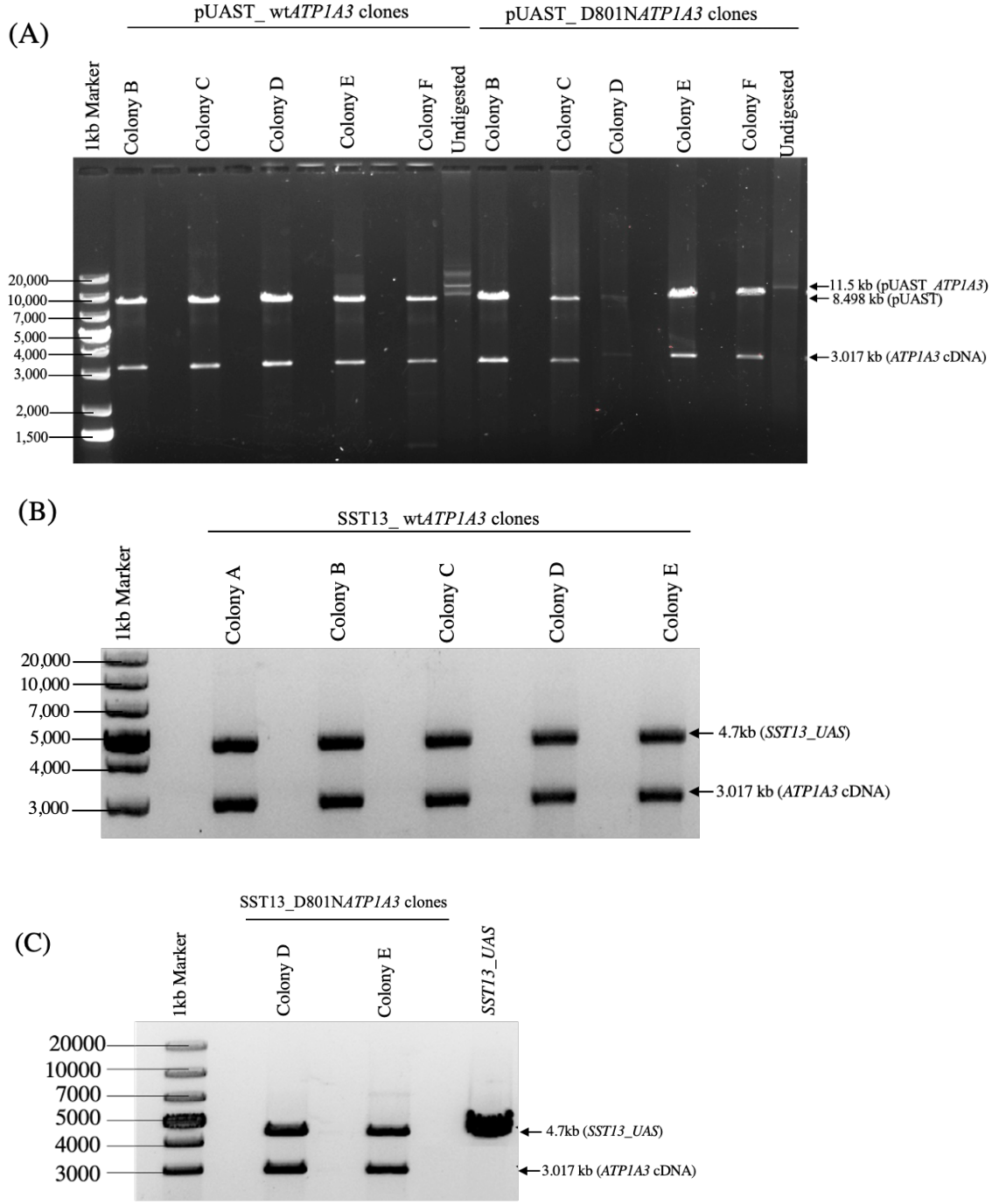

Figure 9. Screening of *UAS_ATP1A3* recombinant clones by *BgIII* and *XhoI* restriction digest analysis. (A) 0.8% agarose gel result of digested wildtype and mutated pUAST_ATP1A3 isolated plasmids. Expected size of insert, vector backbone and uncut plasmid should be around 3kb, 8kb and 11kb, respectively. **(B)** 0.8% agarose gel result of digested wildtype and **(C)** mutated SST13-UAS_ATP1A3 isolated

plasmids. Expected size of insert, vector backbone should be around 4.7kb and 3.1kb respectively.

4.1.4 Detection of *UAS_ ATP1A3* construct in *D. melanogaster*

DNA sequence chromatograms of a small fragment of the wildtype and mutated human *ATP1A3* cDNA sequence from *UAS_ATP1A3* transgenic flies revealed no disagreements and reconfirmed the D801N mutation as a result of a G>A substitution at position 2401in the cDNA sequence (Figure 10).

(A)

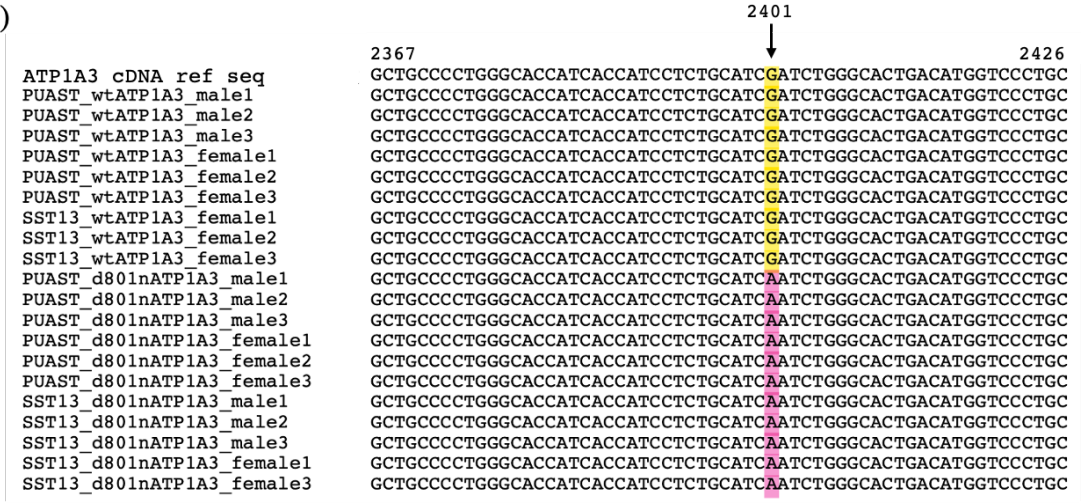

Figure 10. Multiple alignment of the partial DNA sequence obtained from sequencing of human ATP1A3 cDNA fragment in *UAS_ATP1A3* transgenic fly lines. (A) Wildtype and mutated ATP1A3 sequences were aligned against the human ATP1A3 cDNA reference sequence from the ATP1A3 mRNA variant 1 sequence (NCBI: NM_152296.5) which revealed G (highlighted in yellow) to A (highlighted in pink) nucleotide substitution in D801N flies at position c.2401 in the sequence compared to flies carrying the wildtype ATP1A3 sequence.

4.1.5 Detection of *ATP1A3* mRNA in *Gal4/UAS* transgenic flies by qualitative RT-PCR analysis

The human *ATP1A3* cDNA was detected in *Gal4/UAS_ATP1A3* fly samples represented on agarose gel as a clear band around 385-bp akin to the pcDNA3.1(+)-*ATP1A3* vector sample, serving as a positive control for *ATP1A3* expression (Figure 11A). The positive control sample presents with a thicker band than *Gal4/UAS_ATP1A3* samples (Figure

11A). Moreover, no band was visible in WT CS control samples which acted as a negative control for *ATP1A3* expression (Figure 11A). Expression of the fly *ATP**α*** was also detected in *Gal4/UAS_ATP1A3* fly samples represented on agarose gel as a clear band around 475-bp (Figure 11B). No band was visible in pcDNA3.1(+)-*ATP1A3* vector which acted as a negative control for *ATP**α*** expression (Figure 11B).

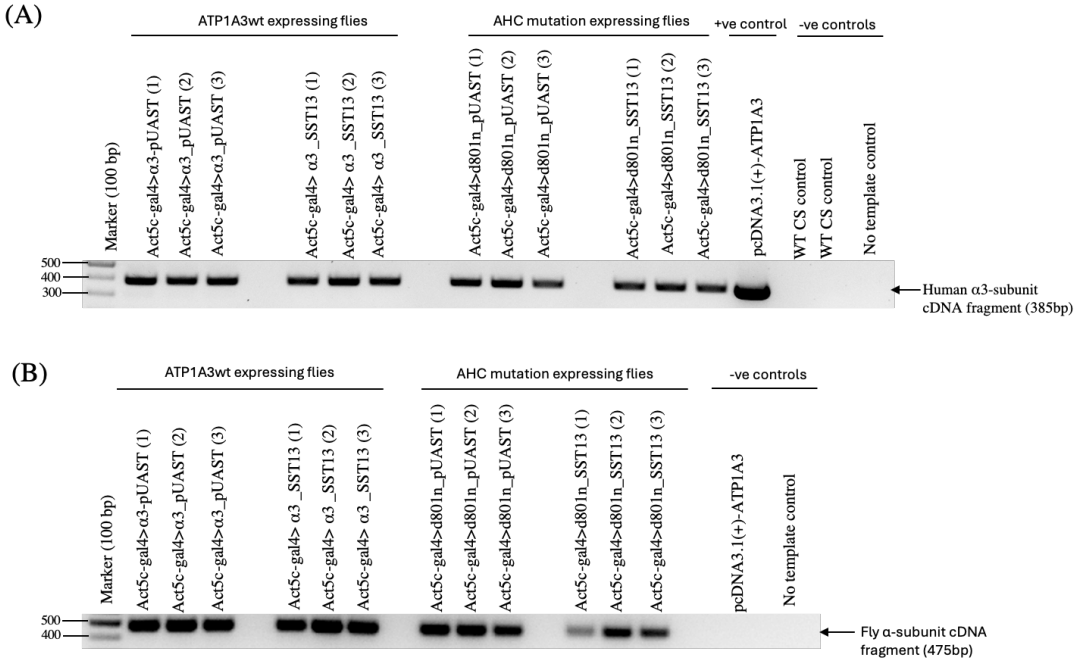

Figure 11. Reverse transcription-PCR analysis of human *ATP1A3* and fly *Atpα* expression in transgenic Gal4/UAS adult flies. Agarose gel electrophoresis (1.2% agarose) showcased PCR amplification of **(A)** human ATP1A3 and **(B)** fly ATP***α*** cDNA synthesized from total RNA extracted from whole body adults. Expected bands seen at 385-bp and 475-bp correspond to the coding region of human ATP1A3 variant 1 and fly Atp***α*** variant b transcripts respectively. The WT CS fly samples serve as a negative control for human ATP1A3 expression meanwhile the pcDNA3.1(+)-ATP1A3 vector serves as a negative control for fly Atp***α*** expression. The no template control serves as a control for DNA and reagent contamination.

4.1.6 Detection of the human ATP1A3 protein in *Gal4/UAS* flies by western blot analysis

A signal around 90kDa was consistently detected in fly *Gal4/UAS_ATP1A3* samples at varying concentrations (5-50μg) when probed with the Anti-h/m-NKA α3 polyclonal

antibody and Anti-α (h/m/d-α subunits) antibody at varying dilutions (Figure 12A, 12B,12D & 12F). Meanwhile a signal around 90kDa was not consistently detected in fly *Gal4/UAS_ATP1A3* samples at varying concentrations (5-50μg) when probed with the Anti-h/m-NKA α3 XVIF9-G10 monoclonal antibody at increasing concentrations (Figure 12A, 12B, 12C, 12D & 12E). Moreover, a signal akin to fly *Gal4/UAS_ATP1A3* samples was detected in fly *UAS-ATP1A3*, *Act5C-Gal4/CyO* and WT CS negative controls when probed with both Anti-h/m-NKA α3 antibodies (Figure 12A, 12B, 12C,12D & 12F). Similarly, a signal around 90kDa was detected consistently in positive control mouse samples (5-10 μg) when probed with both Anti-h/m-NKA α3 antibodies (Figure 12A, 12E & 12F). A signal around 55kDa was detected in the mouse sample only when probed with the loading control β-Tubulin antibody (Figure 12A). A signal around 42kDa was consistently detected in *Gal4/UAS_ATP1A3* fly samples at varying concentrations (5- 50μg) when probed with β-Actin antibody which acted as a loading control (Figure 12A, 12B, 12C, 12D, 12E & 12F).

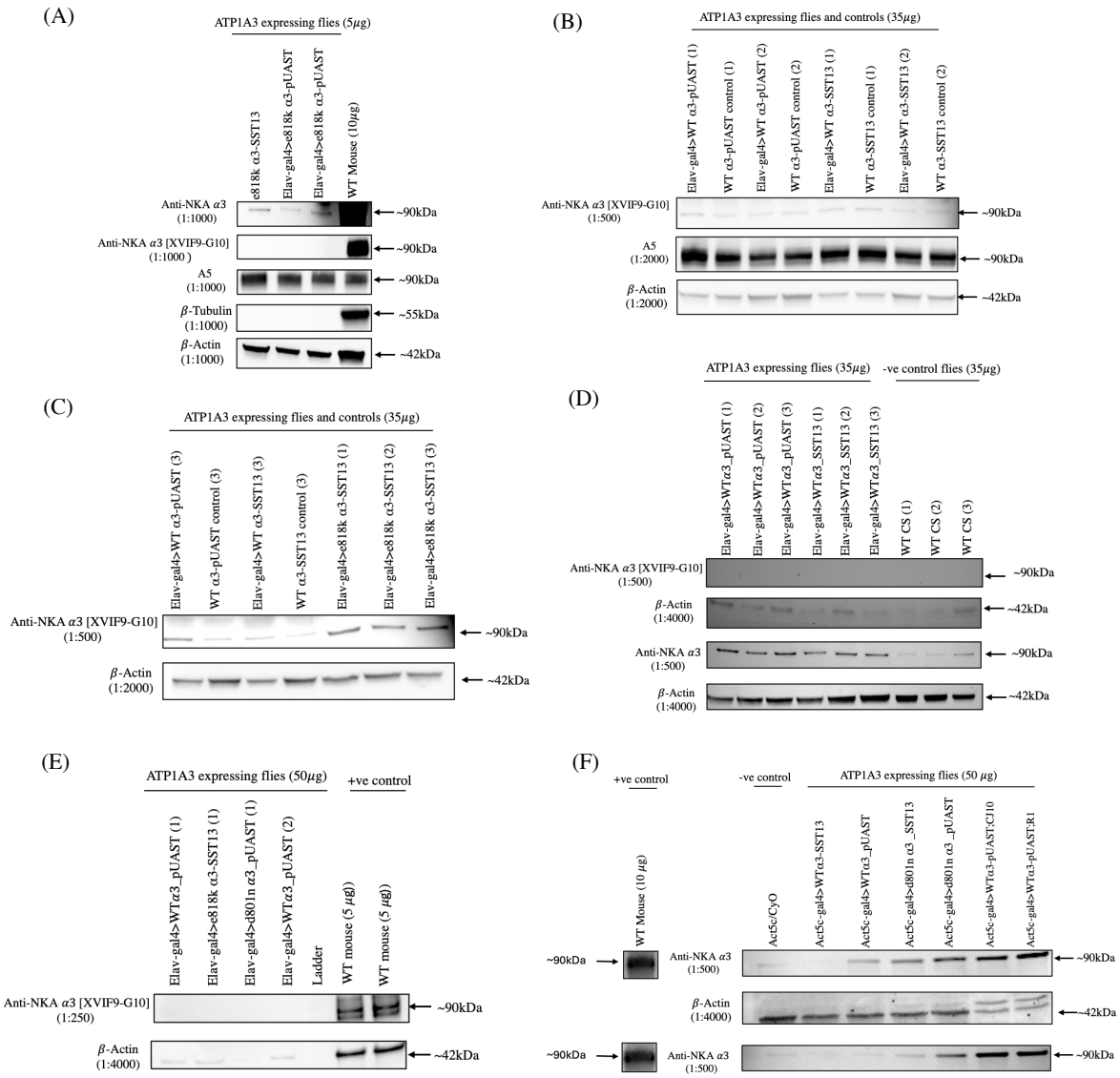

Figure 12. Investigation into optimal detection of the human ATP1A3 protein in transgenic Gal4/UAS adult flies. The presence of the human protein Na+/K+ ATPase alpha subunit 3 (h-NKA α3) in whole fly head (Elav-gal4) or whole body (Act5C-gal4) homogenates (5-50μg per lane) was evaluated by western blot analysis using the polyclonal anti-α3 antibody (Anti-h/m-NKA α3), monoclonal anti-α3 antibody (Anti-h/m-NKA α3 [XVIF9-G10]) and an anti-α (h/m/d- α subunits) antibody (a5) at varying dilutions (annotated on figure). In this analysis, β-Actin was used as the loading control to showcase that protein loading was the same across the gel. Each row is a cropped image representing results and the corresponding molecular weight generated when membrane was probed with the primary antibodies listed above.

4.1.7 Discussion

The heterozygous nature of the *ATPα* mutations in flies during backcrossing scheme was confirmed using the PCR/RE digest method established in this research and finally by Sanger sequencing. Heterozygosity in *CJ10* mutants was indicated by a single overlapping peak corresponding to the wildtype G and mutant A nucleotide (Figure 7C), replicating results previously reported by Ashmore et al. (2009) work. In *ATPα R1,* heterozygosity was indicated by presence of the wildtype A, T, C and G nucleotides overlapped with T, G, G and T nucleotides indicating the absence of the 4-bp (A, T, C and G) and disruption to the *ATPα* ORF (Figure 8C and D). This research is the first to report a sequence chromatogram of the *ATPα R1* mutation. Moreover, this research provides a genotyping method that could be used for routine genotyping of the *ATPα CJ10* and *R1* mutants in future experiments, thus overcoming limitations such as the longer turnaround time and high cost as associated with Sanger sequencing.

This research also reports the successful generation of *UAS-ATP1A3* constructs indicated by observations by *BgIII* and *XhoI* restriction digest analysis (Figure 9) and 100% DNA sequence identity between the alignment of the sequenced wildtype *ATP1A3* cDNA fragment from *UAS* transgenic flies with the wildtype *ATP1A3* cDNA reference sequence (Figure 10) obtained from the *ATP1A3* mRNA variant 1 sequence (NCBI: NM_152296.5) obtained from the NCBI database (Brown et al., 2015). The research also verifies the identity of *UAS* transgenic flies carrying a single G>A substitution at position c.2401 corresponding to the human AHC D801N mutation (Heinzen et al., 2014) via sequence alignment (Figure 10). The report of these results confirms the successful integration of the *UAS_ATP1A3*^{WT} and *UAS_ATP1A3*^{D801N} constructs into the fly genome via the phiC31 integrase system (Bischof et al., 2007). Moreover, these

findings add to the body of research validating the effectiveness of NEBuilder® HiFi DNA Assembly Cloning Method in generating constructs for transgenic experiments.

The western blots performed in this research revealed the consistent detection of a single band at approximately 90kDa when extracted protein samples from *Gal4/UAS* flies were probed with the Millipore anti-h/m-NKA α3 antibody (Cat no: 06-172) (Figure 12A, B, D and F), a primary antibody that has been previously used to successfully detect the level of m-NKA α3 in mouse brain and spinal cord samples (Edwards et al., 2013). Thus, the observation of a signal at around 90kDa in *Gal4/UAS_ATP1A3* flies and in mouse samples (Figure 12A, B, D and F), the latter serving as a positive control, indicates expression of the h-NKA α3 protein in the *Gal4/UAS_ATP1A3* flies. Previously, the detection of the h/m-NKA α3 protein was reported at around 100kDa (Shyjan and Levenson, 1989). However, recently it has been reported that the human *ATP1A3* cDNA (from transfected HEK293 cells) runs around 92kDa on westerns blots with goat-specific polyclonal (C16) or mouse-specific monoclonal (H4 or F1) antibodies (Arystarkhova and Sweadner, 2024). In addition, the XVIF9-G10 anti-h/m-NKA α3 antibody (Cat no: Sc-58631) used in this research has been shown to produce a signal at 95kDa (Arystarkhova and Sweadner, 1996). The presence of visually faint bands at ~90kDa in *Gal4/UAS* fly samples probed with the XVIF9-G10 anti-h/m-NKA α3 antibody (Cat no: Sc-58631) (Figure 12B and C) further suggests low expression of the h-NKA α3 protein in *Gal4/UAS* flies. However, the detection of a very faint band at ~90kDa in the wildtype CS and *Act5C-Gal4/CyO* samples (Figure 12D and F), which served a negative control in experiments, weakens the interpretation of results described above. This observation suggests that the Millipore anti-h/m-NKA α3 antibody (Cat no: 06-172) is able to weakly bind to the fly *ATPα* protein, in addition to the target h-NKA α3 protein. This is plausible considering the large epitope (aa 320-514 of NKA α3) of

the Millipore anti-h/m-NKA α3 antibody (Shyjan and Levenson, 1989) has a 80-90% sequence identity to fly ATPα protein isoforms when epitope sequence was put into NCBI BLAST search (Johnson et al., 2008). To confirm cross-reactivity of the Millipore anti-h/m-NKA α3 antibody (Cat no: 06-172), western blot experiments would need be repeated with additional negative controls for the h-NKA α3 protein expression. Moreover, confidence in the expression of the h-NKA α3 protein in *Gal4*/*UAS* flies is limited by the lack of success in consistently detecting the h-NKA α3 protein in *Gal4*/*UAS* fly samples when probed with the XVIF9-G10 anti-h/m-NKA α3 antibody (Cat no: Sc-58631), which is known to have greater specificity to the h/m-NKA α3-subunit than the Millipore anti-h/m-NKA α3 antibody as it detects the protein within 50 amino acids of the N-terminus, a region that is less conserved in other h/m-NKA α-subunits (α1, α2) (Arystarkhova and Sweadner, 1996; Edwards et al., 2013). The observation of a signal at ~90kDa in mouse sample probed with a5 antibody (Cat no: a5), which is reported to detect all h/m-NKA alpha subunits ($\alpha1, \alpha2, \alpha3$ and $\alpha4$) (Mobasheri et al., 2012) provides evidence to suggest that the signal detected by Millipore anti-h/m-NKA α3 and the XVIF9-G10 anti-h/m-NKA α3 antibodies is likely the h-NKA α3 protein. However, this is weakened by the observation of a signal at the same size in *UAS*_α3 fly samples probed with the h/m-NKA α3 antibodies (Figure 12B-D and F). A signal in these flies was not expected as *Gal4* expression driver is not present in these flies. Moreover, the presence of a signal in *UAS*_ α3 flies samples parallel to size of signal detected by the h/m-NKA α3 antibodies when probed with the a5 antibody (Figure 12A and B) suggests either the h/m-NKA α3 antibodies is able pick up the fly ATPα protein or leaky expression of the *ATP1A3* is occurring in *UAS* flies. This can be said because the a5 is a pan-specific anti-α antibody known to successfully detect the fly ATPα protein (Lebovitz et al., 1989; Ashmore et al., 2009). *UAS-attB* vectors,

particularly the *pUAST-attB* used in this research to generate transgenic flies, have been reported to have leaky expression (Gluderer et al., 2010). This research is the first to report testing of these α3 antibodies in *Drosophila*, suggesting the possibility of cross-reactivity of the Millipore and XVIF9-G10 anti-h/m-NKA α3 antibodies. In summary, the western blots performed in this research using the Millipore and XVIF9-G10 anti-h/m-NKA α3 antibodies were unable to confidently confirm the presence of the h-NKA α3 protein in *Gal4*/*UAS* flies.

In this research, the expression of the wildtype and mutated *ATP1A3* transgene in *Gal4*/*UAS* flies was also examined by qualitative RT-PCR analysis (Figure 11). The agarose gel results revealed a clear ~385-bp band in each *Gal4*/*UAS* fly sample (Figure 11A), corresponding to the expected size of the *ATP1A3* cDNA fragment based on the primer design and in silico analysis of the human *ATP1A3* sequence. The observed band in *Gal4*/*UAS* fly samples, which mirrored the band size seen in positive controls (Figure 11A), indicates that the total RNA extracted from flies contained the *ATP1A3* mRNA transcript, which was subsequently reversed transcribed into cDNA using random primers. Furthermore, the absence of a band in wildtype CS samples (Figure 11A), serving as the negative control for *ATP1A3* cDNA amplification, and no observations of additional bands, further suggests that the designed primers were highly specific to amplification of the *ATP1A3* cDNA sequence, and that the PCR was free from contaminants such as genomic DNA, demonstrating that the DNase treatment employed was effective. Moreover, the observation of a clear ~475-bp band in all *Gal4*/*UAS* fly samples (Figure 11B), corresponding to the predicted fragment size from the fly *ATPα* cDNA, and absence of a band in the pcDNA3.1(+)-*ATP1A3* sample which serves a negative control for *ATPα* expression (Figure 11B), further validates the reverse transcriptase and PCR process used in this research. However, these results do not to

provide quantitative analysis of *ATP1A3* expression in *Gal4/UAS* transgenic flies, which would require real-time PCR analysis. This may be worthwhile as western blot analysis using validated h/m-NKA $\alpha 3$ antibodies (Edwards et al., 2013) has not been able to verify h-NKA α3 expression in transgenic flies.

4.2 Behavioural analysis of AHC-relevant phenotypes in *D. melanogaster ATPα* mutants

This chapter aims to address the extent to which *ATPα* mutants (p.Gly477Ser; CJ10 and p.Ile905Trpfs*8; R1) replicate the behavioural phenotypes observed in m-NKA α3 mutant mice and AHC patients. By assessing motor-related, stress-induced and circadian behaviours which make up essential, major and minor criteria of AHC diagnosis (Table 1), this will provide critical insight into the functional equivalence between NKA α and h-NKA α3. Additionally, comparing the missense (p.Gly477Ser; CJ10) and null (p.Ile905Trpfs*8; R1) mutation will help to distinguish shared versus mutation-specific phenotypes, shedding light on how different molecular mechanisms of *ATPα* dysfunction contributes to AHC pathology.

4.2.1 Climbing performance of *ATPα* mutants

4.2.1.1 Height Climbed

In negative geotaxis assay, distance climbed in 3 s was assessed as a measure of gross motor function in 2-3-day old *ATPα* mutant flies. The height climbed by *ATPα* mutant and CS control flies in 3s was affected by genotype (Table 36). The median distance climbed by CS, CS-*CJ10*/+ and CS-*R1*/+ flies was 4.48 cm (IQR: 2.51-5.33 cm), 2.11 cm (IQR: 0.01-3.56 cm) and 2.26 cm (IQR: 0.93-4.08 cm) respectively (Figure 13A). Post-hoc test revealed height climbed by CS-*CJ10*/+ and CS-*R1*/+ flies was significantly shorter than CS controls (Table 36, Figure 13A). Meanwhile, no significant difference was found between CS-*CJ10*/+ and CS-*R1*/+ mutants (Table 36, Figure 13A). The results indicate deficit in the climbing performance of CS-*CJ10*/+ and CS-*R1*/+ mutants via measure of height climbed in 3s.

Table 36. GLM analysis of the height climbed in 3 s by ATPα mutants and CS controls. Post-hoc results were corrected for multiple testing using Holm-Bonferroni method, where P < 0.05 is indicated in bold.

	Data	Explanatory Variable(s)	Test statistic	df	*P*-value
GLM	All fly strains	Genotype * Sex	2.2609	2, 144	**0.1079**
		Sex	2.0269	1, 148	0.1566
		Genotype	8.6264	2, 147	**0.0002868**
Post-hoc Tests	CS-*CJ10*/+ vs CS	Genotype	-3.856	147	**0.0005**
	CS-*R1*/+ vs CS	Genotype	-2.325	147	**0.0429**
	CS-*CJ10*/+ vs CS-*R1*/+	Genotype	-1.744	147	0.0832

4.2.1.2 Climbing Speed

In negative geotaxis assay, time taken to climb above 4 cm target line was assessed as an additional measure of gross motor function in 2-3-day old *ATP*α mutant flies. The climbing speed of *ATP*α mutants and CS controls was affected by genotype (Table 37). The median time taken by CS, CS-*CJ10*/+ and CS-*R1*/+ flies was 2.67 s (IQR: 2.13-4.29 s), 4.33 s (IQR: 3.27-5.82 s) and 4.48 s (IQR: 3.05-6.41 s) (Figure 13B). Post-hoc test revealed CS-*CJ10*/+ and CS-*R1*/+ flies took significantly longer than CS controls to climb above the target line (Table 37, Figure 13). Meanwhile, no significant difference was found between CS-*CJ10*/+ and CS-*R1*/+ flies (Table 37, Figure 13B). The results indicate deficit in the climbing performance of CS-*CJ10*/+ and CS-*R1*/+ mutants via measure of time taken to climb above 4 cm target line.

Table 37. GLM analysis of the climbing speed of *ATPα* mutants and CS controls. Post-hoc results were corrected for multiple testing using Holm-Bonferroni method, where P < 0.05 is indicated in bold.

	Data	Explanatory Variable(s)	Test statistic	df	*P*-value
GLM	All fly strains	Genotype * Sex	1.0677	2, 132	0.3468
		Sex	1.3105	2, 136	0.2543
		Genotype	8.4142	2, 135	**0.0003596**
Post-hoc Tests	CS-*CJ10*/+ vs CS	Genotype	3.438	135	**0.0016**
	CS-*R1*/+ vs CS	Genotype	3.629	135	**0.0012**
	CS-*CJ10*/+ vs CS-*R1*/+	Genotype	0.143	135	0.8864

4.2.1.3 Climbing Latency

In negative geotaxis assay, time taken to initiate vertical movement following commencement of negative geotaxis was assessed as an additional measure of gross motor function in 2-3-day old *ATP*α mutant flies. The climbing latency of *ATP*α mutants and CS controls was affected by both genotype and sex, but not their interaction (Table 38). The significant effect of sex was seen within CS-*CJ10*/+ flies only, males were found to take significantly longer than females to begin climbing (Table 38, Figure 13C). Moreover, the significant of genotype was seen in both males and females (Table 38). The time taken for CS, CS-*CJ10*/+ and CS-*R1*/+ males to initiate vertical movement was 0.88 s (IQR: 0.28-1.37 s), 2.36 s (IQR: 0.8-3.12 s) and 1.68 s (IQR: 0.5-2.34 s) respectively (Figure 13C). For CS, CS-*CJ10*/+ and CS-*R1*/+ females the time taken was 0.50 s (IQR: 0.25-1.43 s), 1.38 s (IQR: 0.72-1.79 s) and 1.19 s (IQR: 0.59-1.5 s) respectively (Figure 13C). Post-hoc comparisons of males showed CS-*CJ10*/+ and CS-*R1*/+ mutants took significantly longer than CS control males to begin climbing (Table

38, Figure 13C). Meanwhile, no significant difference was found between CS-*CJ10*/+ and CS-*R1*/+ mutant males (Table 38, Figure 13C). Post-hoc comparisons of females showed CS-*CJ10*/+ mutants took significantly longer than CS control females (Table 38, Figure 13C). Meanwhile, CS-*R1*/+ females did not significantly differ from CS-*CJ10*/+ or CS control females (Table 38, Figure 13C). The results indicate deficit in climbing performance of CS-*CJ10*/+ males, CS-*R1*/+males and CS-*CJ10*/+ females via measure of climbing latency,

Table 38. GLM analysis of climbing latency of *ATPα* mutants and CS controls. Post-hoc results were corrected for multiple testing using Holm-Bonferroni method, where P < 0.05 is indicated in bold.

	Data	Explanatory Variable(s)	Test statistic	df	*P*-value
GLM	All fly strains	Genotype * Sex	0.0004	2, 136	0.9998
		Sex	8.3218	1, 138	**0.000387**
		Genotype	8.1115	2, 139	**0.0004657**
	CS-*CJ10*/+	Sex	5.3626	1, 45	**0.02519**
	CS-*R1*/+	Sex	2.9524	1, 46	0.09248
	CS	Sex	0.6398	1, 45	0.428
	Males	Genotype	4.6896	2, 64	**0.001257**
	Females	Genotype	4.4218	2, 75	**0.0153**
Post-hoc Tests of males	CS-*CJ10*/+ vs CS	Genotype	2.673	64	**0.0315**
	CS-*R1*/+ vs CS	Genotype	2.410	64	**0.0377**
	CS-*CJ10*/+ vs CS-*R1*/+	Genotype	-0.283	64	0.7779
	CS-*CJ10*/+ vs CS	Genotype	2.739	75	**0.0231**

Post-hoc Tests of females	CS-*R1*/+ vs CS	Genotype	1.379	75	0.5164
	CS-*CJ10*/+ vs CS-*R1*/+	Genotype	-1.613	75	0.3328

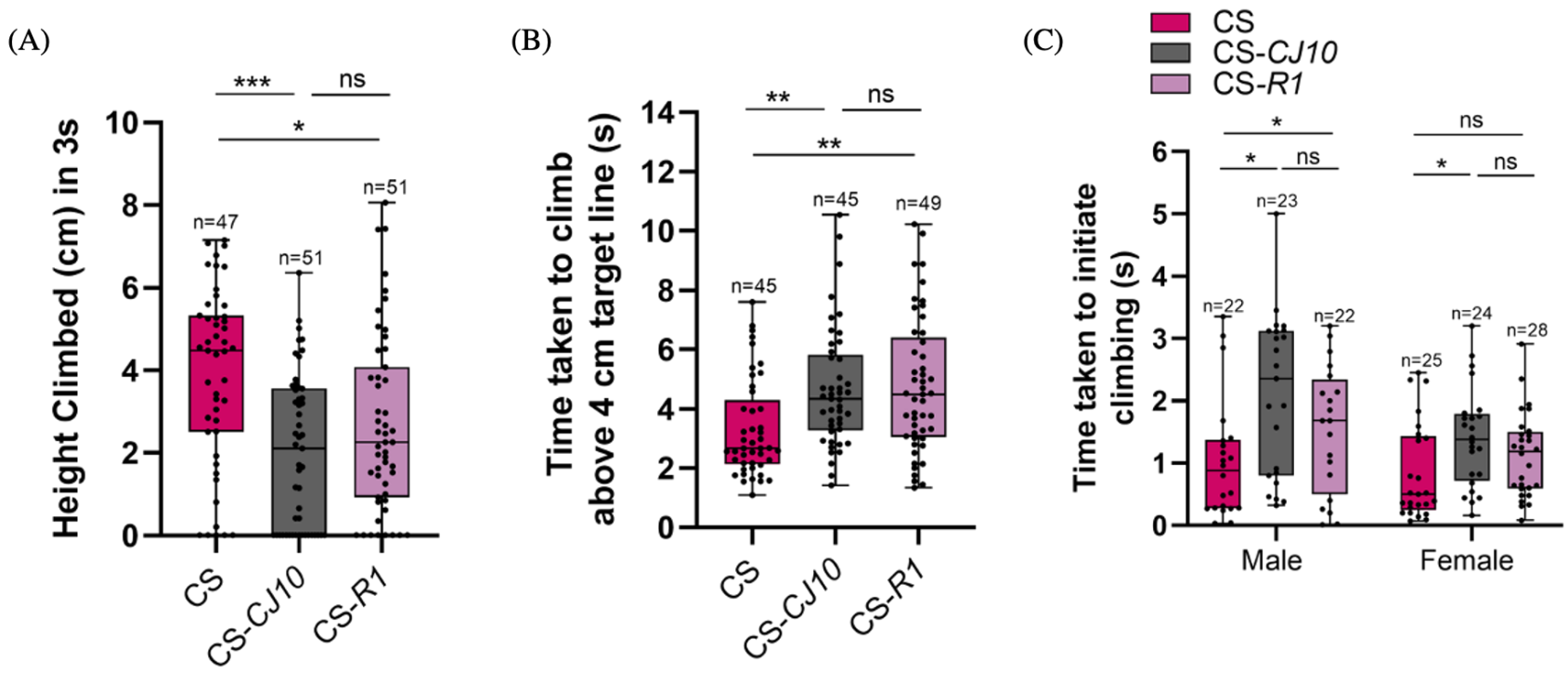

Figure 13. Climbing performance in response to negative geotaxis in young (2–3-day old) virgin *D. melanogaster* heterozygous for *ATP*α mutant alleles (CJ10 and R1), along with wildtype Canton-S (CS) controls . **(A)** Height (cm) climbed in 3 seconds (s) following commencement of negative geotaxis. Final sample size displayed on graph excludes flies that did not fall to bottom of vial. **(B)** Time taken to climb above the 4 cm target line. Final sample size displayed on graph B excludes flies that did not successfully complete the task and were classified as outliers based on Grubbs test ($P<0.05$). **(C)** Time taken (s) to initiate vertical movement following commencement of negative geotaxis, final sample size displayed on graph excludes outliers based on Iterative Grubbs test ($P<0.05$). Median and Interquartile range (IQR) values are shown. Whiskers represent the maximum and minimum non-outlier values. Black circles overlaying graphs represent all non-outlier data points.* $P< 0.05$, ** $P < 0.01$; *** $P < 0.001$; ns, not significant as determined by GLM analysis.

4.2.1.4 Discussion

AHC disease is characterised by a range of movement-related disorders (Mikati et al., 2021), thus locomotion (i.e., walking) was studied in the *ATPα* mutants flies. This research revealed that flies heterozygous for the *ATPα CJ10* (p.Gly744Ser) mutation, equivalent to the human Gly755Ser AHC mutation (Heinzen et al., 2014), and the *R1* null (p. Ile905Trpfs*8) mutation (Ashmore et al., 2009; Öztürk-Çolak et al., 2024). display defective locomotor function. Previously, climbing in young *CJ10/TM6* and *R1/TM3* mutants by qualitative measure was reported as normal (Ashmore et al., 2009). However, in this research quantitative measure of vertical movement suggests otherwise. Climbing performance of 2-3-day old CS-*CJ10*/+ and CS-*R1*/+ mutant flies was characterised by a shorter height climbed in 3 s (Figure 13A), longer time period required to climb above target line (Figure 13B) and a longer climbing latency relative to the wildtype CS strain (Figure 13C). Height climbed by CS control, CS-*CJ10*/+ and CS-*R1*/+ mutant flies in 3 s was 4.48 cm, 2.16 cm and 2.26 cm respectively(Figure 13A). Time taken by to climb above the target line by CS control, CS-*CJ10*/+ and CS-*R1*/+ mutant flies was 2.67 s, 4.37 s and 4.48 s (Figure 13B). The time taken by for CS, CS-*CJ10*/+ and CS-*R1*/+ males to initiate vertical movement was 0.88 s, 2.36 s and 1.68 s respectively and for CS, CS-*CJ10*/+ and CS-*R1*/+ females, time taken was 0.50 s, 1.38 s and 1.19 s respectively (Figure 13C). A recent study reported that females typically have a greater climbing ability than males (Zhong et al., 2022). This was indicated in this research in regard to time taken for flies to initiate vertical movement following startling, irrespective of genotype females were significantly quicker to begin climbing than males (Figure 13C). In relation to genotype, this sex difference was only statistically different with the CS-*CJ10*/+ genotype (Figure 13C). The ability of *ATPα* mutant flies to perform the climbing task in this research corroborates the previous report of intact gross locomotion in mutant flies (Ashmore et al., 2009). The present findings

also validate the previous report of young wildtype fly strains climbing a height of 4-5 cm in 3 s (Nichols et al., 2012). More importantly, the results from the assay indicate that the *CJ10*/+ and *R1*/+ mutations affects walking speed therefore suggesting that normal function of the d-NKA α-subunit is important for modulating speed of motion in flies. It is unlikely that a defect in speed of movement of *ATP*α mutants is a muscle atrophy-related phenotype as previous study of the muscle tissue in aged *ATP*α mutants showed no signs of abnormalities (Ashmore et al., 2009). Climbing defects in *Drosophila* have been associated with degeneration of dopaminergic neurons in the fly brain (Riemensperger et al., 2013), however it is unlikely that degeneration is responsible for the *ATP*α-induced decline in climbing performance of flies as signs of neurodegeneration were observed only in aged *CJ10*/+ and *R1*/+ mutant flies (Ashmore et al., 2009). In the present study, negative geotaxis was performed on 2-3-day old flies. The observed phenotype is likely due to impaired d-NKA α activity causing abnormal depolarization of mushroom body (MB)-associated neurons (i.e., Kenyon cells, dopaminergic neurons and MB output neurons) which have been shown to underpin the regulation of startled-induced locomotion such as negative geotaxis (Sun et al., 2018). This proposed mechanism is supported by the report of partial loss-of-function in the d-NKA pump in both *CJ10*/+ and *R1*/+ mutants (Ashmore et al., 2009) and reports of the activation of Kenyon cells, a type of interneuron, which lead to a reduction in startle-induce climbing performance in *Gal4*/*UAS* flies expressing a heat-induced cation channel (*dTrpA1*) in the mushroom body (Riemensperger et al., 2013; Sun et al., 2018). It is understood that animals modulate their locomotor speed through processing visual information (Creamer et al., 2018). It is plausible that the slowness in these *ATP*α mutants may also be attributed to insufficient d-NKA pump activity affecting the normal function of lamina neurons (L1, L2 L3 and L4) in the visual system which process visual information from the photoreceptors were reported to contribute to walking speed (Silies

et al., 2013). Moreover, neuronal d-NKA pump activity has been implicated in in visual signaling as knockdown of the *ATPα* and the neuron-specific *β*-subunit in photoreceptors lead to blindness in flies (Luan et al., 2014). Another possible explanation for slowness in flies could be related to sustained activation of serotonergic neurons in the fly ventral nerve cord (VNC) as a result of impaired d-NKA *α* activity. This is proposed as serotonergic (5-HT) neurons are reported to extensively innervate the network of nerves in fly legs, and optogenetics activation of this neuron population in the VCN reveal coordinated but reduced speed in free walking flies (Howard et al., 2019).

4.2.2 General Locomotor Activity in *ATP*α mutants

4.2.2.1 Activity in 24 h Cycle

4.2.2.1.1 Males

In Zantiks system, the total distance travelled during a 24 h period was assessed as a measure of general locomotor activity in young *ATP*α mutant males. No significant difference was found among age-matched CS control, CS-*CJ10*/+ and CS-*R1*/+ mutant males (Table 39). The median distance travelled by CS control, CS-*CJ10*/+ and CS-*R1*/+ mutant males was 35,396 mm (IQR: 13,287-48,827 mm), 26,263 mm (IQR: 19,839-33,119 mm) and 27,475 mm (IQR: 15,792-33,928 mm) respectively (Figure 14E). The results indicate no deficit in general locomotor activity of CS-*CJ10*/+ and CS-*R1*/+ mutant males via measure of activity in a 24 h period.

Table 39. GLM analysis of the total distance travelled in 24 h by *ATPα* mutants and WT control males.

	Data	Explanatory Variable(s)	Test statistic	df	*P*-value
GLM	All fly strains	Genotype	1.9498	2, 88	0.1484

4.2.2.1.2 Females

In Zantiks system, the total distance travelled during a 24 h period was assessed as a measure of general locomotor activity in young *ATP*α mutant females. Distance travelled in 24 h by *ATP*α mutant and CS control females was affected by genotype (Table 40). Post-hoc comparisons revealed distanced travelled by CS-*R1*/+ mutant females was significantly shorter than CS control females (Table 40, Figure 14F). Meanwhile, no significant difference was found between CS control and CS-*CJ10*/+ mutant females or between *ATP*α mutant females (Table 40, Figure 14F). The median distance travelled by age-matched CS control, CS-*CJ10*/+ and CS-*R1*/+ mutant females was 19,534 mm (IQR: 11,185 -28,949 mm), 17,962 mm (IQR: 11,069-22,167 mm) and 14,660 mm (IQR: 9,589-18,606 mm) respectively (Figure 14F). The results indicate deficit in general locomotion of CS-*R1*/+ mutant females via measure of activity during the day.

Table 40. GLM analysis of the total distance travelled in 24 h by ATPα mutants and WT control females. Post-hoc results were corrected for multiple testing using Holm-Bonferroni method, where P < 0.05 is indicated in bold.

	Data	Explanatory Variable(s)	Test statistic	df	*P*-value
GLM	All fly strains	Genotype	4.8931	2, 93	**0.009539**
Post-hoc Test	CS-*CJ10*/+ vs CS	Genotype	-1.835	93	0.1394
	CS-R/+1 vs CS	Genotype	-3.010	93	**0.0101**
	CS-*CJ10*/+ vs CS-*R1*/+	Genotype	-1.279	93	0.2042

4.2.2.2 Activity in Light Phase

4.2.2.2.1 Males

In Zantiks system, the total distance travelled during a 12 h light phase was assessed as an additional measure of general locomotor activity in young *ATP*α mutant males. No significant difference was found among age-matched CS control, CS-*CJ10*/+ and CS-*R1*/+ mutant males (Table 41). The median distance travelled by CS control, CS-*CJ10*/+ and CS-*R1*/+ mutant males was 17,385 mm (IQR: 9,211-24,202 mm), 13,497 mm (IQR: 10,459-16,779 mm) and 15,946 mm (IQR: 10,825-19,046 mm) respectively (Figure 14E). The results indicate no deficit in general locomotor activity of CS-*CJ10*/+ and CS-*R1*/+ mutant males via measure of activity during dark phase.

Table 41. GLM analysis of the total distance travelled in the 12 h light phase by *ATPα* mutants and WT control males.

	Data	Explanatory Variable(s)	Test statistic	df	*P*-value
GLM	All fly strains	Genotype	2.1527	2, 88	0.1222

4.2.2.2.2 Females

In Zantiks system, the total distance travelled during a 12 h light phase was assessed as an additional measure of general locomotor activity in young *ATP*α mutant females. Distance travelled in light phase by *ATP*α mutant and CS control females was affected by genotype (Table 42). Post-hoc comparisons revealed distanced travelled by both CS-*CJ10*/+ and CS-*R1*/+ mutant females was significantly shorter than CS control females (Table 42, Figure 14F). Meanwhile, no significant difference was found between *ATP*α mutant females (Table 42, Figure 14F). The median distance travelled by age-matched CS control, CS-*CJ10*/+ and CS-*R1*/+ mutant females was 12,404 mm (IQR: 9,331-

19,498 mm), 10,127 mm (IQR: 6,786-12,861 mm) and 9,208 mm (IQR: 6,778-10,566 mm) respectively (Figure 14F). The results indicate deficit in general locomotion of CS-*CJ10*/+ and CS-*R1*/+ mutant females via measure of activity during light phase.

Table 42. GLM analysis of the total distance travelled in the 12 h light period by *ATPα* mutants and WT control females. Post-hoc results were corrected for multiple testing using Holm-Bonferroni method, where P < 0.05 is indicated in bold.

	Data	Explanatory Variable(s)	Test statistic	df	*P*-value
GLM	All fly strains	Genotype	6.5956	2, 91	**0.002114**
Post-hoc Test	CS-*CJ10*/+ vs CS	Genotype	-2.749	92	**0.0144**
	CS-R/+1 vs CS	Genotype	-3.235	92	**0.0051**
	CS-*CJ10*/+ vs CS-*R1*/+	Genotype	-0.558	92	0.5783

4.2.2.3 Activity in Dark Phase

4.2.2.3.1 Males

In Zantiks system, the total distance travelled during a 12 h dark phase was assessed as an additional measure of general locomotor activity in young *ATP*α mutant males. No significant difference was found among age-matched CS control, CS-*CJ10*/+ and CS-*R1*/+ mutant males (Table 43). The median distance travelled by CS control, CS-*CJ10*/+ and CS-*R1*/+ mutant males was 17,894 mm (IQR: 6,482-22,770 mm), 13,109 mm (IQR: 9,359-16,244 mm) and 11,482 mm (IQR: 5,726-17,564 mm) respectively (Figure 14E). The results indicate no deficit in general locomotor activity of CS-*CJ10*/+ and CS-*R1*/+ mutant males via measure of activity during dark phase.

Table 43. GLM analysis of the total distance travelled in the 12 h dark phase by *ATPα* mutants and WT control males.

	Data	Explanatory Variable(s)	Test statistic	df	*P*-value
GLM	All fly strains	Genotype	1.6951	2, 88	0.1895

4.2.2.3.2 Females

In Zantiks system, the total distance travelled during a 12 h dark phase was assessed as an additional measure of general locomotor activity in young *ATP*α mutant females. No significant difference was found among age-matched CS control, CS-*CJ10*/+ and CS-*R1*/+ mutant females (Table 44). The median distance travelled by CS control, CS-*CJ10*/+ and CS-*R1*/+ mutant females was 8,067 mm (IQR: 2,029-11,373 mm), 6,687 mm (IQR: 3,450-8,576 mm) and 4,857 mm (IQR: 2,931-6,775 mm) respectively (Figure 14F). The results indicate no deficit in general locomotion of CS-*CJ10*/+ and CS-*R1*/+ mutant females via measure of activity during dark phase.

Table 44. GLM analysis of the total distance travelled in the 12 h dark phase by *ATPα* mutants and WT control males.

	Data	Explanatory Variable(s)	Test statistic	df	*P*-value
GLM	All fly strains	Genotype	2.4289	2, 91	0.09383

4.2.2.4 Locomotor Response to Light Changes

4.2.2.4.1 Males

In Zantiks system, the difference in distance travelled 10 minutes before and after light changes was assessed as measure of locomotor response to lighting changes in young *ATP*α mutant and CS control males. No significant difference was found among the

change in distance of *ATP*α mutant and CS control males during the transition from dark to light (i.e., dawn) or light to dark (i.e., dusk) (Table 45, Figure 14G). The median change in distance by CS control, CS-*CJ10*/+ and CS-*R1*/+ mutant males during dawn was 213.7 mm (IQR: 79.4-425.1 mm), 120.4 mm (IQR: 25.2-291.1 mm) and 221.1 mm (IQR: 104.9-410.3 mm) respectively (Figure 14G). The median change in distance by CS control, CS-*CJ10*/+ and CS-*R1*/+ mutant males during dusk was 110.8 mm (IQR: 52.7-438.5 mm), 157.2 mm (IQR: 8.525-386.7 mm) and 337.9 mm (IQR: 70.1-560.2 mm) respectively (Figure 14G). The results indicate that the CS-*CJ10*/+ and CS-*R1*/+ mutations have no significant impact on male locomotor response to light changes.

Table 45. Kruskal Wallis analysis of the locomotor response in *ATPα* mutants and WT control males during lighting changes.

	Data	Explanatory Variable(s)	Test statistic	df	*P*-value
Dawn (dark to light transition)					
KW	All fly strains	Genotype	1.980	2	0.3715
Dusk (light to dark transition)					
KW	All fly strains	Genotype	3.244	2	0.1975

4.2.2.4.2 Females

In Zantiks system, the difference in distance travelled 10 minutes before and after light changes was assessed as measure of locomotor response to lighting changes in young *ATP*α mutant and CS control females. A significant effect of genotype was found among the locomotor response of *ATP*α mutant and CS control females during the transition from dark to light (i.e., dawn) (Table 46). Post-hoc comparisons revealed locomotor response of CS-*R1*/+ mutant females to dawn was significantly higher than CS-*CJ10*/+

mutant females, but not relative to CS control females (Table 46, Figure 14H). Meanwhile no significant difference was found between CS-*CJ10*/+ mutant and CS controls females (Table 46, Figure 14H). The median change in distance by CS control, CS-*CJ10*/+ and CS-*R1*/+ mutant females during dawn was 46.3 mm (IQR: -17.7-115.6 mm), 29.6 mm (IQR: -29.4-73.62 mm) and 117.2 mm (IQR: 56.3-154.4 mm) respectively (Figure 14H). Additionally, no significant difference was found among the locomotor response of *ATP*α mutant and CS control females during the transition from light to dark (i.e., dusk) (Table 46, Figure 14H).The mean change in distance by CS control, CS-*CJ10*/+ and CS-*R1*/+ mutant females during dusk was 51.0 mm (IQR: -12.3-138.4 mm), 98.6 mm (IQR: 18.21-190.1 mm) and 70.5 mm (IQR: -5.3-126.9 mm) respectively (Figure 14H). The results indicate that the *CJ10*/+ and *R1*/+ mutations do not have a significant impact on female locomotor response to light changes.

Table 46. GLM analysis of the locomotor response in *ATPα* mutants and WT control females during lighting changes. Post-hoc results were corrected for multiple testing using Dunn's method, where P < 0.05 is indicated in bold.

	Data	Explanatory Variable(s)	Test statistic	df	*P*-value
Dawn (dark to light transition)					
GLM	All fly strains	Genotype	4.7098	2, 91	**0.01131**
Post-hoc Test	CS-*CJ10*/+ vs CS	Genotype	1.196	91	0.2347
	CS-R/+1 vs CS	Genotype	-1.838	91	0.1385
	CS-*CJ10*/+ vs CS-*R1*/+	Genotype	-3.049	91	**0.009**
Dusk (light to dark transition)					
GLM	All fly strains	Genotype	1.1249	2, 91	0.3292

MALES **FEMALES**

(A)

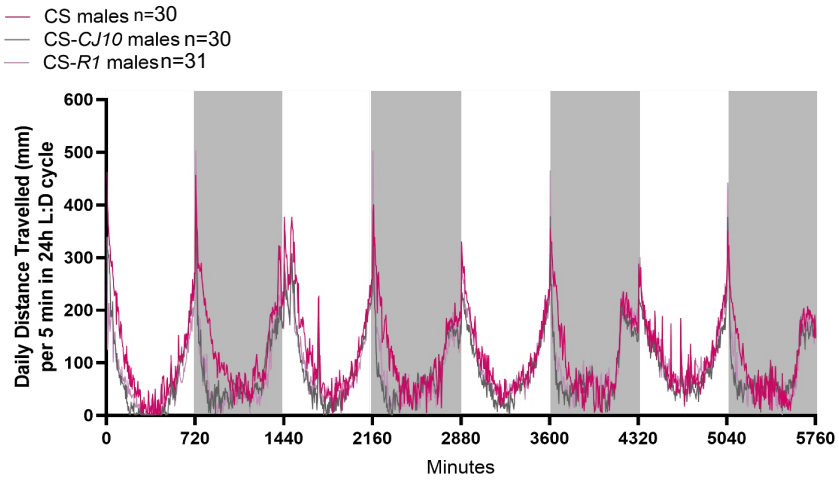

(B)

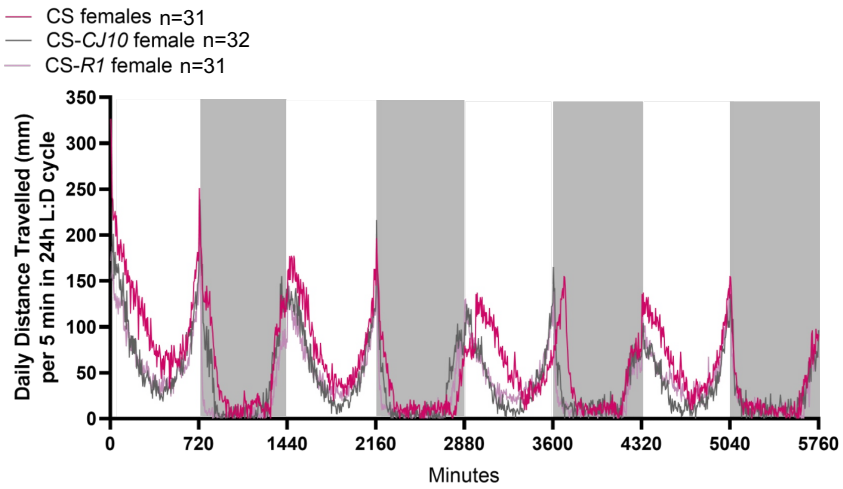

(C)

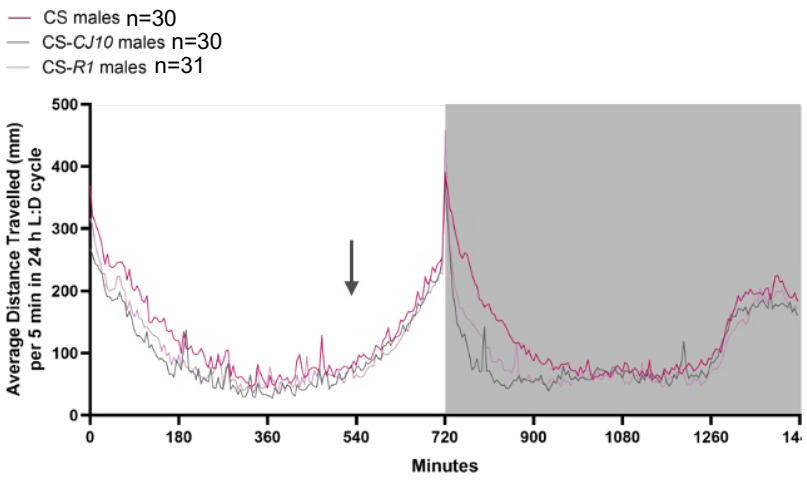

(D)

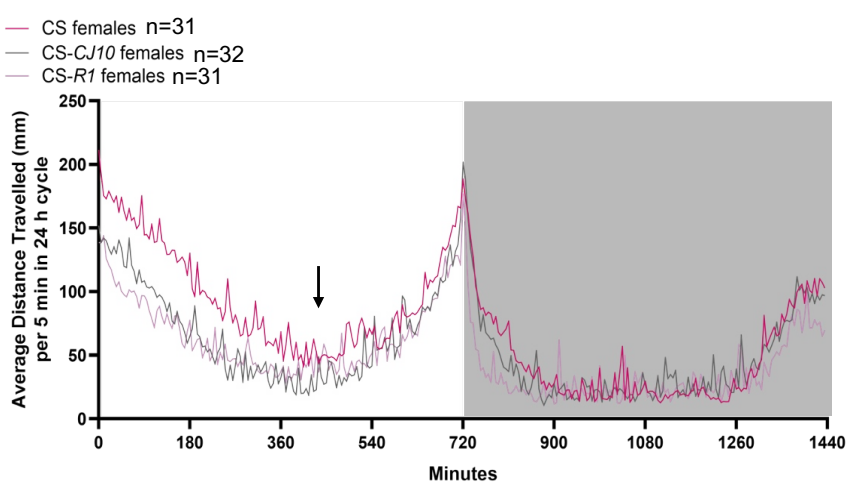

(E)

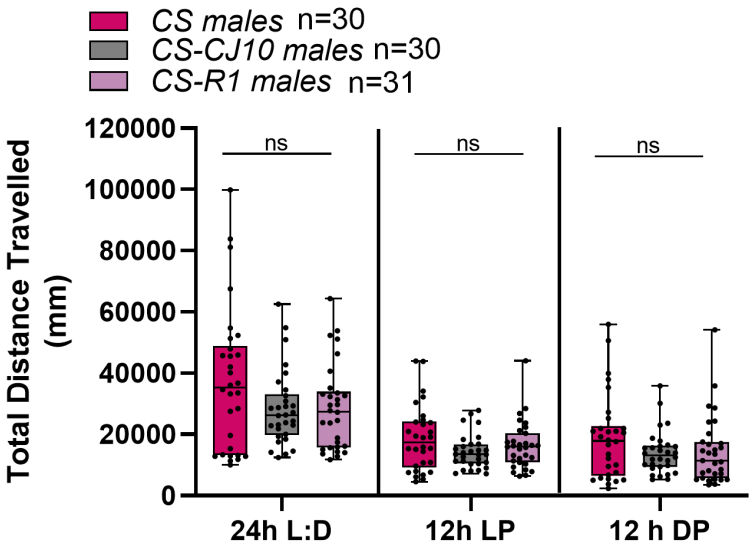
CS males n=30
CS-CJ10 males n=30
CS-R1 males n=31
Total Distance Travelled (mm)
120000
100000
80000
60000
40000
20000
0
ns
ns
ns
24h L:D
12h LP
12 h DP

(F)

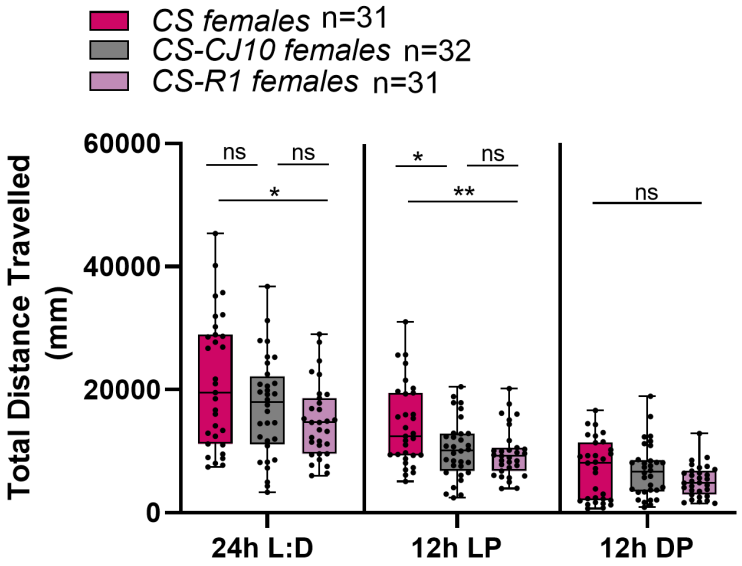
CS females n=31
CS-CJ10 females n=32
CS-R1 females n=31
Total Distance Travelled (mm)
60000
40000
20000
0
ns
ns
*
*
ns
**
ns
24h L:D
12h LP
12h DP

(G)

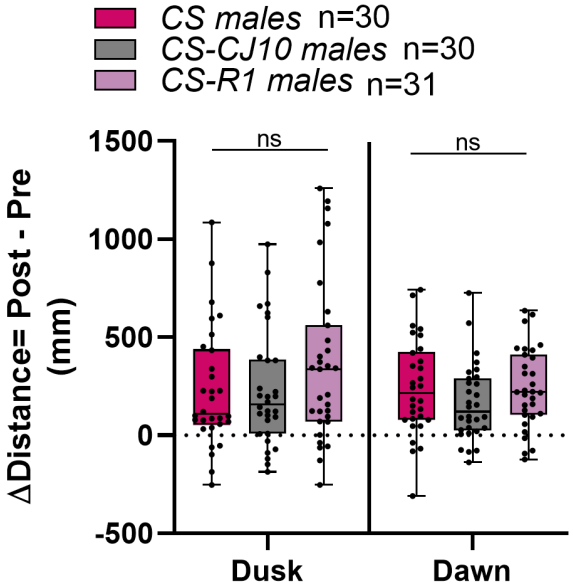
CS males n=30
CS-CJ10 males n=30
CS-R1 males n=31
ΔDistance= Post - Pre (mm)
1500
1000
500
0
-500
ns
ns
Dusk
Dawn

(H)

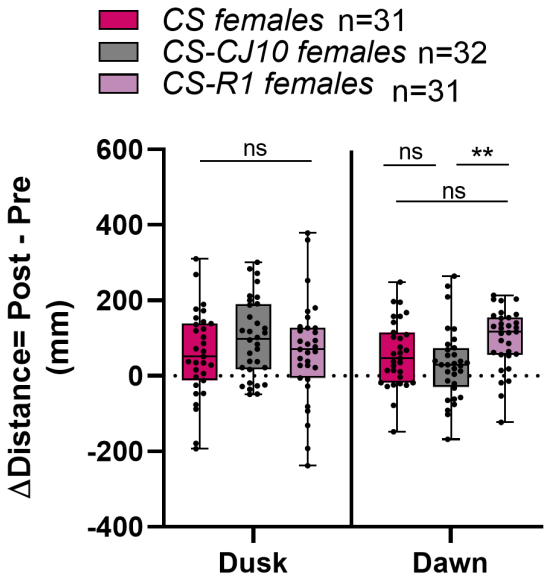
CS females n=31
CS-CJ10 females n=32
CS-R1 females n=31
ΔDistance= Post - Pre (mm)
600
400
200
0
-200
-400
ns
ns
ns
**
Dusk
Dawn

Figure 14. General locomotor behaviour over four days in the Zantiks system in young (3-4-day old) virgin male and female *D. melanogaster* heterozygous for *ATPα* mutant alleles (CJ10 and R1), along with wildtype Canton-S (CS) controls. Day-wise activity trace represents the mean distance travelled in millimetre (mm) by >30 individual males **(A)** and females **(B)** in 5-minute (min) bins, over 4 consecutive days of a 12-hour light (white background) and 12-hour dark (shaded background) phases. Activity trace average across four days to present the mean distance travelled by >30 individual males **(C)** and females **(D)** in 5 min bins within a 24-hour light and dark (24h L:D) cycle. The arrow in C-D represents the beginning of anticipatory increase in locomotive activity. Total distance travelled in a 24-hour light and dark cycle, 12-hour light and 12-hour dark phase by >30 individual males **(E)** and females **(F)** across 4 full days. Comparison of average change in distance travelled (Δ) 10 min before (Pre) and 10 min after (Post) the transition from dark to light phase (dawn) and light to dark phase (dusk) by males **(G)** and females **(H)**. Change was calculated by the distance travelled 10 min after lighting transition minus distance travelled 10 min before lighting transition, average across three days. The data in E-H shows median, IQR with whisker representing the maximum and minimum non-outlier values. The black circles overlaying E-H graphs represent individual mean values, each calculated from 4 days of data per fly. Final sample size displayed on graph excludes flies that died at any point during the 4-day experiment. Significant difference is represented by asterisks * $P < 0.05$; ** $P < 0.01$; ; *** $P < 0.001$; ns, not significant as determined by GLM analysis (Fig. E, F and H) or Kruskal Wallis analysis (Fig. G).

4.2.2.5 Discussion

This research reports the use of an automated video tracking system as an optimization method to measure general locomotor activity of *ATPα* mutants flies in an open field arena. The method of tracking flies to study locomotor behaviour is acknowledged as a valid assay option to study locomotor behaviour (Donelson et al., 2012; Scaplen et al., 2019; Milojevic et al., 2024). In this research, the earlier use of the *Drosophila* Activity Monitor (DAM) system which characterises fly locomotor activity by the frequency of infrared beam breaks as they walk across a glass tube (Pfeiffenberger et al., 2010) showed that both 3-4-day old *ATPα* mutant males and female exhibited low levels of activity relative to age-matched CS control flies (data not shown). However, could not be sure if this was a true representation of the general locomotor behaviour in *ATPα* mutants as the climbing assay carried out in this research indicated flies are slow thus there is a possibility that flies were unable to carry out task of moving up and down the glass vial. Moreover, the DAM system does not account for fly preference to spend more time at one end of the tube thus underestimating locomotor activity and overestimating sleep behaviour (Donelson et al., 2012; Scaplen et al., 2019). The use of a tracking showed reduced locomotor activity in *ATPα* mutant females only (Figure 14F). Although wildtype males generally showed higher activity than both CS-*CJ10*/+ and CS-*R1*/+ mutant males, no significant difference in distance travelled during a 12 h light: 12 h dark cycle was observed (Figure 14E). This suggests sex-specific effects of the *ATPα* mutations on general locomotor behaviour. In this research, males and females were assayed separately due to reports of sex differences in *Drosophila* locomotor activity (Helfrich-Förster, 2000; Videlier et al., 2019), so the study did not explore possible genotype-by-sex interaction. Sex differences in this study was indicated by virgin males travelling a total distance in a 24 h cycle that was 1.5x greater than virgin females regardless of genotype (Figure 14E and F). In females, a marked reduction in

activity was observed in CS-*CJ10*/+ and CS-*R1*/+ mutants relative to CS controls during the 12 h light phase (Figure 14F). The median distance travelled by *ATPα* mutant females in the light phase differed by >2m . Waking activity levels are considered a useful measure of hypo/hyperactivity in flies (Wu et al., 2008). This result suggests that CS-*CJ10*/+ and CS-*R1*/+ mutant females are hypoactive, a phenotype that has also been reported in both male and female AHC E815K mice (Helseth et al., 2018). Further, the indication of hypoactivity in young (3-4 day old) *ATPα* mutant females in this study corroborates the previous report of the diminished locomotor ability of older (9-11 day old) *ATPα* mutant females using the DAM system (Ashmore et al., 2009). This highlights the ability of the tracking system approach to generate reproducible results and suggests the hypoactive phenotype exhibited by *ATPα* mutant females are not age-dependent. Hypoactivity in *Drosophila* has been associated with deficiency in the neurotransmitter dopamine in the CNS. This was evidenced by visual tracking of young dopamine-deficient flies exhibiting reduced activity (Riemensperger et al., 2011). Thus, the phenotype observed in *ATPα* mutant females might be explained by a decrease in dopamine signaling resulting from insufficient activity of mutant d-NKA α to maintain ion balance in dopaminergic neurons, although further research would be required to investigate this. Moreover, the assay suggests that circadian clock function is normal in both *ATPα* mutant males and females. This is indicated by a bimodal locomotive rhythm (i.e., a peak in the morning and evening) an increase in activity around the 3 h mark prior to lighting changes (Figure 14C and 14D, arrows), showing that mutants are able to anticipate morning and evening periods (Chiu et al., 2010; Mazzotta et al., 2020). Normal circadian patterns in *CJ10* and *R1* mutants have previously been reported in Ashmore et al. (2009) work.

4.2.3 Sleep in *ATP*α mutants

4.2.3.1 Total Sleep Time in a 24 h Cycle

4.2.3.1.1 Males

In Zantiks system, the total duration of sleep in a 24 h period was assessed as a measure of sleep behaviour in young *ATP*α mutant males. No significant difference was found among *ATP*α mutant and CS control males (Table 47). The median duration of total sleep in 24 h by CS control, CS-*CJ10*/+ and CS-*R1*/+ mutant males was 183.8 min (IQR: 85.0-433.4 min), 259.4 min (IQR: 186.3-386.3 min) and 232.5 min (IQR: 130.0-346.3 min) respectively (Figure 15E). The results indicate no aberrant sleep behaviour in CS-*CJ10*/+ and CS-*R1*/+ mutant males via measure of total sleep time in the 24 h period.

Table 47. GLM analysis of the total sleep time of *ATPα* mutants and WT control males in 24 h.

	Data	Explanatory Variable(s)	Test statistic	df	*P*-value
GLM	All fly strains	Genotype	0.4594	2, 88	0.6332

4.2.3.1.2 Females

In Zantiks system, the total duration of sleep in a 24 h period was assessed as a measure of sleep behaviour in young *ATP*α mutant females. No significant difference was found among *ATP*α mutant and CS control females (Table 48). The median duration of total sleep in 24 h by CS control, CS-*CJ10*/+ and CS-*R1*/+ mutant females was 355 min (IQR: 107.5-580.0 min), 432.5 min (IQR: 285.9-629.7 min) and 336.3 min (IQR: 232.5-483.8 min) respectively (Figure 15F). The result indicate no aberrant sleep behaviour in

CS-*CJ10*/+ and CS-*R1*/+ mutant females via measure of total sleep time in the 24 h period.

Table 48. GLM analysis of the total sleep time of *ATPα* mutants and WT control females in 24 h.

	Data	Explanatory Variable(s)	Test statistic	df	*P*-value
GLM	All fly strains	Genotype	0.66782	2, 91	0.3147

4.2.3.2 Total Sleep Time in the Light Phase

4.2.3.2.1 Males

In Zantiks system, the total duration of sleep in a 12 h light period was assessed as a measure of sleep behaviour in young *ATP*α mutant males. A significant effect of genotype was found among *ATP*α mutant and CS control male (Table 49). Post-hoc comparisons showed duration of sleep during the light phase by CS-*R1*/+ mutant males was significantly shorter than by CS-*CJ10*/+ mutants but not CS control males (Table 49, Figure 15E). Meanwhile, no significant difference was found between CS-*CJ10*/+ mutants and CS control males (Table 49 Figure 15E). The median duration of total sleep by CS control, CS-*CJ10*/+ and CS-*R1*/+ mutant females during 12 h light phase was 73.13 min (IQR: 33.8-159.4 min), 115.6 min (IQR: 65.9-145.0 min) and 65.0 min (IQR: 40.0-100.0 min) respectively (Figure 15E). Relative to CS control males, the results indicate no aberrant sleep behaviour in CS-*CJ10*/+ and CS-*R1*/+ males via measure of total sleep time during the 12 h light phase.

Table 49. GLM analysis of the total sleep time of *ATPα* mutants and WT control males in the 12 h light phase. Post-hoc results were corrected for multiple testing using Holm-Bonferroni method, where P < 0.05 is indicated in bold.

	Data	Explanatory Variable(s)	Test statistic	df	*P*-value
GLM	All fly strains	Genotype	4.2984	2, 88	**0.01659**
Post-hoc Test	CS-*CJ10* vs CS	Genotype	2.523	88	0.5907
	CS-R1 vs CS	Genotype	2.178	88	0.0642
	CS-*CJ10* vs CS-*R1*	Genotype	2.695	88	**0.0253**

4.2.3.2.2 Females

In Zantiks system, the total duration of sleep in a 12 h light period was assessed as a measure of sleep behaviour in young *ATP*α mutant females. A significant effect of genotype was found among *ATP*α mutant and CS control female (Table 50). Post-hoc comparisons revealed total sleep time in light phase by CS-*CJ10*/+ mutant females was significantly longer than by CS-*R1*/+ mutants and CS control females (Table 50, Figure 15F). Meanwhile, no significant difference was found between CS-*R1*/+ mutants and CS control females (Table 50, Figure 15F). The median duration of total sleep by CS control, CS-*CJ10*/+ and CS-*R1*/+ mutant females during 12 h light phase was 70.0 min (IQR: 19.7-148.4 min), 123.1 min (IQR: 77.2-211.3 min) and 82.5 min (IQR: 23.8-140.0 min) respectively (Figure 15F). The results indicate aberrant sleep behaviour in CS-*CJ10*/+ females via measure of total sleep time during the 12 h light phase.

Table 50. GLM analysis of the total sleep time of *ATPα* mutants and WT control females in the 12 h light phase. Post-hoc results were corrected for multiple testing using Holm-Bonferroni method, where P < 0.05 is indicated in bold.

	Data	Explanatory Variable(s)	Test statistic	df	*P*-value
GLM	All fly strains	Genotype	4.5166	2, 91	**0.01348**
Post-hoc Test	CS-*CJ10*/+ vs CS	Genotype	2.523	91	**0.0132**
	CS-R1/+ vs CS	Genotype	0.241	91	0.8368
	CS-*CJ10*/+vs CS-*R1*/+	Genotype	2.313	91	**0.0159**

4.2.3.3 Total Sleep Time in the Dark Phase

4.2.3.3.1 Males

In Zantiks system, the total duration of sleep in a 12 h dark period was assessed as a measure of sleep behaviour in young *ATP*α mutant males. No significant difference was found among *ATP*α mutant and CS control males (Table 51). The median duration of total sleep by CS control, CS-*CJ10*/+ and CS-*R1*/+ mutant males during dark phase was 121.3 min (IQR: 39.1-209.1 min), 199.4 min (IQR: 91.9-238.1 min) and 150.0 min (IQR: 63.8-237.5 min) respectively (Figure 15E). The results indicate no aberrant sleep behaviour in CS-*CJ10*/+ and CS-*R1*/+ mutant females via measure of total sleep time during the 12 h dark phase.

Table 51. GLM analysis of the total sleep time in *ATPα* mutants and WT control males in the 12 h dark phase.

	Data	Explanatory Variable(s)	Test statistic	df	*P*-value
GLM	All fly strains	Genotype	0.9004	2, 88	0.4101

4.2.3.3.2 Females

In Zantiks system, the total duration of sleep in a 12 h dark period was assessed as a measure of sleep behaviour in young *ATP*α mutant females. No significant difference was found among *ATP*α mutant and CS control females (Table 52). The median duration of total sleep by CS control, CS-*CJ10*/+ and CS-*R1*/+ mutant females during dark phase was 278.8 min (IQR: 81.3-461.3 min), 308.8 min (IQR: 200.0-372.2 min) and 317.5 min (IQR: 221.3-403.8 min) respectively (Figure 15F). The result indicate no aberrant sleep behaviour in CS-*CJ10*/+ and CS-*R1*/+ mutant females via measure of total sleep time during the 12 h dark phase.

Table 52. GLM analysis of the total sleep time of *ATPα* mutants and WT control females in the 12 h dark phrase.

	Data	Explanatory Variable(s)	Test statistic	df	*P*-value
GLM	All fly strains	Genotype	0.0452	2, 91	0.9558

4.2.3.4 Sleep Bout Frequency in 24 h Cycle

4.2.3.4.1 Males

In Zantiks system, the total number of separate sleep periods in 24 h was assessed as an additional measure of sleep behaviour in young *ATP*α mutant males. No significant difference was found among *ATP*α mutant and CS control males (Table 53). The median number of sleep bouts by CS control, CS-*CJ10*/+ and CS-*R1*/+ mutant males in 24 h was 19 (IQR: 11-32), 23 (IQR: 19-30) and 21 (IQR: 14-29) bouts respectively (Figure 15G). The results indicate no aberrant sleep behaviour in CS-*CJ10*/+ and CS-*R1*/+ mutant males via measure of the total number of sleep bouts in the 24 h phase.

Table 53. GLM analysis of the number of sleep bouts of *ATPα* mutants and WT controls males in 24 h.

	Data	Explanatory Variable(s)	Test statistic	df	*P*-value
GLM	All fly strains	Genotype	0.5485	2, 88	0.5798

4.2.3.4.2 Females

In Zantiks system, the total number of separate sleep periods in 24 h was assessed as an additional measure of sleep behaviour in young *ATP*α mutant females. A significant effect of genotype was found among *ATP*α mutant and CS control female (Table 56). Post-hoc comparisons revealed number of sleep episodes in the 24h L:D cycle by CS-*CJ10*/+ and CS-*R1*/+ mutant females was significantly higher than by CS control females (Table 54, Figure 15H). Meanwhile, no significant difference was found between CS-*CJ10*/+ and CS-*R1*/+ mutant females (Table 54, Figure 15H). The median number of sleep bouts by CS control, CS-*CJ10*/+ and CS-*R1*/+ mutant females in 24 h was 24 (IQR 14-34), 31 (IQR: 25-34) and 32 (IQR: 22-39) bouts respectively (Figure 15H). The results indicate aberrant sleep behaviour in CS-*CJ10*/+ and CS-*R1*/+ mutant females via measure of the total number of sleep bouts in the 24 h phase.

Table 54. GLM analysis of the number of sleep bouts of *ATPα* mutants and WT controls females in 24 h. Post-hoc results were corrected for multiple testing using Holm-Bonferroni method, where P < 0.05 is indicated in bold.

	Data	Explanatory Variable(s)	Test statistic	df	*P*-value
GLM	All fly strains	Genotype	5.2986	2, 91	**0.006657**
	CS-*CJ10*/+ vs CS	Genotype	2.944	91	**0.0123**

Post-hoc Test	*CS-R1*/+ *vs* CS	Genotype	2.683	91	**0.0173**
	CS-*CJ10*/+vs CS-*R1*/+	Genotype	0.240	91	0.8111

4.2.3.5 Sleep Bout Frequency in the Light Phase

4.2.3.5.1 Males

In Zantiks system, the total number of separate sleep periods in 12 h light phase was assessed as an additional measure of sleep behaviour in young *ATP*α mutant males. No significant difference was found among *ATP*α mutant and CS control males (Table 55). The median number of sleep bouts by CS control, CS-*CJ10*/+ and CS-*R1*/+ mutant males in 12 h light phase was 8 (IQR: 4-15), 10 (IQR: 7-14) and 7 (IQR: 5-10) bouts respectively (Figure 15G). The results indicate no aberrant sleep behaviour in CS-*CJ10*/+ and CS-*R1*/+ mutant males via measure of the total number of sleep bouts during the 12 h light phase.

Table 55. GLM analysis of the number of sleep bouts of *ATPα* mutants and WT controls males in the 12 h light phase.

	Data	Explanatory Variable(s)	Test statistic	df	*P*-value
GLM	All fly strains	Genotype	2.9727	2, 88	0.05632

4.2.3.5.2 Females

In Zantiks system, the total number of separate sleep periods in 12 h light phase was assessed as an additional measure of sleep behaviour in young *ATP*α mutant females. A significant effect of genotype was found among *ATP*α mutant and CS control female (Table 56). Post-hoc comparisons revealed number of sleep episodes during the light phase by CS-*CJ10*/+ mutant females was significantly higher than by CS control

females (Table 56, Figure 15H). Meanwhile, no significant difference was found between CS-*R1*/+ mutant and CS control females or between CS-*CJ10*/+ and CS-*R1*/+ mutant females (Table 56, Figure 15H). The median number of sleep bouts by CS control, CS-*CJ10*/+ and CS-*R1*/+ mutant females in 12 h light phase was 8 (IQR: 3-13), 12 (IQR: 7-15) and 9 (IQR: 3-13) bouts respectively (Figure 15H). The results indicate aberrant sleep behaviour in CS-*CJ10*/+ females via measure of the total number of sleep bouts during the 12 h light phase.

Table 56. GLM analysis of the number of sleep bouts of *ATPα* mutants and WT controls females in the 12 h light phase. Post-hoc results were corrected for multiple testing using Holm-Bonferroni method, where P < 0.05 is indicated in bold.

	Data	Explanatory Variable(s)	Test statistic	df	*P*-value
GLM	All fly strains	Genotype	3.8539	2, 91	**0.02474**
Post-hoc Test	CS-*CJ10*/+ vs CS	Genotype	2.536	91	**0.0388**
	CS-R1/+ vs CS	Genotype	0.302	91	0.7632
	CS-*CJ10*/+ vs CS-*R1*/+	Genotype	2.231	91	0.0562

4.2.3.6 Sleep Bout Frequency in the Dark Phase

4.2.3.6.1 Males

In Zantiks system, the total number of separate sleep periods in 12 h dark phase was assessed as an additional measure of sleep behaviour in young *ATP*α mutant males. No significant difference was found among *ATP*α mutant and CS control males (Table 57). The median number of sleep bouts by CS control, CS-*CJ10*/+ and CS-*R1*/+ mutant males in 12 h dark phase was 12 (IQR: 4-17), 14 (IQR: 8-17) and 16 (IQR: 7-20) bouts respectively (Figure 15G). The results indicate no aberrant sleep behaviour in CS-

CJ10/+ and CS-*R1*/+ mutant males via measure of the total number of sleep bouts during the 12 h dark phase.

Table 57. GLM analysis of the number of sleep bouts of *ATPα* mutants and WT controls males in the 12 h dark phase.

	Data	Explanatory Variable(s)	Test statistic	df	*P*-value
GLM	All fly strains	Genotype	0.7348	2, 88	0.4825

4.2.3.6.2 Females

In Zantiks system, the total number of separate sleep periods in 12 h dark phase was assessed as an additional measure of sleep behaviour in young *ATP*α mutant females. A significant effect of genotype was found among *ATP*α mutant and CS control female (Table 58). Post-hoc comparisons revealed number of sleep bouts during the dark phase by CS-*R1*/+ and *CJ10*/+ mutant females was significantly higher than by CS control females (Table 58, Figure 15H). Meanwhile, no significant difference was found between CS-*CJ10*/+ and CS-*R1*/+ mutant females (Table 58, Figure 15H). The median number of sleep bouts in 24 h by CS control, CS-*CJ10*/+ and CS-*R1*/+ mutant females was 17 (IQR:9-21), 19 (IQR: 16-21) and 21 (IQR: 19-26) respectively (Figure 15H). The results indicate aberrant sleep behaviour in CS-*R1*/+ mutant females via measure of the total number of sleep bouts during the 12 h dark phase.

Table 58.GLM analysis of the number of sleep bouts of *ATPα* mutants and WT controls females in the 12 h dark phase. Post-hoc results were corrected for multiple testing using Holm-Bonferroni method, where P < 0.05 is indicated in bold.

	Data	Explanatory Variable(s)	Test statistic	df	*P*-value

GLM	All fly strains	Genotype	9.2921	2, 91	**0.0002127**
Post-hoc Test	CS-*CJ10*/+ vs CS	Genotype	2.477	91	**0.0302**
	CS-R1/+ vs CS	Genotype	4.296	91	**0.0001**
	CS-*CJ10*/+ vs CS-*R1*/+	Genotype	1.853	91	0.0672

4.2.3.7 Sleep Bout Length in 24 h Cycle

4.2.3.7.1 Males

In Zantiks system, the length of separate sleep periods in a 24 h period was assessed as an additional measure of sleep behaviour in young *ATP*α mutant males. A significant effect of genotype was found among *ATP*α mutant and CS control males (Table 59). Post-hoc comparisons showed the length of sleep episodes in 24 h by CS-*R1*/+ mutant males was significantly shorter than CS-*CJ10*/+ mutant males (Table 59, Figure 15I). Meanwhile, no significant difference was found between *ATP*α mutants and CS control males (Table 59, Figure 15I). The median length of sleep bouts in 24 h by CS control, CS-*CJ10*/+ and CS-*R1*/+ mutant males was 20.4 min (IQR: 17.7-25.6 min), 21.4 min (19.9-25.2 min) and 18.45 (16.6-20.5 min) min respectively (Figure 15I). Relative to CS control males, the results indicate no aberrant sleep behaviour in CS-*CJ10*/+ and CS-*R1*/+ males via measure of the length of sleep bouts in the 24 h phase.

Table 59. GLM analysis of the length of sleep bouts of *ATPα* mutants and WT controls males in 24 h. Post-hoc results were corrected for multiple testing using Holm-Bonferroni method, where *P* < 0.05 is indicated in bold.

	Data	Explanatory Variable(s)	Test statistic	df	*P*-value
GLM	All fly strains	Genotype	3.7125	2, 85	**0.02846**

Post-hoc Test	CS-*CJ10* vs CS	Genotype	0.531	85	0.5957
	CS-R1 vs CS	Genotype	2.044	85	0.0818
	CS-*CJ10* vs CS-*R1*	Genotype	2.562	85	**0.0313**

4.2.3.7.2 Females

In Zantiks system, the length of separate sleep periods in a 24 h period was assessed as an additional measure of sleep behaviour in young *ATP*α mutant females. A significant effect of genotype was found among *ATP*α mutant and CS control females (Table 60). Post-hoc comparisons showed the length of sleep episodes in 24 h by CS-*R1*/+ mutant females was significantly shorter than by CS-*CJ10*/+ mutant females (Table 60, Figure 15J). Meanwhile, no significant difference was found between *ATP*α mutants and CS control females (Table 60, Figure 15J). The median length of sleep bouts in 24 h by CS control, CS-*CJ10*/+ and CS-*R1*/+ mutant females was 27.2 min (15.3-32.2 min), 26.9 min (IQR: 20.1-34.6 min) and 21.9 min (16.9-24.5 min) respectively (Figure 15J). Relative to CS control females, the results indicate no aberrant sleep behaviour in CS-*CJ10*/+ and CS-*R1*/+ females via measure of the length of sleep bouts in the 24 h phase.

Table 60. GLM analysis of the length of sleep bouts of *ATPα* mutants and WT controls females in 24 h. Post-hoc results were corrected for multiple testing using Holm-Bonferroni method, where P < 0.05 is indicated in bold.

	Data	Explanatory Variable(s)	Test statistic	df	*P*-value
GLM	All fly strains	Genotype	3.5644	2, 91	**0.03233**
Post-hoc Test	CS-*CJ10*/+ vs CS	Genotype	0.764	91	04468
	CS-R1/+ vs CS	Genotype	1.834	91	0.1397

	CS-*CJ10*/+ vs CS-*R1*/+	Genotype	2.599	91	**0.0327**

4.2.3.8 Sleep Bout Length in the Light Phase

4.2.3.8.1 Males

In Zantiks system, the duration of separate sleep periods in a 12 h light phase was assessed as an additional measure of sleep behaviour in young *ATP*α mutant females. A significant effect of genotype was found among *ATP*α mutant and CS control female (Table 61). Post-hoc comparisons showed the mean length of sleep bouts during light by CS-*R1*/+ mutant males was significantly shorter than by CS-*CJ10*/+mutants and CS control males (Table 61, Figure 15I). Meanwhile, no significant difference was found CS-*CJ10*/+ and CS control males (Table 61, Figure 15I). The median length of sleep bouts by CS control, CS-*CJ10*/+ and CS-*R1*/+ mutant males in 12 h light phase was 9.6 min (IQR: 7.9-12 min), 10.2 min (IQR: 9.1-11.7 min) and 8.9 min (IQR: 7.4-9.9 min) respectively (Figure 15I). The results indicate aberrant sleep behaviour in CS-*R1*/+ mutant males via measure of sleep bout lengths during the 12 h light phase.

Table 61. GLM analysis of the length of sleep bouts of *ATPα* mutants and WT controls males in the 12 h light phase. Post-hoc results were corrected for multiple testing using Holm-Bonferroni method, where P < 0.05 is indicated in bold.

	Data	Explanatory Variable(s)	Test statistic	df	*P*-value
GLM	All fly strains	Genotype	4.2523	2, 85	**0.01737**
Post-hoc Test	CS-*CJ10* vs CS	Genotype	0.224	85	0.8230
	CS-R1 vs CS	Genotype	2.405	85	**0.0324**
	CS-*CJ10* vs CS-*R1*	Genotype	2.646	85	**0.0245**

4.2.3.8.2 Females

In Zantiks system, the duration of separate sleep periods in a 12 h light phase was assessed as an additional measure of sleep behaviour in young *ATP*α mutant females. A significant effect of genotype was found among *ATP*α mutant and CS control female (Table 62). Post-hoc comparisons revealed the length of sleep bouts by CS-*CJ10*/+mutant females was significantly longer than by CS-*R1*/+ mutants and CS control females during light phase (Table 62, Figure 15J). Meanwhile, no significant difference was found between CS-*R1*/+ mutants and CS control females (Table 62, Figure 15J). The median length of sleep bouts in CS control, CS-*CJ10*/+ and CS-*R1*/+ mutant females was 8.7 min (IQR: 6.1-12.0 min), 11.5 min (IQR: 8.7-14.5 min) and 8.6 min (IQR: 6.8-10.2 min) respectively (Figure 15J). The results indicate aberrant sleep behaviour in CS-*CJ10*/+ females via measure of sleep bout lengths during the 12 h light phase.

Table 62. GLM analysis of the length of sleep bouts of *ATPα* mutants and WT controls females in the 12 h light phase. Post-hoc results were corrected for multiple testing using Holm-Bonferroni method, where P < 0.05 is indicated in bold.

	Data	Explanatory Variable(s)	Test statistic	df	*P*-value
GLM	All fly strains	Genotype	5.3513	2, 90	**0.007508**
Post-hoc Test	CS-*CJ10*/+ vs CS	Genotype	2.456	90	**0.0281**
	CS-R1/+ vs CS	Genotype	0.359	90	0.8358
	CS-*CJ10*/+ vs CS-*R1*/+	Genotype	2.826	90	**0.0141**

4.2.3.9 Sleep Bout Length in the Dark Phase

4.2.3.9.1 Males

In Zantiks system, the duration of separate sleep periods in a 12 h dark phase was assessed as an additional measure of sleep behaviour in young *ATP*α mutant males. No significant effect was found among *ATP*α mutant and CS control males (Table 63, Figure 15I). The median length of sleep bouts by CS control, CS-*CJ10*/+ and CS-*R1*/+ mutant males in 12 h dark phase was 10.3 min (IQR: 8.9-13.7 min), 12 min (IQR: 10.5-14.4 min) and 10 min (IQR: 8.0-12.8 min) respectively (Figure 15I). The results indicate no aberrant sleep behaviour in *ATP*α mutant males by measure of sleep bout lengths during the 12 h dark phase.

Table 63. GLM analysis of the length of sleep bouts of *ATPα* mutants and WT controls males in the 12 h dark phase.

	Data	Explanatory Variable(s)	Test statistic	df	*P*-value
GLM	All fly strains	Genotype	2.5387	2, 86	0.08488

4.2.3.9.2 Females

In Zantiks system, the duration of separate sleep periods in a 12 h dark phase was assessed as an additional measure of sleep behaviour in young *ATP*α mutant females. A significant effect of genotype was found among *ATP*α mutant and CS control female (Table 64). Post-hoc comparisons revealed the median duration of sleep episodes in dark phase by CS-*R1*/+ mutant females was significantly shorter than CS control females (Table 64, Figure 15J). Meanwhile, no significant difference was found between CS-*CJ10*/+ mutants and CS control females or between CS-*CJ10*/+ and CS-*R1*/+ mutants females (Table 64, Figure 15J). The median duration of sleep bouts in CS control, CS-

CJ10/+ and CS-*R1*/+ mutant females was 17.1 min (8.9-21.7 min), 15.8 min (IQR: 11.6-20.4 min) and 12.7 min (IQR: 10.1-14.7 min) respectively (Figure 15J). The results indicate aberrant sleep behaviour in CS-*R1*/+ females via measure of sleep bout lengths during the 12 h dark phase.

Table 64. GLM analysis of the mean length of sleep bouts of *ATPα* mutants and WT controls females in the 12 h dark phase. Post-hoc results were corrected for multiple testing using Holm-Bonferroni method, where P < 0.05 is indicated in bold.

	Data	Explanatory Variable(s)	Test statistic	df	*P*-value
GLM	All fly strains	Genotype	4.1003	2, 91	**0.01972**
Post-hoc Test	CS-*CJ10*/+ vs CS	Genotype	0.542	91	0.5878
	CS-R1/+ vs CS	Genotype	2.671	91	**0.0227**
	CS-*CJ10*/+ vs CS-*R1*/+	Genotype	2.183	91	**0.0580**

4.2.3.10 Sleep Latency

4.2.3.10.1 Males

In Zantiks system, the time taken until first sleep bout following the switch to 12 h dark phase was assessed as an additional measure of sleep behaviour in young *ATP*α mutant males. A significant effect of genotype was found among *ATP*α mutant and CS control male (Table 65). Post-hoc comparisons revealed latency to sleep in CS-*CJ10*/+ mutant males was significantly shorter than in CS control males (Table 65, Figure 15K). Meanwhile, no significant difference was found between CS-*R1*/+ mutants and CS control males or between CS-*CJ10*/+ and CS-*R1*/+ mutant males (Table 65, Figure 15K). The median time taken for CS control, CS-*CJ10*/+ and CS-*R1*/+ mutant males to fall asleep was 181.3 min (IQR: 70.6-305.9 min), 80.0 min (IQR: 50.6-110.3 min) and

88.8 min (IQR: 47.5-191.3 min)respectively (Figure 15K). The results indicate aberrant sleep behaviour in CS-*CJ10*/+ mutant males by measure of sleep latency during the 12 h dark phase.

Table 65. GLM analysis of the sleep latency of *ATPα* mutants and WT control males in the 12 h dark phase. Post-hoc results were corrected for multiple testing using Holm-Bonferroni method, where P < 0.05 is indicated in bold.

	Data	Explanatory Variable(s)	Test statistic	df	*P*-value
GLM	All fly strains	Genotype	7.4436	2, 88	**0.001031**
Post-hoc Test	CS-*CJ10* vs CS	Genotype	3.005	88	**0.0080**
	CS-R1 vs CS	Genotype	1.714	88	0.1071
	CS-*CJ10* vs CS-*R1*	Genotype	1.930	88	0.1071

4.2.3.10.2 Females

In Zantiks system, the time taken until first sleep bout following the switch to 12 h dark phase was assessed as an additional measure of sleep behaviour in young *ATP*α mutant females. A significant effect of genotype was found among *ATP*α mutant and CS control female (Table 66). Post-hoc comparisons revealed latency to sleep in CS-*CJ10*/+ and CS-*R1*/+ mutant females was significantly shorter than in CS control females (Table 66, Figure 15M). Meanwhile, no significant difference was found CS-*CJ10*/+ and CS-*R1*/+ mutant females (Table 66, Figure 15M). The median time taken for CS control, CS-*CJ10*/+ and CS-*R1*/+ mutant females to fall asleep was 97.9 min (31.5-184.4 min), 71.6 min (IQR: 45.3-94.1 min) and 62.8min (IQR: 36.2-82.3 min) respectively (Figure 15M). The results indicate aberrant sleep behaviour in CS-*CJ10*/+ and CS-*R1*/+ mutant females via measure of sleep latency during the 12 h dark phase.

Table 66. Table 67. GLM analysis of the sleep latency of *ATPα* mutants and WT control females in the 12 h dark phase. Post-hoc results were corrected for multiple testing using Holm-Bonferroni method, where P < 0.05 is indicated in bold.

	Data	Explanatory Variable(s)	Test statistic	df	*P*-value
GLM	All fly strains	Genotype	7.4083	2, 89	**0.001057**
Post-hoc Test	CS-*CJ10* vs CS	Genotype	2.517	89	**0.0237**
	CS-R1 vs CS	Genotype	3.089	89	**0.0060**
	CS-*CJ10* vs CS-*R1*	Genotype	0.818	89	0.1071

4.2.3.11 Wake Time After Sleep Onset

4.2.3.11.1 Males

In Zantiks system, the time awake after first sleep bout during 12 h dark phase was assessed as an additional measure of sleep behaviour in young *ATP*α mutant females. A significant effect of genotype was found among *ATP*α mutant and CS control male (Table 67). Post-hoc comparisons showed time awake during the dark phase by CS-*CJ10*/+ and CS-*R1*/+ mutant males was significantly longer than by CS control males (Table 67, Figure 15L). Meanwhile, no significant difference was found CS-*CJ10*/+ and CS-*R1*/+ mutant males (Table 67, Figure 15L). The median time awake by CS control, CS-*CJ10*/+ and CS-*R1*/+ mutant males was 401.3 min (IQR: 348.8-481.6 min), 466.0 min (IQR: 418.0-537.0 min)and 442.5 min (IQR: 393.8-497.5 min) respectively (Figure 15L). The results indicate aberrant sleep behaviour in CS-*CJ10*/+ and CS-*R1*/+ mutant males via measure of time awake after sleep onset during the 12 h dark phase.

Table 68. GLM analysis of the time awake after sleep onset in *ATPα* mutants and WT control males during the 12 h dark phase. Post-hoc results were corrected for multiple testing using Holm-Bonferroni method, where P < 0.05 is indicated in bold.

	Data	Explanatory Variable(s)	Test statistic	df	*P*-value
GLM	All fly strains	Genotype	6.9595	2, 88	**0.001563**
Post-hoc Test	CS-*CJ10* vs CS	Genotype	3.648	88	**0.0013**
	CS-R1 vs CS	Genotype	-2.516	88	**0.0274**
	CS-*CJ10* vs CS-*R1*	Genotype	1.162	88	0.2485

4.2.3.11.2 Females

In Zantiks system, the time awake after first sleep bout during 12 h dark phase was assessed as an additional measure of sleep behaviour in young *ATP*α mutant females. A significant effect of genotype was found among *ATP*α mutant and CS control female (Table 68). Post-hoc comparisons revealed time awake during the dark phase by CS-*CJ10*/+ and CS-*R1*/+ mutant females was significantly longer than CS control females (Table 68, Figure 15N). Meanwhile, no significant difference was found CS-*CJ10*/+ and CS-*R1*/+ mutant females. The median time awake by CS control, CS-*CJ10*/+ and CS-*R1*/+ mutant females was 288.8 min (IQR: 225.0-407.5 min), 351.3 min (IQR: 276.3-415.0 min) and 393.1 min (IQR: 337.5-448.8 min) respectively (Figure 15N). The results indicate aberrant sleep behaviour in CS-*CJ10*/+ and CS-*R1*/+ females via measure of time awake after sleep onset during the 12 h dark phase.

Table 69. GLM analysis of the time awake after asleep onset of *ATPα* mutants and WT controls females during the 12 h dark phase. Post-hoc results were corrected for multiple testing using Holm-Bonferroni method, where P < 0.05 is indicated in bold.

	Data	Explanatory Variable(s)	Test statistic	df	*P*-value
GLM	All fly strains	Genotype	3.5593	2, 90	**0.03252**
Post-hoc Test	CS-*CJ10*/+ vs CS	Genotype	0.905	90	**0.0333**
	CS-R1/+ vs CS	Genotype	2.594	90	**0.0005**
	CS-*CJ10*/+ vs CS-*R1*/+	Genotype	1.703	90	0.1840

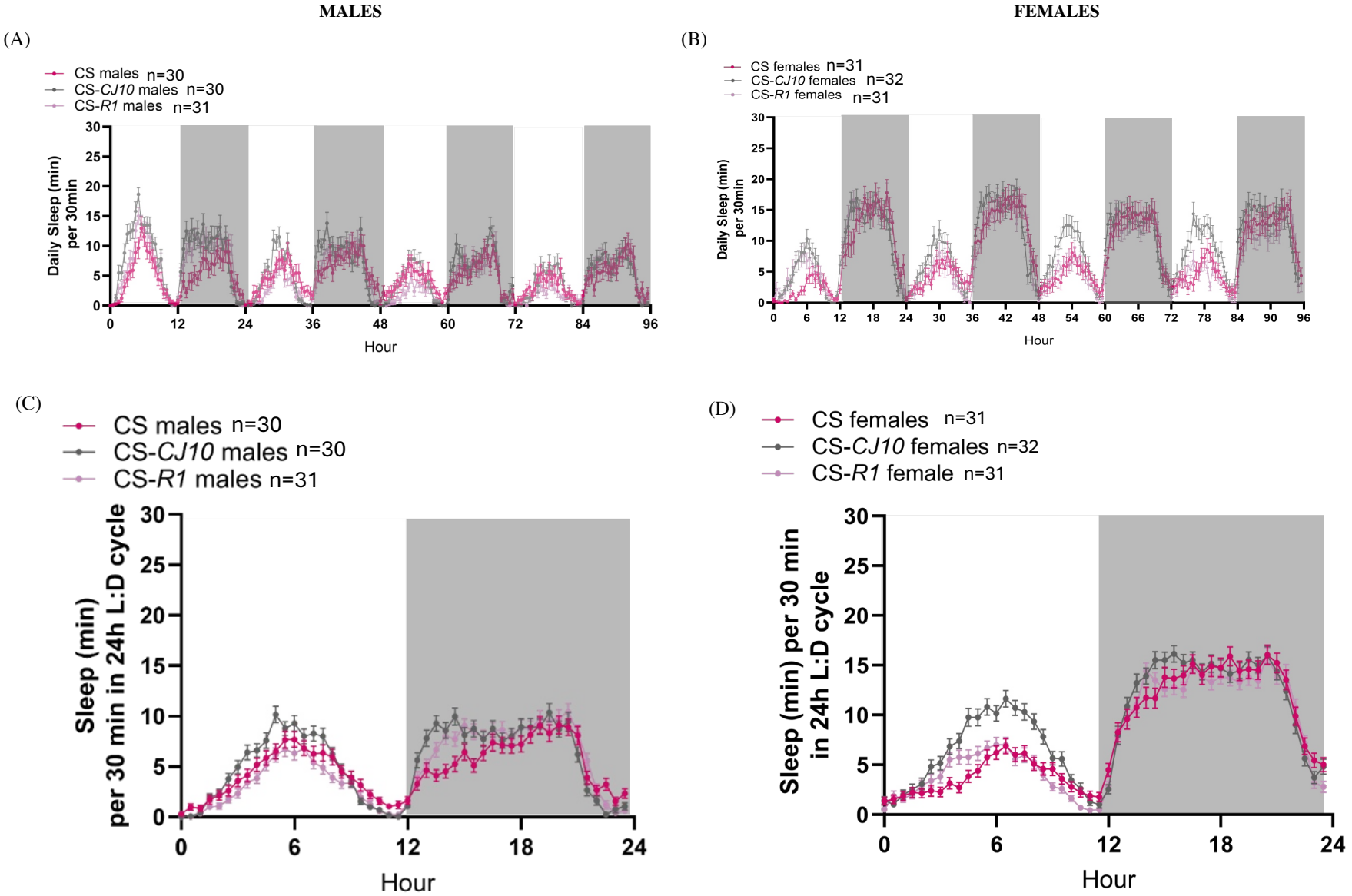
MALES
FEMALES
(A)
CS males n=30
CS-CJ10 males n=30
CS-R1 males n=31
Daily Sleep (min) per 30min
Hour
(B)
CS females n=31
CS-CJ10 females n=32
CS-R1 females n=31
Daily Sleep (min) per 30min
Hour
(C)
CS males n=30
CS-CJ10 males n=30
CS-R1 males n=31
Sleep (min) per 30 min in 24h L:D cycle
Hour
(D)
CS females n=31
CS-CJ10 females n=32
CS-R1 female n=31
Sleep (min) per 30 min in 24h L:D cycle
Hour

(E)

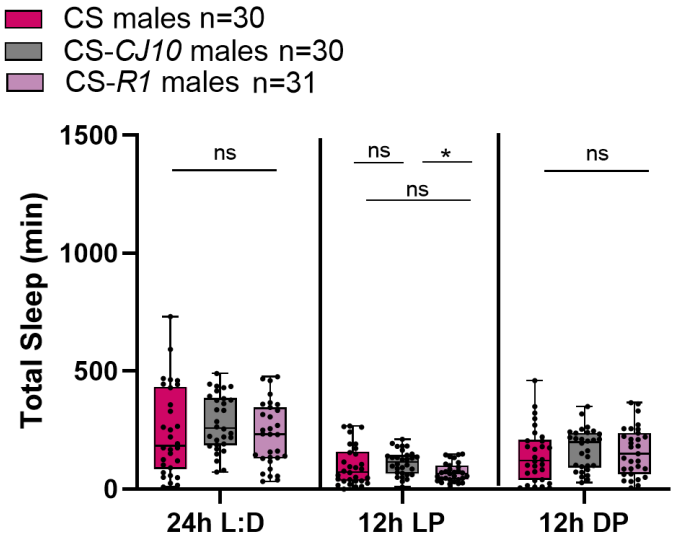
CS males n=30
CS-CJ10 males n=30
CS-R1 males n=31
Total Sleep (min)
1500
1000
500
0
ns
ns
*
ns
ns
24h L:D
12h LP
12h DP

(F)

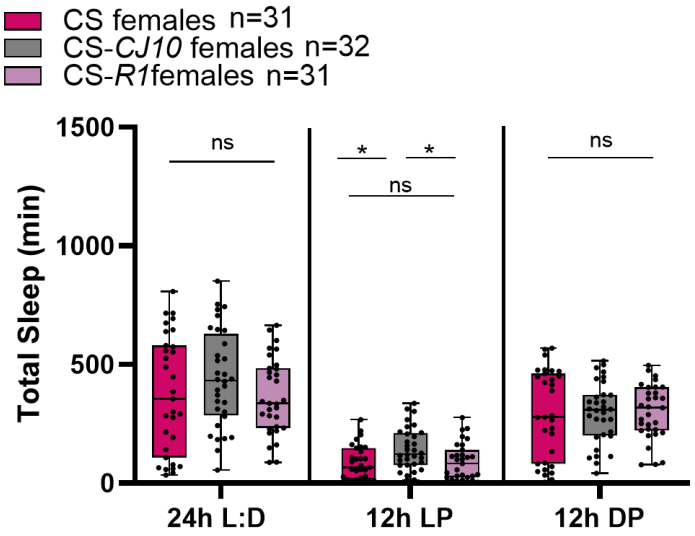
CS females n=31
CS-CJ10 females n=32
CS-R1females n=31
Total Sleep (min)
1500
1000
500
0
ns
*
*
ns
ns
24h L:D
12h LP
12h DP

(G)

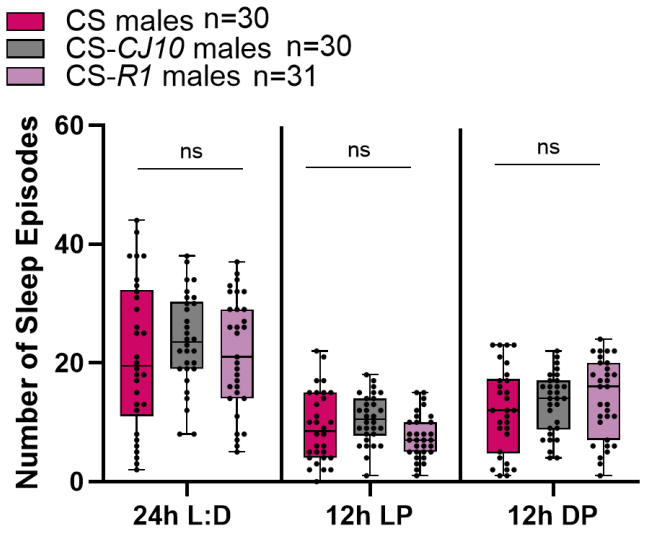
CS males n=30
CS-CJ10 males n=30
CS-R1 males n=31
Number of Sleep Episodes
60
40
20
0
ns
ns
ns
24h L:D
12h LP
12h DP

(H)

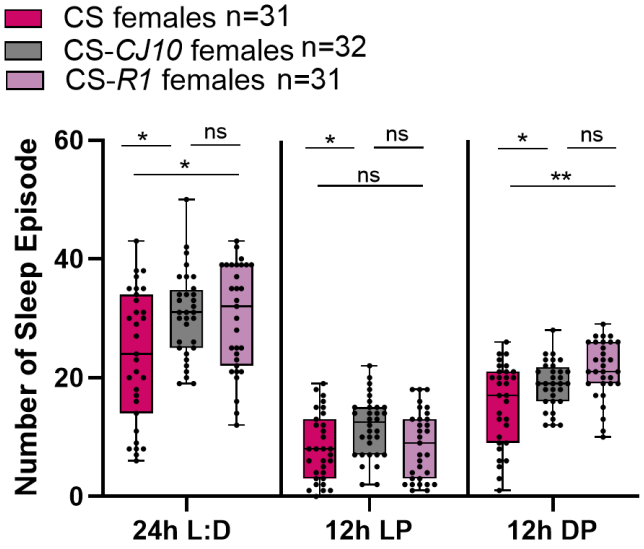
CS females n=31
CS-CJ10 females n=32
CS-R1 females n=31
Number of Sleep Episode
60
40
20
0
*
ns
*
ns
*
ns
ns
*
ns
**
24h L:D
12h LP
12h DP

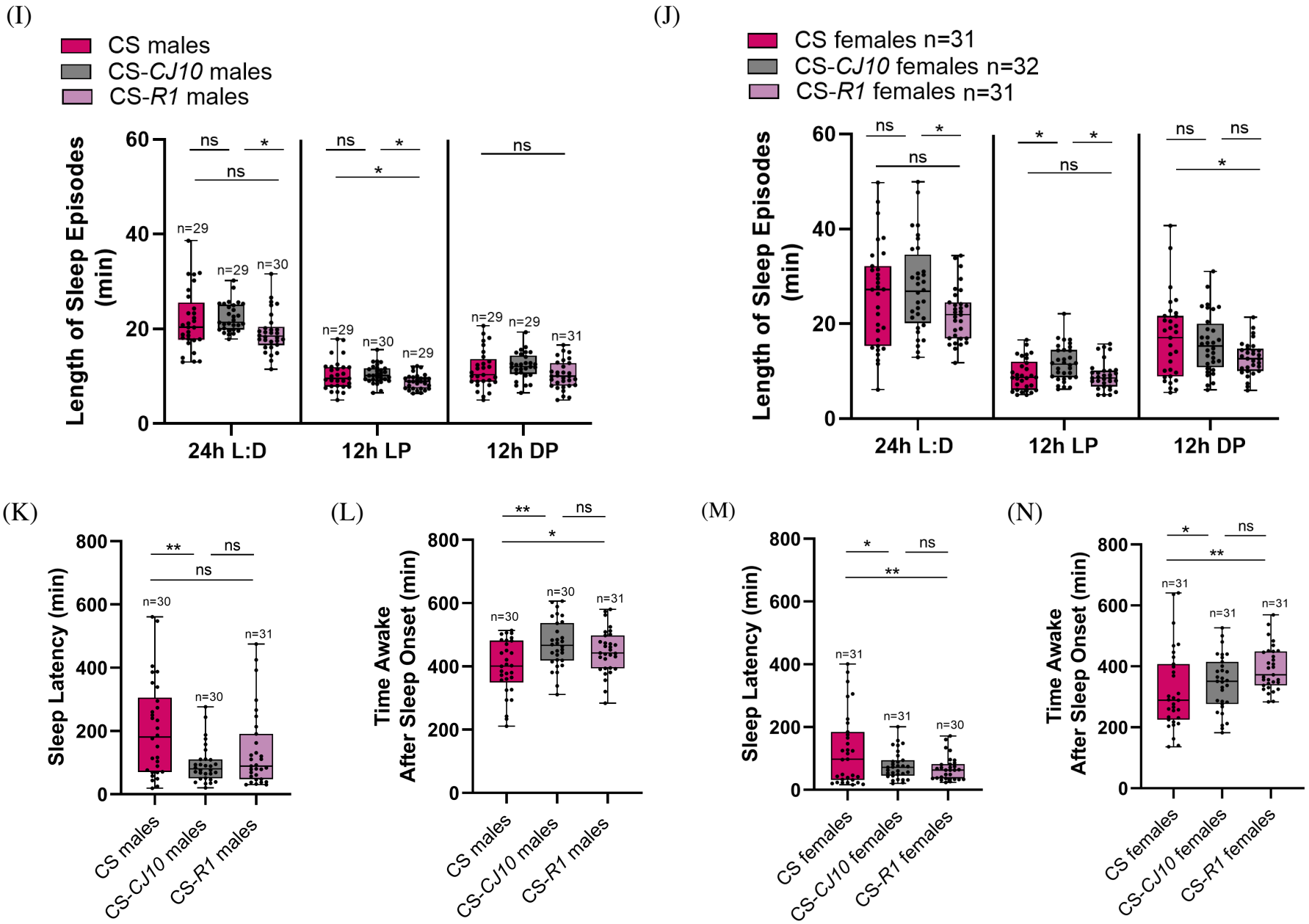
(I)
CS males
CS-CJ10 males
CS-R1 males
Length of Sleep Episodes (min)
24h L:D
12h LP
12h DP
(J)
CS females n=31
CS-CJ10 females n=32
CS-R1 females n=31
(K)
Sleep Latency (min)
CS males
CS-CJ10 males
CS-R1 males
(L)
Time Awake After Sleep Onset (min)
(M)
CS females
CS-CJ10 females
CS-R1 females
(N)

Figure 15. Sleep behaviour in young (3-4-day old) virgin male and female *D. melanogaster* heterozygous for *ATPα* mutant alleles (CJ10 and R1), along with wildtype Canton-S (CS) controls. The day-wise sleep trace represents the mean amount inactivity in minutes (min) by >30 individual males **(A)** and females **(B)** in 30-minute (min) bins, over 4 consecutive days of a 12-hour light (white background) and 12-hour dark (shaded background) phases. The sleep trace average across four days to present the mean amount of inactivity by >30 individual males **(C)** and females **(D)** in 30 min bins within a 24-hour light and dark (24h L:D) cycle. The data in A-D are presented as means with error bars corresponding to the SEM. Total Sleep Time in a 24-hour light and dark (24h L:D) cycle, 12-hour light and 12-hour dark phase for males **(E)** and females **(F)** across 4 full days. Total number of Sleep Bouts in 24-hours, 12-hour light and 12-hour dark phase for males **(G)** and females **(H)** across 4 full days. Total length of Sleep Bouts in Bouts in 24-hours, 12-hour light and 12-hour dark phase for males **(I)** and females **(J)** across 4 full days. Time taken for first sleep bout following lights off for males **(K)** and females **(M)**. Time awake after first sleep bout following lights off for males **(L)** and females **(N)**. The E-N data are presented with median, IQR and whiskers representing the maximum and minimum non-outlier values although G, M and O data are normally distributed. The black circles overlaying E-N graphs represent individual mean values, each calculated from 4 days of locomotor data per fly. Final sample size displayed on graph excludes flies that died at any point during the 4-day experiment and outliers based on Iterative Grubbs test ($P<0.05$). Significant difference is represented by asterisks * $P < 0.05$; ** $P < 0.01$; *** $P < 0.001$; ns, not significant as determined by GLM analysis.

4.2.3.12 Discussion

Sleep is relevant to AHC as hemiplegic and paroxysmal attacks are reported to be relieved upon sleep (Mikati et al., 2021). Moreover, sleep abnormalities such as insomnia, obstructive sleep apnoea and delayed sleep-wake syndrome have been reported in children with AHC (Kansagra et al., 2019).

In this research, five consecutive minutes of inactivity, derived from locomotor activity data from fly tracking was used as a surrogate measurement for sleep defined in flies as five consecutive minutes of inactivity (Chiu et al., 2010). In this present study, aberrant sleep behaviour was observed in both *CS-CJ10*/+ and *CS-R1*/+ mutant males and females to varying extents. In females during the 12 h light phase, the assay suggests that the *ATPα CJ10* (p.Gly744Ser) mutation causes excessive daytime sleep (hypersomnia) indicated by significantly extended total sleep time in CS-*CJ10*/+ mutants relative to *CS-R1*/+ mutant and CS control females (Figure 15F). This is further confirmed during the 12 h light phase by CS-*CJ10*/+ mutant females showing an significantly increased frequency of sleep episodes relative to CS control females (Figure 15H) and a longer duration of sleep episodes relative to CS-*R1*/+ mutant and CS control females (Figure 15J). These behaviours were exclusive to CS-*CJ10*/+ mutant females, suggesting that manifestation of hypersomnia is not a shared phenotype. Although, hypersomnia is not specific to AHC, this finding demonstrates that d-NKA *α* dysfunction resulting from *ATPα CJ10* mutation, equivalent to the human AHC p. Gly755Ser mutation, causes sleep disturbances in flies. Also, in females during the 12 h dark phase, the assay suggests that the *ATPα R1* null (p. Ile905Trpfs*8) mutation causes repetitive short interruption of sleep (sleep fragmentation), as indicated by a significantly increased frequency of sleep episodes in CS-*R1*/+mutant females relative to CS controls (Figure 15H) and a shorter duration of sleep episodes in CS-*R1*/+ relative to CS-*CJ10*/+

mutant and CS control females (Figure 15J). These behaviours were exclusive to CS-*R1*/+ mutant females suggesting that display of sleep fragmentation is not a shared phenotype. In males during the 12 h light phase, the assay suggests that the *ATPα R1* null (p. Ile905Trpfs*8) mutation causes suppressed daytime sleep, as indicated by the display of a significantly shorter duration of sleep episodes in *R1*/+ mutants relative to *CS-CJ10*/+ mutant and CS control males (Figure 15I). . Moreover, in the 12 h dark phase, the assay suggests that both the *ATPα R1* null and *CJ10* mutation affects the ability of males and females to stay asleep (insomnia), as indicated by a significantly longer time spent awake after the first sleep bout in *CS-R1*/+ mutant females and both *ATPα* mutant males relative to CS controls (Figure 15L and N). These results suggest that this AHC-relevant phenotype is specific to the *R1* mutation as both males and females showed sleep fragmentation phenotype.

Sleep is under circadian control, as timing of sleep is controlled during a 24 h cycle (Dubowy and Sehgal, 2017). This sleep data suggests further that the *ATPα* mutants exhibit normal clock function, as indicated herein by a siesta period in the middle of the day (~6 h) and more sleep during the dark phase than the light phase (Dubowy and Sehgal, 2017; Mazzotta et al., 2020). The observation herein of comparable levels of daytime and nighttime sleep in males is considered a typical feature of *D. melanogaster* sleep (Ishimoto et al., 2012). The variability in total sleep during the 12 h dark phase, characterized by short-sleeping, which was exhibited particularly by wildtype CS females (Figure 15F) is likely attributed to the ability of the Zantiks tracking system to detect micromovements in flies (Milojevic et al., 2024). This is supported by reports of a machine learning-based video-tracking system recording that wildtype CS males and females were asleep 50% of the time on average (Geissmann et al., 2019). This contrasts

with the *Drosophila* Activity Monitor (DAM) system, which recorded that flies were asleep 80% of the time on average during 12 h dark phase (Geissmann et al., 2019).

The manifestation of aberrant sleep phenotypes in *ATPα* mutant flies highlight the importance of d-NKA α function for sleep regulation. Regulation of *Drosophila* sleep is governed by the balance of sleep-promoting (5-HT and GABA), wake-promoting (dopamine, octopamine and histamine) and sleep/wake-promoting (acetylcholine and glutamate) neurotransmitters (NT), which activate or silence neurons within the fly's sleep centers composed of the MB, central complex (CC) and fan-shape body (FB) to control sleep (Mazzotta et al., 2020). It is reported that high-frequency neuronal bursting is necessary for sleep behaviour in *Drosophila* (Fernandez-Chiappe et al., 2021). Considering this, the presentation of sleep abnormalities in *ATPα* mutants could be a result of the impaired ability of the d-NKA pump to quickly restore the ion balance to create the electrochemical gradient across the membrane for AP generation in neurons, thus affecting secondary cellular processes, such as the release of inhibitory or excitatory NT required for normal sleep control. This hypothesis is supported by mutagenesis studies which report that dopamine-deficient flies exhibit extended sleep during night and day (Riemensperger et al., 2011). In another study, it was reported that *Gal4*/*UAS* flies, expressing a bacterial derived voltage-gated sensitive sodium channel (*UAS-NaChBac*) under a dopaminergic *Gal4* driver (TH-*Gal4*), which depolarizes and increases excitability in dopaminergic neurons, showed an increased frequency of sleep episodes and a decreased duration of sleep episodes (Xie et al., 2019), as reported here in *CS-R1*/+ mutant females (Figure 15H and J).

4.2.4 Cold-shock Behaviour of *ATPα* mutants

4.2.4.1 Paralysis Outcome

In 4°C cold shock assay, the percentage of 2-5-day old flies paralysed was recorded as measure of cold shock behaviour. Upon exposure to cold conditions, flies exhibited behaviours such as leg shaking, leg extension, high-frequency wing fluttering and fast body rotations in the horizontal plane before immobility. The percentage of CS-*CJ10*/+ flies that experienced cold-induced paralysis was significantly higher than CS control and CS-*R1*/+ flies (Table 69, Figure 16B). No significant difference was found between CS controls and CS-*R1*/+ mutants (Table 69). It was observed that 45 out of 52 (86.54%) CS-*CJ10*/+ flies, 31 out of 51 (60.68%) CS-*R1*/+ flies and 27 out of 56 (48.21%) CS controls experienced cold-induced paralysis (Figure 16B). The results indicates heightened sensitivity to cold in CS-*CJ10*/+ mutant flies via measure of paralysis outcome at 4°C.

Table 70. Fisher's Exact analysis of the percentage of paralysed *ATPα* mutants and WT controls at 4℃. Pairwise Fisher's Exact analyses were corrected for multiple testing using Holm-Bonferroni method, where P < 0.05 is indicated in bold.

	Data	Explanatory Variable(s)	*P*-value
Fisher's Exact Test	All fly strains	Sex	0.9077
	All fly strains	Genotype	**0.0000725**
Pairwise Fisher's Exact Test	CS-*CJ10*/+ vs CS	Genotype	**0.0000948**
	CS-*R1*/+ vs CS	Genotype	0.244
	CS-*CJ10*/+ vs CS-*R1*/+	Genotype	**0.0072**

4.2.4.2 Paralysis Onset Time

In 4°C cold shock assay, the time taken for paralysis onset of 2-5-day old flies was recorded as an additional measure of cold shock behaviour. No significant differences

was found among the time to paralysis of CS-*CJ10*/+, CS-*R1*/+ and CS control flies (Table 70, Figure 16C). The median time to paralysis of CS-*CJ10*/+, CS-*R1*/+ and CS control flies was 165.0 s (IQR: 88.5-237.5 s), 175.0 s (IQR: 104.0-269.0 s) and 143.5 s (IQR: 120.3-216.5 s) respectively (Figure 16C). The results indicate no heightened sensitivity to cold in *ATP*α mutants via measure of time to paralysis with a 360 s cutoff.

Table 71. GLM analysis of the time to paralysis of *ATPα* mutants and WT controls at 4℃.

	Data	Explanatory Variable(s)	Test statistic	df	*P*-value
GLM	All fly strains	Genotype * Sex	0.4632	2, 97	0.6306
		Sex	0.0396	1, 101	0.8426
		Genotype	1.2501	1, 100	0.2909

4.2.4.3 Paralysis Onset Time of All Flies

In 4°C cold shock assay, when all tested 2-5-day old flies were accounted for, a genotype effect was found. Post-hoc comparison of revealed time to paralysis of CS-*CJ10*/+ flies were significantly longer than CS control flies and CS-*R1*/+ flies (Table 71, Figure 16D). Also, no significant difference was found between CS-*R1*/+ and CS control females (Table 71, Figure 16D). The median time to paralysis of CS-*CJ10*/+, CS-*R1*/+ and CS control flies was 360.0 s (IQR: 143.3-360.0 s), 189.0 s (IQR: 92.75-264.5 s) and 296.0 s (IQR: 144.0-360.0 s) respectively (Figure 16D). The results indicate heightened sensitivity to cold in CS-*CJ10*/+ flies via measure of paralysis onset time of all tested flies.

Table 72. KW and MWU analysis of the time to paralysis of all tested *ATPα* mutants and WT controls at 4℃. Post-hoc results were corrected for multiple testing using Dunn's method, where P < 0.05 is indicated in bold.

	Data	Explanatory Variable(s)	Test statistic	df	*P*-value
MWU	CS-*CJ10*/+	Sex	283	1	0.3226
	CS-*R1*/+	Sex	296	1	0.5803
	CS	Sex	333.5	1	0.3217
KW	All fly strain	Genotype	15.53	2	**0.0004**
Post-hoc Test	CS-*CJ10*/+ vs CS	Genotype			**0.0007**
	CS-*R1*/+ vs CS	Genotype			> 0.9999
	CS-*CJ10*/+ vs CS-*R1*/+	Genotype			**0.0064**

4.2.4.4 Paralysis Recovery Time

In 4°C cold shock assay, the time taken for 2-5-day old flies to recovery from paralysis was recorded as an additional measure of cold shock behaviour. Time taken for *ATP*α mutants and CS controls to recover from paralysis was affected by both genotype and sex, but not their interaction (Table 72). The significant effect of sex was found within CS-*R1*/+ mutants only, CS-*R1*/+ females took significantly longer than CS-*R1*/+ males to recovery from paralysis (Table 72, Figure 16E). The significant effect of genotype was found in both males and females (Table 72). The mean time taken by CS-*CJ10*/+ males and females was 182.0 s (SD: 54.8 s) and 200.5 s (SD: 41.6 s) respectively (Figure 16E). The average time taken by CS-*R1*/+ males and females was 140.9 s (SD: 39.4 s) and 186.1 s (SD: 57.3 s) respectively (Figure 16E). The average time taken by CS males and females was 93.5 s (SD: 34.1 s) and 121.7 s (SD: 47.4 s) respectively (Figure 16E). Post-hoc comparisons of males showed CS-*CJ10*/+ mutants took significantly longer to recover from paralysis compared to CS-*R1*/+ mutant and CS control males (Table 72, Figure 16E). Meanwhile, no significant difference was found between recovery times of CS-*R1*/+ and CS control males (Table 72, Figure 16E). Post-hoc comparisons of females

showed CS-*CJ10*/+ and CS-*R1*/+ mutants took significantly longer to recover from paralysis compared CS control females (Table 72, Figure 16E). Meanwhile, no significant difference was found between recovery times of CS-*CJ10*/+ and CS-*R1*/+ mutant females (Table 72, Figure 16E). The results indicate heightened sensitivity to cold in CS-*CJ10*/+ mutant males, CS-*CJ10*/+ and CS-*R1*/+ mutant females via measure of paralysis onset time of all tested flies.

Table 73. GLM analysis of the recovery time of *ATPα* mutants and WT controls at 24-25℃. Post-hoc results were corrected for multiple testing using Holm-Bonferroni method, where P < 0.05 is indicated in bold.

	Data	Explanatory Variable(s)	Test statistic	df	*P*-value
GLM	All fly strains	Genotype * Sex	0.8582	2, 96	0.4271
		Genotype	19.047	2, 99	**$1.003*10^{-7}$**
		Sex	5.9436	1, 100	**0.01654**
	CS-*CJ10*/+	Sex	1.633	1, 43	0.2081
	CS-*R1*/+	Sex	6.7526	1, 29	**0.01456**
	CS	Sex	0.4936	1, 24	0.4891
	Males	Genotype	9.4078	2, 50	**0.0003405**
	Females	Genotype	11.038	2, 46	**0.0001215**
Post-hoc Test for males	CS-*CJ10*/+ vs CS	Genotype	-4.267	50	**0.0003**
	CS-*R1*/+ vs CS	Genotype	-1.833	50	0.0727
	CS-*CJ10*/+ vs CS-*R1*/+	Genotype	2.468	50	**0.0341**
Post-hoc Test for females	CS-*CJ10*/+ vs CS	Genotype	-1.507	67	**0.0001**
	CS-*R1*/+ vs CS	Genotype	-2.51	67	**0.0026**
	CS-*CJ10*/+ vs CS-*R1*/+	Genotype	-1.262	67	0.3804

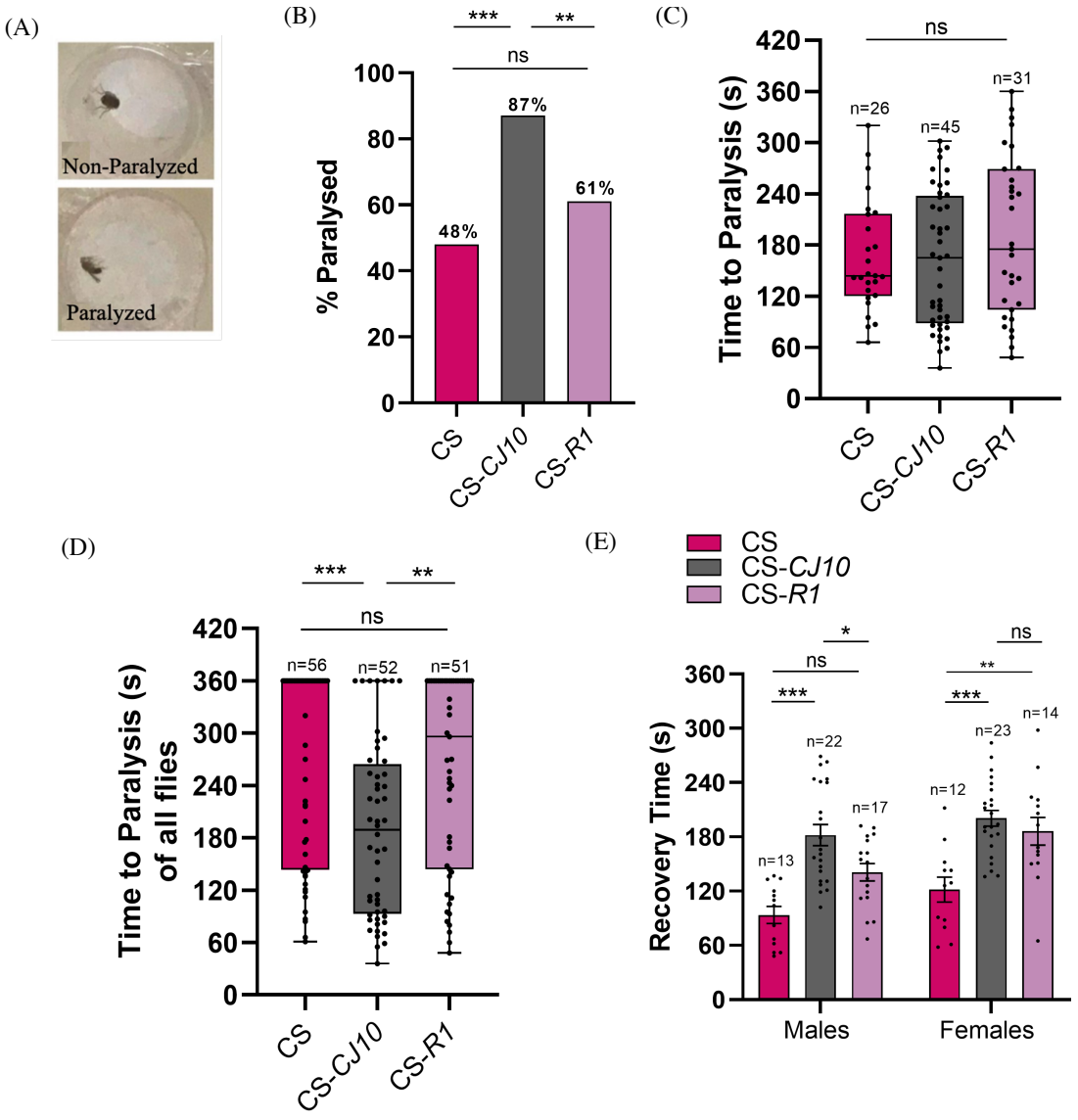

Figure 16. Cold shock paralysis behaviour at 4℃ in young (2-5-day old) *D. melanogaster* heterozygous for *ATPα* mutant alleles(CJ10 and R1), along with wildtype Canton-S (CS) controls. (A) Visual representation of paralysis outcome of flies following cold shock. **(B)** Total flies paralysed (%) during cold shock. **(C)** Time taken in seconds (s) for flies to become paralysed within 360 s. Final sample size displayed on graph excludes flies that did not become paralysed within 360 s. **(D)** Time taken in seconds(s) for paralysis onset when all tested flies are accounted for. **(E)** Time taken (s) for flies to recovery from paralysis in a 24-25℃ water bath. Data shown as mean ± SEM (bar graphs) or median and IQR (box-plot). Whiskers represent the maximum and minimum non-outlier values. Black circles overlaying graphs represent all non-outlier data points based on Iterative Grubbs test (P<0.05). * P < 0.05; ** P < 0.01; *** P < 0.001; ns, not significant as determined by Fisher's Exact test (Fig. B), GLM analysis (Fig. C and E) and Kruskal Wallis analysis (Fig. D).

4.2.4.5 Discussion

Hemiplegia and quadriplegia, forms of paralysis, are a distinct feature of AHC disease that are spontaneous but also known to be triggered or worsened by environmental stressors such as changes in temperature (Verret and Steele, 1971; Mikati et al., 2000; Sweney et al., 2009; Mikati et al., 2021). Mouse models of AHC (*Atp1a3* $^{D801N/+}$ and $^{E815K/+}$) have been reported to mimic hemiplegia under the stressful condition of forced swimming in warm (35℃) water (Hunanyan et al., 2015; Helseth et al., 2018). In flies, heat-induced paralysis was a reported phenotype of aged *CJ10/TM6* mutants (p.Gly744Ser) only, characterised by a significantly longer recovery time from paralysis compared to control flies (Ashmore et al., 2009). The present study reports novel findings to indicate that both young CS-*CJ10*/+ and CS-*R1*/+ mutant flies have a heightened sensitivity to cold conditions. In CS-*CJ10*/+ mutants this was characterised by: (1) a significantly higher proportion of paralysis than CS controls and *CS-R1*/+ mutant flies (Figure 16B); (2) significantly shorter time to paralysis than CS controls and *CS-R1*/+ flies when all flies were accounted for (Figure 16D) and (3) significantly longer recovery time compared to CS controls and *CS-R1*/+ flies in males and compared to CS controls in female (Figure 16E). In *CS-R1*/+ mutants, heightened sensitivity to cold was characterised in females only by significantly longer recovery time compared CS controls (Figure 16E). It has been reported in warm-acclimated flies that d-NKA pump activity is reduced in the brain, blood and muscles during cold exposure leading to the increase of K^+ ions as ion balance is lost (Armstrong et al., 2012; MacMillan et al., 2015; Cheslock et al., 2021). It is understood that cold exposure leads to neural shutdown resulting from the generation of widespread neuronal depolarization (known as spreading depolarisation) in the fly CNS defined by the rapid increase in K^+ ions concentration in the extracellular space surrounding neuronal and glial cells, thus loss of neuromuscular function leading to paralysis (Armstrong et al., 2012; Robertson et al.,

2020; Cheslock et al., 2021; Andersen et al., 2022). The importance of ionoregulation in the neuromuscular system is suggested by the report of d-NKA being highly expressed in muscle and nerve cells (Lebovitz et al., 1989). With this understanding a possible explanation for the increased susceptibility to cold-induced paralysis in CS-*CJ10*/+ mutants is likely a result of a faster onset of spreading depolarization (SD) resulting from the inability of the mutant d-NKA α to maintain ion balance in the extracellular space in the fly CNS. The prolonged recovery time in both CS-*CJ10*/+ and CS-*R1*/+ mutants (Figure 16E) could potentially be explained by the inability of the mutant d-NKA α to efficiently restore the electrochemical gradient in nerve cells in the fly brain following SD to facilitate the generation of AP thus propagation of the neuromuscular communication. The reduced d-NKA activity in response to cold could explain observations of cold-induced paralysis in CS control flies, however paralysis outcome in these flies was significantly less than CS-*CJ10*/+ mutants (Figure 16B) suggesting that d-NKA α function in wildtype flies could delay the SD event in response cold. A previous study had also reported cold-induced paralysis at very cold temperatures (2℃) but not at a cooler temperature (10℃) (Dean et al., 2018). Thus, in future work, it would be interesting to examine cold-induced behaviour of mutants at slightly cooler temperature to determine whether the fly equivalent of the AHC p.Gly755Ser mutation causes cold-induced paralysis. Moreover, significant differences seen between CS-*CJ10*/+ and *CS-R1*/+ mutant flies (Figure 16B and E) highlight the importance of the p.Gly477 residue in facilitating the normal function of d-NKA α in response to cold. Moreover, this assay revealed sex differences in paralysis recovery time thus adding to the body of research indicating that responses to cold stress can differ between *D. melanogaster* males and females strains (David et al., 1998; Bubliy et al., 2002; Garcia and Teets, 2019; Garcia et al., 2020; Andersen et al., 2022).

4.2.5 Transgenic rescue of behavioural phenotypic deficits of *ATPα* mutants

4.2.5.1 Introduction

Transgenic rescue is an experimental approach used to confirm that observed phenotypic defects in animals is a direct consequence of a specific genetic mutation as opposed to other variables. Briefly, the experiment involves reintroducing a wildtype copy(s) of the transgene into the animal with the specific genetic mutation to determine whether the wildtype gene function improves any phenotypic effects initially observed in the mutant animal. In AHC research, phenotypic rescue of low body mass, epileptic seizures, fine motor dysfunction and cognitive impairment was reported in heterozygous *Myshkin* (Atp1a3 Ile810Asn) mice expressing a transgenic WT *Atp1a3* gene via bacterial artificial chromosome transgenesis (Clapcote et al., 2009; Kirshenbaum et al., 2016a). It is understood that rescue was a result of the WT *Atp1a3* transgene from a different mouse species increasing brain m-NKA activity by 25% in heterozygous *Myshkin* mice (Clapcote et al., 2009; Kirshenbaum et al., 2016a). Thus, providing supporting evidence of the direct correlation between the loss-of-function of h-NKA α_3 activity and the manifestation of AHC clinical features. In the results chapter of this thesis (section 4.2.1-4.2.4), it showcases flies heterozygous for the *ATPα CJ10* (p.Gly744Ser) mutation equivalent to the human Gly755Ser AHC mutation (Heinzen et al., 2014) and the *R1* null (p. Ile905Trpfs*8) mutation also displayed phenotypic deficits relevant to the neurodevelopmental disorder. Thus, the aim of this chapter is to determine whether the human *ATP1A3* and fly *ATPα* gene products are functionally equivalent to rescue phenotypic abnormalities reported in heterozygous *CJ10* and *R1* mutant flies. To address this question, the *Gal4*/*UAS* system was exploited. Generated flies hemizygous for the human $ATP1A3^{WT}$ cDNA (*pUAST-*$ATP1A3^{WT}$) and heterozygous for the *ATPα CJ10* (p.Gly744Ser) and R1 (p. Ile905Trpfs*8) mutations were crossed to a ubiquitous *Gal4* fly line (*Act5C-Gal4*/*CyO*) to drive ubiquitous expression of the $ATP1A3^{WT}$ cDNA

within the heterozygous *ATPα* mutant backgrounds (*Act5C-Gal4/pUAST-α3;CJ10/+* and *Act5C-Gal4/pUAST-α3;R1/+*) for assessment of transgenic rescue of their climbing performance and cold-induced sensitivity by negative geotaxis and cold-shock assay respectively.

4.2.5.2 Rescue of *ATPα CJ10* mutant Climbing Performance

4.2.5.2.1 Height Climbed

In negative geotaxis assay, distance climbed in 3 s was assessed as a measure of gross motor function in 2-3-day old *Act5C-Gal4/pUAST-α3;CJ10/+* flies. No significant effect was found between height climbed in 3 s by *Act5C-Gal4/pUAST-α3;CJ10/+* flies compared to *pUAST-α3;CJ10/+* flies and *Act5C-Gal4/CyO* controls (Table 73). The median distance climbed by *Act5C-Gal4/pUAST-α3;CJ10/+, pUAST-α3;CJ10/+* and *Act5C-Gal4/CyO* flies was 1.55 cm (IQR: 0.51-3.14 cm), 1.66 cm (IQR: 0.64-4.08 cm), and 2.79 cm (IQR: 1.01-4.13 cm), respectively (Figure 17A). The results indicate no deficit in *CJ10* mutants without transgene expression (*pUAST-α3;CJ10/+*), therefore, unable to assess ubiquitous $\alpha 3^{WT}$ expression in rescuing climbing performance of *CJ10/+* mutants via measure of height climbed in 3 s.

Table 74. GLM on the height climbed in 3 s by *Gal4/UAS_α3;CJ10/+* flies compared to parental controls. Post-hoc results were corrected for multiple testing using Holm-Bonferroni method, where P < 0.05 is indicated in bold.

	Data	Explanatory Variable(s)	Test statistic	df	*P*-value
GLM	All fly strains	Genotype * Sex	0.1385	2, 151	0.8708
	All fly strains	Sex	1.6102	1, 155	0.2064
	All fly strains	Genotype	2.0283	2, 154	0.1351

4.2.5.2.2 Climbing Speed

In negative geotaxis assay, time taken to climb above 4 cm target line was assessed as an additional measure of gross motor function in 2-3-day old *Act5C-Gal4/pUAST-α3;CJ10/+* flies. A main effect of sex was found to affect climbing speed of *pUAST-α3;CJ10/+* and *Act5C-Gal4/CyO* flies (Table 74).The median time of *Act5C-Gal4/pUAST-α3;CJ10/+, pUAST-α3;CJ10/+* and *Act5C-Gal4/CyO* males was 4.57 s (IQR: 3.45-5.49 s), 4.08 s (IQR: 2.77-5.16 s) and 3.53 s (IQR: 2.67-4.82 s), respectively (Figure 17B). For *Act5C-Gal4/pUAST-α3;CJ10/+, pUAST-α3;CJ10/+* and *Act5C-Gal4/CyO* females, the median time was 5.03 s (IQR: 3.30-8.1 s), 5.51 s (IQR: 2.56-8.33 s), and 5.93 s respectively (Figure 17B). The results indicate no deficit in *CJ10* mutants without transgene expression (*pUAST-α3;CJ10/+*), therefore, unable to assess ubiquitous $\alpha 3^{WT}$ expression in rescuing climbing performance of *CJ10/+* mutants via measure of time required to reach target line (Figure 17B).

Table 75. GLM analysis of the climbing speed of *Gal4/UAS_α3;CJ10/+* flies compared to parental controls. Post-hoc results were corrected for multiple testing using Holm-Bonferroni method, where P < 0.05 is indicated in bold.

	Data	Explanatory Variable(s)	Test statistic	df	*P*-value
GLM	All fly strains	Genotype * Sex	1.1769	2, 118	0.31192
	All fly strains	Genotype	0.9145	2, 121	0.4035
	All fly strains	Sex	22.429	1, 122	**$5.944*10^{-6}$**
	Act5C-Gal4/pUAST-α3;CJ10/+ flies	Sex	2.1661	1, 32	0.1508

	pUAST-α3;CJ10/+ flies	Sex	10.81	1, 41	**0.002077**
	Act5C-Gal4/*CyO* controls	Sex	12.444	1, 45	**0.0009785**

4.5.2.2.3 Climbing Latency

In negative geotaxis assay, time taken to initiate vertical movement following commencement of negative geotaxis was assessed as an additional measure of gross motor function in 2-3-day old *Act5C-Gal4*/*pUAST-α3;CJ10*/+ flies. A main effect of genotype-by-sex interaction was found among *Act5C-Gal4*/*pUAST-α3;CJ10*/+ flies, *pUAST-α3;CJ10*/+ flies and *Act5C-Gal4*/*CyO* controls (Table 75). The median time of *Act5C-Gal4*/*pUAST-α3;CJ10*/+, *pUAST-α3;CJ10*/+ and *Act5C-Gal4*/*CyO* males was 1.66 s (IQR: 1.03-2.56 s), 1.47 s (IQR: 0.70-2.47 s) and 1.29 s (IQR: 0.82-2.37 s), respectively (Figure 17C). For *Act5C-Gal4*/*pUAST-α3;CJ10*/+, *pUAST-α3;CJ10*/+ and *Act5C-Gal4*/*CyO* females, the median time was 1.77 s (IQR: 0.62-3.45 cm), 1.68 s (IQR: 0.67-3.44 s), and 0.80 s (IQR: 0.35-1.08 s), respectively (Figure 17C). Re-analysis of data grouped by sex showed a significant effect of genotype in females only (Table 75). Post-hoc comparisons of females showed climbing latency of *Act5C-Gal4*/*pUAST-α3;CJ10*/+ flies was significantly longer than *Act5C-Gal4*/*CyO*, but not relative to *pUAST-a3;CJ10* flies (Table 75, Figure 17C). The climbing latency of *pUAST-a3;CJ10* females was also significantly longer than *Act5C-Gal4*/*CyO* control females (Table 75, Figure 17C). The results indicate the climbing deficit in *CJ10* female mutants without transgene expression (*pUAST-α3;CJ10*/+) was not rescued by ubiquitous $a3^{WT}$ expression via measure of climbing latency.

Table 76. GLM analysis of the climbing latency of *Gal4/UAS_α3;CJ10/+* flies compared to parental controls. Post-hoc results were corrected for multiple testing using Holm-Bonferroni method, where *P* < 0.05 is indicated in bold.

	Data	Explanatory Variable(s)	Test statistic	df	*P*-value
GLM	All fly strains	Genotype * Sex	3.329	2, 129	**0.03132**
	Males	Genotype	0.4841	2, 64	0.6185
	Females	Genotype	6.0579	2, 65	**0.003868**
Post-hoc Tests of females	*Act5C-Gal4/pUAST-α3;CJ10/+* vs *pUAST-α3;CJ10/+* flies	Genotype	0.474	65	0.6369
	Act5C-Gal4/pUAST-α3;CJ10/+ flies vs *Act5c-Gal4/CyO* control	Genotype	2.545	65	**0.0266**
	pUAST-α3;CJ10/+ flies vs *Act5c-Gal4/CyO* control	Genotype	2.969	65	**0.0125**

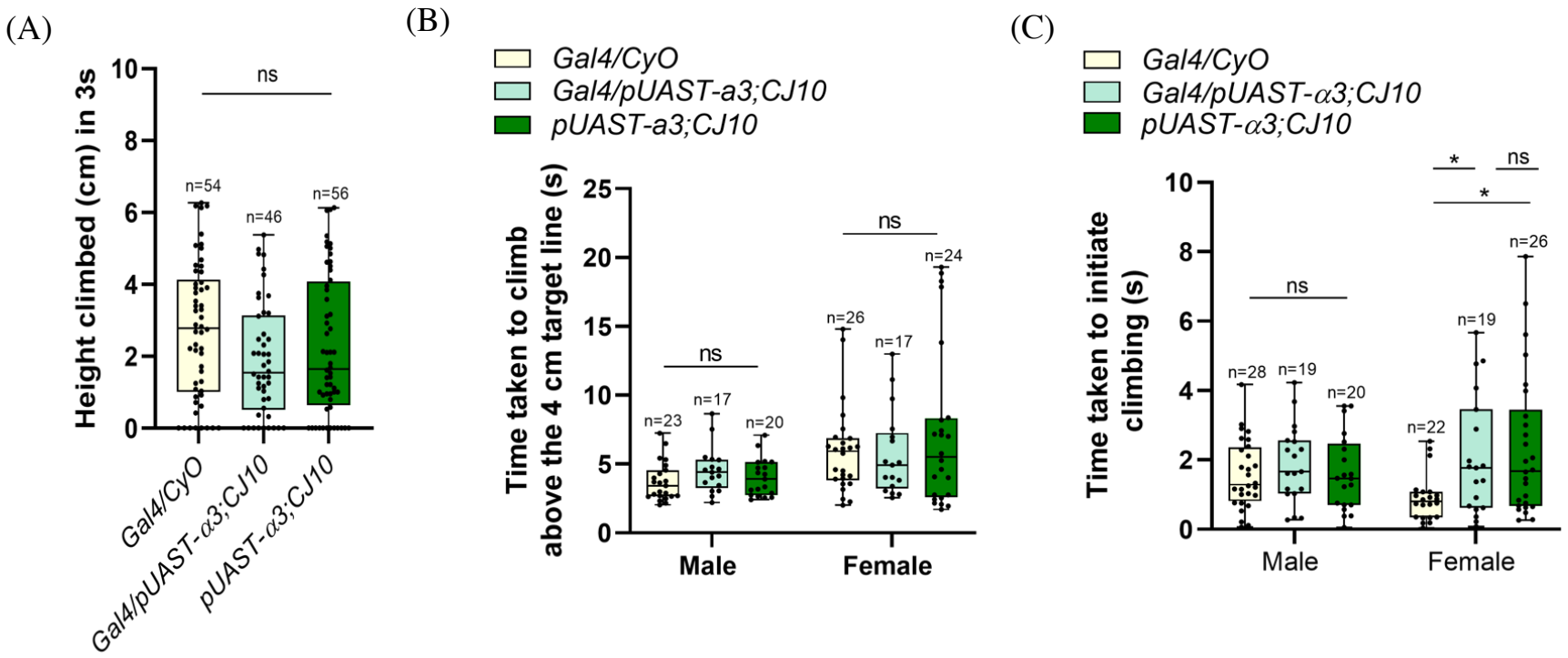

Figure 17. The effect of ubiquitous wildtype *ATP1A3* expression on the climbing performance of young (2-3-day old) virgin heterozygous *CJ10* flies in negative geotaxis assay. (A) Height (cm) climbed in 3 seconds (s) following commencement of negative geotaxis. Final sample size displayed on graph excludes flies that did not fall to bottom of vial. **(B)** Time taken to climb above the 4 cm target line. Final sample size displayed on graph B excludes flies that did not successfully complete the task and were classified as outliers based on Iterative Grubbs test (P<0.05). **(C)** Time taken (s) to initiate vertical movement following commencement of negative geotaxis, final sample size displayed on graph excludes flies that stayed at the bottom of vials following commencement of negative geotaxis and outliers based on Iterative Grubbs test (P<0.05). Median and Interquartile range (IQR) values are shown. Whiskers represent the maximum and minimum non-outlier values. Black circles overlaying graphs represent all non-outlier data points.* P< 0.05, ** P < 0.01; *** P < 0.001; ns, not significant as determined by GLM analysis.

4.2.5.3 Rescue of *ATPα R1* mutant Climbing Performance

4.2.5.3.1 Height Climbed

In negative geotaxis assay, distance climbed in 3 s was assessed as a measure of gross motor function in 2-3-day old *Act5C-Gal4/pUAST-α3;R1/+* flies. No significant effect of genotype was found between height climbed in 3 s by *Act5C-Gal4/pUAST-α3;R1/+* flies compared to *pUAST-α3;R1/+* flies and *Act5C-Gal4/CyO* controls (Table 76, Figure 18A). The median distance climbed by *Act5C-Gal4/pUAST-α3;R1/+, pUAST-α3;R1/+* and *Act5C-Gal4/CyO* flies was 2.95 cm (IQR: 0.64-4.65 cm),, 2.12 cm (IQR: 0.48-3.64 cm), and 2.79 cm (IQR: 1.01-4.13cm), respectively (Figure 18A). The results indicate no deficit in *R1* mutants without transgene expression (*pUAST-α3;R1/+*), therefore unable to assess ubiquitous $\alpha 3^{WT}$ expression in rescuing climbing performance of *R1/+* mutants via measure of height climbed within 3 s.

Table 77. GLM analysis of the height climbed in 3 s by *Gal4/UAS_α3;R1/+* flies compared to parental controls.

	Data	Explanatory Variable(s)	Test statistic	df	*P*-value
GLM	All fly strains	Genotype * Sex	0.6321	2, 156	0.5328
	All fly strains	Sex	0.1609	1, 160	0.6888
	All fly strains	Genotype	0.3763	2, 159	0.687

4.2.5.3.2 Climbing Speed

In negative geotaxis assay, time taken to climb above 4 cm target line was assessed as an additional measure of gross motor function in 2-3-day old *Act5C-Gal4/pUAST-α3;R1/+* flies. No significant effect was found between the climbing speed of *Act5C-*

Gal4/pUAST-α3;R1/+ flies compared to *pUAST-α3;R1/+* flies and *Act5C-Gal4/CyO* controls (Table 77). The median time of *Act5C-Gal4/pUAST-α3;R1/+, pUAST-α3;R1/+* and *Act5C-Gal4/CyO* males was 3.58 s (IQR: 2.85-5.53 s), 3.81 s (IQR: 2.98-5.22 s), and 4.07 s (IQR: 2.83-6.16 s), respectively (Figure 18B). The results indicate no deficit in *R1* mutants without transgene expression (*pUAST-α3;R1/+*), therefore, unable to assess ubiquitous $\alpha 3^{WT}$ expression in rescuing speed of vertical movement in *R1/+* mutants via measure of time taken to climb above 4 cm target line.

Table 78. GLM analysis of the climbing speed of *Gal4/UAS_α3;R1/+* flies compared to parental controls.

	Data	Explanatory Variable(s)	Test statistic	df	*P*-value
GLM	All fly strains	Genotype * Sex	2.5931	2, 129	0.0786
	All fly strains	Sex	0.203	1, 133	0.653
	All fly strains	Genotype	0.2221	2, 132	0.8011

4.2.5.3.3 Climbing Latency

In negative geotaxis assay, time taken to initiate vertical movement following commencement of negative geotaxis was recorded as an additional measure of gross motor function in 2-3-day old *Act5C-Gal4/pUAST-α3;R1/+* flies. The climbing latency of *Act5C-Gal4/pUAST-α3;R1/+* flies compared to *pUAST-α3;R1/+* flies and *Act5C-Gal4/CyO* controls was affected by genotype and sex, but not their interaction (Table 78). The median time of *Act5C-Gal4/pUAST-α3;R1/+, pUAST-α3;R1/+* and *Act5C-Gal4/CyO* males was 1.37 s (IQR: 0.51-3.07 s), 1.99 s (IQR: 1.25-3.55 s), and 1.29 s (IQR: 0.82-2.37 s), respectively (Figure 18C). For *Act5C-Gal4/pUAST-α3;R1/+,*

pUAST-α3;R1/+ and *Act5C-Gal4*/*CyO* females, the median time was 1.40 s (IQR: 1.07-1.85 s), 1.35 s (IQR: 0.56-1.93 s) and 0.80 s (IQR: 0.35-1.08 s) respectively (Figure 18C). The significant effect of sex was found within *pUAST-a3;R1*/+ and *Act5C-Gal4*/*CyO* flies, males took significantly longer than females to initiate climbing (Table 78, Figure 18C). The significant effect of genotype was seen in females only (Table 78). Post-hoc comparisons of females showed climbing latency of *Act5C-Gal4*/*pUAST-α3;R1*/+ flies was significantly longer than *Act5C-Gal4*/*CyO* controls, but not relative to *pUAST-a3;R1*/+ flies (Table 78, Figure 18C). The climbing latency of *pUAST-a3;R1*/+ females was not found to significantly differ to *Act5C-Gal4*/*CyO* control females (Table 78, Figure 18C). The results indicate no deficit in *R1* mutants without transgene expression (*pUAST-α3;R1*/+), therefore, unable to assess ubiquitous $\alpha 3^{WT}$ expression in rescuing climbing performance of *R1*/+ mutants via measure of time taken to initiate climbing.

Table 79. GLM analysis of the climbing latency of *Gal4*/*UAS_α3;R1*/+ flies compared to parental controls. Post-hoc results were corrected for multiple testing using Holm-Bonferroni method, where P < 0.05 is indicated in bold.

	Data	Explanatory Variable(s)	Test statistic	df	*P*-value
GLM	All fly strains	Genotype * Sex	2.6866	2, 135	0.07176
		Genotype	2.7223	2, 138	**0.046**
		Sex	6.3188	1, 139	**0.01309**
	Act5C-Gal4/*pUAST-α3;R1*/+ flies	Sex	0.0183	1, 139	0.8932
	pUAST-α3;R1/+ flies	Sex	12.197	1, 47	**0.001054**

	Act5c-Gal4/CyO control	Sex	4.6222	1, 49	**0.03652**
	Males	Genotype	2.7223	2, 68	0.07289
	Females	Genotype	3.5685	2, 67	**0.03368**
Post-hoc Test for females	*Act5C-Gal4/pUAST-α3;R1/+* vs *pUAST-α3;R1/+* flies	Genotype	-1.507	67	0.4092
	Act5C-Gal4/pUAST-α3;R1/+ flies vs *Act5c-Gal4/CyO* control	Genotype	-2.51	67	**0.0435**
	pUAST-α3;R1/+ flies vs *Act5c-Gal4/CyO* control	Genotype	-1.262	67	0.6340

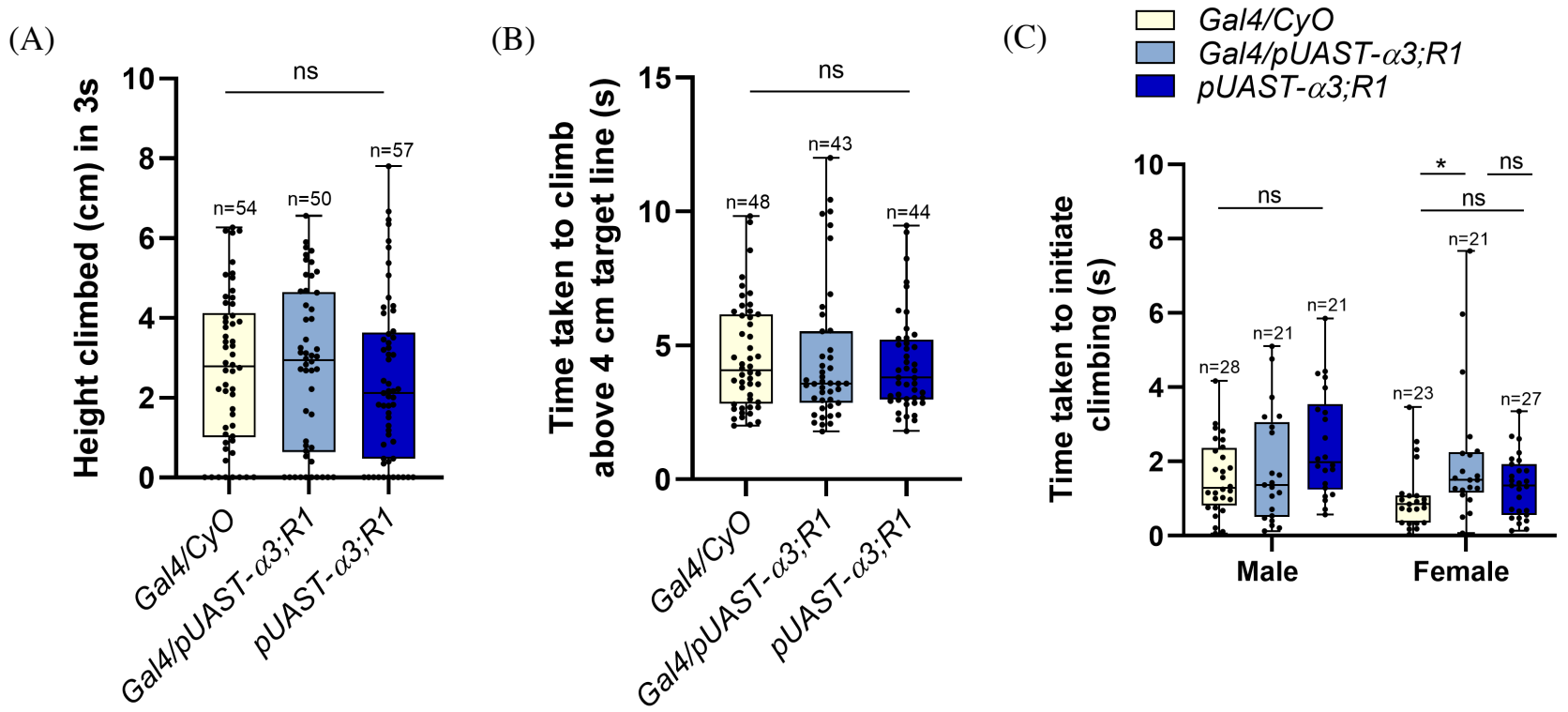

Figure 18. The effect of ubiquitous wildtype *ATP1A3* expression on the climbing performance of young (2-3-day old) virgin **heterozygous *R1* flies in negative geotaxis assay. (A)** Height (cm) climbed in 3 seconds (s) following commencement of negative geotaxis. Final sample size displayed on graph excludes flies that did not fall to bottom of vial. **(B)** Time taken to climb above the 4 cm target line. Final sample size displayed on graph B excludes flies that did not successfully complete the task and were classified as outliers based on Iterative Grubbs test ($P<0.05$). **(C)** Time taken (s) to initiate vertical movement following commencement of negative geotaxis, final sample size displayed on graph excludes flies that stayed at the bottom of vials following commencement of negative geotaxis and outliers based on Iterative Grubbs test ($P<0.05$). Median and Interquartile range (IQR) values are shown. Whiskers represent the maximum and minimum non-outlier values. Black circles overlaying graphs represent all non-outlier data points.* $P< 0.05$, ** $P < 0.01$; *** $P < 0.001$; ns, not significant as determined by GLM analysis.

4.2.5.4 Rescue of *ATPα CJ10* Cold shock Behaviour

4.2.5.4.1 Paralysis Outcome

In 4°C cold shock assay, the percentage of 4-7-day old flies paralysed was recorded as measure of cold shock behaviour. A main effect of genotype was found (Table 79). The *Act5C-Gal4/pUAST-α3;CJ10/+* flies that experienced cold-induced paralysis within 360 s was significantly higher than *Act5C-Gal4/CyO* controls but not relative to *pUAST-α3;CJ10/+* flies (Table 79, Figure 19A). The percentage of paralysed *pUAST-α3;CJ10/+* flies was also significantly higher than *Act5C-Gal4/CyO* controls (Table 79, Figure 19A). It was observed that 39 out of 47 (82.98%) *Act5C-Gal4*/pUAST-*α3;CJ10* flies, 49 out of 54 (90.74%) *pUAST-α3;CJ10* flies and 14 out of 63 (22.22%) *Act5c-Gal4/CyO* controls experienced cold-induced paralysis (Figure 19A). The results indicate cold-sensitivity in *CJ10/+* mutants without transgene expression (*pUAST-α3;CJ10/+*) was not rescued by ubiquitous $\alpha 3^{WT}$ expression via measure of paralysis outcome.

Table 80. Fisher's Exact analysis of the percentage of *Gal4/UAS_α3;CJ10/+* flies compared parental controls at 4°C. Pairwise Fisher's Exact analyses were corrected for multiple testing using Holm-Bonferroni method, where P < 0.05 is indicated in bold.

	Data	Explanatory Variable(s)	*P*-value
Fisher Exact Test	All fly strains	Sex	0.9622
	All fly strains	Genotype	**$2.20*10^{-16}$**
Pairwise Fisher's Exact Test	*Act5C-Gal4/pUAST-α3;CJ10/+* vs *pUAST-α3;CJ10/+* flies	Genotype	0.539
	Act5C-Gal4/pUAST-α3;CJ10/+ flies vs *Act5c-Gal4/CyO* control	Genotype	**$7.94*10^{-11}$**

	pUAST-α3;CJ10/+ flies vs *Act5c-Gal4*/*CyO* control	Genotype	**4.35*10^{-14}**

4.2.5.4.2 Paralysis Onset Time

In 4°C cold shock assay, the time taken for paralysis onset of 4-7-day old flies was recorded as an additional measure of cold shock behaviour. The time to paralysis of *Act5C-Gal4*/*pUAST-α3;CJ10*/+ flies compared to *pUAST-α3;CJ10*/+ flies and *Act5C-Gal4*/*CyO* controls was affected by both genotype and sex, but not their interaction (Table 80). The significant effect of sex was seen within *Act5C-Gal4*/*pUAST-α3;CJ10*/+ flies only, time to paralysis of females was significantly longer than males (Table 80, Figure 19B). The significant effect of genotype was seen in males and females (Table 80). Post-hoc comparison of males revealed time to paralysis of *Act5C-Gal4*/*pUAST-α3;CJ10*/+ males (median: 117 s , IQR: 92.5-146.5 s) was not significantly different to p*UAST-α3;CJ10*/+ control males (median: 80 s , IQR: 53.5-136.5 s) but relative to *Act5C-Gal4*/*CyO* control males (median: 184.0 s , IQR: 161.0-215.0 s) was significantly shorter (Table 80, Figure 19B). Time to paralysis of *pUAST-α3;CJ10*/+ males was also significantly shorter than *Act5C-Gal4*/*CyO* control males (Table 80, Figure 19B). Post-hoc comparison of females revealed time to paralysis of *Act5C-Gal4*/*pUAST-α3;CJ10*/+ females (median: 138.0 s , IQR: 124.0-264.0 s) was significantly longer than p*UAST-α3;CJ10*/+ control females (median: 98.0s , IQR: 68.0-137.8 s) but relative to *Act5C-Gal4*/*CyO* control females (median: 209.0 s , IQR: 158.0-248.0 s) no significant difference was found (Table 80, Figure 19B). Similarly to males, time to paralysis of *pUAST-α3;CJ10*/+ females was significantly shorter than in *Act5C-Gal4*/*CyO* control females (Table 80, Figure 19B). The results indicate that ubiquitous $\alpha3^{WT}$ expression moderately rescued cold-sensitivity in only *CJ10*/+ female mutants via measure of flies that experienced paralysis within 360 s cut-off.

Table 81. GLM analysis of the time to paralysis of *Gal4/UAS_α3;CJ10/+* flies compared to parental controls at 4℃. Post-hoc results were corrected for multiple testing using Holm-Bonferroni method, where P < 0.05 is indicated in bold.

	Data	Explanatory Variable(s)	Test statistic	df	*P*-value
GLM	All fly strains	Genotype * Sex	1.1139	2, 102	0.322
		Genotype	14.681	2, 105	**$2.388*10^{-6}$**
		Sex	7.9228	1, 106	**0.005821**
	Act5C-Gal4/pUAST-α3;CJ10/+ flies	Sex	11.318	1, 39	**0.001764**
	pUAST-α3;CJ10/+ flies	Sex	0.5361	1, 52	0.4673
	Act5c-Gal4/CyO control	Sex	1.3003	1, 12	0.2764
	Males	Genotype	10.343	2, 55	**0.0001583**
	Females	Genotype	8.8831	2, 47	**0.0005341**
Post-hoc Test for males	*Act5C-Gal4/pUAST-α3;CJ10/+* vs *pUAST-α3;CJ10/+* flies	Genotype	1.787	55	0.0795
	Act5C-Gal4/pUAST-α3;CJ10/+ flies vs *Act5c-Gal4/CyO* control	Genotype	3.178	55	**0.0049**
	pUAST-α3;CJ10/+ flies vs *Act5c-Gal4/CyO* control	Genotype	4.515	55	**0.0001**

Post-hoc Test for females	*Act5C-Gal4/pUAST-α3;CJ10/+* vs *pUAST-α3;CJ10/+* flies	Genotype	-3.465	47	**0.0023**
	Act5C-Gal4/pUAST-α3;CJ10/+ flies vs *Act5c-Gal4/CyO* control	Genotype	-0.771	47	0.4444
	pUAST-α3;CJ10/+ flies vs *Act5c-Gal4/CyO* control	Genotype	-3.687	47	**0.0018**

4.2.5.4.3 Paralysis Onset Time of All Flies

In 4°C cold shock assay, when all tested 4-7-day old flies were accounted for, an effect of sex and genotype was found between the time to paralysis of *Act5C-Gal4/pUAST-α3;CJ10/+* flies compared to *pUAST-α3;CJ10/+* flies and *Act5C-Gal4/CyO* controls (Table 81). The significant effect of sex was seen within *Act5C-Gal4/pUAST-α3;CJ10/+* flies only, time to paralysis of females was significantly longer than males (Table 81, Figure 19C). The significant effect of genotype was seen in males and females (Table 81). Post-hoc comparison of males revealed time to paralysis of *Act5C-Gal4/pUAST-α3;CJ10/+* males (median: 130.5 s , IQR: 92.5-165.0 s) was not significantly different to p*UAST-α3;CJ10/+* control males (median: 118.0 s , IQR: 58.3-181.5 s) but relative to *Act5C-Gal4/CyO* control males (median: 360.0s , IQR: 0 s) was significantly shorter (Table 81, Figure 19C). Time to paralysis of *pUAST-α3;CJ10/+* males was also significantly shorter than *Act5C-Gal4/CyO* control males (Table 81, Figure 19C). Post-hoc comparison of females revealed time to paralysis of *Act5C-Gal4/pUAST-α3;CJ10/+* females (median: 177.0s , IQR: 126-324 s) was significantly longer than p*UAST-α3;CJ10/+* control females (median: 98.0s , IQR: 65.8-139.8 s) but

relative to *Act5C-Gal4/CyO* control females (median: 360.0s , IQR: 0 s) was significantly shorter (Table 81, Figure 19C). Similarly to males, time to paralysis of *pUAST-α3;CJ10/+* females was significantly shorter than in *Act5C-Gal4/CyO* control females (Table 81, Figure 19C). The results are a further indicate that ubiquitous $\alpha 3^{WT}$ expression moderately rescued cold-sensitivity in only *CJ10/+* female mutants via measure of paralysis onset time of all tested flies.

Table 82. KW and MWU analysis of the time to paralysis of all tested *Gal4/UAS_α3;CJ10/+* flies compared to parental controls at 4°C. Post-hoc results were corrected for multiple testing using Dunn's method, where P < 0.05 is indicated in bold.

	Data	Explanatory Variable(s)	Test statistic	df	*P*-value
KW	All fly strain	Sex	82.56	5	**<0.0001**
	All fly strain	Genotype	82.63	2	**<0.0001**
MWU	*Act5C-Gal4/pUAST-α3;CJ10/+* flies	Sex	178	1	**0.0363**
	pUAST-α3;CJ10/+ flies	Sex	344	1	0.7343
	Act5C-Gal4/CyO control	Sex	493	1	0.9472
KW	Males	Genotype	37.96	2	**<0.0001**
	Females	Genotype	44.53	2	**<0.0001**
Post-hoc Test for males	*Act5C-Gal4/pUAST-α3;CJ10/+* vs *pUAST-α3;CJ10/+* flies	Genotype			>0.9999
	Act5C-Gal4/pUAST-α3;CJ10/+ flies vs *Act5c-Gal4/CyO* control	Genotype			**<0.0001**

	pUAST-α3;CJ10/+ flies vs *Act5c-Gal4/CyO* control	Genotype			**<0.0001**
Post-hoc Test for females	*Act5C-Gal4/pUAST-α3;CJ10*/+ vs *pUAST-α3;CJ10*/+ flies	Genotype			**0.0201**
	Act5C-Gal4/pUAST-α3;CJ10/+ flies vs *Act5c-Gal4/CyO* control	Genotype			**0.001**
	pUAST-α3;CJ10/+ flies vs *Act5c-Gal4/CyO* control	Genotype			**<0.0001**

4.2.5.4.4 Paralysis Recovery Time

In 4°C cold shock assay, the time taken for 4-7-day old flies to recovery from paralysis was recorded as an additional measure of cold-shock behaviour. A main effect of genotype was found between *Act5C-Gal4/pUAST-α3*;CJ10/+ compared to *pUAST-α3;CJ10*/+ flies and *Act5C-Gal4/CyO* controls (Table 82). The median recovery time of *Act5C-Gal4/pUAST-α3*;CJ10/+, *pUAST-α3;CJ10*/+ and *Act5C-Gal4/CyO* flies was 100 s (IQR: 84.0-115.0 s), 139 s (IQR: 87.0-194.0 s), 46 s (IQR: 21.8-63.0 s), respectively (Figure 19D) .Post-hoc test revealed *Act5C-Gal4/pUAST-α3;CJ10*/+ flies had a significantly shorter recovery time than *pUAST-α3;CJ10*/+ flies but a significantly longer recovery time than *Act5C-Gal4*/CyO controls (Table 82, Figure 19D). The results indicate that ubiquitous $\alpha 3^{WT}$ expression moderately rescued cold-sensitivity in *CJ10*/+ mutants via measure of recovery time from paralysis.

Table 83. GLM analysis of the recovery time of *Gal4/UAS_α3;CJ10/+* flies compared to parental controls at 24-25℃. Post-hoc results were corrected for multiple testing using Holm-Bonferroni method, where P < 0.05 is indicated in bold.

	Data	Explanatory Variable(s)	Test statistic	df	*P*-value
GLM	All fly strains	Genotype * Sex	1.4787	2, 97	0.233
	All fly strains	Sex	1.2576	1, 101	0.2648
	All fly strains	Genotype	32.215	2, 100	**$1.59*10^{-11}$**
Post-hoc Test	*Act5C/pUAST-α3;CJ10*/+ vs *pUAST-α3;CJ10*/+ flies	Genotype	3.351	100	**0.0011**
	Act5C/pUAST-α3;CJ10/+ flies vs *Act5C-Gal4/CyO* control	Genotype	4.741	100	**<0.0001**
	pUAST-α3;CJ10/+ flies vs *Act5C-Gal4/CyO* control	Genotype	5.859	100	**<0.0001**

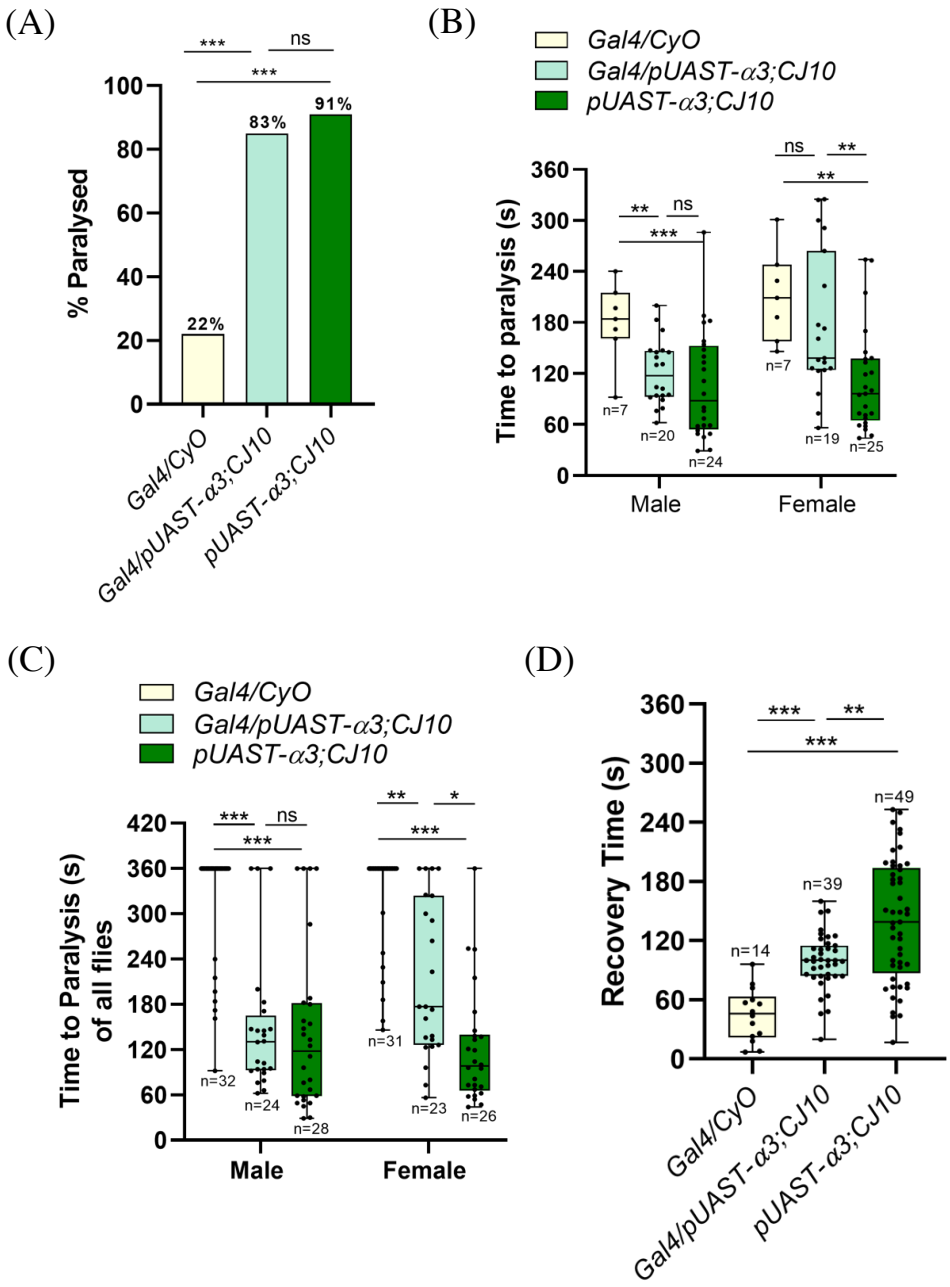

Figure 19. The effect of ubiquitous wildtype *ATP1A3* expression on cold-shock paralysis behaviour of young (4-7-day old) virgin heterozygous CJ10 adult at 4℃. **(A)** Total flies paralysed (%) during cold-shock. **(B)** Time taken in seconds (s) for flies to become paralysed within 360s. Final sample size displayed on graph excludes flies that did not become paralysed within 360 s. **(C)** Time taken in seconds(s) for paralysis onset when all tested flies are accounted for. **(D)** Time taken (s) for flies to recover from paralysis in a 24-25℃ water bath. All data shown as median and IQR (box plots). Whiskers represent the maximum and minimum non-outlier values. Black circles overlaying graphs represent all non-outlier data points. * $P < 0.05$; ** $P < 0.01$; *** $P < 0.001$; ns, not significant as determined by Fisher's Exact test (Fig. A), GLM analysis (Fig. B and D) and Kruskal Wallis analysis (Fig. C).

4.2.5.5 Rescue of *ATPα DTS1R1* Cold-shock Behaviour

4.2.5.5.1 Paralysis Outcome

In 4°C cold shock assay, the percentage of 4-7-day old flies paralysed was recorded as measure of cold shock behaviour. A main effect of genotype was found (Table 83). The *Act5C-Gal4/pUAST-α3;R1//+* flies that experienced cold-induced paralysis within 360 s was significantly higher than *Act5C-Gal4/CyO* controls but not relative to *pUAST-α3;R1/+* flies (Table 83, Figure 20A). It was observed that 33 out of 52 (63.46%) *Act5C/pUAST-α3;R1/+* flies, 39 out of 53 (73.58%) *pUAST-α3;R1/+* flies and 14 out of 63 (22.22%) *Act5C-Gal4/CyO* controls experienced cold-induced paralysis (Figure 20A). The results indicate cold-sensitivity in *R1/+* mutants without transgene expression (*pUAST-α3;R1/+*) was not rescued by ubiquitous $\alpha 3^{WT}$ expression via measure of paralysis outcome.

Table 84. Fisher's Exact analysis of the percentage of paralysed Gal4/UAS_α 3;R1/+flies compared parental controls at 4°C. Pairwise Fisher's Exact analyses were corrected for multiple testing using Holm-Bonferroni method, where P < 0.05 is indicated in bold.

	Data	Explanatory Variable(s)	*P*-value
Fisher's Exact Test	All fly strains	Sex	0.5223
	All fly strains	Genotype	**$1.464*10^{-8}$**
Pairwise Fisher's Exact Test	*Act5C-Gal4/pUAST-α3;R1/+* vs *pUAST-α3;R1/+* flies	Genotype	0.298
	Act5C-Gal4/pUAST-α3;R1/+ flies vs *Act5c-Gal4/CyO* control	Genotype	**0.0000193**
	pUAST-α3;R1/+ flies vs *Act5c-Gal4/CyO* control	Genotype	**$9.66*10^{-8}$**

4.2.5.5.2 Paralysis Onset Time

In 4°C cold shock assay, the time taken for paralysis onset of 4-7-day old flies was recorded as an additional measure of cold shock behaviour. No significant effect was found among time to paralysis of *Act5C-Gal4/pUAST-α3;R1/+* flies relative to *pUAST-α3;R1/+* flies and *Act5C-Gal4/CyO* controls (Table 84, Figure 20B). The median time of *Act5C-Gal4/pUAST-α3;R1/+*, *pUAST-α3;R1/+* and *Act5C-Gal4/CyO* flies was 146 s (IQR: 103.5-238.5 s), 169 s (IQR: 116.0-219.0 s), and 191.5 s (IQR: 160.3-231.8 s), respectively (Figure 20B). The results indicate no deficit in *R1* mutants without transgene expression (*pUAST-α3;R1/+*), therefore, unable to assess ubiquitous $\alpha 3^{WT}$ expression in rescuing cold-sensitivity in *R1/+* mutants via measure of flies that experienced paralysis within 360 s cut-off.

Table 85. GLM analysis of the paralysis onset time of *Gal4/UAS_α3;R1/+* flies compared to parental controls at 4°C.

	Data	Explanatory Variable(s)	Test statistic	df	*P*-value
GLM	All fly strains	Genotype * Sex	0.209	2, 80	0.8119
	All fly strains	Sex	0.6641	1, 84	0.4174
	All fly strains	Genotype	0.7252	2, 83	0.4873

4.2.5.5.3 Paralysis Onset Time of All Flies

In 4°C cold shock assay, when all tested 4-7-day old flies were accounted for, an effect of sex and genotype was found between the time to paralysis of *Act5C-Gal4/pUAST-α3;R1/+* flies compared to *pUAST-α3;R1/+* flies and *Act5C-Gal4/CyO* controls (Table 85). The significant effect of sex was not seen within genotypes, so data was merge together (Table 85, Figure 20C). The median time to paralysis of *Act5C-Gal4/pUAST-*

α3;R1/+, *pUAST-α3;R1*/+ and *Act5C-Gal4*/*CyO* control flies was 240.5 s (IQR: 123.3-360 s), 208 s (IQR: 125.0-360 s), and 360 s (IQR: 0 s), respectively (Figure 20C). Post-hoc comparison of males revealed time to paralysis of *Act5C-Gal4*/*pUAST-α3;R1*/+ was not significantly different to p*UAST-α3;R1*/+ but relative to *Act5C-Gal4*/*CyO* controls was significantly shorter (Table 85, Figure 20C). The results indicate cold-sensitivity of *R1* mutants without transgene expression (*pUAST-α3;R1*/+) was not rescued by ubiquitous $\alpha 3^{WT}$ expression via measure of paralysis onset time of all tested flies.

Table 86. KW and MWU analysis of the time to paralysis of all tested *Gal4*/*UAS_α3;R1*/+ flies compared to parental controls at 4℃. Post-hoc results were corrected for multiple testing using Dunn's method, where P < 0.05 is indicated in bold.

	Data	Explanatory Variable(s)	Test statistic	df	*P*-value
KW	All fly strain	Sex	34.80	5	**<0.0001**
	All fly strain	Genotype	34.57	2	**<0.0001**
MWU	*Act5C-Gal4*/*pUAST-α3;R1*/+ flies	Sex	328	1	0.9735
	pUAST-α3;R1/+ flies	Sex	326	1	0.6591
	Act5C-Gal4/*CyO* control	Sex	493	1	0.9472
Post-hoc Test	*Act5C-Gal4*/*pUAST-α3;R1*/+ vs *pUAST-α3;R1*/+ flies	Genotype			0.8702
	Act5C-Gal4/*pUAST-α3;R1*/+ flies vs *Act5c-Gal4*/*CyO* control	Genotype			**<0.0001**
	pUAST-α3;R1/+ flies vs *Act5c-Gal4*/*CyO* control	Genotype			**<0.0001**

4.2.5.5.4 Paralysis Recovery Time

In 4°C cold shock assay, the time taken for 4-7-day old flies to recovery from paralysis was recorded as an additional measure of cold-shock behaviour. A main effect of genotype was found between the recovery time of *Act5C-Gal4/pUAST-α3;R1/+* compared to *pUAST-α3;R1/+* flies and *Act5C-Gal4/CyO* controls (Table 86). The median recovery time of *Act5C-Gal4/pUAST-α3;R1/+*, *pUAST-α3;R1/+* and *Act5C-Gal4/CyO* controls was 62 s (IQR: 12-78 s), 104 s (IQR: 23.0-144.0 s), and 46 s (IQR: 22-63 s), respectively (Figure 20D). Post-hoc test revealed the recovery time of *Act5C-Gal4/pUAST-α3;R1/+* flies was significantly shorter than *pUAST-α3;R1/+* flies but not relative to *Act5C-Gal4/CyO* controls (Table 86, Figure 20D). The recovery time of *pUAST-α3;R1/+* flies was found to be significantly longer than *Act5C-Gal4/CyO* controls (Table 86, Figure 20D). The results indicate ubiquitous $\alpha 3^{WT}$ expression moderately rescued cold-sensitivity in *R1/+* mutants via measure of recovery time from paralysis.

Table 87. GLM analysis of the recovery time of *Gal4/UAS_α3;R1/+* flies compared to parental controls at 24-25°C. Post-hoc results were corrected for multiple testing using Holm-Bonferroni method, where P < 0.05 is indicated in bold.

	Data	Explanatory Variable(s)	Test statistic	df	*P*-value
GLM	All fly strains	Genotype * Sex	0.2522	2, 80	0.7777
	All fly strains	Sex	0.7938	1, 84	0.3755
	All fly strains	Genotype	7.8777	2, 83	**0.000737**
Post-hoc Test	*Act5C-Gal4/pUAST-α3;R1/+* vs *pUAST-α3;R1/+* flies	Genotype	3.036	83	**0.0096**

	Act5C-Gal4/pUAST-α3;R1/+ flies vs *Act5C-Gal4/CyO* control	Genotype	0.730	83	0.4674
	pUAST-α3;R1/+ flies vs *Act5C-Gal4/CyO* control	Genotype	2.623	83	**0.0207**

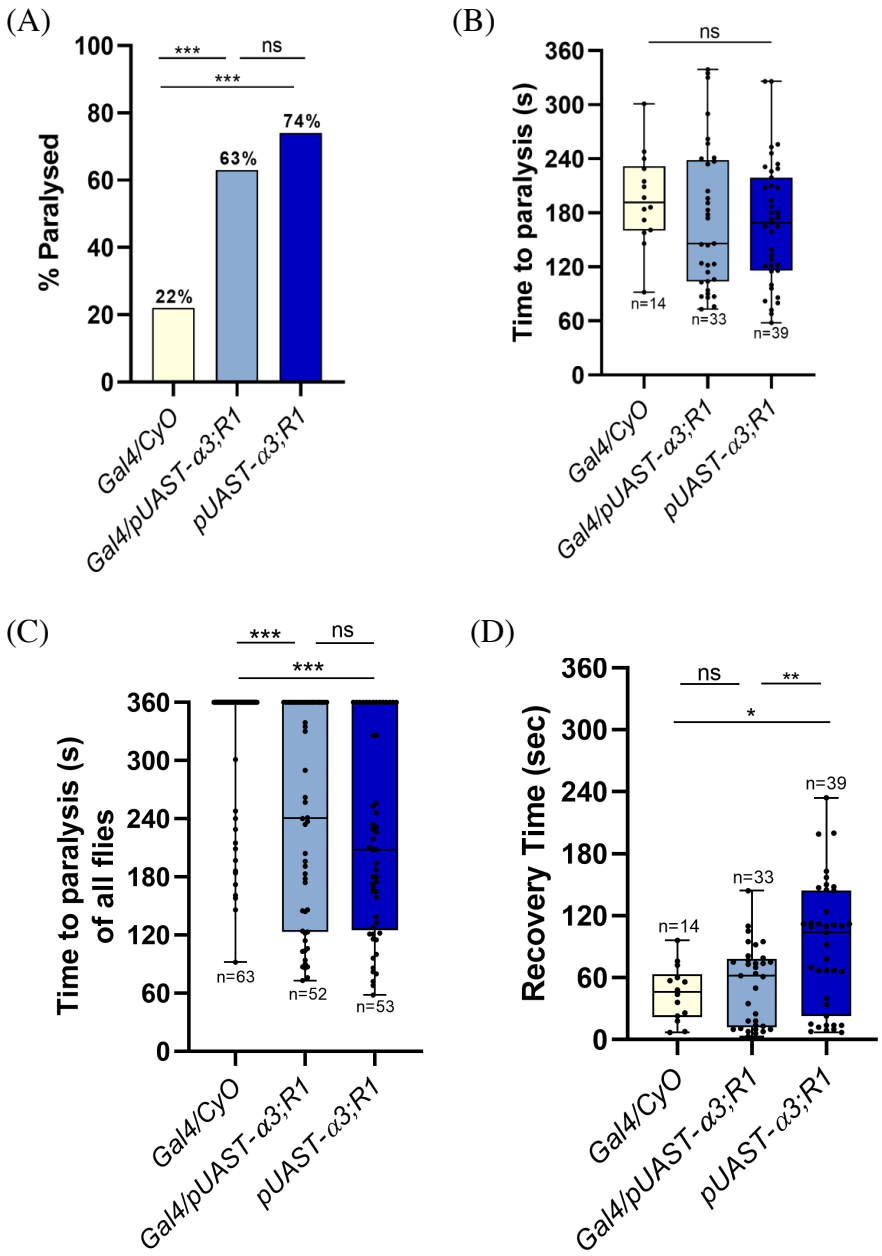

Figure 20. The effect of ubiquitous wildtype *ATP1A3* expression on cold-shock paralysis behaviour of young (4-7-day old) heterozygous *R1* adult flies at 4℃. (A) Total flies paralysed (%) during cold-shock. **(B)** Time taken in seconds (s) for flies to become paralysed within 360s. Final sample size displayed on graph excludes flies that did not become paralysed within 360 s. **(C)** Time taken in seconds(s) for paralysis onset when all tested flies are accounted for. **(D)** Time taken (s) for flies to recovery from paralysis in a 24-25℃ water bath. All data shown as median and IQR (box plots). Whiskers represent the maximum and minimum non-outlier values. Black circles overlaying graphs represent all non-outlier data points. * $P < 0.05$; ** $P < 0.01$; *** $P < 0.001$; ns, not significant as determined by Fisher's Exact test (Fig. A), GLM analysis (Fig. B and D) and Kruskal Wallis analysis (Fig. C).

4.2.5.6 Discussion

This research is the first to report the transgenic rescue of phenotypic deficits in young heterozygous *ATPα CJ10* (p.Gly744Ser) and *R1* (p. Ile905Trpfs*8) mutant flies by ubiquitous expression of a copy of the human *ATP1A3*^{WT} transgene via the *Gal4-UAS* system. The *ATPα CJ10* (p.Gly744Ser) and *R1* (p. Ile905Trpfs*8) mutants carry the fly equivalent of the human Gly755Ser AHC mutation (Heinzen et al., 2014) or a null mutation (Ashmore et al., 2009) respectively. The 4℃ cold shock assay revealed decreased sensitivity to cold stress in *Act5C-Gal4/pUAST-α3;CJ10/+* and *Act5C-Gal4/pUAST-α3;R1/+* flies. This was indicated by the ability of both *Act5C-Gal4/pUAST-α3;CJ10/+* and *Act5C-Gal4/pUAST-α3;R1/+* fly lines to recover significantly faster from paralysis than the p*UAST* parental fly lines (Figure 19D and Figure 20D). The median recovery time of 4-7-day old *Act5C-Gal4/pUAST-α3;CJ10/+* and *Act5C-Gal4/pUAST-α3;R1/+* flies was reduced by more than 30 s relative to age-matched p*UAST* parental flies (Figure 19D and Figure 20D). In addition to this, the assay revealed the ability of *Act5C-Gal4/pUAST-α3;CJ10/+* females to withstand exposure to cold stress for significantly longer than p*UAST* parental females (Figure 19B and C). The median time to paralysis in 4-7-day old *Act5C-Gal4/pUAST-α3;CJ10/+* females differed by ~18% compared to age-matched p*UAST* parental females (Figure 19B and C). These findings suggest that the human α3-subunit is functionally equivalent to that of the fly α-subunit, adding to the body of research that reports the successful functionality of the h-NKA in the fly system (Dalla et al., 2013). Moreover, the rescue of a heterozygous null phenotype, whereby the *Act5C-Gal4/pUAST-α3; R1/+* flies recovered from paralysis within a similar timeframe to that of control flies(Figure 20D), provides strong evidence to suggest the capability of the human α3-subunit to functional replace the inactive copy of the fly α-subunit for restoring wildtype function. However,

a high degree of functional conservation between the human α3-subunit and fly α-subunit cannot be concluded as *CJ10*/+ mutant phenotypes associated with cold shock were not rescued to an extent comparable to control flies in this study. The *Act5C-Gal4*/*pUAST-α3; CJ10*/+ flies were significantly quicker to paralysis and took significantly longer to recovery from paralysis relative to *Act5C-Gal4*/*CyO* controls (Figure 19B and D). They did, however, have paralysis onset and recovery times that were similar to those of CS flies. CS flies showed a median paralysis onset time of 145 s (IQR = 228.3-120.3) (Figure 16C) and a recovery time of 112.5 s (IQR = 138.5-65.75) (Figure 16E) compared to paralysis onset of 134.5 s (IQR = 176.0-94.5) (Figure 19B) and a recovery time of 100 s (IQR = 63.0-21.75) (Figure 19D) for *Act5C-Gal4*/*pUAST-α3;CJ10*/+ flies. A possible explanation for failure of the human *ATP1A3*^{WT} transgene to rescue *CJ10*/+ mutant phenotypes to the level displayed by *Act5C-Gal4*/*CyO* control flies could be due to the endogenous d-NKA α/β combination being functionally better than the h-NKAα3/ β combination for optimal NKA activity in fly neurones. It could also be associated with insufficient transgene expression. The *ATP1A3*^{WT} transgene may not have been expressed to a level comparable with endogenous levels of the wildtype *ATPα* gene in fly neurones, such that the available wildtype gene product was not sufficient to restore normal phenotypic behaviour. Incomplete rescue by insufficient transgene expression could be attributed to the fact that only a single copy of the *pUAST-α3* transgene was expressed in the fly. Alternatively, it could be due to the use of the *Act5C-Gal4* driver as opposed to the *tub-Gal4* driver that has been reported to be ~2.5 time stronger than *Act5C-Gal4* (Ni et al., 2009).

Cold shock rescue experiments also revealed that ubiquitous expression of the *ATP1A3*^{WT} transgene could not rescue the cold shock response of *CJ10*/+ and *R1*/+ mutant flies via measure of paralysis outcome (Figure 19A and Figure 20A). This was

indicated by no significant difference in the percentage of paralysed *CJ10*/+ and *R1*/+ mutants with transgene expression (*Act5C-Gal4/pUAST-α3;CJ10*/+ and *Act5C-Gal4/pUAST-α3;R1*/+ flies) compared to mutants without (*pUAST-α3;CJ10*/+ and *pUAST-α3;R1*/+ flies) (Figure 19A and Figure 20A). This is further evidence to suggest that the endogenous d-NKA α/β combination is functionally better than the h-NKAα3/β combination for optimal NKA activity in fly neurones. The cold shock rescue experiment also revealed sex differences indicated by the ability of *Act5C-Gal4/pUAST-α3;CJ10*/+ females to withstand exposure to cold stress for significantly longer than their male counterparts (Figure 19B and Figure 19C). The median time to paralysis of 4-7-day old *Act5C-Gal4pUAST-α3;CJ10*/+ males and females differed by ~16% (Figure 19B and Figure 19C), thus adding to the body of knowledge that responses to cold stress can differ between *D. melanogaster* males and females (Garcia and Teets, 2019; Garcia et al., 2020; Andersen et al., 2022), specifically males showing higher sensitivity to cold than females (David et al., 1998; Bubliy et al., 2002). Moreover, the significant difference between the *Act5C-Gal4pUAST-α3;CJ10*/+ sexes is likely driving the milder rescue of paralysis onset in *CJ10*/+ mutant females compared with *CJ10*/+ mutant males. Interestingly, sex differences were observed only in *Act5C-Gal4pUAST-α3;CJ10*/+ flies. Similarly, a study reported transgenic females driven by the *Act5C-Gal4* driver took significantly longer than males to become paralysed upon exposure to high temperatures, however, the reason for this was reported to be unknown (Thum et al., 2006).

The negative geotaxis rescue experiments revealed climbing latency deficit in *CJ10*/+ females without transgene expression (*pUAST-α3;CJ10*/+) was not rescued by ubiquitous $a3^{WT}$ expression (Figure 17C). Moreover, no deficit observed by *pUAST-α3;CJ10*/+ and *pUAST-α3;R1*/+ via measure of distance climbed in 3 s or climbing

speed and climbing latency for *pUAST-α3;R1*/+ (Figure 17A-B and Figure 18A-C), meant that it was not possible to assess the ability of ubiquitous $\alpha 3^{WT}$ expression to rescue climbing performance of *ATPα* mutants. The lack of a deficit in *pUAST-α3;CJ10*/+ and *pUAST-α3;R1*/+ flies was not expected due to previous observation in this research of CS-*CJ10*/+ and CS-*R1*/+ mutant flies showing a clear deficit in climbing performance (Figure 13A-C). A possible explanation for this could be related to leaky expression of the *pUAST-α3* transgene within the genome of *pUAST-α3;CJ10*/+ and *pUAST-α3;R1*/+ flies. The *pUAST-attB* vector (Bischof et al., 2007) used in this research has the potential for leaky expression evidenced by a study reporting rescue of the lethality phenotype in a *Drosophila* mutant carrying only the *UAS* construct (Gluderer et al., 2010). Thus, it is important to confirm or rule out the event of leaky expression as could mask phenotypic rescues by wildtype *ATP1A3* or mutant phenotypes of the D801N transgenic lines. To validate the notion of possible leaky expression, real-time PCR should be carried out in future work to quantify levels the human transgene if any in all *UAS* fly lines.

4.2.6 Characterization of AHC-relevant phenotypes in ATP1A3^{D801N} transgenic flies

4.2.6.1 Introduction

Phenocopy experiments help to examine whether and to what extent an animal system can be used to model a human disease to gain a better understanding of the disease pathophysiology and treatment. In AHC research, essential and major criteria of AHC diagnosis such as hemiplegia and dystonia respectively (Table 1) have both been mimicked in heterozygous *Mashlool* (Asp801Asn) mice, which carry the most common AHC mutation in humans (Hunanyan et al., 2015). With the establishment of the *Gal4/UAS* system, this chapter aims to evaluate whether and to what extent the expression of the human Asp801Asn (D801N) mutation induces AHC-relevant phenotypes in *D. melanogaster*, further validating the suitability as a model organism for studying AHC pathophysiology and treatment options. Moreover, this experiment will also help to identify conserved verses species-specific phenotypes of NKA α3 dysfunction. To investigate this, two UAS vectors, pUAST and SST13 (Bischof et al., 2007; Zhang et al., 2022), were used to facilitate expression of the *ATP1A3*^{D801N} transgene. These UAS vectors differ in their integration and selection systems. The pUAST vector carries a fully functional *white* gene, whereas SST13 vector contains a partial, non-functional *white* gene and uses the split-white system, requiring a complementary *white* gene fragment at the attP landing site for full *white* gene function (Bischof et al., 2007; Suh et al., 2015). This system reduces off-target insertions and improve screening efficiency (Bischof et al., 2007). The transgenes were integrated at distinct attP landing sites on either the second (*pUAST-α3*$^{D801N/+}$) or the third (*SST13-α3*$^{D801N/+}$) chromosome (detailed in Section 3.2.3). Flies hemizygous for the *UAS-ATP1A3*^{D801N} transgene were crossed to the *Act5C-Gal4/CyO* driver line to achieve ubiquitous expression of the human mutant transgene. The resulting transgenic flies were examined using negative geotaxis and cold-shock assay to determine whether the

invertebrate models recapitulate core motor symptoms of AHC. Moreover, using different UAS vectors integrated at distinct chromosomal locations allows for the evaluation of transgene expression difference influenced by vector design and chromosomal context.

4.2.6.2 Climbing performance of *ATP1A3* D801N transgenic flies

4.2.6.2.1 Height climbed

In the negative geotaxis assay, distance climbed in 3 s was assessed as a measure of gross motor function in 2-3-day old $a3^{D801N/+}$ transgenic flies. A main effect of genotype was found in both *Act5C-Gal4*/*UAS-*$\alpha3^{D801N/+}$ fly lines relative to their parental controls (Table 87). The *Act5c-Gal4*/*pUAST-*$a3^{D801/+N}$ flies and *pUAST-*$a3^{D801N/+}$ controls climbed a mean distance of 5.49 cm (SD: 2.05 cm) and 4.94 cm (SD: 2.37 cm) respectively (Figure 21A). For *Act5c-Gal4*/*SST13-*$a3^{D801N/+}$ flies and *SST13-*$a3^{D801N/+}$ controls, the mean distance climbed was 5.23 cm (SD: 2.09 cm) and 4.72 cm (SD: 2.02 cm) respectively (Figure 21A). The *Act5c-Gal4*/*CyO* controls climbed a mean distance of 3.63 cm (SD: 1.74 cm) (Figure 21A). Post-hoc tests revealed both *Act5C-Gal4*/*UAS-*$\alpha3^{D801N/+}$ fly lines climbed significantly further than *Act5C-Gal4*/*CyO* controls but not further than *UAS-*$\alpha3^{D801N/+}$ controls (Table 87, Figure 21A). The height climbed by both *UAS-*$\alpha3^{D801N/+}$ control lines was also found to be significantly higher than *Act5C-Gal4*/*CyO* controls (Table 87, Figure 21A). The results indicate no deficit in the climbing performance of *Act5C-Gal4*/*UAS-*$\alpha3^{D801N/+}$ flies via measure of height climbed in 3s.

Table 88. GLM analysis of the height climbed in 3 s by *Gal4*/*UAS_α3D801N*/+ flies relative to parental controls. Post-hoc results were corrected for multiple testing using Holm-Bonferroni method, where P < 0.05 is indicated in bold.

	Data	Explanatory Variable(s)	Test statistic	df	*P*-value

Act5C-Gal4/pUAST-α3$^{D801N/+}$ Analysis					
GLM	*Act5C-Gal4/pUAST-α3$^{D801N/+}$* vs controls	Genotype * Sex	0.7379	2, 129	0.4801
	Act5C-Gal4/pUAST-α3$^{D801N/+}$ vs controls	Sex	0.8064	1, 133	0.3708
	Act5C-Gal4/pUAST-α3$^{D801N/+}$ vs controls	Genotype	9.7268	2, 132	**0.0001147**
Post-hoc Test	*Act5C-Gal4/pUAST-α3$^{D801N/+}$* vs *pUAST-α3$^{D801N/+}$* flies	Genotype	1.225	132	0.2227
	Act5C-Gal4/pUAST-α3$^{D801N/+}$ vs *Act5C-Gal4/CyO* flies	Genotype	4.261	132	**0.0001**
	pUAST-α3$^{D801N/+}$ control vs *Act5C-Gal4/CyO* flies	Genotype	3.117	132	**0.0045**
Act5C-Gal4/SST13-α3$^{D801N/+}$ Analysis					
GLM	*Act5C-Gal4/SST13-α3$^{D801N/+}$* vs controls	Genotype * Sex	0.7706	2, 127	0.4649
	Act5C-Gal4/SST13-α3$^{D801N/+}$ vs controls	Sex	1.288	1, 131	0.2585
	Act5C-Gal4/SST13-α3$^{D801N/+}$ vs controls	Genotype	9.449	2, 130	**0.0001474**
Post-hoc Test	*Act5C-Gal4/SST13-α3$^{D801N/+}$* vs *SST13-α3$^{D801N/+}$* flies	Genotype	1.039	130	0.3010
	Act5C-Gal4/SST13-α3$^{D801N/+}$ vs *Act5C-Gal4/CyO* flies	Genotype	4.205	130	**0.0001**

	SST13-α3$^{D801N/+}$ control vs *Act5C-Gal4/CyO* flies	Genotype	3.129	130	**0.0043**

4.2.6.2.2 Climbing Speed

In negative geotaxis assay, time taken to climb above 4 cm target line was assessed as another measure of gross motor function in 2-3-day old *a3*$^{D801N/+}$ transgenic flies. A main effect of genotype was found among the climbing speed of both *Act5C-Gal4/UAS-α3*$^{D801N/+}$ fly lines and their parental controls (Table 88). The median climbing time for *Act5C-Gal4/pUAST-a3*$^{D801N/+}$ flies and pUAST-*a3*$^{D801N/+}$ controls was 2.29 s (IQR: 1.63-2.88 s) and 2.30 s (IQR: 1.68-2.71 s) respectively (Figure 21B). For *Act5C-Gal4/SST13-a3*$^{D801N/+}$ flies and *SST13-a3*$^{D801N/+}$ controls, the median climbing time was 2.41 s (IQR: 1.98-3.11 s)and 2.65 s (IQR: 2.02-3.41 s) (Figure 21B).The median climbing time for *Act5C-Gal4/CyO* controls was 3.08 s (IQR: 2.67-4.26 s) (Figure 21B). Post-hoc tests revealed both *Act5C-Gal4/UAS-α3*$^{D801N/+}$ fly lines had a significantly faster climbing speed relative to *Act5C-Gal4/CyO* but not to *UAS-α3*$^{D801N/+}$ parental controls (Table 88, Figure 21B). Both *UAS-α3*$^{D801N/+}$ flies were also found to be significantly faster than *Act5C-Gal4/CyO* control animals (Table 88, Figure 21B). The results indicate no deficit in the climbing performance of *Act5C-Gal4/UAS-α3*$^{D801N/+}$ flies via measure of time required to reach target line.

Table 89. GLM analysis of the climbing speed of *Gal4/UAS_α3D801N/+* flies relative to parental controls. Post-hoc results were corrected for multiple testing using Holm-Bonferroni method, where P < 0.05 is indicated in bold.

	Data	Explanatory Variable(s)	Test statistic	df	*P*-value
Act5C-Gal4/pUAST-α3$^{D801N/+}$ Analysis					

GLM	*Act5C-Gal4/pUAST-*$\alpha 3^{D801N/+}$ vs controls	Genotype * Sex	0.4748	2, 118	0.6232
	Act5C-Gal4/pUAST-$\alpha 3^{D801N/+}$ vs controls	Sex	0.6773	1, 122	0.4121
	Act5C-Gal4/pUAST-$\alpha 3^{D801N/+}$ vs controls	Genotype	12.336	2, 121	**$1.331*10^{-5}$**
Post-hoc Test	*Act5C-Gal4/pUAST-*$\alpha 3^{D801N/+}$ vs *pUAST-*$\alpha 3^{D801N/+}$ flies	Genotype	-0.797	121	0.4267
	Act5C-Gal4/pUAST-$\alpha 3^{D801N/+}$ vs *Act5C-Gal4/CyO* flies	Genotype	3.672	121	**0.0007**
	pUAST-$\alpha 3^{D801N/+}$ control vs *Act5C-Gal4/CyO* flies	Genotype	4.405	121	**0.0001**
Act5C-Gal4/SST13-$\alpha 3^{D801N/+}$ Analysis					
GLM	*Act5C-Gal4/SST13-*$\alpha 3^{D801N/+}$ vs controls	Genotype * Sex	0.405	2, 126	0.6678
	Act5C-Gal4/SST13-$\alpha 3^{D801N/+}$ vs controls	Sex	0.9057	1, 130	0.343
	Act5C-Gal4/SST13-$\alpha 3^{D801N/+}$ vs controls	Genotype	5.8596	2, 129	**0.0036666**
Post-hoc Test	*Act5C-Gal4/SST13-*$\alpha 3^{D801N/+}$ vs *SST13-*$\alpha 3^{D801N/+}$ flies	Genotype	0.569	129	0.5638
	Act5C-Gal4/SST13-$\alpha 3^{D801N/+}$ vs *Act5C-Gal4/CyO* flies	Genotype	3.176	129	**0.0056**

	SST13-α3$^{D801N/+}$ control vs *Act5C-Gal4/CyO* flies	Genotype	2.583	129	**0.0218**

4.2.6.2.3 Climbing Latency

In negative geotaxis assay, time taken to initiate vertical movement following commencement of negative geotaxis was recorded as an additional measure of gross motor function in 2-3-day old *a3$^{D801N/+}$* transgenic flies. No significant difference was found between climbing latency of *Act5C-Gal4/UAS-α3$^{D801N/+}$* fly lines and their parental controls (Table 89). The median climbing latency of *Act5C-Gal4/pUAST-a3$^{D801N/+}$* flies and pUAST-*a3$^{D801N/+}$* controls was 0.51 s (IQR: 0.27-1.06 s) and 0.47 s (IQR: 0.17-0.91 s) respectively (Figure 21C). For *Act5C-Gal4/SST13-a3$^{D801N/+}$* flies and *SST13-a3$^{D801N/+}$* controls, the median climbing latency was 0.63 s (IQR: 0.29-1.23 s) and 0.65 s (IQR: 0.32-1.04 s) (Figure 21C).The median climbing time for *Act5C-Gal4/CyO* controls was 0.84 s (IQR: 0.49-1.05 s) (Figure 21C). The results indicate no deficit in climbing performance of *Act5C-Gal4/UAS-α3$^{D801N/+}$* flies via measure of time taken to initiate vertical movement.

Table 90. GLM analysis of the climbing latency of *Gal4/UAS_α3D801N/+* flies relative to parental controls.

	Data	Explanatory Variable(s)	Test statistic	df	*P*-value
Act5C-Gal4/pUAST-α3$^{D801N/+}$ Analysis					
GLM	*Act5C-Gal4/pUAST-α3$^{D801N/+}$* vs controls	Genotype * Sex	0.0623	2, 121	0.9396
	Act5C-Gal4/pUAST-α3$^{D801N/+}$ vs controls	Sex	0.0469	1, 125	0.8289

	Act5C-Gal4/pUAST-$\alpha 3^{D801N/+}$ vs controls	Genotype	0.6533	2, 124	0.5221
Act5C-Gal4/SST13-$\alpha 3^{D801N/+}$ Analysis					
GLM	*Act5C-Gal4/SST13-*$\alpha 3^{D801N/+}$ vs controls	Genotype * Sex	0.2923	2, 124	0.747
	Act5C-Gal4/SST13-$\alpha 3^{D801N/+}$ vs controls	Sex	0.727	1, 128	0.3955
	Act5C-Gal4/SST13-$\alpha 3^{D801N/+}$ vs controls	Genotype	1.8433	2, 127	0.1625

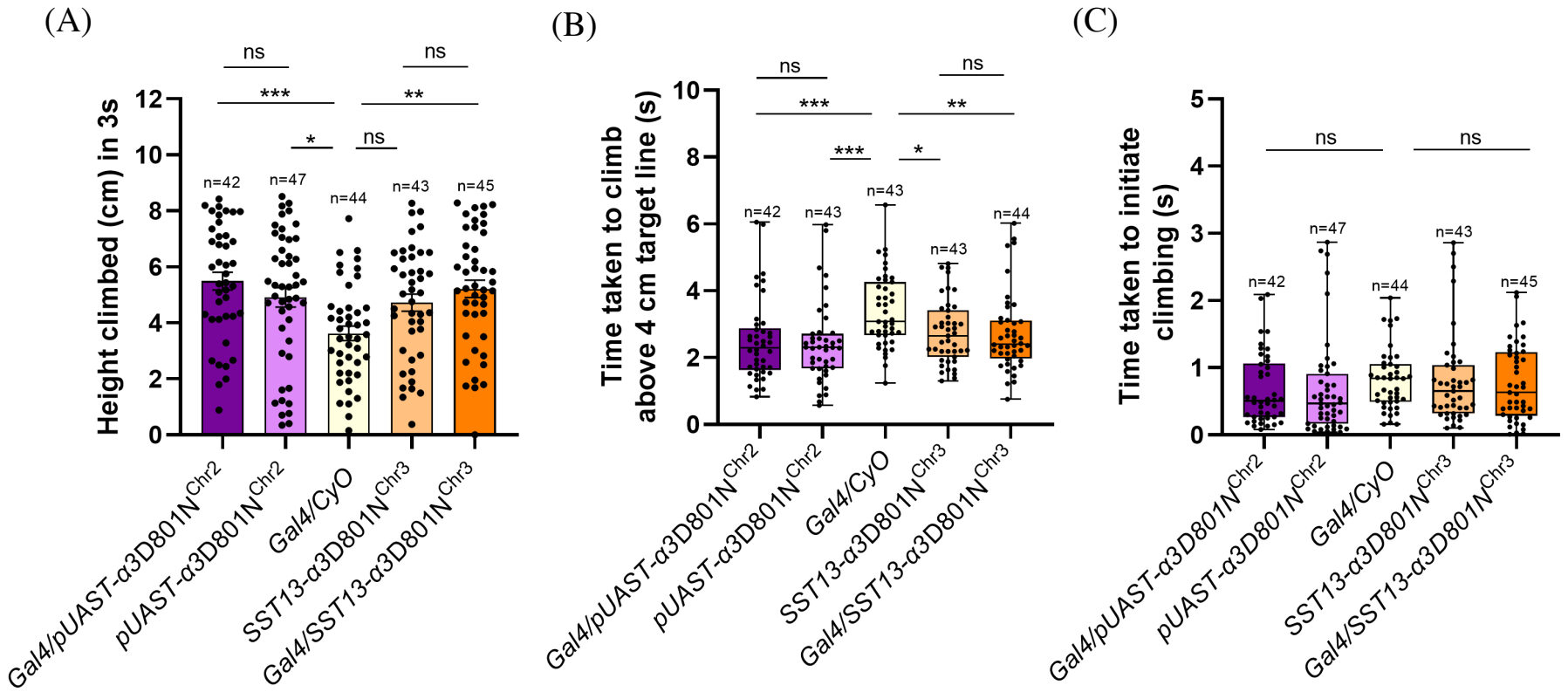

Figure 21. Assessment of climbing performance of young (2–3-day old) *D. melanogaster* hemizygous for the *ATP1A3*$^{D801N/+}$ transgene using the negative geotaxis assay. (A) Height (cm) climbed in 3 seconds (s) following commencement of negative geotaxis. Final sample size displayed on graph excludes flies that did not fall to bottom of vial. **(B)** Time taken to climb above the 4 cm target line. Final sample size displayed on graph B excludes flies that did not successfully complete the task and were classified as outliers based on Iterative Grubbs test (P<0.05). **(C)** Time taken (s) to initiate vertical movement following commencement of negative geotaxis. Data shown as mean ± SEM (bar graph) or median and IQR (box-plot). Whiskers represent the maximum and minimum non-outlier values. Black circles overlaying graphs represent all non-outlier data points. * $P < 0.05$; ** $P < 0.01$; *** $P < 0.001$; ns, not significant as determined by GLM analysis**.** The

Gal4/pUAST-α3$^{D801N/+}$ and Gal4/SST13-α3$^{D801N/+}$ genotypes represents the flies expressing the human mutant transgene, while *pUAST-α3$^{D801N/+}$ and SST13-α3$^{D801N/+}$* fly genotypes do not express the transgene due to the absence of the Gal4 driver. Both pUAST and SST13 are UAS vectors, but they differ in that SST13 makes use of the split-white system for efficient transgene insertion. The genotypes are denoted by 'Chr2' and 'Chr3' signifies that the human *D801N* transgene was inserted at an attP landing site on chromosome 2 or chromosome 3.

4.2.6.3 Cold shock behaviour of *ATP1A3* D801N transgenic flies

4.2.6.3.1 Paralysis Outcome at 4°C

In cold shock assay, the percentage of 4-7-day old *Act5C-Gal4/UAS-α3$^{D801N/+}$* flies that experienced cold-induced paralysis at 4°C did not significantly differ to age-matched parental control animals (Table 90). It was observed that 0 out of 37 (0%) *Act5C-Gal4/pUAST-α3$^{D801N/+}$* flies, 0 out of 46 (0%) *Act5C-Gal4/SST13-α3$^{D801N/+}$* flies, 0 out of 39 (0%) *pUAST-α3$^{D801N/+}$* flies, 0 out of 37 (0%) *SST13-α3$^{D801N/+}$* flies and 1 out 41 (2.44%) *Act5C-Gal4* control animals displayed cold-induced paralysis at 4°C. The results indicate no increased sensitivity to cold in *Act5C-Gal4/UAS-α3$^{D801N/+}$* flies by measure of paralysis outcome at 4°C

Table 91. Fisher's Exact analysis on the percentage of paralysed *Gal4/UAS_α3D801N/+* flies relative to parental controls at 4°C.

	Data	Explanatory Variable(s)	*P*-value
Fisher's Exact Test	*Act5C-Gal4/pUAST-α3$^{D801N/+}$* vs controls	Genotype	1
	Act5C-Gal4/SST13-α3$^{D801N/+}$ vs controls	Genotype	1

4.2.6.3.2 Paralysis Outcome at 2°C

In cold shock assay, the percentage of 4-7-day old *Act5C-Gal4/UAS-α3$^{D801N/+}$* flies that experienced cold-induced paralysis at 2°C did not significantly differ to age-matched parental control animals (Table 91, Figure 22A). It was observed that 18 out of 34 (52.94%) *Act5C-Gal4/pUAST-α3$^{D801N/+}$* flies, 16 out of 35 (45.71%) *Act5C-Gal4/SST13-α3$^{D801N/+}$* flies, 18 out of 32 (56.25%) *pUAST-α3$^{D801N/+}$*, 13 out of 22 (59.09%) *SST13-α3$^{D801N/+}$* and 22 out 34 (64.71%) *Act5C-Gal4/CyO* control animals displayed cold-

induced paralysis at 2°C (Figure 90). The results indicate no increased sensitivity to cold in *Act5C-Gal4/UAS-α3$^{D801N/+}$* flies by measure of paralysis outcome at 2°C.

Table 92. Fisher's Exact analyses on the percentage of paralysed *Gal4/UAS_α3D801N/+* flies relative to parental controls at 2°C.

	Data	Explanatory Variable(s)	*P*-value
Fisher's Exact Test	*Act5C-Gal4/pUAST-α3$^{D801N/+}$* vs controls	Sex	0.8952
	Act5C-Gal4/pUAST-α3$^{D801N/+}$ vs controls	Genotype	0.6274
	Act5C-Gal4/SST13-α3$^{D801N/+}$ vs controls	Sex	0.8796
	Act5C-Gal4/SST13-α3$^{D801N/+}$ vs controls	Genotype	0.279

4.2.6.3.3 Paralysis Onset Time

In 2°C cold shock assay, time taken until onset of paralysis was recorded as an additional measure of cold shock behaviour. Paralysis onset times of 5-8-day old *Act5C-Gal4/pUAST-α3$^{D801N/+}$* flies did not significantly differ to age-matched parental control animals (Table 92). The median time of *Act5C-Gal4/pUAST-α3$^{D801N/+}$* flies and *pUAST-a3$^{D801N/+}$* controls was 216.0 s (IQR: 141.3 -268.5 s) and 208.0 s (IQR: 167.8-249.8 s) respectively (Figure 22B). Meanwhile, a main effect of genotype was found among *Act5C-Gal4/SST13-α3$^{D801N/+}$* flies and parental controls (Table 92). Post-hoc test revealed *Act5C-Gal4/SST13-α3$^{D801N/+}$* flies took significantly longer to become paralysed than *Act5c-Gal4/CyO* flies but not relative to *SST13-α3$^{D801N/+}$* flies (Table 92, Figure 22B).The median time of *Act5C-Gal4/SST13-α3$^{D801N/+}$* flies and *SST13-α3$^{D801N/+}$* controls was 246.5 s (IQR: 208.8-304.3 s) and 222.0 s (IQR: 174.5-291.0 s) respectively (Figure 22B) . For *Act5C-Gal4/CyO* controls, the median time was 168.0 s (IQR: 160.8-212.5

s) (Figure 22B). The results indicate no increased sensitivity to cold in *Act5C-Gal4/UAS-α3$^{D801N/+}$* flies by measure of paralysis onset time at 2℃.

Table 93. GLM analysis of the time to paralysis of *Gal4/UAS_α3D801N/+* flies relative to parental controls at 2℃. Post-hoc results were corrected for multiple testing using Holm-Bonferroni method, where P < 0.05 is indicated in bold.

	Data	Explanatory Variable(s)	Test statistic	df	*P*-value
Act5C-Gal4/pUAST-α3$^{D801N/+}$ Analysis					
GLM	*Act5C-Gal4/pUAST-α3$^{D801N/+}$* vs controls	Genotype * Sex	0.5021	2, 52	0.6082
	Act5C-Gal4/pUAST-α3$^{D801N/+}$ vs controls	Sex	2.7347	2, 56	0.1038
	Act5C-Gal4/pUAST-α3$^{D801N/+}$ vs controls	Genotype	1.4546	2, 55	0.2423
Act5C-Gal4/SST13-α3$^{D801N/+}$ Analysis					
GLM	*Act5C-Gal4/pUAST-α3$^{D801N/+}$* vs controls	Genotype * Sex	0.72221	2, 45	0.4913
	Act5C-Gal4/pUAST-α3$^{D801N/+}$ vs controls	Sex	0.0004	1, 49	0.9836
	Act5C-Gal4/SST13-α3$^{D801N/+}$ vs controls	Genotype	6.4055	2, 48	**0.003422**
Post-hoc Test	*Act5C-Gal4/SST13-α3$^{D801N/+}$* vs SST13-*α3$^{D801N/+}$* control	Genotype	0.943	48	0.3550
	Act5c-Gal4/SST13-α3$^{D801N/+}$ vs *Act5C-Gal4/CyO* control	Genotype	3.321	48	**0.0032**

	SST13-α3$^{D801N/+}$ control vs *Act5C-Gal4/CyO* control	Genotype	2.170	134	0.0531

4.2.6.3.4 Paralysis Onset Time of All tested Flies

In 2°C cold shock assay, when all tested 5-8-day old flies were accounted for, no significant difference was found between the time to paralysis of both *Act5C-Gal4/pUAST-α3$^{D801N/+}$* fly lines relative to parental control flies (Table 93). The median time of *Act5C-Gal4/pUAST-α3$^{D801N/+}$* flies and *pUAST-a3$^{D801N/+}$* controls was 327.0 s (IQR: 206.8-360.0 s) and 328.0 s (IQR: 201.5-360.0 s) respectively (Figure 22C). Meanwhile, a main effect of genotype was found among *Act5C-Gal4/SST13-α3$^{D801N/+}$* flies and parental controls (Table 93). Post-hoc test revealed *Act5C-Gal4/SST13-α3$^{D801N/+}$* flies took significantly longer to become paralysed than *Act5c-Gal4/CyO* flies but not relative to *SST13-α3$^{D801N/+}$* flies (Table 93, Figure 22C). The median time of *Act5C-Gal4/SST13-α3$^{D801N/+}$* flies, and *SST13-α3$^{D801N/+}$* controls was 360.0 s (IQR: 248.0-360.0 s) and 327.5 s (IQR: 211.8-360.0 s) respectively (Figure 22C). The median time for *Act5C-Gal4/CyO* controls was 216.0 s (IQR: 165.8-360.0 s) (Figure 22C). The results are a further indication of a lack of increased sensitivity to cold in *Act5C-Gal4/UAS-α3$^{D801N/+}$* flies by measure of paralysis onset time of all flies tested at 2°C.

Table 94. KW analysis of the time to paralysis of all tested *Gal4/UAS_α3D801N/+* flies relative to parental controls at 2°C. Post-hoc results were corrected for multiple testing using Dunn's method, where P < 0.05 is indicated in bold.

	Data	Explanatory Variable(s)	KW statistic	*P*-value
Act5C-Gal4/pUAST-α3$^{D801N/+}$ Analysis				

KW	*Act5C-Gal4/pUAST-α3$^{D801N/+}$* vs controls	Sex	4.444	0.4874
	Act5C-Gal4/pUAST-α3$^{D801N/+}$ vs controls	Genotype	2.969	0.2266
Act5C-Gal4/SST13-α3$^{D801N/+}$ Analysis				
KW	*Act5C-Gal4/SST13-α3$^{D801N/+}$* vs controls	Sex	8.911	0.1127
	Act5C-Gal4/SST13-α3$^{D801N/+}$ vs controls	Genotype	8.278	**0.0159**
Post-hoc Test	*Act5C-Gal4/SST13-α3$^{D801N/+}$* vs *SST13-α3$^{D801N/+}$* control	Genotype		0.5520
	Act5C-Gal4/SST13-α3$^{D801N/+}$ vs *Act5C-Gal4/CyO* control	Genotype		**0.0121**
	SST13-α3$^{D801N/+}$ control vs *Act5C-Gal4/CyO* control	Genotype		0.6790

4.2.6.3.5 Paralysis Recovery Time

In 2°C cold shock assay, the time taken for 5-8-day old flies to recovery from paralysis was recorded as an additional measure of cold-shock behaviour. No significant difference was found between the recovery times of both *Act5C-Gal4/UAS-α3$^{D801N/+}$* fly lines relative to parental control animals (Table 94). The median recovery time of *Act5C-Gal4/pUAST-α3$^{D801N/+}$* flies and *pUAST-α3$^{D801N/+}$* controls was 71.0 s (IQR: 52.0-83.0 s) and 86.0 s (IQR: 48.3-114.3 s) respectively (Figure 22D). For *Act5C-Gal4/SST13-α3$^{D801N/+}$* flies and *SST13-α3$^{D801N/+}$* controls, the median recovery time was 63.5 s (IQR: 46.8-102.5 s) and 55.0 s (IQR: 20.0-106.5 s) respectively (Figure 22D). For *Act5C-*

Gal4/CyO controls, the median recovery time was 62.5 s (IQR: 54.8-75.5 s) (Figure 22D). The results indicate no increased sensitivity to cold in *Act5C-Gal4/UAS-α3$^{D801N/+}$* flies by measure of recovery time at 24-25°C.

Table 95. GLM of the recovery time of paralysed *Gal4/UAS_α3D801N/+* flies relative to parental controls at 2°C.

	Data	Explanatory Variable(s)	Test statistic	df	*P*-value
Act5C-Gal4/pUAST-α3$^{D801N/+}$ Analysis					
GLM	*Act5C-Gal4/pUAST-α3$^{D801N/+}$* vs controls	Genotype * Sex	0.7015	2, 55	0.5004
	Act5C-Gal4/pUAST-α3$^{D801N/+}$ vs controls	Sex	1.1993	1, 57	0.2781
	Act5C-Gal4/pUAST-α3$^{D801N/+}$ vs controls	Genotype	0.6671	2, 56	0.5172
Act5C-Gal4/SST13-α3$^{D801N/+}$ Analysis					
GLM	*Act5C-Gal4/SST13-α3$^{D801N/+}$* vs controls	Genotype * Sex	0.6704	2, 45	0.5165
	Act5C-Gal4/SST13-α3$^{D801N/+}$ vs controls	Sex	0.2348	2, 49	0.6301
	Act5C-Gal4/SST13-α3$^{D801N/+}$ vs controls	Genotype	0.0346	2, 48	0.966

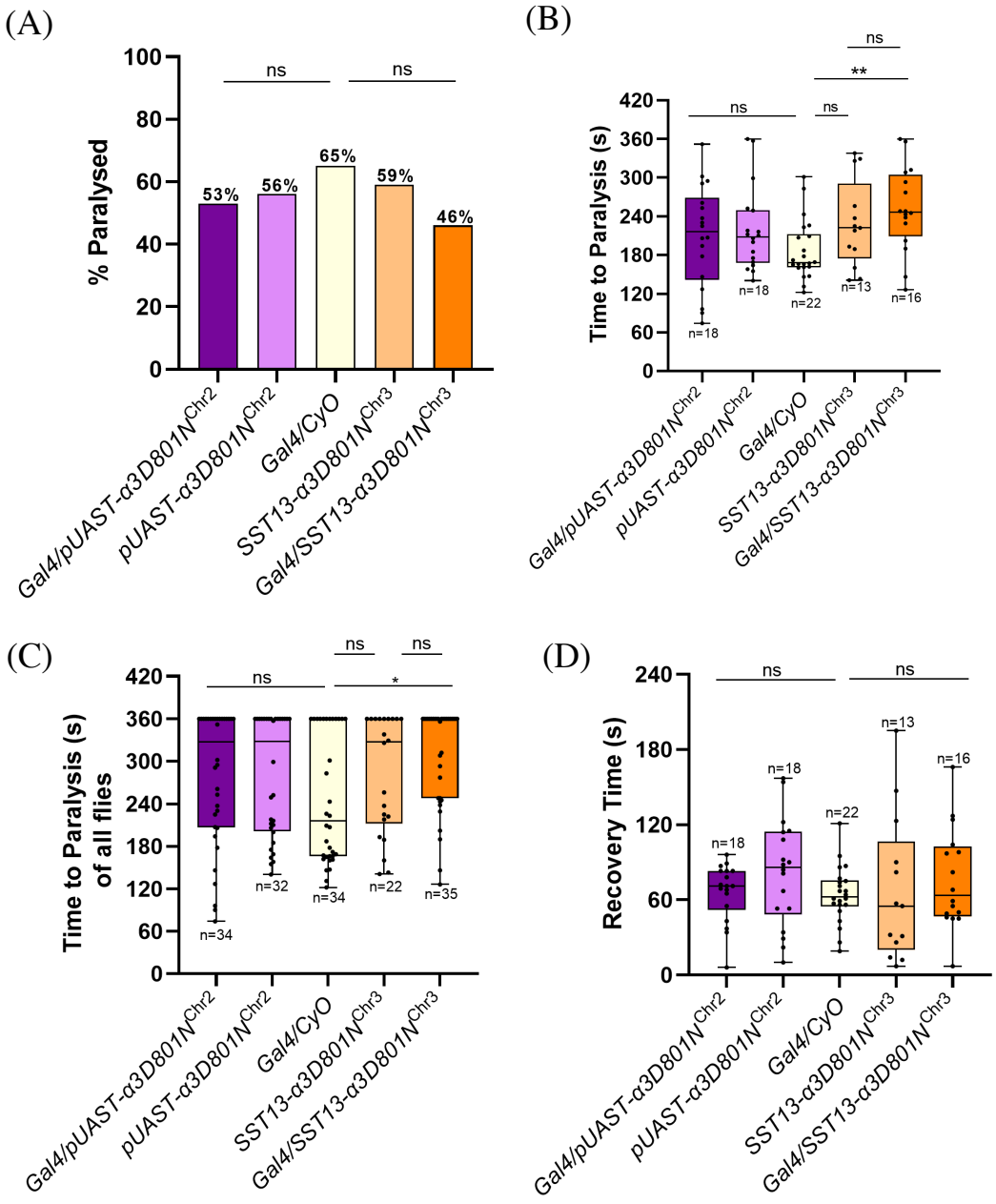

Figure 22. Cold-shock paralysis behaviour at 2℃ in young (5-8-day old) *D. melanogaster* adults hemizygous for the *ATP1A3$^{D801N/+}$* transgene. (A) Total flies paralysed (%) during cold-shock. **(B)** Time taken in seconds(s) for paralysis onset of flies within 360 s. Final sample size displayed on graph excludes flies that did not become paralysed within 360 s. **(C)** Time taken in seconds(s) for paralysis onset when all tested flies are accounted for. **(D)** Time taken (s) for flies to recovery from paralysis in a 24-25℃ water bath. All data shown as median and IQR (box-plot). Whiskers represent the maximum and minimum non-outlier values. Black circles overlaying graphs represent all non-outlier data points. * $P < 0.05$; ** $P < 0.01$; *** $P < 0.001$; ns, not significant as determined by Fisher's Exact test (Fig. A), GLM analysis (Fig. B and D) and Kruskal Wallis analysis (Fig. C). The Gal4/pUAST-α3D801N/+ and

Gal4/SST13-α3D801N/+ genotypes represents the flies expressing the human mutant transgene, while pUAST-α3D801N/+ and SST13-α3D801N/+ fly genotypes do not express the transgene due to the absence of the Gal4 driver. Both pUAST and SST13 are UAS vectors, but they differ in that SST13 makes use of the split-white system for efficient transgene insertion. The genotypes are denoted by 'Chr2' and 'Chr3' signifies that the human D801N transgene was inserted at an attP landing site on chromosome 2 or chromosome 3.

4.2.6.4 Discussion

Generated transgenic flies that expressed the human *ATP1A3*^{D801N} mutant transgene via the *Gal4-UAS* system, confirmed qualitatively by RT-PCR (Figure 11A) and western blot analysis (Figure 12) , could not be validated in this research as an alternative model of AHC. This was due to the novel *Act5C-Gal4*/*UAS-α3*$^{D801N/+}$ fly lines displaying behavioural responses that did not mimic relevant observations reported in mouse AHC models. The negative geotaxis assay revealed that movement and coordination of the *Act5C-Gal4*/*UAS-α3*$^{D801N/+}$ fly lines were intact. This was indicated by the ability of both *Act5C-Gal4*/p*UAST-α3*$^{D801N/+}$ and *Act5C-Gal4*/*SST13-α3*$^{D801N/+}$ fly lines to perform significantly better at the climbing tasks than the *Act5C-Gal4*/*CyO* parental line (Figure 21A-B). The *Act5C-Gal4*/*CyO* flies were intended to act as a wildtype control in this study since the mutant transgene was not present in the fly's genome, as confirmed by RT-PCR analysis. The average distance climbed in 3 s by 2-3-day old *Act5C-Gal4*/*CyO* control, *Act5C-Gal4*/p*UAST-α3*$^{D801N/+}$ and *Act5C-Gal4*/*SST13-α3*$^{D801N/+}$ flies was 3.60 cm, 5.49 cm, and 5.23 cm respectively (Figure 21A). The average distances climbed by both *Act5C-Gal4*/*UAS-α3*$^{D801N/+}$ fly lines were comparable to distances reported for young wildtype flies (i.e., ~4-5 cm) at the 3 s time-point (Nichols et al., 2012) but not to the wildtype CS control flies used in this research which exhibited an average distance of 3.88 cm in 3 s .However, the CS data was not normally distributed, so comparison with the median which was 4.88 cm in 3 s (Figure 13A), shows behaviour of D801N

transgenic flies were comparable to the wildtype control used here. This is further evidence to suggest that the gross motor control of the transgenic flies is intact and therefore seems to be unaffected by the ubiquitous expression of the *ATP1A3*$^{D801N/+}$ transgene. By contrast, heterozygous *Mashlool* (*Atp1a3*$^{D801N/+}$) mice are reported to display impaired motor coordination in the balance beam and rotarod assays (Hunanyan et al., 2015). The median time taken for the young *Act5C-Gal4*/*CyO* control, *Act5C-Gal4*/p*UAST-α3*$^{D801N/+}$ and *Act5C-Gal4*/*SST13-α3*$^{D801N/+}$ flies to climb pass the 4 cm target line was 3.26 s, 2.23 s and 2.39 s respectively (Figure 21B), indicating that both *Act5C-Gal4*/*UAS-α3*^{D801N} fly lines can climb above 4 cm in less than 3 s – less than the time reported for young wildtype flies (Nichols et al., 2012) and the wildtype CS control flies used in this research which took a median time of 2.67 s to climb above 4 cm (Figure 13B). Moreover, the measure of climbing time was a further confirmation that the *Act5C-Gal4*/*UAS-α3*$^{D801N/+}$ flies were significantly faster than the *Act5C-Gal4*/*CyO* control flies. In future work it would be interesting to characterise the general locomotor activity of *Act5C-Gal4*/*UAS-α3*$^{D801N/+}$ flies in the Zantiks system to determine whether the climbing performance of these transgenic mutants is an indicator of hyperactivity, a phenotype of described in AHC (I810N, D801N, D801Y) mouse models (Hunanyan et al., 2015; Kirshenbaum et al., 2015; Holm, T.H. et al., 2016). As both poor climbing performance and reduced locomotor activity was observed in CS-*CJ10*/+ and CS-*R1*/+ females during light phase (Figure 14F). The poor performance of *Act5C-Gal4*/*CyO* control flies, which appears to be driving the genotype effect in this study, could be related to the general fitness of the selected *Gal4* line. It is understood that, over time, fly stocks with a balancer can accumulate unwanted mutations, some of which may negatively impact the fly's overall fitness/health (Miller et al., 2019; Miller et al., 2020). Specifically, second chromosome balancer lines such as *CyO* have been reported to carry mutations that disrupt protein-coding genes (Miller et al., 2018). This includes the

postsynaptic receptor nicotinic Acetylcholine Receptor α6 (nAChRα6) gene, which is primarily expressed in the *Drosophila* nervous system, including regions of the fly brain involved in motor control (Öztürk-Çolak et al., 2024). Mutation of nAChRα6 has been reported to cause abnormal locomotor behaviour in adult flies (Miller et al., 2018; Öztürk-Çolak et al., 2024). Thus, the presence of the *CyO* balancer is a plausible explanation for the significantly slower climbing behaviour of *Act5C-Gal4/CyO* control flies (Figure 21B), even in comparison to *UAS* parental flies (p*UAST-α3*$^{D801N/+}$ and *SST13-α3*$^{D801N/+}$) that harbour the mutant transgene within their genome. The average distance climbed in 3 s by p*UAST-α3*$^{D801N/+}$, *SST13-α3*$^{D801N/+}$ and *Act5c-Gal4/CyO* flies was 4.94 cm, 4.76 cm and 3.60 cm respectively (Figure 21A). Meanwhile, the median time taken for p*UAST-α3*$^{D801N/+}$, *SST13-α3*$^{D801N/+}$ and *Act5c-Gal4/CyO* flies to pass the target line was 2.29 s, 2.75 s and 3.26 s respectively (Figure 21B). Although, the genetic backgrounds of *Gal4* and *UAS* flies differ, genotypes compared to were made to evaluate their behaviour as negative controls for transgene expression. Moreover, the climbing assay should be repeated on several occasions with the addition of *Act5C-Gal4/+* (generated by outcross of *Gal4* line to an appropriate WT strain), *Act5C-Gal4/UAS-α3*^{WT} and standard wildtype flies. This would help to address: (1) whether the climbing behaviour of *Act5C-Gal4/CyO* flies was driven by presence of the balancer; (2) confirm that gross motor control of *Act5C-Gal4/UAS-α3*$^{D801N/+}$ flies are intact; and (3) conclude whether the ubiquitous expression of the *ATP1A3*$^{D801N/+}$ transgene affects climbing behaviour of flies.

In addition to locomotor behaviour, stress-induced paralysis, another motor-related phenotype associated with AHC disease (Mikati et al., 2021), and recapitulated in heterozygous Mashlool (*Atp1a3*$^{D801N/+}$) and Matoub (*Atp1a3*$^{E815K/+}$) mouse models (Hunanyan et al., 2015; Helseth et al., 2018), was examined in *ATP1A3*$^{D801N/+}$ transgenic

flies. Here, 4℃ cold shock did not induce paralysis in any *Act5C-Gal4*/*UAS-α3*$^{D801N/+}$ or *UAS-α3*$^{D801N/+}$ parental flies. Cold-induced paralysis was observed in 1 out of 41 *Act5c-Gal4*/*CyO* control flies, which is negligible. The results suggest that ubiquitous expression of the *ATP1A3*$^{D801N/+}$ transgene does not affect the fly's sensitivity to cold at this temperature. Exposure to 2℃ cold shock caused over 50% of *Act5C-Gal4*/*UAS-α3*$^{D801N/+}$, *UAS-α3*$^{D801N/+}$ parental and *Act5c-Gal4*/*CyO* control flies to become paralysed (Figure 22A). However, there was no significant difference between fly lines, suggesting that the ubiquitous expression of the *ATP1A3*$^{D801N/+}$ transgene does not heighten the fly's sensitivity to cold at a colder temperature. This notion is supported by the *Act5C-Gal4*/*UAS-α3*$^{D801N/+}$ flies displaying paralysis onset and recovery times that were not significantly lower compared to *UAS-α3*$^{D801N/+}$ and *Act5c-Gal4*/*CyO* flies (Figure 22B-D), which were employed as negative controls for transgene expression. However, in the case of the *Act5C-Gal4*/*SST13-α3*$^{D801N/+}$ line, flies were observed to take significantly longer than *Act5C-Gal4*/*CyO* control flies to become paralysed (Figure 22B-C). This genotype effect is likely driven by the behaviour of the *Act5C-Gal4*/*CyO* flies. Unexpectedly, the *Act5C-Gal4*/*CyO* flies exhibited a higher paralysis outcome and a quicker onset time to paralysis compared to *Act5C-Gal4*/*UAS-α3*$^{D801N/+}$ and *UAS-α3*$^{D801N/+}$ flies (Figure 22A). It is possible that the genetic burden of the *CyO* balancer could be influencing the behaviour of *Act5C-Gal4*/*CyO* flies (Miller et al., 2018; Miller et al., 2020). To determine whether initial observations are driven by the balancer, the assay should be repeated with the addition of *Act5C-Gal4*/+ and wildtype CS control flies.

Negative geotaxis and cold shock experiments both revealed that the behavioural responses of the *Act5C-Gal4*/*UAS-α3*$^{D801N/+}$ fly lines did not significantly differ to their respective *UAS-α3*$^{D801N/+}$ parental fly lines (Figure 21 and Figure 22). The expected

experimental outcome was for *Act5C-Gal4*/*UAS-α3*$^{D801N/+}$ flies to perform significantly worse than *UAS-α3*$^{D801N/+}$ flies due to the ubiquitous expression of the human *ATP1A3*$^{D801N/+}$ transgene. This assumption was rationalised by the reported observations of the D801N mutation in the *Atp1a3* mice orthologue causing neurological defects in mice (Hunanyan et al., 2015). A plausible explanation for no observed differences could be related to the expression levels of the intact fly *ATPα* gene in transgenic flies, potentially compensating for the effects of the *ATP1A3*$^{D801N/+}$ transgene. A way to address this, is to cross the *UAS-α3*$^{D801N/+}$ transgene into the heterozygous *ATPα* null background (*R1*/+) to produce transgenic flies that carry only one functional copy of the *ATPα* gene and a copy the *ATP1A3*$^{D801N/+}$ transgene. This would help to understand whether the intact function of the d-NKA *α* is the issue.

V General Discussion

In this research, the identification of other AHC-relevant phenotypes including hypoactivity, sleep disturbances, motor performance defects and hypersensitivity to cold-stress paralysis reported in AHC patients and m-NKA α3 mutant mice (described in Table 1 and 4) as a consequence of the heterozygous *ATPα CJ10* (p.Gly744Ser) mutation equivalent to the human Gly755Ser AHC mutation (Heinzen et al., 2014) and the *R1* null (p. Ile905Trpfs*8) mutation (Ashmore et al., 2009; Öztürk-Çolak et al., 2024) in d-NKA *α* suggests functional equivalence to the h-NKA α3. Functional equivalence of the h/d-NKA α between species was validated in this research by ubiquitous expression of the human *ATP1A3* transgene partially or completely rescuing the prolonged paralysis recovery phenotype in the CS-*CJ10*/+ mutant and CS-*R1*/+ mutant flies respectively through the *Gal4*/*UAS* approach (Figure 19D and Figure 20D). Previous studies have also exemplified the effectiveness of the *Gal4*/*UAS* approach to determine functional conservation between human and fly genes to validate the invertebrate system as suitable model for study of human neurological-related diseases (Du et al., 2010; Saini et al., 2011). Moreover, the complete rescue of the heterozygous *R1*/+ null flies indicated by these mutants displaying a paralysis recovery time that is similar to that of the wildtype h-NKA α function in the *Gal4* control flies (Figure 20D) strongly suggests that the role of the d-NKA α-subunit is highly conserved throughout evolution. This is consistent with the overall high degree of homology seen between the d-NKA α and h-NKA α3 protein sequence (~76%,). It is also consistent with the finding that the d-NKA α is able to form a functional complex with the human neuron-specific β-subunit which produces NKA activity that is comparable to the fly endogenous d-NKA αβ complex found in neurons (Dalla et al., 2013). In addition, functional homology between d-NKA α and h-NKA α3 is consistent with observations within this research of the manifestation of AHC-relevant phenotypes as a result of the conserved

hydrophobic Gly residue at position 744 in the fly and 755 in humans (highlighted in pink, Figure 4) being substituted for the hydrophilic Ser residue which this research confirmed by Sanger sequencing (Figure 7D). In this research very few phenotypes were found to be mutation-specific which could suggest that the heterozygous p.Gly744Ser point mutation disrupts d-NKA α function to the same extent as the heterozygous Ile905Trpfs*8 null mutation. Moreover, the observations of the heterozygous *ATPα* p.Gly744Ser point mutation causing worse phenotypes than the heterozygous Ile905Trpfs*8 null mutation in flies, when examined for cold-induced paralysis (Figure 16B and E) and daytime sleep (Figure 15F), suggests possible dominant-negative activity of the *ATPα* p.Gly744Ser mutation. This is supported by the partial rescue of the CS-*CJ10*/+ mutants in cold-stress testing relative to CS-*R1*/+ mutants which were completely rescued by the human wildtype transgene (Figure 19D and Figure 20D). Possible dominant-negative effects of the *ATPα CJ*/+ mutations (listed in Table 5) was previously proposed in Ashmore et al. (2009) work thus these findings described here contributes to the validity of this proposed mechanism. However, it is not possible to conclude from this research that the nature of the p.Gly744Ser mutation is dominant-negative as severe phenotypes in *CJ10*/+ mutants were not consistently seen in here. This could be a future direction to explore, to further validate the functional equivalence of h/d-NKA α between species as ATP1A3 variants have demonstrated dominant-negative activity (Li et al., 2015). Although, the d-NKA α has been shown in this study to be functional equivalent to the h-NKA α3, the examination of d-NKA α-modified flies in this study highlighted sex-specific differences (Figure 13C and Figure 16D-E), suggesting that sex also has an influence on the phenotype observed in *ATPα* mutant flies. This may pose issues in regard to the translatability power of findings as AHC disease is not characterised by sex differences (Uchitel et al., 2021). Moreover, in mouse models of AHC, sex differences are rarely reported, with one report of sex difference in

Atp1a3 D801N/+ mice following gait analysis (Uchitel et al., 2021).. Thus, highlighting the importance in future work to further develop the AHC D801N fly model to provide more convincing evidence, that the fly is a strong candidate to replace or at minimum reduce the use of mice in pre-clinical trials.

VI Conclusion

To conclude, the ability of the d-NKA α-modifed flies to mimic phenotypes relevant to AHC disease in behaviours that are highly conserved across species such as sleep (Zimmerman et al., 2008).suggest that the invertebrate model could be useful in elucidating neural circuits that may underpin AHC symptoms. Moreover, the rescue of an AHC-relevant phenotype of the *ATPα* p.Gly744Ser mutation equivalent to the human Gly755Ser AHC mutation and the null (p. Ile905Trpfs*8) mutation in *D. melanogaster* by the ubiquitous expression of the human *UAS-ATP1A3^{WT}* transgene showcases functional homology between the d-NKA α and h-NKA α3 therefore validating the *D. melanogaster* as a suitable *in vivo* model for AHC research. This is a step in the right direction to successfully implement the replacement principle of the 3Rs (Russell and Burch, 1959).

VII Future Direction

The transgenic rescue of a *ATPα* mutant phenotype facilitated the further assessment of the function of the human ATP1A3 p.Asp801Asn mutation in flies. However, this was deemed unsuccessful as no phenotypic defects akin to *ATPα* mutant flies was observed in flies ubiquitously expressing the mutant transgene. As previously discussed, this is likely to be a result of the intact endogenous fly *ATPα* gene masking the potential mutant transgene effects. Thus, future work would involve crossing the mutant transgene into the heterozygous null background to produce a fly line carrying one functional copy of the *ATPα* on the third chromosome and a copy of the *UAS-ATP1A3^{D801N}* on the second

chromosome, liken to the of genotype of fly lines used in rescue experiment. Following this, climbing and cold shock assays will be repeated on these new sets of transgenic flies with appropriate controls. Alongside this continuation of rescue experiments to gather more evidence for functional homology of d-NKA α such as determining whether homozygous lethality and mechanical-induced paralysis (Ashmore et al., 2009) can be rescued in *ATPα* mutants by the *UAS-ATP1A3^{Wt}* transgene. All future behavioural experiments with transgenic flies would include a standard wildtype control like CS flies. As AHC disease is suggested to be progressive in nature indicated by exacerbated motor, intellectual disability symptoms and progressive brain atrophy (Sasaki et al., 2014; Sasaki et al., 2017; Uchitel et al., 2021). It could be of interest to conduct phenocopy experiments in older transgenic flies.

Another area of focus relates to application of real-time PCR to facilitate the quantitative verification of the amount of human *ATP1A3* transgene and endogenous fly *ATPα* gene that is expressed in the brain of *Gal4/UAS_α3* and *UAS_α3* control transgenic fly lines. This would help to address several questions like: (1) whether the transgenes are being expressed to a level comparable to the wildtype ATP*α* gene and (2) whether leaky expression is occurring in *UAS_α3* fly lines.

Finally, would carry out further western blot studies with different standard wildtype controls (CS, W1118 and Dahomey) to determine whether the Millipore anti-h/m-NKA *α*3 and XVIF9-G10 anti-h/m-NKA *α*3 antibodies cross-react with the h-NKA *α* protein to definitively establish whether these primary antibodies can be used to identify and quantify the expression of the human wildtype or mutant ATP1A3 transgene in *Gal4/UAS* flies.

VIII REFERENCES

Adams, M.D., Celniker, S.E., Holt, R.A., Evans, C.A., Gocayne, J.D., Amanatides, P.G., Scherer, S.E., Li, P.W., Hoskins, R.A. and Galle, R.F. 2000. The genome sequence of Drosophila melanogaster. *Science.* **287**(5461), pp.2185-2195.

Aicardi, J. 1987. Alternating hemiplegia of childhood. *International Pediatrics.* **Volume 2**(Issue 2), pp.115-119.

Aicardi, J., Bourgeois, M. and Goutieres, F. 1995. Alternating hemiplegia of childhood: clinical findings and diagnostic criteria. *Alternating hemiplegia of childhood.* pp.3-18.

Algahtani, H., Ibrahim, B., Shirah, B., Aldarmahi, A. and Abdullah, A. 2017. More than a decade of misdiagnosis of alternating hemiplegia of childhood with catastrophic outcome. *Case reports in medicine.* **2017**.

Alyoubi, R., Park, I., Embuido, J. and Hwang, P. 2016. 1. Alternating hemiplegia of childhood into adulthood (AHCA): Case series and literature update. *Clinical Neurophysiology.* **127**(4), pe160.

Andersen, M.K., Robertson, R.M. and MacMillan, H.A. 2022. Plasticity in Na+/K+-ATPase thermal kinetics drives variation in the temperature of cold-induced neural shutdown of adult Drosophila melanogaster. *Journal of Experimental Biology.* **225**(24), pjeb244923.

Armstrong, G.A., Rodríguez, E.C. and Robertson, R.M. 2012. Cold hardening modulates K+ homeostasis in the brain of Drosophila melanogaster during chill coma. *Journal of Insect Physiology.* **58**(11), pp.1511-1516.

Arystarkhova, E., Haq, I.U., Luebbert, T., Mochel, F., Saunders-Pullman, R., Bressman, S.B., Feschenko, P., Salazar, C., Cook, J.F. and Demarest, S. 2019. Factors in the disease severity of ATP1A3 mutations: impairment, misfolding, and allele competition. *Neurobiology of disease.* **132**, p104577.

Arystarkhova, E. and Sweadner, K.J. 1996. Isoform-specific monoclonal antibodies to Na, K-ATPase α subunits: evidence for a tissue-specific post-translational modification of the α subunit. *Journal of Biological Chemistry.* **271**(38), pp.23407-23417.

Arystarkhova, E. and Sweadner, K.J. 2024. Na, K-ATPase Expression Can Be Limited Post-Transcriptionally: A Test of the Role of the Beta Subunit, and a Review of Evidence. *International Journal of Molecular Sciences.* **25**(13), p7414.

Ashmore, L.J., Hrizo, S.L., Paul, S.M., Van Voorhies, W.A., Beitel, G.J. and Palladino, M.J. 2009. Novel mutations affecting the Na, K ATPase alpha model complex neurological diseases and implicate the sodium pump in increased longevity. *Human genetics.* **126**, pp.431-447.

Auvin, S., Joriot-Chekaf, S., Cuvellier, J., Pandit, F., Cuisset, J., Ruchoux, M. and Vallee, L. 2006. Small vessel abnormalities in alternating hemiplegia of childhood: pathophysiologic implications. *Neurology.* **66**(4), pp.499-504.

Azarias, G., Kruusmägi, M., Connor, S., Akkuratov, E.E., Liu, X.-L., Lyons, D., Brismar, H., Broberger, C. and Aperia, A. 2013. A specific and essential role for Na, K-ATPase α3 in neurons co-expressing α1 and α3. *Journal of Biological Chemistry.* **288**(4), pp.2734-2743.

Bass, T.M., Grandison, R.C., Wong, R., Martinez, P., Partridge, L. and Piper, M.D. 2007. Optimization of dietary restriction protocols in Drosophila. *The Journals of Gerontology Series A: Biological Sciences and Medical Sciences.* **62**(10), pp.1071-1081.

Bassi, M., Bresolin, N., Tonelli, A., Nazos, K., Crippa, F., Baschirotto, C., Zucca, C., Bersano, A., Dolcetta, D. and Boneschi, F. 2004. A novel mutation in the ATP1A2 gene causes alternating hemiplegia of childhood. *Journal of medical genetics.* **41**(8), pp.621-628.

Bates, D., Maechler, M., Bolker, B., Walker, S., Christensen, R.H.B., Singmann, H., Dai, B., Grothendieck, G., Green, P. and Bolker, M.B. 2015. Package 'lme4'. *convergence.* **12**(1), p2.

Baumann, O., Salvaterra, P.M. and Takeyasu, K. 2010. Developmental changes in β-subunit composition of Na, K-ATPase in the Drosophila eye. *Cell and tissue research.* **340**, pp.215-228.

Bischof, J., Maeda, R.K., Hediger, M., Karch, F. and Basler, K. 2007. An optimized transgenesis system for Drosophila using germ-line-specific φC31 integrases. *Proceedings of the National Academy of Sciences.* **104**(9), pp.3312-3317.

Blanco, G. and Mercer, R.W. 1998. Isozymes of the Na-K-ATPase: heterogeneity in structure, diversity in function. *American Journal of Physiology-Renal Physiology.* **275**(5), pp.F633-F650.

Boelman, C., Lagman-Bartolome, A.M., MacGregor, D.L., McCabe, J., Logan, W.J. and Minassian, B.A. 2014. Identical ATP1A3 mutation causes alternating hemiplegia of childhood and rapid-onset dystonia parkinsonism phenotypes. *Pediatric Neurology.* **51**(6), pp.850-853.

Bøttger, P., Tracz, Z., Heuck, A., Nissen, P., Romero-Ramos, M. and Lykke-Hartmann, K. 2011. Distribution of Na/K-ATPase alpha 3 isoform, a sodium-potassium P-type pump associated with rapid-onset of dystonia parkinsonism (RDP) in the adult mouse brain. *Journal of Comparative Neurology.* **519**(2), pp.376-404.

Bourgeois, M., Aicardi, J. and Goutières, F. 1993. Alternating hemiplegia of childhood. *The Journal of pediatrics.* **122**(5), pp.673-679.

Brown, G.R., Hem, V., Katz, K.S., Ovetsky, M., Wallin, C., Ermolaeva, O., Tolstoy, I., Tatusova, T., Pruitt, K.D. and Maglott, D.R. 2015. Gene: a gene-centered information resource at NCBI. *Nucleic acids research.* **43**(D1), pp.D36-D42.

Bubliy, O.A., Riihimaa, A., Norry, F.M. and Loeschcke, V. 2002. Variation in resistance and acclimation to low-temperature stress among three geographical strains of Drosophila melanogaster. *Journal of thermal biology.* **27**(5), pp.337-344.

Carvalho, G.B., Ja, W.W. and Benzer, S. 2009. Non-lethal PCR genotyping of single Drosophila. *Biotechniques.* **46**(4), pp.312-314.

Casaer, P., Aicardi, J., Curatolo, P., Dias, K., Maia, M., Motte, J., Pineda, M., Pouplard, F., Preney-Cramatte, S. and Stephenson, J. 1987. Flunarizine in alternating hemiplegia in childhood. An international study in 12 children. *Neuropediatrics.* **18**(04), pp.191-195.

Catterson, J.H., Knowles-Barley, S., James, K., Heck, M.M., Harmar, A.J. and Hartley, P.S. 2010. Dietary modulation of Drosophila sleep-wake behaviour. *PloS one.* **5**(8), pe12062.

Cavener, D.R. 1987. Comparison of the consensus sequence flanking translational start sites in Drosophila and vertebrates. *Nucleic acids research.* **15**(4), pp.1353-1361.

Chart, D.A.S. 2019. Molecular Cloning Overview. *UPDATE.* p20.

Cheslock, A., Andersen, M.K. and MacMillan, H.A. 2021. Thermal acclimation alters Na+/K+-ATPase activity in a tissue-specific manner in Drosophila melanogaster. *Comparative Biochemistry and Physiology Part A: Molecular & Integrative Physiology.* **256**, p110934.

Chiu, J.C., Low, K.H., Pike, D.H., Yildirim, E. and Edery, I. 2010. Assaying locomotor activity to study circadian rhythms and sleep parameters in Drosophila. *JoVE (Journal of Visualized Experiments).* (43), pe2157.

Clapcote, S.J., Duffy, S., Xie, G., Kirshenbaum, G., Bechard, A.R., Rodacker Schack, V., Petersen, J., Sinai, L., Saab, B.J. and Lerch, J.P. 2009. Mutation I810N in the α3 isoform of Na+, K+-ATPase causes impairments in the sodium pump and hyperexcitability in the CNS. *Proceedings of the national academy of sciences.* **106**(33), pp.14085-14090.

Clausen, M.V., Hilbers, F. and Poulsen, H. 2017. The structure and function of the Na, K-ATPase isoforms in health and disease. *Frontiers in physiology.* **8**, p371.

Colonna, T.E., Huynh, L. and Fambrough, D.M. 1997. Subunit interactions in the Na, K-ATPase explored with the yeast two-hybrid system. *Journal of Biological Chemistry.* **272**(19), pp.12366-12372.

Contreras, E.G. and Klämbt, C. 2023. The Drosophila blood-brain barrier emerges as a model for understanding human brain diseases. *Neurobiology of Disease.* **180**, p106071.

Cordani, R., Stagnaro, M., Pisciotta, L., Tiziano, F.D., Calevo, M.G., Nobili, L., De Grandis, E. and Consortium, I.A. 2021. Alternating Hemiplegia of Childhood: Genotype–Phenotype Correlations in a Cohort of 39 Italian Patients. *Frontiers in Neurology.* p369.

Creamer, M.S., Mano, O. and Clark, D.A. 2018. Visual control of walking speed in Drosophila. *Neuron.* **100**(6), pp.1460-1473. e1466.

Dalla, S., Swarts, H.G., Koenderink, J.B. and Dobler, S. 2013. Amino acid substitutions of Na, K-ATPase conferring decreased sensitivity to cardenolides in insects compared to mammals. *Insect Biochemistry and Molecular Biology.* **43**(12), pp.1109-1115.

David, R.J., Gibert, P., Pla, E., Petavy, G., Karan, D. and Moreteau, B. 1998. Cold stress tolerance in Drosophila: analysis of chill coma recovery in D. melanogaster. *Journal of Thermal Biology.* **23**(5), pp.291-299.

De Vries, B., Stam, A., Beker, F., Van Den Maagdenberg, A., Vanmolkot, K., Laan, L., Ginjaar, I., Frants, R., Lauffer, H. and Haan, J. 2008. CACNA1A mutation linking hemiplegic migraine and alternating hemiplegia of childhood. *Cephalalgia.* **28**(8), pp.887-891.

Dean, D., Weinstein, H., Amin, S., Karno, B., McAvoy, E., Hoy, R., Recknagel, A., Jarvis, C. and Deitcher, D. 2018. Extending julius seizure, a bang-sensitive gene, as a model for studying epileptogenesis: Cold shock, and a new insertional mutation. *Fly.* **12**(1), pp.55-61.

DeAndrade, M.P., Yokoi, F., van Groen, T., Lingrel, J.B. and Li, Y. 2011. Characterization of Atp1a3 mutant mice as a model of rapid-onset dystonia with parkinsonism. *Behavioural brain research.* **216**(2), pp.659-665.

Delorme, C., Hainque, E. and Roze, E. 2017. Alternating upper limb monoplegia due to ATP1A3 mutation. *Pediatric Neurology.* **68**, pp.79-80.

Desguerre, I., Aubart, M., Hashimoto, Y., Poirier, K., Kaminska, A., Alison, M., Boddaert, N., Munnich, A. and Campbell, M. 2023. Reply: De novo mutations in CLDN5: alternating hemiplegia of childhood or not? *Brain.* **146**(8), pp.e59-e60.

Doke, S.K. and Dhawale, S.C. 2015. Alternatives to animal testing: A review. *Saudi Pharmaceutical Journal.* **23**(3), pp.223-229.

Donelson, N., Kim, E.Z., Slawson, J.B., Vecsey, C.G., Huber, R. and Griffith, L.C. 2012. High-resolution positional tracking for long-term analysis of Drosophila sleep and locomotion using the "tracker" program. *PloS one.* **7**(5), pe37250.

Du, F., Ozdowski, E.F., Kotowski, I.K., Marchuk, D.A. and Sherwood, N.T. 2010. Functional conservation of human Spastin in a Drosophila model of autosomal dominant-hereditary spastic paraplegia. *Human molecular genetics.* **19**(10), pp.1883-1896.

Dubowy, C. and Sehgal, A. 2017. Circadian rhythms and sleep in Drosophila melanogaster. *Genetics.* **205**(4), pp.1373-1397.

Edwards, I.J., Bruce, G., Lawrenson, C., Howe, L., Clapcote, S.J., Deuchars, S.A. and Deuchars, J. 2013. Na+/K+ ATPase α1 and α3 isoforms are differentially expressed in α-and γ-motoneurons. *Journal of Neuroscience.* **33**(24), pp.9913-9919.

Ejima, A. and Griffith, L.C. 2011. Assay for courtship suppression in Drosophila. *Cold Spring Harb Protoc.* **2011**(2), pt5575.

Fernandez-Chiappe, F., Frenkel, L., Colque, C.C., Ricciuti, A., Hahm, B., Cerredo, K., Muraro, N.I. and Ceriani, M.F. 2021. High-frequency neuronal bursting is essential for circadian and sleep behaviors in Drosophila. *Journal of Neuroscience.* **41**(4), pp.689-710.

Foley, K.P., Leonard, M.W. and Engel, J.D. 1993. Quantitation of RNA using the polymerase chain reaction. *Trends in Genetics.* **9**(11), pp.380-385.

Gajam, S., Peterson, R.R., Mathew, A.A. and Thomas, A. 2022. Sporadic hemiplegic migraine with CACNA1A mutation masquerading as acute meningoencephalitis. *Annals of Indian Academy of Neurology.* **25**(3), p528.

Garcia, M.J., Littler, A.S., Sriram, A. and Teets, N.M. 2020. Distinct cold tolerance traits independently vary across genotypes in Drosophila melanogaster. *Evolution.* **74**(7), pp.1437-1450.

Garcia, M.J. and Teets, N.M. 2019. Cold stress results in sustained locomotor and behavioral deficits in Drosophila melanogaster. *Journal of Experimental Zoology Part A: Ecological and Integrative Physiology.* **331**(3), pp.192-200.

Gargano, J.W., Martin, I., Bhandari, P. and Grotewiel, M.S. 2005. Rapid iterative negative geotaxis (RING): a new method for assessing age-related locomotor decline in Drosophila. *Experimental gerontology.* **40**(5), pp.386-395.

Geering, K. 2005. Function of FXYD proteins, regulators of Na, K-ATPase. *Journal of bioenergetics and biomembranes.* **37**, pp.387-392.

Geering, K. 2006. FXYD proteins: new regulators of Na-K-ATPase. *American Journal of Physiology-Renal Physiology.* **290**(2), pp.F241-F250.

Geering, K. 2008. Functional roles of Na, K-ATPase subunits. *Current opinion in nephrology and hypertension.* **17**(5), pp.526-532.

Geissmann, Q., Beckwith, E.J. and Gilestro, G.F. 2019. Most sleep does not serve a vital function: Evidence from Drosophila melanogaster. *Science advances.* **5**(2), peaau9253.

Gergont, A. and Kaciński, M. 2014. Alternating hemiplegia of childhood: New diagnostic options. *Neurologia i neurochirurgia polska.* **48**(2), pp.130-135.

Ghosh, A. and Sheeba, V. 2022. VANESSA—Shiny Apps for Accelerated Time-series Analysis and Visualization of Drosophila Circadian Rhythm and Sleep Data. *Journal of biological rhythms.* **37**(2), pp.222-231.

Gluderer, S., Brunner, E., Germann, M., Jovaisaite, V., Li, C., Rentsch, C.A., Hafen, E. and Stocker, H. 2010. Madm (Mlf1 adapter molecule) cooperates with Bunched A to promote growth in Drosophila. *Journal of biology.* **9**, pp.1-15.

Gramates, L.S., Marygold, S.J., Santos, G.d., Urbano, J.-M., Antonazzo, G., Matthews, B.B., Rey, A.J., Tabone, C.J., Crosby, M.A. and Emmert, D.B. 2016. FlyBase at 25: looking to the future. *Nucleic acids research.* pgkw1016.

Harris, J.J., Jolivet, R. and Attwell, D. 2012. Synaptic energy use and supply. *Neuron.* **75**(5), pp.762-777.

Hashimoto, Y., Poirier, K., Boddaert, N., Hubert, L., Aubart, M., Kaminska, A., Alison, M., Desguerre, I., Munnich, A. and Campbell, M. 2022. Recurrent de novo mutations in CLDN5 induce an anion-selective blood–brain barrier and alternating hemiplegia. *Brain.* **145**(10), pp.3374-3382.

Heinzen, E.L., Arzimanoglou, A., Brashear, A., Clapcote, S.J., Gurrieri, F., Goldstein, D.B., Jóhannesson, S.H., Mikati, M.A., Neville, B. and Nicole, S. 2014. Distinct neurological disorders with ATP1A3 mutations. *The Lancet Neurology.* **13**(5), pp.503-514.

Heinzen, E.L., Swoboda, K.J., Hitomi, Y., Gurrieri, F., Nicole, S., de Vries, B., Tiziano, F.D., Fontaine, B., Walley, N.M. and Heavin, S. 2012. De novo mutations in ATP1A3 cause alternating hemiplegia of childhood. *Nature genetics.* **44**(9), pp.1030-1034.

Helfrich-Förster, C. 2000. Differential control of morning and evening components in the activity rhythm of Drosophila melanogaster—sex-specific differences suggest a different quality of activity. *Journal of biological rhythms.* **15**(2), pp.135-154.

Helseth, A.R., Hunanyan, A.S., Adil, S., Linabarger, M., Sachdev, M., Abdelnour, E., Arehart, E., Szabo, M., Richardson, J. and Wetsel, W.C. 2018. Novel E815K knock-in mouse model of alternating hemiplegia of childhood. *Neurobiology of disease.* **119**, pp.100-112.

Hochrein, L., Machens, F., Gremmels, J., Schulz, K., Messerschmidt, K. and Mueller-Roeber, B. 2017. AssemblX: a user-friendly toolkit for rapid and reliable multi-gene assemblies. *Nucleic Acids Research.* **45**(10), pp.e80-e80.

Hoei-Hansen, C.E., í Dali, C., Lyngbye, T.J., Duno, M. and Uldall, P. 2014. Alternating hemiplegia of childhood in Denmark: clinical manifestations and ATP1A3 mutation status. *European Journal of Paediatric Neurology.* **18**(1), pp.50-54.

Holm, R., Toustrup-Jensen, M.S., Einholm, A.P., Schack, V.R., Andersen, J.P. and Vilsen, B. 2016. Neurological disease mutations of α3 Na+, K+-ATPase: Structural and functional perspectives and rescue of compromised function. *Biochimica et Biophysica Acta (BBA)-Bioenergetics.* **1857**(11), pp.1807-1828.

Holm, T.H., Isaksen, T.J., Glerup, S., Heuck, A., Bøttger, P., Füchtbauer, E.-M., Nedergaard, S., Nyengaard, J.R., Andreasen, M. and Nissen, P. 2016. Cognitive deficits caused by a disease-mutation in the α3 Na+/K+-ATPase isoform. *Scientific reports.* **6**(1), p31972.

Holm, T.H. and Lykke-Hartmann, K. 2016. Insights into the pathology of the α3 Na+/K+-ATPase ion pump in neurological disorders; lessons from animal models. *Frontiers in physiology.* **7**, p209.

Howard, C.E., Chen, C.-L., Tabachnik, T., Hormigo, R., Ramdya, P. and Mann, R.S. 2019. Serotonergic modulation of walking in Drosophila. *Current Biology.* **29**(24), pp.4218-4230. e4218.

Huang, D., Liu, M., Wang, H., Zhang, B., Zhao, D., Ling, W., Wang, M., Feng, J., Shen, Y. and Chen, X. 2021. De novo ATP1A2 variants in two Chinese children with alternating hemiplegia of childhood upgraded the gene–disease relationship and variant classification: a case report. *BMC Medical Genomics.* **14**(1), pp.1-6.

Hunanyan, A.S., Fainberg, N.A., Linabarger, M., Arehart, E., Leonard, A.S., Adil, S.M., Helseth, A.R., Swearingen, A.K., Forbes, S.L. and Rodriguiz, R.M. 2015. Knock-in mouse model of alternating hemiplegia of childhood: behavioral and electrophysiologic characterization. *Epilepsia.* **56**(1), pp.82-93.

Ikeda, K., Satake, S.I., Onaka, T., Sugimoto, H., Takeda, N., Imoto, K. and Kawakami, K. 2013. Enhanced inhibitory neurotransmission in the cerebellar cortex of Atp1a3-deficient heterozygous mice. *The Journal of physiology.* **591**(13), pp.3433-3449.

Incorpora, G., Pavone, P., Polizzi, A., Cocuzza, M., Privitera, M., Pavone, L. and Ruggieri, M. 2012. An 11-year follow-up study of neonatal-onset, bath-induced alternating hemiplegia of childhood in twins. *Journal of Child Neurology.* **27**(5), pp.657-662.

Isaac, R.E., Li, C., Leedale, A.E. and Shirras, A.D. 2010. Drosophila male sex peptide inhibits siesta sleep and promotes locomotor activity in the post-mated female. *Proceedings of the Royal Society B: Biological Sciences.* **277**(1678), pp.65-70.

Isaksen, T.J., Kros, L., Vedovato, N., Holm, T.H., Vitenzon, A., Gadsby, D.C., Khodakhah, K. and Lykke-Hartmann, K. 2017. Hypothermia-induced dystonia and abnormal cerebellar activity in a mouse model with a single disease-mutation in the sodium-potassium pump. *PLoS genetics.* **13**(5), pe1006763.

Ishii, A., Saito, Y., Mitsui, J., Ishiura, H., Yoshimura, J., Arai, H., Yamashita, S., Kimura, S., Oguni, H. and Morishita, S. 2013. Identification of ATP1A3 mutations by exome sequencing as the cause of alternating hemiplegia of childhood in Japanese patients. *PloS one.* **8**(2), pe56120.

Ishimoto, H., Lark, A. and Kitamoto, T. 2012. Factors that differentially affect daytime and nighttime sleep in Drosophila melanogaster. *Frontiers in neurology.* **3**, p24.

Ito, T., Narugami, M., Egawa, K., Yamamoto, H., Asahina, N., Kohsaka, S., Ishii, A., Hirose, S. and Shiraishi, H. 2018. Long-term follow up of an adult with alternating hemiplegia of childhood and a p. Gly755Ser mutation in the ATP1A3 gene. *Brain and Development.* **40**(3), pp.226-228.

Jen, J., Wan, J., Palos, T., Howard, B. and Baloh, R. 2005. Mutation in the glutamate transporter EAAT1 causes episodic ataxia, hemiplegia, and seizures. *Neurology.* **65**(4), pp.529-534.

Jenett, A., Rubin, G.M., Ngo, T.-T., Shepherd, D., Murphy, C., Dionne, H., Pfeiffer, B.D., Cavallaro, A., Hall, D. and Jeter, J. 2012. A GAL4-driver line resource for Drosophila neurobiology. *Cell reports.* **2**(4), pp.991-1001.

Johnson, M., Zaretskaya, I., Raytselis, Y., Merezhuk, Y., McGinnis, S. and Madden, T.L. 2008. NCBI BLAST: a better web interface. *Nucleic acids research.* **36**(suppl_2), pp.W5-W9.

Kanai, R., Cornelius, F., Ogawa, H., Motoyama, K., Vilsen, B. and Toyoshima, C. 2021. Binding of cardiotonic steroids to Na+, K+-ATPase in the E2P state. *Proceedings of the National Academy of Sciences.* **118**(1), pe2020438118.

Kanai, R., Ogawa, H., Vilsen, B., Cornelius, F. and Toyoshima, C. 2013. Crystal structure of a Na+-bound Na+, K+-ATPase preceding the E1P state. *Nature.* **502**(7470), pp.201-206.

Kanavakis, E., Xaidara, A., Papathanasiou-Klontza, D., Velentza, S. and Youroukos, S. 2003. Alternating hemiplegia of childhood: a syndrome inherited with an autosomal dominant trait. *Developmental Medicine & Child Neurology.* **45**(12), pp.833-836.

Kansagra, S., Ghusayni, R., Kherallah, B., Gunduz, T., McLean, M., Prange, L., Kravitz, R.M. and Mikati, M.A. 2019. Polysomnography findings and sleep disorders in children with alternating hemiplegia of childhood. *Journal of Clinical Sleep Medicine.* **15**(1), pp.65-70.

Kinoshita, P.F., Leite, J.A., Orellana, A.M.M., Vasconcelos, A.R., Quintas, L.E., Kawamoto, E.M. and Scavone, C. 2016. The influence of Na+, K+-ATPase on glutamate signaling in neurodegenerative diseases and senescence. *Frontiers in physiology.* **7**, p195.

Kirshenbaum, G.S., Clapcote, S.J., Duffy, S., Burgess, C.R., Petersen, J., Jarowek, K.J., Yücel, Y.H., Cortez, M.A., Snead III, O.C. and Vilsen, B. 2011. Mania-like behavior induced by genetic dysfunction of the neuron-specific Na+, K+-ATPase α3 sodium pump. *Proceedings of the National Academy of Sciences.* **108**(44), pp.18144-18149.

Kirshenbaum, G.S., Dachtler, J., Roder, J.C. and Clapcote, S.J. 2015. Characterization of cognitive deficits in mice with an alternating hemiplegia-linked mutation. *Behavioral neuroscience.* **129**(6), p822.

Kirshenbaum, G.S., Dachtler, J., Roder, J.C. and Clapcote, S.J. 2016a. Transgenic rescue of phenotypic deficits in a mouse model of alternating hemiplegia of childhood. *Neurogenetics.* **17**, pp.57-63.

Kirshenbaum, G.S., Dawson, N., Mullins, J.G., Johnston, T.H., Drinkhill, M.J., Edwards, I.J., Fox, S.H., Pratt, J.A., Brotchie, J.M. and Roder, J.C. 2013. Alternating hemiplegia of childhood-related neural and behavioural phenotypes in Na+, K+-ATPase α3 missense mutant mice. *PloS one.* **8**(3), pe60141.

Kirshenbaum, G.S., Idris, N.F., Dachtler, J., Roder, J.C. and Clapcote, S.J. 2016b. Deficits in social behavioral tests in a mouse model of alternating hemiplegia of childhood. *Journal of neurogenetics.* **30**(1), pp.42-49.

Kramer, U., Nevo, Y., Margalit, D., Shorer, Z. and Harel, S. 2000. Alternating hemiplegia of childhood in half-sisters. *Journal of Child Neurology.* **15**(2), pp.128-130.

Krupinski, T. and Beitel, G.J. 2009. Unexpected roles of the Na-K-ATPase and other ion transporters in cell junctions and tubulogenesis. *Physiology.* **24**(3), pp.192-201.

Kryvenko, V., Vagin, O., Dada, L.A., Sznajder, J.I. and Vadász, I. 2021. Maturation of the Na, K-ATPase in the endoplasmic reticulum in health and disease. *The Journal of Membrane Biology.* **254**(5), pp.447-457.

Kusunoki, S., Kido, J., Momosaki, K., Sawada, T., Kashiki, T., Matsumoto, S. and Nakamura, K. 2021. Effect of Flunarizine on Alternating Hemiplegia of Childhood in a Patient with the p. E815K Mutation in ATP1A3: A Case Report. *Case Reports in Neurology.* **12**(3), pp.299-306.

Lazarov, E., Hillebrand, M., Schröder, S., Ternka, K., Hofhuis, J., Ohlenbusch, A., Barrantes-Freer, A., Pardo, L.A., Fruergaard, M.U. and Nissen, P. 2020. Comparative analysis of alternating hemiplegia of childhood and rapid-onset dystonia-parkinsonism

ATP1A3 mutations reveals functional deficits, which do not correlate with disease severity. *Neurobiology of Disease.* **143**, p105012.

Lebovitz, R.M., Takeyasu, K. and Fambrough, D. 1989. Molecular characterization and expression of the (Na++ K+)-ATPase alpha-subunit in Drosophila melanogaster. *The EMBO journal.* **8**(1), pp.193-202.

Li, M., Jazayeri, D., Corry, B., McSweeney, K.M., Heinzen, E.L., Goldstein, D.B. and Petrou, S. 2015. A functional correlate of severity in alternating hemiplegia of childhood. *Neurobiology of disease.* **77**, pp.88-93.

Li, Y., Liu, X., Wang, C., Su, Z., Zhao, K., Yang, M., Chen, S. and Zhou, L. 2022. Molecular and clinical characteristics of ATP1A3-related diseases. *Frontiers in Neurology.* **13**, p924788.

Lingrel, J.B. and Kuntzweiler, T. 1994. Na+, K (+)-ATPase. *The Journal of biological chemistry.* **269**(31), pp.19659-19662.

Luan, Z., Reddig, K. and Li, H.-S. 2014. Loss of Na+/K+-ATPase in Drosophila photoreceptors leads to blindness and age-dependent neurodegeneration. *Experimental neurology.* **261**, pp.791-801.

MacMillan, H.A., Ferguson, L.V., Nicolai, A., Donini, A., Staples, J.F. and Sinclair, B.J. 2015. Parallel ionoregulatory adjustments underlie phenotypic plasticity and evolution of Drosophila cold tolerance. *Journal of Experimental Biology.* **218**(3), pp.423-432.

Malik, B.R. and Hodge, J.J. 2014. Drosophila adult olfactory shock learning. *JoVE (Journal of Visualized Experiments).* (90), pe50107.

Mazzotta, G.M., Damulewicz, M. and Cusumano, P. 2020. Better sleep at night: how light influences sleep in Drosophila. *Frontiers in Physiology.* **11**, p997.

McBride, S.M., Holloway, S.L. and Jongens, T.A. 2013. Using Drosophila as a tool to identify pharmacological therapies for fragile X syndrome. *Drug Discovery Today: Technologies.* **10**(1), pp.e129-e136.

Measuring pixel difference. n.d. [Online]. [Accessed 13 September 2022]. Available from: https://zantiks.com/support/tutorials-for-zanscript/measuring-pixel-difference

Mikati, M., Maguire, H., Barlow, C., Ozelius, L., Breakefield, X., Klauck, S., Korf, B., O'Tuama, S. and Dangond, F. 1992. A syndrome of autosomal dominant alternating hemiplegia: clinical presentation mimicking intractable epilepsy; chromosomal studies; and physiologic investigations. *Neurology.* **42**(12), pp.2251-2251.

Mikati, M., O'Tuama, L. and Dangond, F. 1995. Autosomal dominant alternating hemiplegia of childhood. *Alternating hemiplegia of childhood. New York: Raven.* pp.125-134.

Mikati, M.A., Kramer, U., Zupanc, M.L. and Shanahan, R.J. 2000. Alternating hemiplegia of childhood: clinical manifestations and long-term outcome. *Pediatric neurology.* **23**(2), pp.134-141.

Mikati, M.A., Panagiotakaki, E. and Arzimanoglou, A. 2021. Revision of the diagnostic criteria of alternating hemiplegia of childhood. *European Journal of Paediatric Neurology.* **32**, pp.A4-A5.

Miller, D.E., Cook, K.R. and Hawley, R.S. 2019. The joy of balancers. *PLoS genetics.* **15**(11), pe1008421.

Miller, D.E., Cook, K.R., Hemenway, E.A., Fang, V., Miller, A.L., Hales, K.G. and Hawley, R.S. 2018. The molecular and genetic characterization of second chromosome balancers in Drosophila melanogaster. *G3: Genes, Genomes, Genetics.* **8**(4), pp.1161-1171.

Miller, D.E., Kahsai, L., Buddika, K., Dixon, M.J., Kim, B.Y., Calvi, B.R., Sokol, N.S., Hawley, R.S. and Cook, K.R. 2020. Identification and characterization of breakpoints and mutations on Drosophila melanogaster balancer chromosomes. *G3: Genes, Genomes, Genetics.* **10**(11), pp.4271-4285.

Milojevic, S., Ghosh, A., Makevic, V., Stojkovic, M., Capovilla, M., Tosti, T., Budimirovic, D. and Protic, D. 2024. Circadian Rhythm and Sleep Analyses in a Fruit

Fly Model of Fragile X Syndrome Using a Video-Based Automated Behavioral Research System. *International journal of molecular sciences.* **25**(14), p7949.

Mishra, N.K., Peleg, Y., Cirri, E., Belogus, T., Lifshitz, Y., Voelker, D.R., Apell, H.-J., Garty, H. and Karlish, S.J. 2011. FXYD proteins stabilize Na, K-ATPase: amplification of specific phosphatidylserine-protein interactions. *Journal of Biological Chemistry.* **286**(11), pp.9699-9712.

Mitchell, T.J., Zugarramurdi, C., Olivera, J.F., Gatto, C. and Artigas, P. 2014. Sodium and proton effects on inward proton transport through Na/K pumps. *Biophysical journal.* **106**(12), pp.2555-2565.

Miyazaki, T., Williams, J.A. and Toda, H. 2022. Measuring sleep in Drosophila. *Behavioral Neurogenetics.* Springer, pp.39-56.

Mobasheri, A., Trujillo, E., Arteaga, M.-F. and Martín-Vasallo, P. 2012. Na+, K+-ATPase subunit composition in a human chondrocyte cell line; evidence for the presence of α1, α3, β1, β2 and β3 isoforms. *International journal of molecular sciences.* **13**(4), pp.5019-5034.

Morth, J.P., Pedersen, B.P., Toustrup-Jensen, M.S., Sørensen, T.L.-M., Petersen, J., Andersen, J.P., Vilsen, B. and Nissen, P. 2007. Crystal structure of the sodium–potassium pump. *Nature.* **450**(7172), pp.1043-1049.

Moseley, A.E., Williams, M.T., Schaefer, T.L., Bohanan, C.S., Neumann, J.C., Behbehani, M.M., Vorhees, C.V. and Lingrel, J.B. 2007. Deficiency in Na, K-ATPase α isoform genes alters spatial learning, motor activity, and anxiety in mice. *Journal of Neuroscience.* **27**(3), pp.616-626.

Mundiyanapurath, S., Certel, S. and Kravitz, E.A. 2007. Studying aggression in Drosophila (fruit flies). *JoVE (Journal of Visualized Experiments).* (2), pe155.

Nagarajan, U. and Georgiou, M. 2022. Screening mutants by single fly genomic PCR. *Notch Signaling Research: Methods and Protocols.* Springer, pp.15-25.

Neville, B. and Ninan, M. 2007. The treatment and management of alternating hemiplegia of childhood. *Developmental Medicine & Child Neurology.* **49**(10), pp.777-780.

Ng, H.W., Ogbeta, J.A. and Clapcote, S.J. 2021. Genetically altered animal models for ATP1A3-related disorders. *Disease Models & Mechanisms.* **14**(10), pdmm048938.

Nguyen, P.T., Deisl, C., Fine, M., Tippetts, T.S., Uchikawa, E., Bai, X.-c. and Levine, B. 2022. Structural basis for gating mechanism of the human sodium-potassium pump. *Nature communications.* **13**(1), p5293.

Ni, J.-Q., Liu, L.-P., Binari, R., Hardy, R., Shim, H.-S., Cavallaro, A., Booker, M., Pfeiffer, B.D., Markstein, M. and Wang, H. 2009. A Drosophila resource of transgenic RNAi lines for neurogenetics. *Genetics.* **182**(4), pp.1089-1100.

Nichols, C.D., Becnel, J. and Pandey, U.B. 2012. Methods to assay Drosophila behavior. *Journal of visualized experiments: JoVE.* (61).

Okamura, H., Yasuhara, J., Fambrough, D. and Takeyasu, K. 2003. P-type ATPases in Caenorhabditis and Drosophila: implications for evolution of the P-type ATPase subunit families with special reference to the Na, K-ATPase and H, K-ATPase subgroup. *The Journal of membrane biology.* **191**, pp.13-24.

Öztürk-Çolak, A., Marygold, S.J., Antonazzo, G., Attrill, H., Goutte-Gattat, D., Jenkins, V.K., Matthews, B.B., Millburn, G., Dos Santos, G. and Tabone, C.J. 2024. FlyBase: updates to the Drosophila genes and genomes database. *Genetics.* **227**(1), piyad211.

Paciorkowski, A.R., McDaniel, S.S., Jansen, L.A., Tully, H., Tuttle, E., Ghoneim, D.H., Tupal, S., Gunter, S.A., Vasta, V. and Zhang, Q. 2015. Novel mutations in ATP1A3 associated with catastrophic early life epilepsy, episodic prolonged apnea, and postnatal microcephaly. *Epilepsia.* **56**(3), pp.422-430.

Palladino, M.J., Bower, J.E., Kreber, R. and Ganetzky, B. 2003. Neural dysfunction and neurodegeneration indrosophila na+/k+ atpase alpha subunit mutants. *Journal of Neuroscience.* **23**(4), pp.1276-1286.

Panagiotakaki, E., De Grandis, E., Stagnaro, M., Heinzen, E.L., Fons, C., Sisodiya, S., de Vries, B., Goubau, C., Weckhuysen, S. and Kemlink, D. 2015. Clinical profile of patients with ATP1A3 mutations in alternating hemiplegia of childhood—a study of 155 patients. *Orphanet journal of rare diseases.* **10**, pp.1-13.

Panagiotakaki, E., Gobbi, G., Neville, B., Ebinger, F., Campistol, J., Nevšímalová, S., Laan, L., Casaer, P., Spiel, G. and Giannotta, M. 2010. Evidence of a non-progressive course of alternating hemiplegia of childhood: study of a large cohort of children and adults. *Brain.* **133**(12), pp.3598-3610.

Pandey, U.B. and Nichols, C.D. 2011. Human disease models in Drosophila melanogaster and the role of the fly in therapeutic drug discovery. *Pharmacological reviews.* **63**(2), pp.411-436.

Paul, S.M., Palladino, M.J. and Beitel, G.J. 2007. A pump-independent function of the Na, K-ATPase is required for epithelial junction function and tracheal tube-size control.

Paul, S.M., Ternet, M., Salvaterra, P.M. and Beitel, G.J. 2003. The Na+/K+ ATPase is required for septate junction function and epithelial tube-size control in the Drosophila tracheal system.

Pavone, P., Pappalardo, X.G., Ruggieri, M., Falsaperla, R. and Parano, E. 2022. Alternating hemiplegia of childhood: a distinct clinical entity and ATP1A3-related disorders: A narrative review. *Medicine.* **101**(31).

Pfeiffenberger, C., Lear, B.C., Keegan, K.P. and Allada, R. 2010. Locomotor activity level monitoring using the Drosophila Activity Monitoring (DAM) System. *Cold Spring Harbor Protocols.* **2010**(11), ppdb. prot5518.

Pfeiffer, B.D., Jenett, A., Hammonds, A.S., Ngo, T.-T.B., Misra, S., Murphy, C., Scully, A., Carlson, J.W., Wan, K.H. and Laverty, T.R. 2008. Tools for neuroanatomy and neurogenetics in Drosophila. *Proceedings of the National Academy of Sciences.* **105**(28), pp.9715-9720.

Pfeiffer, B.D., Ngo, T.-T.B., Hibbard, K.L., Murphy, C., Jenett, A., Truman, J.W. and Rubin, G.M. 2010. Refinement of tools for targeted gene expression in Drosophila. *Genetics.* **186**(2), pp.735-755.

Post, R.L., Hegyvary, C. and Kume, S. 1972. Activation by adenosine triphosphate in the phosphorylation kinetics of sodium and potassium ion transport adenosine triphosphatase. *Journal of Biological Chemistry.* **247**(20), pp.6530-6540.

Prokop, A. 2015. A rough guide to Drosophila mating schemes (version 6.2). *Neuron.* **72**, pp.202-230.

Prokop, A. 2016. Fruit flies in biological research. *Biological Sciences Review.* **28**(2), pp.2-5.

Qiao, B., Li, C., Allen, V.W., Shirasu-Hiza, M. and Syed, S. 2018. Automated analysis of long-term grooming behavior in Drosophila using ak-nearest neighbors classifier. *Elife.* **7**, pe34497.

Reiter, L.T., Potocki, L., Chien, S., Gribskov, M. and Bier, E. 2001. A systematic analysis of human disease-associated gene sequences in Drosophila melanogaster. *Genome research.* **11**(6), pp.1114-1125.

Richards, K.S., Bommert, K., Szabo, G. and Miles, R. 2007. Differential expression of Na+/K+-ATPase α-subunits in mouse hippocampal interneurones and pyramidal cells. *The Journal of physiology.* **585**(2), pp.491-505.

Riemensperger, T., Isabel, G., Coulom, H., Neuser, K., Seugnet, L., Kume, K., Iché-Torres, M., Cassar, M., Strauss, R. and Preat, T. 2011. Behavioral consequences of dopamine deficiency in the Drosophila central nervous system. *Proceedings of the National Academy of Sciences.* **108**(2), pp.834-839.

Riemensperger, T., Issa, A.-R., Pech, U., Coulom, H., Nguyễn, M.-V., Cassar, M., Jacquet, M., Fiala, A. and Birman, S. 2013. A single dopamine pathway underlies progressive locomotor deficits in a Drosophila model of Parkinson disease. *Cell reports.* **5**(4), pp.952-960.

Robertson, R.M., Dawson-Scully, K.D. and Andrew, R.D. 2020. Neural shutdown under stress: an evolutionary perspective on spreading depolarization. *Journal of Neurophysiology.* **123**(3), pp.885-895.

Rosewich, H., Ohlenbusch, A., Huppke, P., Schlotawa, L., Baethmann, M., Carrilho, I., Fiori, S., Lourenco, C.M., Sawyer, S. and Steinfeld, R. 2014. The expanding clinical and genetic spectrum of ATP1A3-related disorders. *Neurology.* **82**(11), pp.945-955.

Rosewich, H., Sweney, M.T., DeBrosse, S., Ess, K., Ozelius, L., Andermann, E., Andermann, F., Andrasco, G., Belgrade, A. and Brashear, A. 2017. Research conference summary from the 2014 international task force on ATP1A3-related disorders. *Neurology: Genetics.* **3**(2), pe139.

Rosewich, H., Thiele, H., Ohlenbusch, A., Maschke, U., Altmüller, J., Frommolt, P., Zirn, B., Ebinger, F., Siemes, H. and Nürnberg, P. 2012. Heterozygous de-novo mutations in ATP1A3 in patients with alternating hemiplegia of childhood: a whole-exome sequencing gene-identification study. *The Lancet Neurology.* **11**(9), pp.764-773.

Roubergue, A., Philibert, B., Gautier, A., Kuster, A., Markowicz, K., Billette de Villemeur, T., Vuillaumier-Barrot, S., Nicole, S., Roze, E. and Doummar, D. 2015. Excellent response to a ketogenic diet in a patient with alternating hemiplegia of childhood. *JIMD Reports, Volume 15.* pp.7-12.

Roubergue, A., Roze, E., Vuillaumier-Barrot, S., Fontenille, M.J., Méneret, A., Vidailhet, M., Fontaine, B., Doummar, D., Philibert, B. and Riant, F. 2013. The multiple faces of the ATP1A3-related dystonic movement disorder. *Movement disorders: official journal of the Movement Disorder Society.* **28**(10), pp.1457-1459.

Roy, M., Sivan-Loukianova, E. and Eberl, D.F. 2013. Cell-type–specific roles of Na+/K+ ATPase subunits in Drosophila auditory mechanosensation. *Proceedings of the National Academy of Sciences.* **110**(1), pp.181-186.

Ruffin, V.A., Salameh, A.I., Boron, W.F. and Parker, M.D. 2014. Intracellular pH regulation by acid-base transporters in mammalian neurons. *Frontiers in physiology.* **5**, p43.

Russell, W.M.S. and Burch, R.L. 1959. *The principles of humane experimental technique.* Methuen.

Saini, N., Georgiev, O. and Schaffner, W. 2011. The parkin mutant phenotype in the fly is largely rescued by metal-responsive transcription factor (MTF-1). *Molecular and cellular biology.* **31**(10), pp.2151-2161.

Samanta, D. 2020. Management of alternating hemiplegia of childhood: a review. *Pediatric neurology.* **103**, pp.12-20.

Sasaki, M., Ishii, A., Saito, Y. and Hirose, S. 2017. Progressive brain atrophy in alternating hemiplegia of childhood. *Movement Disorders Clinical Practice.* **4**(3), pp.406-411.

Sasaki, M., Ishii, A., Saito, Y., Morisada, N., Iijima, K., Takada, S., Araki, A., Tanabe, Y., Arai, H. and Yamashita, S. 2014. Genotype–phenotype correlations in alternating hemiplegia of childhood. *Neurology.* **82**(6), pp.482-490.

Sasaki, M., Sakuma, H., Fukushima, A., Yamada, K.-i., Ohnishi, T. and Matsuda, H. 2009. Abnormal cerebral glucose metabolism in alternating hemiplegia of childhood. *Brain and Development.* **31**(1), pp.20-26.

Scaplen, K.M., Mei, N.J., Bounds, H.A., Song, S.L., Azanchi, R. and Kaun, K.R. 2019. Automated real-time quantification of group locomotor activity in Drosophila melanogaster. *Scientific Reports.* **9**(1), p4427.

Schirinzi, T., Graziola, F., Cusmai, R., Fusco, L., Nicita, F., Elia, M., Travaglini, L., Bertini, E., Curatolo, P. and Vigevano, F. 2018. ATP1A3-related epileptic encephalopathy responding to ketogenic diet. *Brain and Development.* **40**(5), pp.433-438.

Shinoda, T., Ogawa, H., Cornelius, F. and Toyoshima, C. 2009. Crystal structure of the sodium–potassium pump at 2.4 Å resolution. *Nature.* **459**(7245), pp.446-450.

Shyjan, A. and Levenson, R. 1989. Antisera specific for the a1, a2, a3, and b subunits of the Na, K-ATPase: differential expression of a and b subunits in rat tissue membranes. *Biochemistry.* **28**, pp.4531-4535.

Sievers, F. and Higgins, D.G. 2018. Clustal Omega for making accurate alignments of many protein sequences. *Protein Science.* **27**(1), pp.135-145.

Silies, M., Gohl, D.M., Fisher, Y.E., Freifeld, L., Clark, D.A. and Clandinin, T.R. 2013. Modular use of peripheral input channels tunes motion-detecting circuitry. *Neuron.* **79**(1), pp.111-127.

Silva, R.F., Pinho, B.R., Monteiro, N.M., Santos, M.M. and Oliveira, J.M. 2022. Automated analysis of activity, sleep, and rhythmic behaviour in various animal species with the Rtivity software. *Scientific Reports.* **12**(1), p4179.

Simmons, C.Q., Thompson, C.H., Cawthon, B.E., Westlake, G., Swoboda, K.J., Kiskinis, E., Ess, K.C. and George Jr, A.L. 2018. Direct evidence of impaired neuronal Na/K-ATPase pump function in alternating hemiplegia of childhood. *Neurobiology of disease.* **115**, pp.29-38.

Smith, R.S., Florio, M., Akula, S.K., Neil, J.E., Wang, Y., Hill, R.S., Goldman, M., Mullally, C.D., Reed, N. and Bello-Espinosa, L. 2021. Early role for a Na+, K+-ATPase (ATP1A3) in brain development. *Proceedings of the National Academy of Sciences.* **118**(25), pe2023333118.

Stagnaro, M., Pisciotta, L., Gherzi, M., Di Rocco, M., Gurrieri, F., Parrini, E., Prato, G., Veneselli, E. and De Grandis, E. 2018. ATP1A3 spectrum disorders: A video-documented history of 7 genetically confirmed early onset cases. *European Journal of Paediatric Neurology.* **22**(2), pp.264-271.

Sugimoto, H., Ikeda, K. and Kawakami, K. 2014. Heterozygous mice deficient in Atp1a3 exhibit motor deficits by chronic restraint stress. *Behavioural brain research.* **272**, pp.100-110.

Suh, Y.S., Bhat, S., Hong, S.-H., Shin, M., Bahk, S., Cho, K.S., Kim, S.-W., Lee, K.-S., Kim, Y.-J. and Jones, W.D. 2015. Genome-wide microRNA screening reveals that the

evolutionary conserved miR-9a regulates body growth by targeting sNPFR1/NPYR. *Nature communications.* **6**(1), p7693.

Suhail, M. 2010. Na+, K+-ATPase: ubiquitous multifunctional transmembrane protein and its relevance to various pathophysiological conditions. *Journal of clinical medicine research.* **2**(1), p1.

Sun, J., Xu, A.Q., Giraud, J., Poppinga, H., Riemensperger, T., Fiala, A. and Birman, S. 2018. Neural control of startle-induced locomotion by the mushroom bodies and associated neurons in Drosophila. *Frontiers in systems neuroscience.* **12**, p6.

Sun, Y., Jan, L.Y. and Jan, Y.N. 1998. Transcriptional regulation of atonal during development of the Drosophila peripheral nervous system. *Development.* **125**(18), pp.3731-3740.

Sweadner, K.J., Arystarkhova, E., Penniston, J.T., Swoboda, K.J., Brashear, A. and Ozelius, L.J. 2019. Genotype-structure-phenotype relationships diverge in paralogs ATP1A1, ATP1A2, and ATP1A3. *Neurology Genetics.* **5**(1).

Sweney, M.T., Silver, K., Gerard-Blanluet, M., Pedespan, J.-M., Renault, F., Arzimanoglou, A., Schlesinger-Massart, M., Lewelt, A.J., Reyna, S.P. and Swoboda, K.J. 2009. Alternating hemiplegia of childhood: early characteristics and evolution of a neurodevelopmental syndrome. *Pediatrics.* **123**(3), pp.e534-e541.

Swoboda, K.J., Kanavakis, E., Xaidara, A., Johnson, J.E., Leppert, M.F., Schlesinger-Massart, M.B., Ptacek, L.J., Silver, K. and Youroukos, S. 2004. Alternating hemiplegia of childhood or familial hemiplegic migraine?: a novel ATP1A2 mutation. *Annals of Neurology: Official Journal of the American Neurological Association and the Child Neurology Society.* **55**(6), pp.884-887.

Tenney, J.R. and Schapiro, M.B. 2010. Child neurology: alternating hemiplegia of childhood. *Neurology.* **74**(14), pp.e57-e59.

Thum, A.S., Knapek, S., Rister, J., Dierichs-Schmitt, E., Heisenberg, M. and Tanimoto, H. 2006. Differential potencies of effector genes in adult Drosophila. *Journal of Comparative Neurology.* **498**(2), pp.194-203.

Timothy, J.W., Klas, N., Sanghani, H.R., Al-Mansouri, T., Hughes, A.T., Kirshenbaum, G.S., Brienza, V., Belle, M.D., Ralph, M.R. and Clapcote, S.J. 2018. Circadian disruptions in the Myshkin mouse model of mania are independent of deficits in suprachiasmatic molecular clock function. *Biological psychiatry.* **84**(11), pp.827-837.

Titus, S.A., Warmke, J.W. and Ganetzky, B. 1997. The Drosophila erg K+ channel polypeptide is encoded by the seizure locus. *Journal of Neuroscience.* **17**(3), pp.875-881.

Towbin, H., Staehelin, T. and Gordon, J. 1979. Electrophoretic transfer of proteins from polyacrylamide gels to nitrocellulose sheets: procedure and some applications. *Proceedings of the national academy of sciences.* **76**(9), pp.4350-4354.

Uchitel, J., Helseth, A., Prange, L., McLean, M., Ghusayni, R., Sachdev, M., Hunanyan, A. and Mikati, M.A. 2019. The epileptology of alternating hemiplegia of childhood. *Neurology.* **93**(13), pp.e1248-e1259.

Uchitel, J., Wallace, K., Tran, L., Abrahamsen, T., Hunanyan, A., Prange, L., Jasien, J., Caligiuri, L., Pratt, M. and Rikard, B. 2021. Alternating hemiplegia of childhood: evolution over time and mouse model corroboration. *Brain Communications.* **3**(3), pfcab128.

Ugur, B., Chen, K. and Bellen, H.J. 2016. Drosophila tools and assays for the study of human diseases. *Disease models & mechanisms.* **9**(3), pp.235-244.

Ulate-Campos, A., Fons, C., Artuch, R., Castejón, E., Martorell, L., Ozelius, L., Pascual, J. and Campistol, J. 2014. Alternating hemiplegia of childhood with a de novo mutation in ATP1A3 and changes in SLC2A1 responsive to a ketogenic diet. *Pediatric neurology.* **50**(4), pp.377-379.

van der Graaf, K., Srivastav, S., Singh, P., McNew, J.A. and Stern, M. 2022. The Drosophila melanogaster attP40 docking site and derivatives are insertion mutations of msp-300. *PLoS One.* **17**(12), pe0278598.

Van Hillegondsberg, L. and Michaelis, I. 2019. Alternating hemiplegia of childhood: First South African case report and verapamil as a possible treatment option. *SAMJ: South African Medical Journal.* **109**(3), pp.152-153.

Vedovato, N. and Gadsby, D.C. 2014. Route, mechanism, and implications of proton import during Na+/K+ exchange by native Na+/K+-ATPase pumps. *Journal of General Physiology.* **143**(4), pp.449-464.

Verret, S. and Steele, J.C. 1971. Alternating hemiplegia in childhood: a report of eight patients with complicated migraine beginning in infancy. *Pediatrics.* **47**(4), pp.675-680.

Videlier, M., Rundle, H.D. and Careau, V. 2019. Sex-specific among-individual covariation in locomotor activity and resting metabolic rate in Drosophila melanogaster. *The American Naturalist.* **194**(6), pp.E164-E176.

Viollet, L., Glusman, G., Murphy, K.J., Newcomb, T.M., Reyna, S.P., Sweney, M., Nelson, B., Andermann, F., Andermann, E. and Acsadi, G. 2015. Alternating hemiplegia of childhood: retrospective genetic study and genotype-phenotype correlations in 187 subjects from the US AHCF registry. *PloS one.* **10**(5), pe0127045.

Weigand, K.M., Messchaert, M., Swarts, H.G., Russel, F.G. and Koenderink, J.B. 2014. Alternating hemiplegia of childhood mutations have a differential effect on Na+, K+-ATPase activity and ouabain binding. *Biochimica et Biophysica Acta (BBA)-Molecular Basis of Disease.* **1842**(7), pp.1010-1016.

Weller, C.M., Leen, W.G., Neville, B.G., Duncan, J.S., Vries, B.d., Geilenkirchen, M.A., Haan, J., Kamsteeg, E.-J., Ferrari, M.D. and Maagdenberg, A.M.v.d. 2015. A novel SLC2A1 mutation linking hemiplegic migraine with alternating hemiplegia of childhood. *Cephalalgia.* **35**(1), pp.10-15.

Wu, M.N., Koh, K., Yue, Z., Joiner, W.J. and Sehgal, A. 2008. A genetic screen for sleep and circadian mutants reveals mechanisms underlying regulation of sleep in Drosophila. *Sleep.* **31**(4), pp.465-472.

Xie, J., Wang, D., Ling, S., Yang, G., Yang, Y. and Chen, W. 2019. High-salt diet causes sleep fragmentation in young Drosophila through circadian rhythm and dopaminergic systems. *Frontiers in neuroscience.* **13**, p1271.

Yang, X., Gao, H., Zhang, J., Xu, X., Liu, X., Wu, X., Wei, L. and Zhang, Y. 2014. ATP1A3 mutations and genotype-phenotype correlation of alternating hemiplegia of childhood in Chinese patients. *PloS one.* **9**(5), pe97274.

Yap, J.Q., Seflova, J., Sweazey, R., Artigas, P. and Robia, S.L. 2021. FXYD proteins and sodium pump regulatory mechanisms. *Journal of General Physiology.* **153**(4), pe202012633.

Zhang, C., Kim, A.J., Rivera-Perez, C., Noriega, F.G. and Kim, Y.-J. 2022. The insect somatostatin pathway gates vitellogenesis progression during reproductive maturation and the post-mating response. *Nature communications.* **13**(1), p969.

Zhong, L., Yang, Z., Tang, H., Xu, Y., Liu, X. and Shen, J. 2022. Differential analysis of negative geotaxis climbing trajectories in Drosophila under different conditions. *Archives of Insect Biochemistry and Physiology.* **111**(2), pe21922.

Zimmerman, J.E., Naidoo, N., Raizen, D.M. and Pack, A.I. 2008. Conservation of sleep: insights from non-mammalian model systems. *Trends in neurosciences.* **31**(7), pp.371-376.